UNIVERSITY OF CALIFORNIA,
IRVINE

Scaffolds for Neural Stem Cell Tissue Engineering

DISSERTATION

submitted in partial satisfaction of the requirements for the degree of

DOCTOR OF PHILOSOPHY

in Biomedical Engineering

by

Janahan Arulmoli

Dissertation Committee:
Professor Lisa Flanagan, Chair
Professor Elliot Botvinick
Professor Wendy Liu

2016

DEDICATION

To my parents, Kandiah and Jayagowri Arulmoli, for your unending support and for the infinite levels of sacrifice and selflessness you've displayed in providing for your family.

To my grandparents, Viswalingam and Jayaranie Nakulendran, for being the second set of parents throughout my life and your endless encouragement and support.

And to my little brother, Vithuran Arulmoli and little sister, Aarani Arulmoli for being two pillars that have supported me through everything.

Table of Contents

List of Figures

List of Tables

ACKNOWLEDGMENTS

Firstly, I would like to thank Dr. Lisa Flanagan for giving me the opportunity to work in her lab over the past 4 years. I met with you for the first time in my first year of graduate school knowing that we had mutual research interests. I am extremely thankful for your mentorship, guidance, and friendship over the years and for all the collaborative opportunities that you have provided for me. I genuinely believe you possess a grounded and deep understanding of how science should be properly executed in terms of research, mentorship, and lifelong learning. I would also like to thank Dr. Wendy Liu and Dr. Elliot Botvinick for serving on my committee and being excellent collaborators over the years. I thank Dr. Matthew Blurton-Jones and Dr. Lizhi Sun for serving on my qualifying exam committee and finally would like to thank Dr. James Earthman for providing a starting point for my graduate research career.

Although there are many members in the Flanagan lab as well as our collaborating laboratories that I must thank for their assistance in completing these studies, I must acknowledge Dr. Medha Pathak and Dr. Jamison "Sunshine" Nourse, both of whom served as alternate mentors in the lab for me. Sunshine showed me the ropes on everything neural stem cells and taught me the analytical techniques that I used throughout the years in the lab. Medha enlightened me to the wonderful world of mechanotransduction and stretch-activated ion channels and was part of an efficient and fruitful collaboration along with Dr. Francesco Tombola. Medha also inspired me to work hard because of her unparalleled determination to obtain results and make scientific breakthroughs. I must also thank the other members of the Flanagan lab, Lisa McDonnell for being a great lab manager in my earlier years in the lab and Clarissa Ro for being a great friend and an excellent collaborator on the *in vivo* studies. Andrew

Yale has been a great friend, teammate, and fellow graduate student in the lab and Rylan Kautz has also been a great friend and collaborator on the reflectin project. Dr. Mindy Simon was an excellent collaborator and friend during my initial years in the lab working on dielectropheresis-based cell sorting. I must also Urmi Sheth who worked with me as an undergraduate for 2 years and was instrumental in obtaining results for our combination scaffold studies as well as for a large majority of the hyaluronic acid-peptide studies. I'd like to also thank Dr. Shubha Tiwari and Dr. Tayloria Adams for their advice on navigating through the end of graduate school and being excellent collaborators on the neural stem cell sorting and differentiation projects. Dr. Tom Zarembinski and Michael Onorato from BioTime, Inc. have been instrumental collaborators in pushing forward the HA-based scaffold studies and Dr. Evelyn Sawyer from SeaRun Holdings, Inc. has been very generous in providing our lab with salmon fibrinogen and thrombin. I would like to thank Richard Que and Dr. Szu Wang and Dr. Nancy Da Silva for being great colleagues and collaborators on developing recombinant collagen substrates for human neural stem cells. Richard has stuck by me since my UCSD engineering days and provided bioengineering expertise throughout graduate school.

There are several labs that helped us navigate moving our research from the *in vitro* to *in vivo* stages. I wish to thank Dr. Ron Frostig and Cynthia Bee for their stroke expertise and training on TTC staining of brain tissue. I thank Dr. Brian Cummings, Dr. Aileen Anderson, and Dr. Rebecca Nishi for their stem cell transplant expertise. Dr. Daniel Haus and Eric Gold were invaluable in providing training on transplantation and perfusions. I would also like to thank Dr. Weian Zhao, Dr. Wenbin Liao, and Victor Pham for training in the transient middle cerebral artery occlusion model on both mice and rats. The *in vivo* studies would not have been possible without all of your help.

I would like to thank all my friends because I would not have been able to complete this doctorate without your support. First, I want to thank the morning basketball club, my intramural UCI basketball team, and Irvine City League team comprised primarily of graduate students, post-docs, and professors. This provided me not only a great group of people to be around but a consistent outlet to relieve stress while getting to play my favorite sport throughout graduate school. I would like to thank Dr. Peter Donovan for being a great scientist and friend as well as an excellent tennis partner. I am grateful that you have helped rekindle my appreciation and addiction for playing tennis, and for all our post-tennis sessions at Eureka! I would also like to thank my college friends who have stuck by my side throughout graduate school. Whether it was getting together on weekends or light-hearted banter on group chats, I truly appreciate having you in my life.

Lastly, I must thank my everlasting support system – my family. Much of my family live in Southern California, so I am appreciative of the continuous support I've received from aunts, uncles, and cousins. My younger siblings both share parts of my personality and thus understand how I react in many situations, thus I am thankful that I have had them for support through the ups and downs of graduate school. From the beginning, my parents prioritized their children and helped us realize the importance of a solid academic foundation in life. Knowing my parents worked extremely hard to come to America from a war-torn third world country puts many things in perspective and makes me realize that anything really is possible if one sets their mind to it and puts in the time and effort. My grandparents have been there for us throughout my life and despite their advanced age, I am truly lucky that I have been able to spend so much time with them and gotten to appreciate their Sri Lankan cultural roots and values.

CURRICULUM VITAE

Janahan Arulmoli

Education: Ph.D. Biomedical Engineering, University of California, Irvine (2016)

M.S. Biomedical Engineering, University of California, Irvine (2014)

B.S. Chemical Engineering, University of California, San Diego (2009)

Professional Positions:

January 2013-Present: UC Irvine
Doctoral Candidate, Professor Lisa Flanagan's Laboratory

- Investigation of injectable synthetic and natural biomaterials as drug delivery platforms for human neural stem cell (NSC) tissue engineering and transplantation in rodent stroke models – resulted in publication in *Acta Biomaterialia*
- Analysis of the effects of mechanical stimuli on NSC growth and differentiation using device built in-house – resulted in publication in *Scientific Reports* 2015
- Investigated the effects of novel material substrates on NSC behavior – resulted in publication in *ACS Applied Materials and Interfaces* 2015
- Utilized various microfluidic platforms to sort and characterize unlabeled NSC populations using dielectrophoresis (DEP) – resulted in publication in *Biomicrofluidics* 2014
- Involvement of stretch-activated ion channels (SACs) in human NSC differentiation – resulted in publication in *Proceedings of the National Academy of Sciences* 2014
- Encapsulation of NSCs in scaffold biomaterial droplets demonstrating reliability of the microfluidic platform

July 2011-December 2012: UC Irvine
Graduate Student, Professor James Earthman's Laboratory

- Investigation of the combustion properties of titanium microparticles via abrasion from golf clubs and their ability to ignite uncontrolled brush fires – resulted in publication in *Fire and Materials* 2015

June 2009-September 2010: Biogen Idec Inc.
Research Assistant

- Tested antibody binding to cancer stem cells by means of fluorescence-activated cell sorting (FACS) leading to isolation of 2 candidates used in a preclinical subcutaneous mouse model

- Established an assay designed to test the ability of single stem cells to proliferate and form colonies with tumor-like properties which became the established model within the research group

September 2008-April 2010: UCSD Microhemodynamics Laboratory
Researcher, Professors Marcos Intaglietta/Paul C. Johnson Lab

- Research on the rheological properties of blood flow through the arterioles
- Investigation of the ability of polyethylene glycol (PEG) to reduce drag *in vivo* in the arterioles of rats under hemorrhaging conditions
- Aided in the development of an *in vitro* system to test the drag reducing ability of polyethylene glycol (PEG) under high flow rate environments
- Analysis and manipulation of Arthur Guyton's MATLAB model of the human cardiovascular system

Summer 2006, Summer 2007, & Summer 2008: Prodo Laboratories Inc.
Volunteer

- Assistance in surgical pancreatic islet isolation for diabetes research
- Aided in preparation of research presentation for the International Pancreas and Islet Transplant Association Conference in Minnesota (September 2007)
- Enumeration of healthy islet cells after isolation

Summer 2005: Earth Mechanics Inc.
Intern/Laboratory Assistant

- Assisted engineers and technicians in performing laboratory testing of soil samples for bridge foundation design

Research Interests:

Tissue Engineering, Biomaterials, Stem Cells, Materials Science and Engineering

Awards/Honors:

1. Peer-reviewed selection for oral presentation of research – Biomedical Engineering Society (BMES) Annual Meeting 2015

2. Featured Publication, Neural Cell News, February 2015 (Arulmoli et al. Scientific Reports 2015)

3. UC Irvine Public Impact Fellowship 2014-2015 ($1000 stipend award) *Fellowship intended to support and highlight academically excellent students whose research demonstrates the potential to significantly improve or enrich the lives of people in California and beyond.*

4. Selected invitation for oral presentation of research – 15th Annual UC Systemwide Bioengineering Symposium (June 2014)

5. "Best Oral Presentation" Award – 15th Annual UC Systemwide Bioengineering Symposium (June 2014)

6. Featured Publication/News Headline, ESPN/CNN/ABC News, March 2014 (Arulmoli et al. Fire and Materials 2015)

Grants/Fellowships:

2013-2015 Stem Cells in Translational Medicine for Neurological Disorders from the National Institute of Neurological Disorders and Stroke (NINDS/NIH) Training Fellowship T32 NS082174

2014-2015 UC Irvine Public Impact Fellowship

Teaching Experience:

1. Winter 2013: CBEMS 155L Teaching Assistant (Mechanical Behavior of Engineering Materials Lab Course)

2. Fall 2011: BME 110A Teaching Assistant (Biomechanics I Course)

Professional Societies:

2011-Present: BMES (Biomedical Engineering Society) Member
2006-2009: AIChE (American Institute of Chemical Engineers) Member

Mentoring:

Undergraduate Students:
2014-2016: Urmi Sheth (Professor Lisa Flanagan Laboratory)
2013-2014: Patrick Torres (Professor Lisa Flanagan Laboratory)
2011-2012: Bryant Vu (Professor James Earthman Laboratory)

High School Students:
2013-2015: Christina Huang (Professor Lisa Flanagan Laboratory)
Received 1st place in 2015 Palos Verdes High School District Science Fair Competition

Publications:

Original Articles

1. Pathak, M.M., Nourse, J.L., Tran, T., Hwe, J., **Arulmoli, J.**, Le, D.T., Bernardis, E., Flanagan, L.A., Tombola, F. "Stretch-activated ion channel piezo1 directs lineage choice in human neural stem cells" *PNAS* 111(45): 16148-16153, 2014.

2. Simon, M.G., Li, Y., **Arulmoli, J.**, McDonnell, L.P., Akil, A., Nourse, J.L., Lee, A.P., Flanagan, L.A. "Increasing label-free stem cell sorting capacity to reach transplantation-scale throughput" *Biomicrofluidics* 8(6): 064106, 2014.

3. **Arulmoli, J.**, Vu, B., Sung M.J., Mohamed F.A., Earthman, J.C. "Spark production by abrasion of titanium alloys in golf club heads" *Fire Mater*, 39:119-126, 2015.

4. **Arulmoli, J.**, Pathak, M.M., McDonnell, L.P., Nourse, J.L., Tombola, F., Earthman, J.C., Flanagan, L.A. "Static stretch affects neural stem cell differentiation in an extracellular matrix-dependent manner" *Scientific Reports,* 5: 8499, 2015.

5. Phan, L., Kautz, R., **Arulmoli, J.,** Kim, I., Le, D.T., Shenk, M.A., Pathak, M.M., Flanagan, L.A., Tombola, F., Gorodetsky, A.A. "Reflectin as a Material for Neural Stem Cell Growth" *ACS Applied Materials & Interfaces*, 8 (1), 278-284, 2016.

6. Wright, H.J., **Arulmoli, J.**, Motazedi, M., Nelson, L.J., Heinemann, F.S., Flanagan, L.A., Razorenova, O.V. "CDCP1 cleavage is necessary for homodimerization-induced migration of triple-negative breast cancer" *Oncogene*, 1-11, 2016.

7. **Arulmoli, J**., Wright, H.J., Phan, D., Sheth, U., Que, R.A., Botten, G.A., Keating, M., Botvinick, E.L., Pathak, M.M., Zarembinski, T.I., Yanni, D.S., Razorenova, O.V., Hughes, C.C.W., Flanagan, L.A. "Combination scaffolds of salmon fibrin, hyaluronic acid, and laminin for human neural stem cell and vascular tissue engineering" *Acta Biomaterialia*, http://dx.doi.org/10.1016/j.actbio.2016.07.043, 2016.

8. Yale, A.R., Nourse, J.L., Muth, K.R., Ahmed, S.N., **Arulmoli, J.**, Povieng, B., McDonnell, L.P., Flanagan, L.A. "N-glycans influence fate potential in neural stem cells" **(In Preparation)**

Abstracts/Presentations:

Oral Conference Presentations

P1. **Arulmoli, J.,** Pathak, M.M., McDonnell, L.P., Flanagan, L.A. The Effects of Stretch on Neural Stem Cell Differentiation. *15th Annual UC Systemwide Bioengineering Symposium*, Irvine, CA, USA. (June 2014)

P2. **Arulmoli, J.**, Sheth, U., Wright, H.J., Pathak, M.M., Huang, C., Sawyer, E., Zarembinski, T., Yanni, D.S., Razorenova, O., Flanagan, L.A. Salmon fibrin-hyaluronic acid hybrid scaffolds support human neural stem/progenitor cell function. *Biomedical Engineering Society (BMES) Annual Meeting*, Tampa, FL, USA. (October 2015)

P3. **Arulmoli, J.** Human Neural Stem Cell Tissue Engineering – Fishing for Scaffolds. *UC Irvine Biomedical Engineering Department Seminar*, Irvine, CA, USA. (March 2016)

Conference Posters

A1. Yalcin, O., **Arulmoli, J.**, Johnson, P.C., The effects of drag reducing polymers on the rheological properties of blood flow in the microcirculation. *UCSD Science Fair*, La Jolla, CA, USA. (March 2008)

A2. Clanton, D., **Arulmoli, J.**, Chu, P., Antibody binding to LGR5 colorectal cancer stem cell target. *Biogen Idec Inc. Poster Symposium*, La Jolla, CA, USA. (June 2010)

A3. **Arulmoli, J.**, Pathak, M.M., McDonnell, L.P., Flanagan, L.A. Static stretch affects neural stem cell differentiation along the oligodendrocyte lineage. *Keystone Symposium: Engineering Cell Fate and Function*, Olympic Valley, CA, USA. (April 2014)

A4. **Arulmoli, J.**, Pathak, M.M., McDonnell, L.P., Flanagan, L.A. Static stretch affects neural stem cell differentiation along the oligodendrocyte lineage. *Biomedical Engineering Society (BMES) Annual Meeting*, San Antonio, TX, USA. (October 2014)

A5. **Arulmoli, J.**, Wright, H.J., Phan, T.T., Sheth, U., Ro, C.C., Bee, C., Haus, D., Pham, V.B., Liao, W., Razorenova, O.V., Frostig, R., Hughes, C.C.W., Flanagan, L.A. Salmon fibrin-hyaluronic acid-laminin combination scaffolds for human neural stem cell tissue engineering to treat stroke. *UC Irvine Institute for Clinical and Translational Science Research Day*, Irvine, CA, USA. (June 2016)

Extracurricular Activities:

2nd degree black belt in the Korean martial art of Kuk Sool Won

Proficient on the Veena (South Indian classical stringed instrument) having played in several concerts around Southern California and overseas in England from 1993-2007

ABSTRACT OF THE DISSERTATION

Scaffolds for Neural Stem Cell Tissue Engineering

By

Janahan Arulmoli

Doctor of Philosophy in Biomedical Engineering

University of California, 2016

Professor Lisa A. Flanagan, Chair

Stroke is a leading cause of long-term disability and there is a high unmet clinical need for therapies that allow patients to recover lost function. Neural stem cells are good candidates for treating stroke since they can self-renew, secrete beneficial trophic factors, and differentiate into mature central nervous system (CNS) cells; however, most cells die after transplantation. In this work, injectable biomaterials were optimized as transplantation scaffolds for human neural stem/progenitor cells (hNSPCs) with the goal of improving transplanted cell survival. Biomaterials including fibrin, hyaluronic acid, laminin, collagen, and reflectin were combined and tailored to promote hNSPC function. Parameters for scaffold optimization included sensitivity to mechanical stimuli since we discovered that NSPC differentiation can be regulated by static stretch when cells adhere to specific substrate materials and mechanosensing in these cells is regulated by the stretch-activated ion channel Piezo1. Further characteristics of the scaffold included material properties, polymerization and degradation kinetics, ability to support vascularization and hNSPC function, and injectability into naïve and damaged CNS tissue. A novel salmon fibrin-hyaluronic acid-laminin combination scaffold for hNSPC tissue engineering

was developed *in vitro*, and this work marked the first report for the use of both human neural and vascular cells within a biomaterial to promote vascularization. This developed transplant construct was used *in vivo* in a preclinical transient middle cerebral artery occlusion (tMCAO) stroke model in rats as a potential therapeutic.

CHAPTER 1

INTRODUCTION

Neurological disorders represent diseases and injuries to the central nervous system (CNS), such as stroke, traumatic brain injury (TBI), and spinal cord injury (SCI), all of which are debilitating and incurable. Stem cells can self-renew and differentiate into more mature cell types; thereby holding promise as a therapy for these types of ailments. A great challenge to employing stem cells as therapeutics for CNS injury is the dismal survival and integration of transplanted cells. These parameters are of vital importance for the success of such a therapy. Bioengineering strategies that use injectable biomaterial-based scaffolds to protect stem cells and act as an artificial niche within the injured tissue can help combat the issue of transplanted cell death. This work highlights the strategic design and use of novel scaffolds combined from various sources to support stem cell survival and function for the treatment of stroke.

1.1 STROKE AND CURRENT THERAPIES

Stroke is currently the third leading cause of death and a leading cause of long-term disability in the United States imposing direct economic costs of over $70 billion annually[1, 2]. An ischemic stroke occurs when an artery becomes blocked and inhibits blood circulation to the brain. Ischemic strokes can be categorized as either embolic or thrombotic and account for 87% of all stroke occurrences in the United States[1]. In an embolic stroke, a plaque fragment within an artery forms in a different part of the body and moves through the circulatory system where it becomes lodged in the brain, while thrombotic strokes are caused by buildup of plaque on the vessel inner wall, causing blockage of one or more arteries that supply blood to the brain.

Hemorrhagic strokes, which account for the other 13% of stroke incidences, are caused by the rupture of blood vessels leading to decreased blood supply in the brain.

Unfortunately, the high prevalence of stroke has not been met with sufficient restorative therapies to address long-term disability. The most common treatment for ischemic stroke has been the use of thrombolytics to dissolve clots that block blood flow in the brain. Tissue plasminogen activator (tPA) is a Federal Drug Administration (FDA)-approved thrombolytic that is commonly used for treatment of ischemia, and must be administered within 4.5 hours of stroke onset to be effective[3]. This short time window restriction leaves only 5-7% of stroke patients eligible for tPA treatment[3]. For patients ineligible for tPA treatment, the MERCI Retrieval System may be used as it is an FDA-approved device that wraps a stent around the clot within the blood vessel and removes it to restore blood flow. The Penumbra System is an alternative device approved by the FDA for treatment of ischemic stroke and allows for revascularization of blocked blood vessels via a stent that mechanically disrupts and aspirates out the clot *in situ*. These therapies must be employed within 6 hours after stroke onset[3] in order to prevent damage to brain tissue and are thus limited to early intervention. With tPA and stent retrievers as the only available treatments for stroke, there is a pressing need for therapies that can promote recovery and regeneration of dead tissue following insult.

1.2 NEURAL STEM/PROGENITOR CELLS (NSPCS)

Cell therapy in the field of tissue engineering and regenerative medicine most commonly refers to the use of stem cells to replace lost cell types due to injury or to provide beneficial secreted molecules to stimulate repair[4]. Stem cells migrate to areas of injury, actively respond to the microenvironment, secrete neuroprotective compounds, and generate a diverse subset of cells

with various functional capabilities[5]. The transplantation of stem cells into the infarct cavity of the brain poses a unique alternative to current therapies and the potential for recovery outside the short time window of current treatments. Several *in vivo* rodent models have demonstrated that neural stem cell transplantation into damaged brains of rodents can result in migration of cells to the ischemic lesion, differentiation into neuronal and glial cell types, and improved functional recovery[6-8]. The main drawback to direct stem cell transplantation into the damaged area of the brain is that most cells die upon injection[9]. However, the incorporation of the cells into a biocompatible scaffold can greatly alleviate this issue.

Neural stem cells are multipotent stem cells capable of self-renewal and differentiation into the 3 cell types of the CNS: neurons, astrocytes and oligodendrocytes[10]. NSPCs are a heterogeneous population of neural stem cells and committed progenitor cells that are present in the fetal as well as adult brain. Throughout life NSPCs are generated in the subventricular zone (SVZ) of the lateral ventricles and dentate gyrus (DG) of the hippocampus and give rise to new neurons in the brain, a process known as neurogenesis. In the event of ischemic brain injury, many neurons become damaged and patterns of neurogenesis are altered[5]. Global ischemia, which refers to the restriction of blood flow to large areas of the brain, can cause increased neurogenesis in ischemic neurogenic regions such as the SVZ and hippocampus along with increased NSPC proliferation in the SVZ[11, 12]. There is also evidence for the migration of NSPCs out of the SVZ to non-neurogenic regions such as the striatum in response to focal ischemia for up to one year after stroke[13]. However, in many cases endogenous NSPCs migrating to sites of injury fail to differentiate into functional cortical neurons, attesting to the potential value in the transplantation of exogenous NSPCs (Fig. 1.1)[5]. Furthermore, the significant functional deficits suffered by many humans with stroke suggest limited potential of endogenous NSPCs to provide

sufficient repair after stroke. The development of human NSPCs (hNSPCs) as an exogenous cell source makes transplants for human conditions possible.

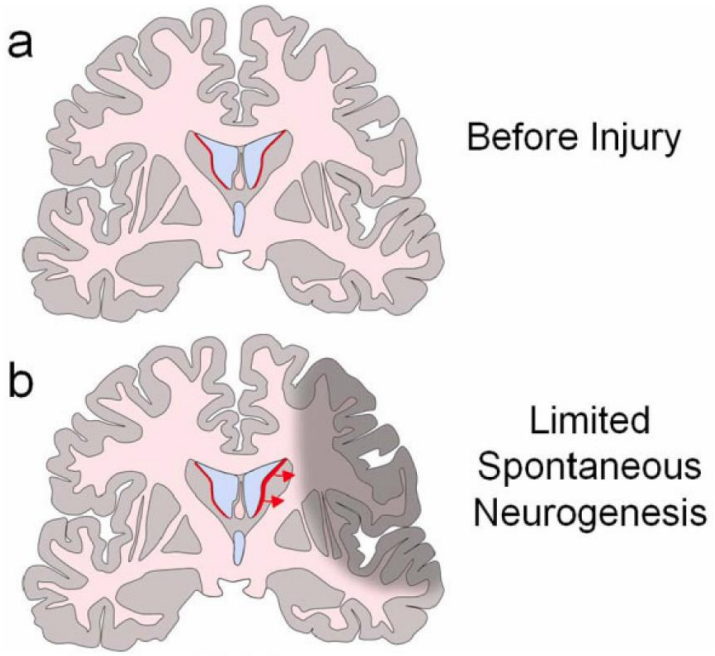

Figure 1.1. Mobilization of endogenous NSCs post-injury. (a) NSCs exist in the SVZ of adult human brains (red outline). (b) Proliferation of NSCs increases after stroke and ensuing migration gives rise to a limited number of new neurons (stroke affected region outlined in gray) Reprinted by permission from John Wiley and Sons: Journal of Comparative Neurology[5], copyright 2009.

Exogenous stem cells can act via multiple mechanisms to restore function after ischemic brain injury (Fig. 1.2)[14]. The transplantation of NSPCs into the ischemic brain is advantageous because of the greater control over cell fate and ability to deliver a chosen amount of cells to the lesion site. There are several delivery variables that must be accounted for when attempting to optimize the number of surviving functional cells at the site of injury. The timing of cellular delivery can yield a variety of results as many groups have transplanted cells at time periods ranging from 1 day to 1 month post-injury. Transplantation of NSPCs as a neuroprotective measure during the acute post-stroke period less than 1 week following injury reduces lesion size

and can prevent further apoptosis[5, 9]. Delivery of stem cells even in the subacute 1 week period after injury has yielded improved motor function in ischemic rats[15]. Transplanting cells in the chronic phase 3-4 weeks after stroke induction attempts to investigate host-graft circuitry in the chronic rather than acute or subacute time frame, as later time points ensure drastic reduction of the inflammatory response and stabilization of long-term behavioral deficits. Even in the chronic stroke transplantation model, stem cells yield improvements in both sensorimotor function and gross motor asymmetry[15, 16]. Thus, transplantation at multiple stages after stroke target different mechanisms of cell-based recovery.

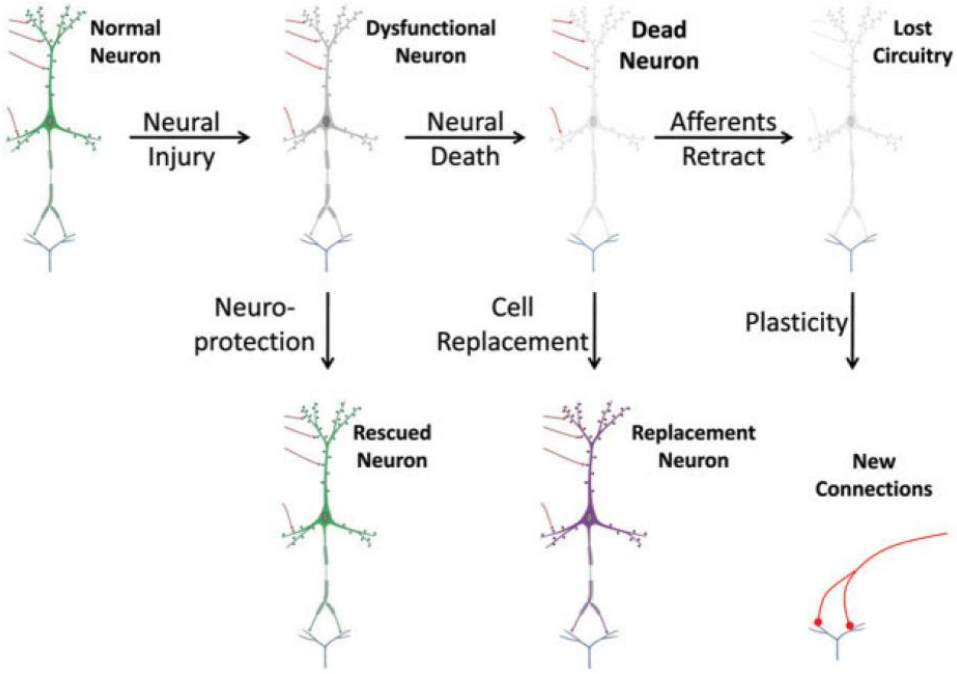

Figure 1.2. Schematic illustrating mechanisms of exogenous stem cell action. (1) Neuroprotection: Neuroprotective actions, which can include modulation of inflammation or secretion of neuroprotective compounds, may rescue damaged neurons and preserve existing neural circuitry. (2) Cell Replacement: Upon neural cell death, transplanted cells can serve to replace the lost cell. Effective replacement depends heavily on the preservation of surrounding cellular and microenvironmental architecture. (3) Plasticity: If original circuits cannot be maintained due to retraction of afferent projections after the neuron dies, transplanted cells can participate in the formation of new circuits via synaptic incorporation or formation of new

connections by host neurons, termed synaptic plasticity. Reprinted by permission from Elsevier Science & Technology Books: Fundamental Neuroscience, 2nd edition[14], copyright 2003.

The administration route of therapeutic NSPCs for stroke can vary as cells may be delivered systemically into the vasculature or locally into the brain. Systemic delivery relies on the migratory tendencies of NSPCs to target areas of injury, but can also risk the homing of cells to different organs or clumping within blood vessels[17]. More commonly, NSPCs are delivered intracerebrally either into the peri-infarct penumbra surrounding the injury, or the infarct core within the lesion site. The peri-infarct region is the area of greatest plasticity and recovery following an ischemic event, therefore transplantation of cells into this site may perturb this process. Injection into the infarct core yields an enormous amount of cell death[18], most likely attributed to the damage in this area and to the absence of blood vessels and presence of inflammatory cells within this region[19].

Ischemia generates an infarct core that contains widespread necrosis and is highly unreceptive to transplanted cells. This is due both to the lack of a support system for transplanted cells such as the extracellular matrix (ECM) and a lack of vascularization. Transplanted cell death can be alleviated by the use of scaffolds to protect exogenous cells from the endogenous ischemic microenvironment. Embedding NSPCs in a biomaterial during transplantation into the infarct core may aid in transplanted cell survival, proliferation, differentiation, and ultimately incorporation into the host tissue to promote recovery.

1.3 BIOMATERIALS AS SCAFFOLDS FOR NSPCS

Biomaterials configured as three-dimensional (3D) scaffold hydrogels provide stem cells with an appropriate microenvironment in order to reproduce the functions of the damaged tissue[20-22]. Scaffolds can be categorized as natural or synthetic, each of which have their

advantages and disadvantages. Natural scaffolds such as collagen, fibrin, and hyaluronic acid are generally more biocompatible, degrade into non-toxic byproducts, and contain innate cell adhesion and signaling elements but can vary batch to batch and are more difficult to scale up for manufacturing. Synthetic scaffolds such as polylacticoglycolic acid (PLGA) or polyethylene glycol (PEG) can be tuned to have ideal mechanical and chemical properties, are optimal for manufacturing purposes, but formation of toxic products during polymerization and degradation can be drawbacks. Key parameters in the design of scaffolds for stem cell transplantation are mechanical properties, biocompatibility, polymerization and degradation rate, and adhesion site availability. It has been shown that stem cell behavior can be directed by the stiffness of the substrate *in vitro*[23-25]. Mechanotransduction describes the process by which cells convert mechanical stimuli into a chemical or electrical response. Mechanical cues, such as stretch, compression, and substrate stiffness are tightly linked to stem cell fate and function, suggesting cells can efficiently alter their behavior in a mechanosensory manner[26, 27]. Cationic stretch-activated ion channels (SACs) are known to detect mechanical forces with great sensitivity and are permeable to Ca^{2+}, a key messenger implicated in cell fate[28, 29]. We investigated the role of SACs as a mechanistic player for transducing mechanical cues in NSPCs. This provides context for the importance of developing biomaterials with material properties in order for stem cells to survive and function, especially within the infarct cavity of stroke where the physical microenvironment is vastly different than that of healthy brain tissue. Due to the non-toxic polymerization, biocompatibility, and injectability of natural biomaterials, we investigate several types of these scaffolds in our studies. By combining different scaffold materials through chemical and physical tethering, we develop novel hydrogels with synergistic properties targeting the support of neural stem cell survival and function.

The combination of stem cells and biomaterial scaffolds offers a hopeful strategy for engineering functional tissues and cellular delivery. The various components that comprise the ECM provide a robust foundation for developing scaffolds based on natural biomaterials. These components include proteins and polysaccharides that play numerous roles *in vivo*, making natural materials a fitting choice for tissue engineering applications. In addition, natural materials tend to be biocompatible and contain sites for cellular adhesion, providing substrates for stem cell survival, growth, and function. Injectability of these materials allows for *in situ* polymerization in addition to the formation of a tight apposition with the lesion cavity, especially in the case of stroke. Since NSPC behavior is highly regulated by the physical environment[23, 30-32], the tuning of these materials to match the mechanical properties of the native brain tissue (~100 – 1000 Pa)[33-35] is a top priority in their design. Fibrin, hyaluronic acid, laminin, collagen, and a novel cephalopod-based protein reflectin are all scaffold materials that can be used with NSPCs as a potential treatment for stroke. Our studies investigate the use of each of these materials both individually and as hybrid combinations to support hNSPC function.

1.3.1 Fibrin

Fibrin is a protein involved in blood clotting during the natural coagulation cascade. In this process, fibrin monomers are formed in the cleaving of fibrinogen by thrombin. Fibrinogen is a complex multimeric protein with Aα, Bβ, and γ chains. Factor XIIIa covalently cross-links fibrin monomers to create a mesh that forms a clot over an injury, which can then be degraded by the enzyme plasmin once wound healing is complete. By varying the concentrations of fibrinogen and thrombin, the mechanical properties and polymerization time of the hydrogel can be modulated, allowing the formation of fibrin scaffolds with varying compliance and polymerization rate[33, 36]. Fibrin contains multiple adhesive sites including RGD sequences that

engage integrins on the cell surface. Along with its favorable cell adhesive properties, bioactive signaling molecules can easily be incorporated into the fibrin scaffold making it highly suitable as a substrate for NSPCs.

The source of fibrin can also play an integral role in its effectiveness as a scaffold material. Fibrin sourced from Atlantic salmon, as opposed to human and bovine fibrin, can encourage greater neurite outgrowth of rodent CNS neurons and better resist degradation by cellular proteases[37]. Furthermore, salmon fibrin promotes functional recovery and improved bladder function in rats with dorsal hemisection spinal cord injuries[38]. The compatibility of fibrin with the CNS makes this an excellent candidate as a scaffold material for use in the treatment of stroke. Subdural transplants of fibrin in conjunction with induced pluripotent stem cells in a rat model of ischemia showcases its ability to reduce total infarct volume, improve motor function, and attenuate inflammatory cytokines [39]. In addition, NSPCs embedded in fibrin scaffolds have improved cell survival and neuronal differentiation in a model of rat spinal cord injury, demonstrating fibrin's effectiveness as a CNS scaffold material[40]. However, one of the downsides to fibrin as a scaffold material is its rapid degradation rate *in vivo*[38] as it breaks down within 7 days of implantation. This presents a roadblock since hNSPCs require a minimum of one month to differentiate *in vivo*. Our strategy to solve this issue is to combine salmon fibrin with alternate materials that possess more resilient degradation properties. Our work signifies the first report of the utilization of salmon fibrin scaffolds in any rodent model of ischemic stroke.

1.3.2 Hyaluronic Acid

Hyaluronic acid (HA) is a naturally occurring polysaccharide in all living organisms[41]. It is a key component of the ECM and is found throughout the body in the vitreous of the eye,

synovial fluid of joints, and brain[42-44]. The structure of HA is a linear polyanion, with repeating disaccharides consisting of D-glucuronic acid and D-N-acetylglucosamine (Fig. 1.3)[44]. The disaccharides, which can be thousands of repeats long allowing for HA polymers of varying molecular weight, can be broken down by hyaluronidase enzymes in the body. HA is advantageous because of its ability to be chemically modified via the carboxylic acid group on the glucuronic acid or C-6 hydroxyl group on the N-acetylglucosamine. These modifications allow for HA materials with varying chemical and mechanical properties for tissue engineering applications[45]. The disadvantage of HA is that many cells will not adhere to HA without these modifications or integration of cell-binding sites within the matrix.

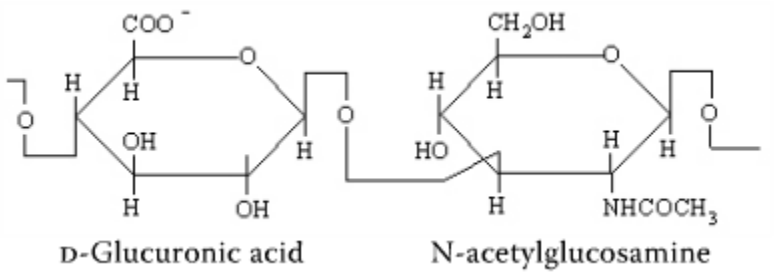

Figure 1.3. Structure of a single disaccharide repeat of HA. Reprinted by permission from American Chemical Society: Biochemistry[44], copyright 1975.

HA content is high in the developing brain and although content declines postnatally, it is still found in brain ventricle regions with ongoing NSPC proliferation[44, 46]. For this reason it has been an attractive material for use in tissue reconstruction with neural stem cells after acute ischemic stroke. HA has an additional advantage as it persists for at least 2 months post-transplant[47]. Incorporation of HA hydrogels seeded with NSPCs into the infarct stroke cavity of mice improves protection against host inflammatory response in addition to inducing a twofold enhancement in cell survival[48]. HA modulus, varied by using different amounts of methacrylate cross-linker, drastically affects NSPC differentiation, with hydrogels mimicking stiffness of

neonatal brain inducing neuronal differentiation and stiffer hydrogels emulating adult brain promoting astrocytic differentiation[49]. In our work, we use HA both as a component of a combination scaffold with fibrin and as an individual scaffold conjugated with various adhesion peptides to assess compatibility with hNSPCs for the purposes of CNS transplantation. The addition of HA in the combination scaffolds can test whether it can slow the rapid degradation rate of fibrin scaffolds. Though full length non-recombinant biomolecules can effectively allow cells to bind in 3D scaffolds, they can be difficult to obtain FDA-approval for due to the possibility of contamination with other biologically active components during purification. Short peptide sequences that are known to have cell-adhesive properties, such as IKVAV and YIGSR sequences derived from laminin or GFOGER derived from collagen, are chemically synthesized, easy to purify, and more simple in obtaining FDA-approval as devices that compliment cellular therapeutics. The HA-peptide scaffolds are investigated since they can be rapidly developed for translation to the clinic.

1.3.3 Laminin

Laminin is an ECM molecule that stimulates hNSPC expansion, migration, and differentiation[50] and can be used as a functionalizing material in neural tissue engineering settings[51, 52]. It has been established as a standardized ECM for NSPC culture[53]. Laminin is not inherently a hydrogel material, so in most cases is conjugated onto other biomaterials as an adhesion mediator. Rats with cerebral focal ischemia treated with Matrigel scaffolds comprised primarily of collagen and laminin seeded with embryonic stem cell-derived hNSPCs had decreased lesion volumes compared to cell-only transplants[54]. Laminin has also been combined with HA to enhance NSPC migration after traumatic brain injury[55]. In our studies, we investigate

the role of laminin in NSPC mechanotransduction and its ability to support hNSPC function in 3D combination scaffolds *in vitro* and *in vivo*.

1.3.4 Collagen

Collagen is widely used as an ECM material because of its biocompatibility, favorable degradation kinetics, and low immunogenicity[56, 57]. It is comprised of a linear triple helical structure and is advantageous for tissue engineering applications due to its abundance in the native ECM[58]. Rat NSPCs cultured in 3D collagen scaffolds proliferate, differentiate into the three lineages of the CNS at similar propensities to standard poly-L-lysine substrates, and extend processes more efficiently than when cultured in suspension[59]. Moreover, NSPCs migrate more efficiently and form protruding networks with neighboring cells within soft collagen matrices (< 100 Pa) as opposed to stiffer scaffolds, again highlighting the importance of matrix mechanics[60]. Collagen used as a scaffold for NSPCs transplanted *in vivo* to treat cerebral ischemia improves exogenous cell differentiation, supports new synapse formation, and functional recovery in rats[61]. The primary bottleneck for using collagen as a scaffold has been its batch-to-batch variation and difficulty in scale-up for manufacturing. For this reason, we develop novel recombinant collagen scaffolds with various cell adhesion sites engineered into the polymer. Compatibility of these scaffolds with hNSPCs with regards to adhesion, proliferation, and differentiation is assessed on each of the engineered substrates as a prerequisite for potential use in a preclinical stroke model.

1.3.5 Reflectin

The CNS of cephalopods has many similarities to its vertebrate counterpart[62]. Along these lines, we investigate the ability of a family of self-assembling cephalopod proteins known as reflectins[63, 64] to support hNSPC behavior. The A1 isoform of reflectin from *Doryteuthis*

(Loligo) pealeii used in our studies has been shown to possess proton conductive and electrical properties[65, 66], which make it attractive as a potential scaffold material for NSPCs. The embryos of cuttlefish, *Sepia officinalis*, express mRNA associated with reflectin in the CNS during developmental stages correlating with neurogenesis and brain development[67, 68]. This provided inspiration for us to ponder reflectin's involvement in neural developmental and its potential biocompatibility with hNSPCs. Our studies mark the discovery of a never-before-used biocompatible substrate for hNSPCs, which may favorably signify its use as a scaffold or implantable device for the treatment of stroke.

1.4 SUMMARY

There is a very high unmet clinical need for stroke therapies that can help the many patients who are not eligible for current therapies such as tPA and clot removal systems. NSPCs stand as a promising therapeutic candidate to help stroke sufferers recover well beyond the limited time window of current treatments. This work aims to characterize the potential of a variety of biomaterials as transplantation scaffolds and substrates for NSPCs. We initially investigate the effect of mechanical stimuli, particularly static stretch, on NSPC differentiation and the involvement of the ECM in these processes, since the mechanics of the microenvironment has been heavily implicated in modulating NSPC behavior[30-32, 69] (Chapter 2). We delve further into the mechanism of NSPC sensing to biophysical cues by studying the role of SACs in governing lineage choice (Chapter 3). We then develop a unique salmon fibrin-HA-laminin combination scaffold optimized to support hNSPC behavior *in vitro*. The inclusion of endothelial cells co-cultured with hNSPCs within this combination scaffold supports vascularization and emulates the *in vivo* neurovascular niche (Chapter 4). Based on these findings, we use this scaffold-hNSPC transplantation construct as a therapy in a preclinical rat

transient middle cerebral artery occlusion (tMCAO) model of stroke (Chapter 5). In concurrence with the development of salmon fibrin-HA-laminin combination scaffolds, we investigate the potential of HA-based scaffolds conjugated with a myriad of adhesion peptides (Chapter 6), novel recombinant collagen engineered with peptide-based cell-adhesion sites (Chapter 7), and the unique cephalopod protein reflectin (Chapter 8) as both 2D and 3D substrates for hNSPCs. In the summary, the overall impact on the neural tissue engineering and regenerative medicine field and future directions of the study are discussed (Chapter 9).

1.5 REFERENCES

1. Roger, V. et al. Heart disease and stroke statistics--2012 update: a report from the American Heart Association. *Circulation* **125** (2012).
2. Lloyd-Jones, D. et al. Heart disease and stroke statistics--2009 update: a report from the American Heart Association Statistics Committee and Stroke Statistics Subcommittee. *Circulation* **119**, 181 (2009).
3. Prabhakaran, S., Ruff, I. & Bernstein, R.A. Acute stroke intervention: a systematic review. *JAMA* **313**, 1451-1462 (2015).
4. Lindvall, O. & Kokaia, Z. Stem cells for the treatment of neurological disorders. *Nature* **441**, 1094-1096 (2006).
5. Burns, T., Verfaillie, C. & Low, W. Stem cells for ischemic brain injury: a critical review. *The Journal of comparative neurology* **515**, 125-144 (2009).
6. Kelly, S. et al. Transplanted human fetal neural stem cells survive, migrate, and differentiate in ischemic rat cerebral cortex. *Proceedings of the National Academy of Sciences of the United States of America* **101**, 11839-11844 (2004).
7. Hayashi, J. et al. Primate embryonic stem cell-derived neuronal progenitors transplanted into ischemic brain. *Journal of cerebral blood flow and metabolism : official journal of the International Society of Cerebral Blood Flow and Metabolism* **26**, 906-914 (2006).
8. Ikeda, R. et al. Transplantation of neural cells derived from retinoic acid-treated cynomolgus monkey embryonic stem cells successfully improved motor function of hemiplegic mice with experimental brain injury. *Neurobiology of disease* **20**, 38-48 (2005).
9. Bliss, T., Guzman, R., Daadi, M. & Steinberg, G. Cell transplantation therapy for stroke. *Stroke; a journal of cerebral circulation* **38**, 817-826 (2007).
10. Gage, F.H. Mammalian Neural Stem Cells. *Science* **287** (2000).
11. Liu, J., Solway, K., Messing, R. & Sharp, F. Increased neurogenesis in the dentate gyrus after transient global ischemia in gerbils. *The Journal of neuroscience : the official journal of the Society for Neuroscience* **18**, 7768-7778 (1998).
12. Tonchev, A., Yamashima, T., Sawamoto, K. & Okano, H. Enhanced proliferation of progenitor cells in the subventricular zone and limited neuronal production in the striatum and neocortex of adult macaque monkeys after global cerebral ischemia. *Journal of neuroscience research* **81**, 776-788 (2005).
13. Kokaia, Z., Thored, P., Arvidsson, A. & Lindvall, O. Regulation of stroke-induced neurogenesis in adult brain--recent scientific progress. *Cerebral cortex (New York, N.Y. : 1991)* **16 Suppl 1**, 7 (2006).
14. Roberts, J.L. & Squire, L.R. Fundamental neuroscience. *San Diego, Academic* (2003).
15. Zhao, L.-R. et al. Human bone marrow stem cells exhibit neural phenotypes and ameliorate neurological deficits after grafting into the ischemic brain of rats. *Experimental neurology* **174**, 11-20 (2002).
16. Pollock, K. et al. A conditionally immortal clonal stem cell line from human cortical neuroepithelium for the treatment of ischemic stroke. *Experimental neurology* **199**, 143-155 (2006).
17. Bliss, T., Andres, R. & Steinberg, G. Optimizing the success of cell transplantation therapy for stroke. *Neurobiology of disease* **37**, 275-283 (2010).
18. Kelly, S. et al. Transplanted human fetal neural stem cells survive, migrate, and differentiate in ischemic rat cerebral cortex. *Proc Natl Acad Sci U S A* **101**, 11839-11844 (2004).
19. Grabowski, M., Johansson, B.B. & Brundin, P. Survival of fetal neocortical grafts implanted in brain infarcts of adult rats: the influence of postlesion time and age of donor tissue. *Exp Neurol* **127**, 126-136 (1994).
20. Evans et al. materialstoday 2006.pdf.
21. Willerth, S.M. & Sakiyama-Elbert, S.E. Combining stem cells and biomaterial scaffolds for constructing tissues and cell delivery. (2008).

22. Zhang, J. et al. Physically associated synthetic hydrogels with long-term covalent stabilization for cell culture and stem cell transplantation. *Advanced materials (Deerfield Beach, Fla.)* **23**, 5098-5103 (2011).
23. Engler, A., Sen, S., Sweeney, H. & Discher, D. Matrix elasticity directs stem cell lineage specification. *Cell* **126**, 677-689 (2006).
24. Kshitiz et al. Control of stem cell fate and function by engineering physical microenvironments. *Integrative Biology* **4** (2012).
25. Murphy, W.L., McDevitt, T.C. & Engler, A.J. Materials as stem cell regulators. *Nat Mater* **13**, 547-557 (2014).
26. D'Angelo, F. et al. Mechanotransduction: tuning stem cells fate. *J Funct Biomater* **2**, 67-87 (2011).
27. Wang, J.H. & Thampatty, B.P. Mechanobiology of adult and stem cells. *International review of cell and molecular biology* **271**, 301-346 (2007).
28. Tonelli, F.M. et al. Stem cells and calcium signaling. *Adv Exp Med Biol* **740**, 891-916 (2012).
29. Leclerc, C., Néant, I. & Moreau, M. The calcium: an early signal that initiates the formation of the nervous system during embryogenesis. *Front Mol Neurosci* **5**, 3 (2012).
30. Saha, K. et al. Substrate modulus directs neural stem cell behavior. *Biophysical journal* **95**, 4426-4438 (2008).
31. Leipzig, N. & Shoichet, M. The effect of substrate stiffness on adult neural stem cell behavior. *Biomaterials* **30**, 6867-6878 (2009).
32. Pathak, M.M. et al. Stretch-activated ion channel Piezo1 directs lineage choice in human neural stem cells. *Proc Natl Acad Sci U S A* **111**, 16148-16153 (2014).
33. Uibo, R. et al. Soft materials to treat central nervous system injuries: evaluation of the suitability of non-mammalian fibrin gels. *Biochimica et biophysica acta* **1793**, 924-930 (2009).
34. Tyler, W.J. The mechanobiology of brain function. *Nat Rev Neurosci* **13**, 867-878 (2012).
35. Levental, I., Georges, P.C. & Janmey, P.A. Soft biological materials and their impact on cell function. *Soft Matter* **3**, 299-306 (2007).
36. Xiaowei, L., Eleni, K., Xiaoyan, L., Ning, Z. & Xuejun, W. Engineering neural stem cell fates with hydrogel design for central nervous system regeneration. *Progress in Polymer Science* **37** (2012).
37. Ju, Y.-E., Janmey, P., McCormick, M., Sawyer, E. & Flanagan, L. Enhanced neurite growth from mammalian neurons in three-dimensional salmon fibrin gels. *Biomaterials* **28**, 2097-2108 (2007).
38. Sharp, K. et al. Salmon fibrin treatment of spinal cord injury promotes functional recovery and density of serotonergic innervation. *Experimental neurology* **235**, 345-356 (2012).
39. Chen, S.-J. et al. Functional improvement of focal cerebral ischemia injury by subdural transplantation of induced pluripotent stem cells with fibrin glue. *Stem cells and development* **19**, 1757-1767 (2010).
40. Johnson, P., Tatara, A., McCreedy, D., Shiu, A. & Sakiyama-Elbert, S. Tissue-engineered fibrin scaffolds containing neural progenitors enhance functional recovery in a subacute model of SCI. *Soft matter* **6**, 5127-5137 (2010).
41. Necas, J., Bartosikova, L., Brauner, P. & Kolar, J. Hyaluronic acid (hyaluronan): a review. *Veterinarni Medicina* (2008).
42. Burdick, J. & Prestwich, G. Hyaluronic acid hydrogels for biomedical applications. *Advanced materials (Deerfield Beach, Fla.)* **23**, 56 (2011).
43. Preston, M. & Sherman, L.S. Neural stem cell niches: roles for the hyaluronan-based extracellular matrix. *Front Biosci (Schol Ed)* **3**, 1165-1179 (2011).
44. Margolis, R.U., Margolis, R.K., Chang, L.B. & Preti, C. Glycosaminoglycans of brain during development. *Biochemistry* **14**, 85-88 (1975).
45. Vanderhooft, J., Alcoutlabi, M., Magda, J. & Prestwich, G. Rheological properties of cross-linked hyaluronan-gelatin hydrogels for tissue engineering. *Macromolecular bioscience* **9**, 20-28 (2009).
46. Preston, M. & Sherman, L. Neural Stem Cell Niches: Critical Roles for the Hyaluronan-Based Extracellular Matrix in Neural Stem Cell Proliferation and Differentiation.
47. Moshayedi, P. & Carmichael, S.T. Hyaluronan, neural stem cells and tissue reconstruction after acute ischemic stroke. *Biomatter* **3** (2013).
48. Zhong, J. et al. Hydrogel matrix to support stem cell survival after brain transplantation in stroke. *Neurorehabilitation and neural repair* **24**, 636-644 (2010).

49. Seidlits, S. et al. The effects of hyaluronic acid hydrogels with tunable mechanical properties on neural progenitor cell differentiation. *Biomaterials* **31**, 3930-3940 (2010).
50. Flanagan, L., Rebaza, L., Derzic, S., Schwartz, P. & Monuki, E. Regulation of human neural precursor cells by laminin and integrins. *Journal of neuroscience research* **83**, 845-856 (2006).
51. Stabenfeldt, S.E., García, A.J. & LaPlaca, M.C. Thermoreversible laminin-functionalized hydrogel for neural tissue engineering. *J Biomed Mater Res A* **77**, 718-725 (2006).
52. Junka, R., Valmikinathan, C.M., Kalyon, D.M. & Yu, X. Laminin Functionalized Biomimetic Nanofibers For Nerve Tissue Engineering. *J Biomater Tissue Eng* **3**, 494-502 (2013).
53. Peltier, J., Agrawal, S., Robertson, M.J. & Schaffer, D.V. In vitro culture and analysis of adult hippocampal neural progenitors. *Methods Mol Biol* **621**, 65-87 (2010).
54. Jin, K. et al. Transplantation of human neural precursor cells in Matrigel scaffolding improves outcome from focal cerebral ischemia after delayed postischemic treatment in rats. *J Cereb Blood Flow Metab* **30**, 534-544 (2010).
55. Addington, C.P. et al. Enhancing neural stem cell response to SDF-1α gradients through hyaluronic acid-laminin hydrogels. *Biomaterials* **72**, 11-19 (2015).
56. Stang, F., Fansa, H., Wolf, G. & Keilhoff, G. Collagen nerve conduits--assessment of biocompatibility and axonal regeneration. *Biomed Mater Eng* **15**, 3-12 (2005).
57. Yoshii, S., Ito, S., Shima, M., Taniguchi, A. & Akagi, M. Functional restoration of rabbit spinal cord using collagen-filament scaffold. *J Tissue Eng Regen Med* **3**, 19-25 (2009).
58. Han, Q. et al. The promotion of neural regeneration in an extreme rat spinal cord injury model using a collagen scaffold containing a collagen binding neuroprotective protein and an EGFR neutralizing antibody. *Biomaterials* **31**, 9212-9220 (2010).
59. Huang, F., Shen, Q. & Zhao, J. Growth and differentiation of neural stem cells in a three-dimensional collagen gel scaffold. *Neural Regen Res* **8**, 313-319 (2013).
60. Shamloo, A., Heibatollahi, M. & Mofrad, M.R. Directional migration and differentiation of neural stem cells within three-dimensional microenvironments. *Integr Biol (Camb)* **7**, 335-344 (2015).
61. Yu, H. et al. Combinated transplantation of neural stem cells and collagen type I promote functional recovery after cerebral ischemia in rats. *Anat Rec (Hoboken)* **293**, 911-917 (2010).
62. Sandeman, D. Homology and convergence in vertebrate and invertebrate nervous systems. *Naturwissenschaften* **86**, 378-387 (1999).
63. Phan, L. et al. Reconfigurable infrared camouflage coatings from a cephalopod protein. *Adv Mater* **25**, 5621-5625 (2013).
64. Phan, L. et al. Infrared invisibility stickers inspired by cephalopods. *Journal of Materials Chemistry C* **3**, 6493-6498 (2015).
65. Ordinario, D.D. et al. Bulk protonic conductivity in a cephalopod structural protein. *Nat Chem* **6**, 596-602 (2014).
66. Ordinario, D.D., Phan, L., Jocson, J.-M., Nguyen, T. & Gorodetsky, A.A. Protonic transistors from thin reflectin films. *APL materials* **3**, 014907 (2015).
67. Bassaglia, Y. et al. ESTs library from embryonic stages reveals tubulin and reflectin diversity in Sepia officinalis (Mollusca—Cephalopoda). *Gene* **498**, 203-211 (2012).
68. Andouche, A., Bassaglia, Y., Baratte, S. & Bonnaud, L. Reflectin genes and development of iridophore patterns in Sepia officinalis embryos (Mollusca, Cephalopoda). *Dev Dyn* **242**, 560-571 (2013).
69. Aurand, E.R., Wagner, J.L., Shandas, R. & Bjugstad, K.B. Hydrogel formulation determines cell fate of fetal and adult neural progenitor cells. *Stem Cell Res* **12**, 11-23 (2014).

CHAPTER 2

STATIC STRETCH AFFECTS NEURAL STEM CELL DIFFERENTIATION IN AN EXTRACELLULAR MATRIX-DEPENDENT MANNER

Authors: **Janahan Arulmoli**[1,2], Medha M. Pathak[3], Lisa P. McDonnell[2,4], Jamison L. Nourse[2,4], Francesco Tombola[3], James C. Earthman[1,5], Lisa A. Flanagan[1,2,4*]

Author Affiliations:

[1]Department of Biomedical Engineering

[2]Sue & Bill Gross Stem Cell Research Center

[3]Department of Physiology & Biophysics

[4]Department of Neurology

[5]Department of Chemical Engineering and Materials Science

[1-5]University of California, Irvine, Irvine, CA, 92697, USA

Keywords: neural stem cell; mechanical stimulation; static stretch; integrin; alpha6; equibiaxial; laminin; fibronectin; oligodendrocyte; neuron; astrocyte

2.1 ABSTRACT

Neural stem and progenitor cell (NSPC) fate is strongly influenced by mechanotransduction as modulation of substrate stiffness affects lineage choice. Other types of mechanical stimuli, such as stretch (tensile strain), occur during CNS development and trauma, but their consequences for NSPC differentiation have not been reported. We delivered a 10% static equibiaxial stretch to NSPCs and examined effects on differentiation. We found static stretch specifically impacts NSPC differentiation into oligodendrocytes, but not neurons or astrocytes, and this effect is dependent on particular extracellular matrix (ECM)-integrin linkages. Generation of oligodendrocytes from NSPCs was reduced on laminin, an outcome likely mediated by the α6 laminin-binding integrin whereas similar effects were not observed for NSPCs on fibronectin. Our data demonstrate a direct role for tensile strain in dictating the lineage choice of NSPCs and indicate the dependence of this phenomenon on specific substrate materials, which should be taken into account for the design of biomaterials for NSPC transplantation.

2.2 INTRODUCTION

Stem cells are the only cells in the body capable of indefinite self-renewal and differentiation into various cell types. *In vivo*, they reside within specific microenvironments, or niches, that contain various chemical and physical signals affecting cell function. CNS neural stem cells are present in the fetal as well as adult brain and are multipotent, thus able to differentiate into neurons, astrocytes and oligodendrocytes[1]. During development, embryonic neural stem cells form the neural tube, which then gives rise to the brain and spinal cord. Throughout life neural stem cells are present in the subventricular zone (SVZ) of the lateral ventricles and dentate gyrus (DG) of the hippocampus. Since the discovery of stem cells, much work has focused on studying the effect of the chemical environment (soluble growth factors, chemokines, morphogens, etc.) on their behavior. However, effort recently has shifted to studying the effects of the physical microenvironment on stem cell behavior.

Mechanotransduction describes the process by which cells convert physical stimuli into chemical or electrical responses. Various mechanical factors of the cellular microenvironment, both passive and active, can greatly influence the maturation and shape of cells, tissues, and organs under both physiological and pathological conditions (Fig. 2.1)[2]. In particular, substrate elasticity, or stiffness, is a passive mechanical cue that has been well studied and greatly impacts stem cell fate during differentiation. For example, human mesenchymal stem cells (hMSCs) express markers of either bone, muscle, or brain cells when differentiated on hard (~25-40 kPa), medium (~5-20 kPa), or soft (~0.1-1 kPa) substrates, respectively[3]. NSPC fate is also strongly influenced by substrate stiffness in a range physiologically relevant for CNS tissue[4], such that softer substrates (<1 kPa) induce neuronal differentiation while stiffer substrates (>1 kPa) encourage generation of astrocytes[5-7].

Stem cells also encounter many active mechanical forces that can affect their differentiation (Fig. 2.1). Uniaxial cyclic strain increases the expression of smooth muscle markers fromhMSCs[8-10]. This active mechanical stimulus coordinates with TGF-β, a soluble factor that also induces smooth muscle markers in these cells, to affect MSC differentiation[10]. Equibiaxial static strain of hMSCs cultured in osteogenic conditions causes increased cell proliferation and production of vascular endothelial growth factor (VEGF) via ERK and p38 mitogen-activated protein kinase pathways[11]. Additionally, active mechanical stimuli affect pluripotent stem cells since local cyclic stresses lead to downregulation of the undifferentiated stem cell marker Oct3/4 in mouse embryonic stem cells[12]. Furthermore, active forces imparted by the microenvironment may impact NSPC differentiation *in vivo*[13]. In normal CNS development, tissue folding and convergent extension cell movements create local physical stresses on endogenous NSPCs[14, 15]. In cases of CNS damage such as traumatic brain injury (TBI), there is acute physical straining of brain tissue that has been modeled *in vitro* via application of equibiaxial stretch, which significantly affects function of neurons and glia[16] There has been little work investigating the influence of mechanical stretch on NSPC differentiation into the three cell types of the CNS, but gradual mechanical stretching enhances neurite elongation and maturation of neurons derived from adult rat hippocampal NSPCs[17]. Since mechanical forces are at play during development and in cases of trauma, it is important to determine their effects on NSPC differentiation.

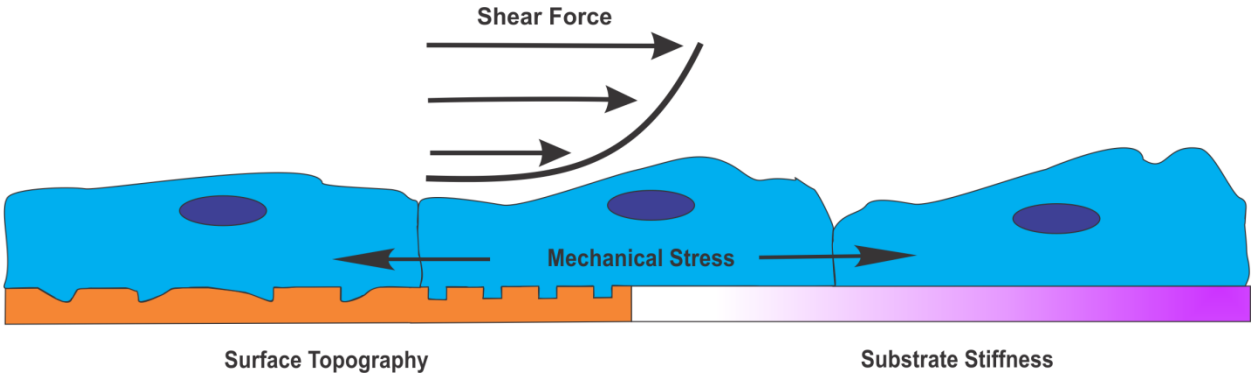

Figure 2.1. Physical regulators of stem cell behavior. Stem cells experience a variety of physical cues within the natural microenvironment that can have significant effects on survival, proliferation, differentiation, and gene expression[2]. Examples of these mechanical cues include shear force from fluid, mechanical stress from cell-cell interactions and cell movements, and surface topology and substrate stiffness through components of the ECM and surrounding cells.

2.3 RESULTS

2.3.1 Static stretch decreases oligodendrocyte differentiation from mNSPCs

We tested whether an active mechanical stimulus alters NSPC differentiation by delivering a 10% static equibiaxial strain to cells via laminin-coated silicone elastomer membranes using a custom-built device, the J-Flex (Fig. 2.2a, b).

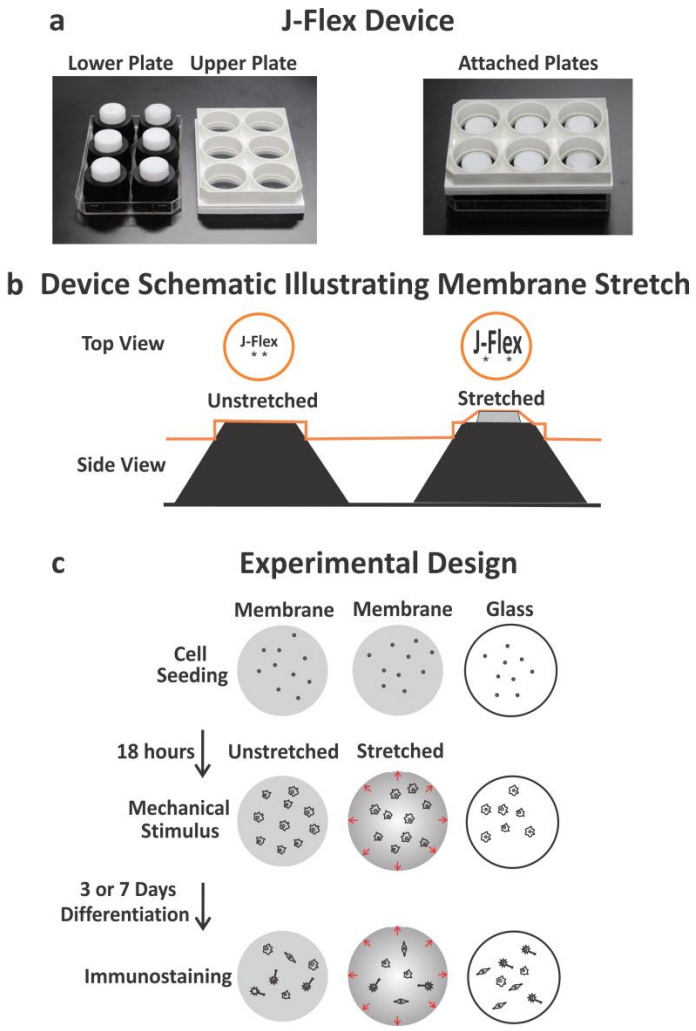

Figure 2.2. Induction of 10% equibiaxial static stretch to adhered NSPCs via the J-flex device. (a) J-Flex device: white polytetrafluoroethylene (Teflon) disks (25mm diameter) attached to black rubber corks (lower plate) press fit into a Flexcell Bioflex plate (standard 6-well size) with silicone elastomer membranes (upper plate). When the two plates are attached, a 10% equibiaxial strain is induced on the silicone elastomer membranes (attached plates). Rubber bands (not shown) were used to keep the plates firmly press-fit. (b) Device schematic illustrating membrane stretch: top and side views of the membrane (orange circles in top view; orange line in side view), cork (black) and Teflon disk (grey) when the plates are attached. The stretched configuration shows displacement (10% equibiaxial) of two markings on the membrane in the top view and the corresponding setup with the cork and disk in the side view (not to scale). (c) Experimental design: mNSPCs were seeded on laminin-coated surfaces (membranes and glass) for 18 hours in proliferation conditions, followed by application of mechanical stimulus (stretched group only) after removal of growth factors (differentiation conditions) to assess formation of neurons (3 days), astrocytes (7 days), or oligodendrocytes (5 or 7 days) by immunostaining post-differentiation.

We utilized mouse NSPCs (mNSPCs) derived from the embryonic cortex and quantified differentiation into neurons, astrocytes, and oligodendrocytes (Fig. 2.2c). We found no direct effect of static stretch on the differentiation of mNSPCs into neurons or astrocytes, which will be discussed further in a later section. However, oligodendrocyte differentiation was markedly affected. Specifically, generation of oligodendrocytes was significantly decreased on stretched compared to unstretched membranes, as illustrated by the number of cells positive for either the more mature oligodendrocyte marker O4 (Fig. 2.3a) or a marker of cells at an earlier stage of oligodendrocyte differentiation, platelet-derived growth factor receptor alpha (PDGFR-α) (Fig. 2.S1). In fact, a single static stretch applied at the onset of differentiation and maintained for several days induced a 2.6-fold reduction in O4-positive oligodendrocytes and a 3.2-fold reduction in earlier stage oligodendrocytes detected by PDGFR-α (Figs. 3a and S1). Stretching the membranes increased membrane stiffness, which was controlled for by seeding and differentiating cells on membranes already undergoing stretch (pre-stretched condition) so that cells encountered the same stiffness as the stretched membranes but did not experience the stretch stimulus. This control distinguished the effects of stretch and stiffness. Oligodendrocyte differentiation was significantly higher on pre-stretched than stretched membranes (O4-positive cells pre-stretched: 2.6±0.4% and stretched: 0.6±0.1%; error represents SEM), showing that the stretch-induced decrease in oligodendrocyte generation was not due to a stiffness change in the membrane. The observed decrease in oligodendrocyte differentiation in response to stretch was also not due to a significant effect on the adhesion, proliferation, or survival of cells on stretched membranes since there was no difference in total cell number counts on unstretched and stretched membranes (Fig. 2.S2a). A single static stretch stimulus reduces the generation of

oligodendrocytes from embryonic mNSPCs, and this effect is not due to either a stiffness change in the membrane or a change in the total cell number in the stretched condition.

We performed analogous experiments with adult rat hippocampal NSPCs to test whether the effects of stretch on oligodendrocyte generation are relevant to adult NSPC populations. A single static stretch induced a remarkably similar 2.6-fold decrease in the production of O4-positive oligodendrocytes from these cells, indicating their sensitivity to stretch (Fig. 2.3b). As seen with mNSPCs, the effect of stretch was not due to a stiffness change since oligodendrocyte differentiation was significantly higher on pre-stretched membranes than stretched membranes (O4-positive cells pre-stretched: 8.1±1.1% and stretched: 5.0±0.4%, $p<0.05$; error represents SEM) nor to changes in the total cell number since this measure was equal on unstretched and stretched membranes (total cell number unstretched: 572±57.4 and stretched: 546.0±80.2, $p=0.792$; error represents SEM).

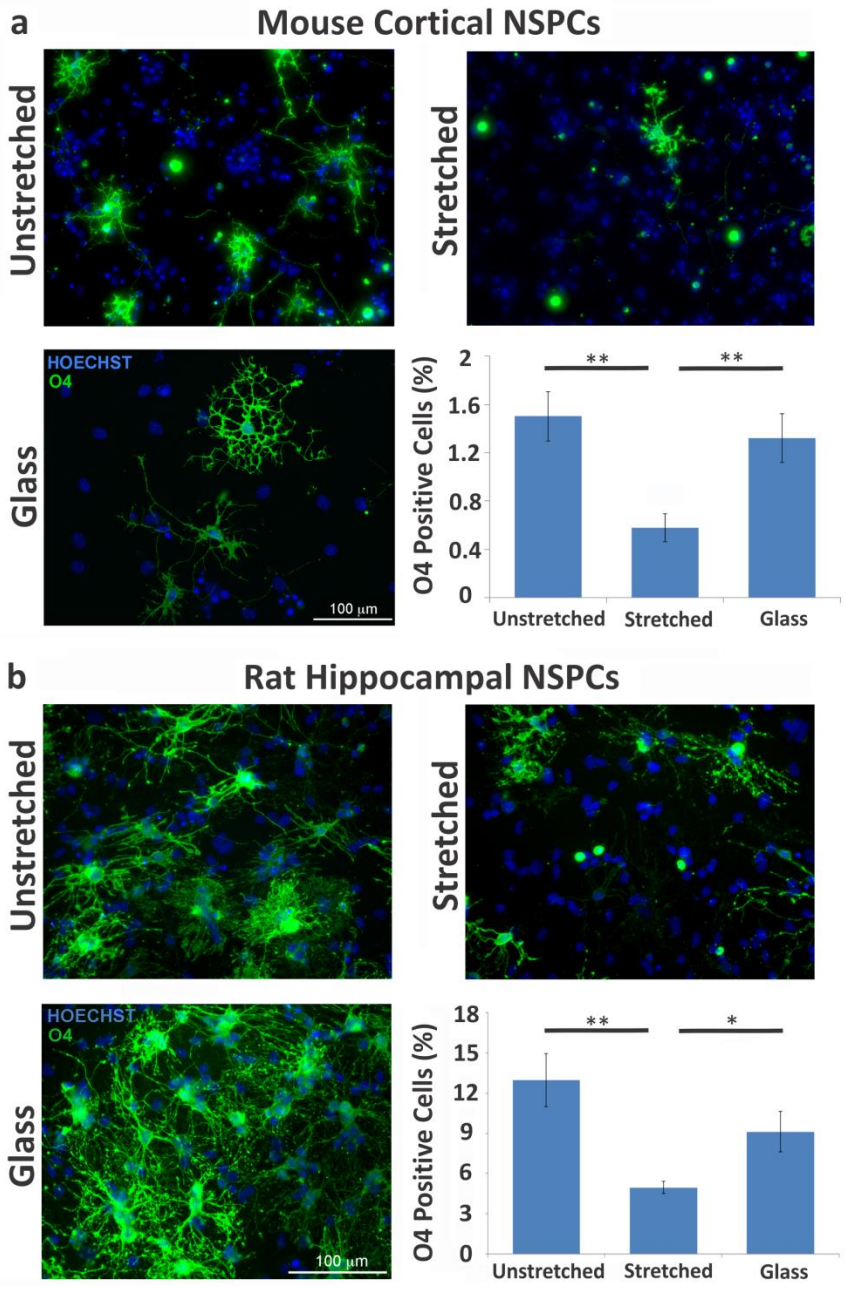

Figure 2.3. Stretch inhibits mNSPC differentiation into oligodendrocytes. (a) Mouse cortical NSPCs and (b) rat hippocampal NSPCs differentiated on unstretched and stretched membranes or glass were stained with oligodendrocyte cell surface marker O4 and Hoechst for nuclear DNA. Static stretch reduces oligodendrocyte differentiation regardless of cell source. (a) P = 0.0003 (unstretched vs. stretched), P = 0.002 (glass vs. stretched). (b) P=0.001 (unstretched vs. stretched), P = 0.016 (glass vs. stretched). **P < 0.01, *P < 0.05. Error bars represent SEM. N=3 independent biological repeats.

2.3.2 Laminin, but not fibronectin, plays a role in stretch-mediated oligodendrocyte differentiation

To investigate the mechanism behind the stretch-induced reduction in oligodendrocyte generation, we tested whether the specific type of ECM coating on the silicone elastomer membranes played a role. We found previously that human and mouse NSPCs cultured on laminin exhibited enhanced migration and differentiation into neurons and astrocytes in comparison to cells cultured on fibronectin or Matrigel[18]. Furthermore, ECMs regulate oligodendrocyte development since fibronectin stimulates proliferation pathways while laminin has been linked to survival and differentiation within this lineage[19-21]. To test the role of ECMs in the stretch-dependent reduction of oligodendrocyte generation from mNSPCs, we performed stretch experiments analogous to those shown previously on laminin (Fig. 2.3), but instead used fibronectin as an ECM (Fig. 2.4a,b). We found no effect of stretch on generation of oligodendrocytes from mNSPCs on fibronectin-coated membranes as illustrated by the similar percentages of O4-expressing cells in the unstretched and stretched groups (Fig. 2.4b).

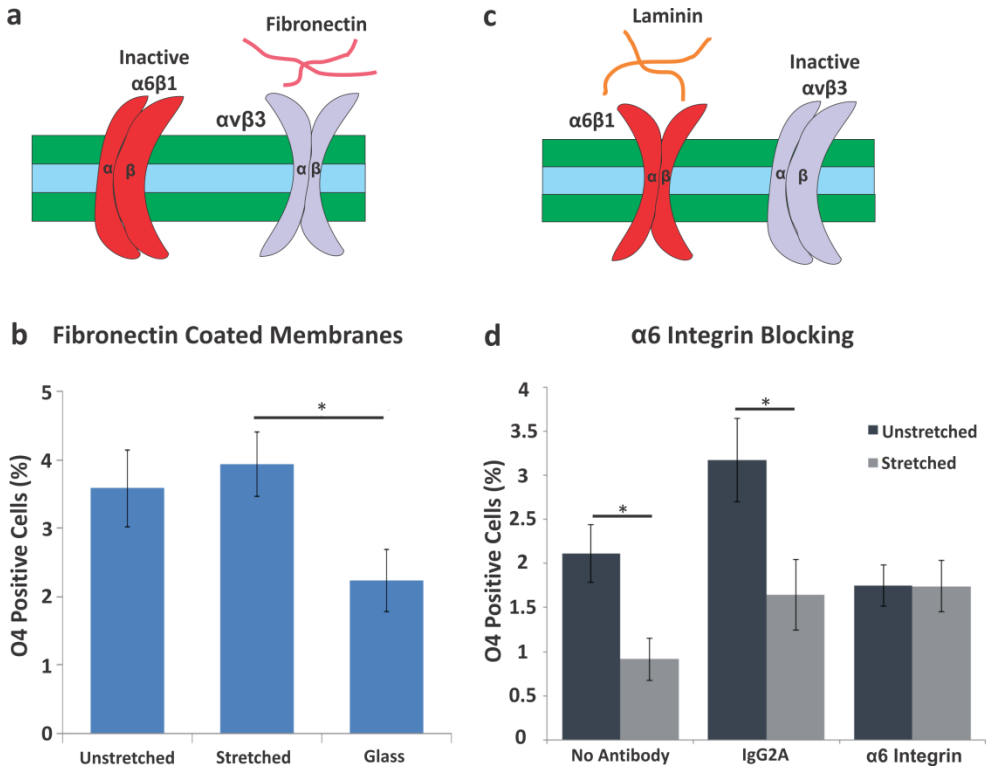

Figure 2.4. ECMs and integrins regulate mNSPC differentiation in response to static stretch. (a) Cells in the oligodendrocyte lineage express the laminin-binding integrin α6β1 but are driven to proliferate by fibronectin via the αVβ3 integrin[19]. (b) Delivery of a static stretch to mNSPCs on fibronectin does not affect differentiation into oligodendrocytes (no significant difference between unstretched vs. stretched group) although there is a difference between the stretched and glass groups. *P<0.05. P=0.013 (stretched vs. glass). Error bars represent SEM. N=3 independent biological repeats. (c) Oligodendrocyte lineage cells can bind laminin through the α6β1 integrin to affect differentiation[20] (d) Inhibiting α6 integrin with a function-blocking antibody negates the effect of stretch on oligodendrocyte differentiation from mNSPCs as shown by a lack of decreased O4 expression for cells on stretched membranes compared to those on unstretched membranes treated with α6 integrin antibody. *P < 0.05 , P = 0.013 (no antibody). P = 0.025 (IgG2A). Error bars represent SEM. N=3 independent biological repeats.

There was a significant difference between the stretched and glass groups, which is not easy to attribute to effects of either stretch or stiffness since differences were not significant between unstretched and stretched or unstretched and glass groups. The lack of an effect of stretch on fibronectin-coated membranes clarifies that the stretch-induced decrease in oligodendrocyte differentiation is specifically related to the cellular interaction with laminin and therefore suggests the involvement of laminin-binding integrins.

2.3.3 E12.5 mNSPCs express functional α6 laminin-binding integrin

Cells bind to ECMs via integrins, which are transmembrane protein heterodimers consisting of α and β subunits. Integrins act as mechanosensors by forming bridges between the ECM and intracellular focal adhesions that connect to the actin cytoskeleton. Mechanical forces affect stem cells by altering the position and conformation of specific ECM components (such as laminin and fibronectin), thus triggering integrin-dependent signaling pathways to stimulate focal adhesion assembly[22]. Integrins have been well studied in the oligodendrocyte lineage and the laminin-binding integrin α6β1 is involved in oligodendrocyte differentiation and is exclusive to laminin without promiscuous binding to other ECMs[19-21, 23, 24]. We showed previously that human NSPCs express α6β1 and its function is critical for migration on laminin[18]. We therefore used a migration assay and a function-blocking antibody against the laminin-binding α6 integrin to discern whether mNSPCs also express functional α6β1 integrin. Treatment of mNSPCs with the α6 integrin function-blocking antibody did not appear to alter adhesion of the cells to laminin, which was based on visual inspection indicating no increase in non-adherent cells in wells treated with α6 antibody compared to controls. However, migration of cells treated with α6 antibody was significantly decreased compared to that of cells treated with IgG2A isotype control antibody or no antibody control (Fig. 2.S3). These results indicate the expression of functional laminin-binding α6 integrins on mNSPCs.

2.3.4 Blocking laminin-binding α6 integrin affects stretch-mediated reduction of oligodendrocyte differentiation

In order to test whether the α6 integrin is involved in the stretch-induced reduction of oligodendrocyte differentiation from mNSPCs on laminin, the α6 integrin function-blocking

antibody was incubated with the cells at the onset of differentiation and stretch. Untreated and IgG2A isotype control antibody treated mNSPCs both revealed a decrease in oligodendrocyte differentiation with the stretch stimulus (Fig. 2.4d). Conversely, treatment of mNSPCs with α6 integrin blocking antibody abrogated the effect of stretch as evidenced by the lack of a marked decrease in generation of O4-positive oligodendrocytes with the application of stretch (Fig. 2.4d). While there was no significant difference in the generation of oligodendrocytes from cells on unstretched membranes in the no antibody control and α6 integrin antibody groups, there was a difference between the IgG2A control antibody and α6 integrin antibody unstretched membrane groups ($p<0.05$). This brings up the possibility that blocking α6 integrin generally reduces oligodendrocytes, which would not be surprising given the role of this integrin in oligodendrocyte differentiation[20]. Alternatively, the IgG2A control antibody may be increasing oligodendrogenesis through an unknown mechanism. In either case, disrupting the function of the α6 integrin blocks the effect of stretch on oligodendrocyte differentiation, which does not occur with the controls. This suggests that the stretch-induced reduction of oligodendrocyte differentiation on laminin ECM may be mediated by the laminin-binding α6 integrin on mNSPCs.

2.3.5 Distinct effects of static stretch and substrate stiffness on mNSPC differentiation

To test whether the observed stretch effect on differentiation is related to the increased stiffness of stretched membranes, we compared oligodendrocyte, neuron, and astrocyte generation on laminin-coated stretched and pre-stretched membranes that do not differ in stiffness (Fig. 2.5a). The stiffness of the pre-stretched control membrane matches that of the stretched membrane without delivering a stretch stimulus to the cells. NSPCs differentiated on pre-stretched membranes generated significantly more oligodendrocytes than cells on either

unstretched or stretched membranes or glass (Fig. 2.5b and 2.S4). Thus, increasing membrane stiffness from 10 kPa to 1.6 MPa induces more oligodendrocytes, but a single stretch at the onset of differentiation completely overcomes the stiffness stimulus and leads to a decrease in oligodendrocyte formation (stretched compared to pre-stretched membranes). Laminin molecules on the pre-stretched membrane might be altered by the stretch, which would be a confounding variable since cells are plated on the membrane after stretch application. To control for this, we stretched the membranes then coated with laminin to avoid perturbation of the laminin molecules (prestretched-then-coated). There were no differences in oligodendrocyte differentiation on pre-stretched [laminin coating → stretch → cell seeding] compared to prestretched-then-coated membranes [stretch → laminin coating → cell seeding] (O4-positive cells pre-stretched: 0.9±0.3% and prestretched-then-coated: 1.1±0.3%; error represents SEM). As observed with the stretch stimulus, the stiffness effect on oligodendrocyte generation was not due to a significant change in the adhesion, proliferation, or survival of cells on pre-stretched membranes since there was no difference in total cell number counts on unstretched and pre-stretched membranes (Fig. 2.S2a). Collectively, these data indicate that two mechanical factors, stiffness and stretch, have significant and varying effects on differentiation of oligodendrocytes from NSPCs.

Static stretch had negligible effects on differentiation of neurons from mNSPCs. Neuronal differentiation, as shown by MAP2-positive cells, significantly increased in the stretched and pre-stretched conditions as compared to the unstretched condition, suggesting a potential stiffness effect (10 kPa unstretched vs. 1.6 MPa stretched and pre-stretched) but no influence of stretch (Fig. 2.5c and 2.S4). Similar results were obtained when neurons were co-stained with two neuronal markers, MAP2 and doublecortin (DCX), which detects immature

neurons (Fig. 2.S5). The total number of cells on unstretched and pre-stretched membranes and glass did not differ, but there were significantly fewer cells on the stretched membranes (Fig. 2.S2b). Thus, the significant increase in the percentage of neurons on pre-stretched membranes compared to the unstretched membranes may indicate an effect of stiffness on neuronal differentiation, but the increased neurogenesis on stretched membranes could indicate a stiffness effect or be due to reduced cell densities on those membranes.

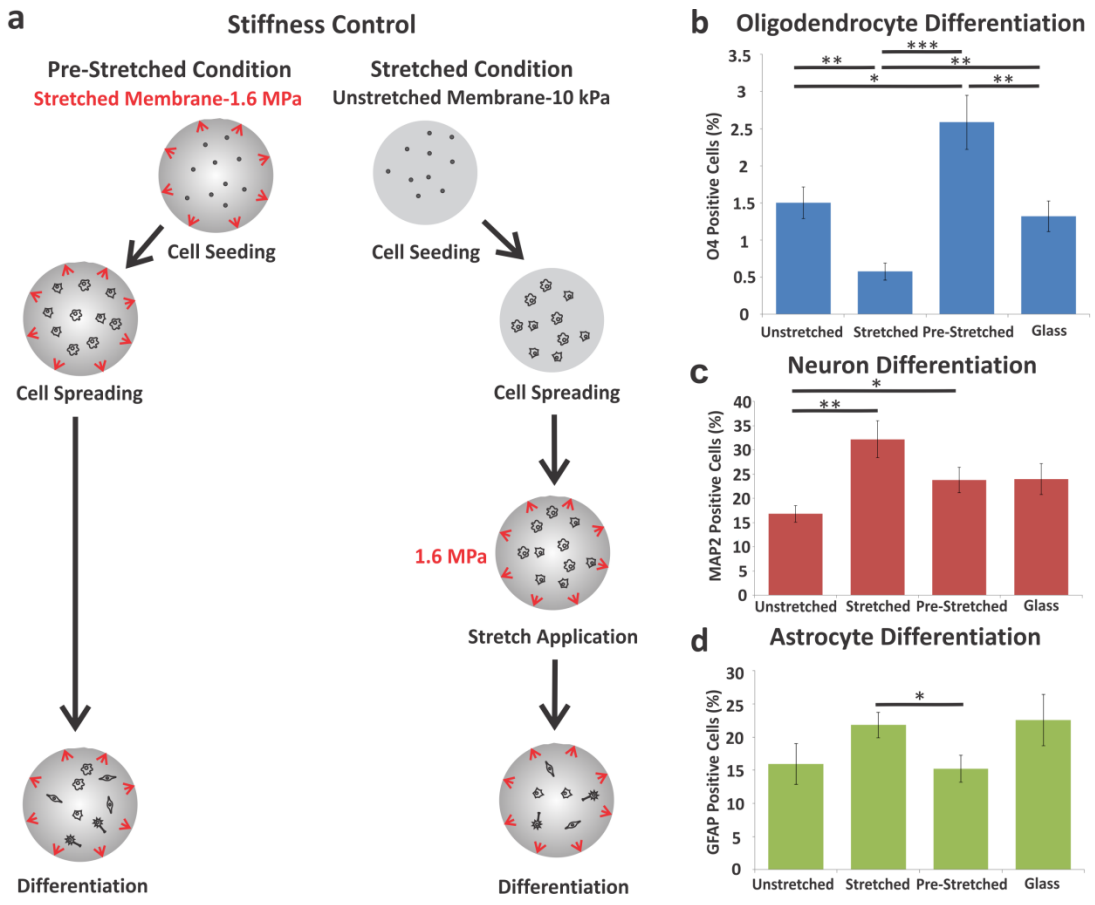

Figure 2.5. Effects of stretched membrane stiffness on NSPC differentiation. (a) Pre-stretched membranes were seeded with mNSPCs when the J-Flex device was already in place in order to control for the stiffness increase associated with the application of stretch at the onset of differentiation. Application of stretch to the membranes is denoted by red arrows. (b) Increase in stiffness upregulates oligodendrocyte differentiation as illustrated by the difference in percentage

of O4-positive cells on pre-stretched vs. unstretched membranes. P = 0.0003 (unstretched vs. stretched). P = 0.01 (unstretched vs. pre-stretched). P = 1.9E-0.6 (pre-stretched vs. stretched). P = 0.002 (glass vs. stretched). P = 0.003 (glass vs. pre-stretched). (c) Stiffer membranes promote differentiation of more neurons from mNSPCs as demonstrated by significantly more MAP2-positive cells on pre-stretched or stretched membranes compared to cells on unstretched membranes. P = 0.002 (unstretched vs. stretched). P = 0.04 (unstretched vs. pre-stretched). (d) Negligible effects of stiffness or stretch on astrocyte generation as shown by minimal differences in GFAP-positive cells between stretched and pre-stretched against unstretched groups. P = 0.03 (pre-stretched vs. stretched). *P < 0.05, **P < 0.01, ***P < 0.0001. Error bars represent SEM. N=3 independent biological repeats.

We found no clear effect of static stretch on astrocyte generation from mNSPCs. We observed neither a stretch nor stiffness-dependent on astrocyte differentiation from mNSPCs since the stretched group demonstrated a significant increase in GFAP positive staining in comparison with the pre-stretched group, but not against the unstretched control group (Fig. 2.5d and S4). Furthermore, there was no difference between the glass and stretched membrane group, and the percentages of GFAP-expressing cells across all conditions were quite similar (less than 1.5 fold difference between any of the groups). The total number of cells on membranes was very similar, but there was a significant difference between the unstretched and glass groups (Fig. 2.S2c). However, since there was no difference in astrocyte differentiation between these groups (Fig. 2.5d), the data suggest that there was not a significant effect of cell adhesion, survival, or proliferation on the generation of astrocytes on the different surfaces. These findings indicate no significant effects of stretch or stiffness on astrocyte differentiation from mNSPCs in our system.

2.4 DISCUSSION

We found a single static stretch significantly and specifically impacts NSPC differentiation along the oligodendrocyte lineage, an effect that is dependent on the ECM composition. Oligodendrocyte differentiation is affected by static stretch on laminin but not fibronectin, and is

potentially mediated by the α6 laminin-binding integrin. The interaction of stretch and specific ECM components may play a pivotal role in NSPC differentiation *in vivo.* The developing brain is rich in laminin[25], and laminin is expressed in the SVZ and DG in the adult brain, which are two NSPC niches that remain throughout life[26, 27]. Active mechanical forces induced during development by robust cell movements and tissue folding and in adult brain tissue by trauma may synergize with laminin ECM in NSPC niches to directly affect differentiation along the oligodendrocyte lineage[13]. Our data demonstrate the significant role mechanical forces such as stretch and ECM-integrin linkages play in dictating the lineage choice of NSPCs. This is the first reported case of a connection among active mechanical forces, specific ECM components , and oligodendrocyte differentiation.

A single active mechanical stretch stimulus was sufficient to induce a change in oligodendrocyte differentiation from NSPCs. Previous studies indicate that a single static stretch affects the function of multiple cell types, including MSCs, endothelial cells, and lung epithelial cells. Human MSCs exposed to static stretch exhibited increased proliferation as well as production and secretion of VEGF[11]. Rat coronary microvascular endothelial cells after static stretch increased proliferation, expression of VEGF receptor and vasculogenesis as demonstrated by formation of *in vitro* tubular structures[28]. Delivering a static stretch to human lung epithelial cells shifted their phenotype from alveolar type II to type I cells[29]. Taken together with our NSPC data, these studies show that a single static stretch activates signaling cascades affecting myriad cell types and functions.

NSPCs on laminin are able to sense an active stretch stimulus and translate the mechanical signal into a reduction in oligodendrocyte generation. ECM binding integrins are critical for mechanosensing in other systems and our data suggest the involvement of the laminin-binding

α6 integrin in the stretch induced decrease in oligodendrocytes. Part of the mechanism by which static stretch affects NSPCs may involve a reduction in integrin clustering since the number of bound ligands per a given surface area is reduced by stretch and clustering is critical for integrin function[30-32]. Integrins are developmentally regulated in the oligodendrocyte lineage, and early precursors express laminin-binding α6β1 as well as the αV fibronectin-binding integrins αVβ1, αVβ3, and αVβ8[24, 33, 34]. While the cells in our study adhered well to fibronectin, this did not translate into an effect of stretch on oligodendrocyte differentiation (Fig. 2.4b). Much of the integrin mechanosensing literature has focused on fibronectin-binding integrins, so little is known regarding the mechanical coupling of the laminin integrins to laminin. Thus, more studies will be necessary to test the role of the α6 laminin-binding integrin as a mechanosensor.

The specificity of NSPC stretch mechanosensing to laminin may be related to the *in vivo* function of these cells since *in vivo* cell niches are particularly rich in laminin ECM and laminin is associated with axons in the developing embryo[36]. For example, contact between developing axons and oligodendrocyte precursors and the associated ligation of precursor α6 integrins aids the further development of these cells into mature oligodendrocytes[36]. Thus, it is likely stem cell populations express mechanosensitive integrins that bind to the appropriate ECMs for that stem cell's niche in order to transduce *in vivo* mechanical signals and direct relevant physiological responses.

Since our experimental system enabled assessment of stretch and stiffness parameters, our data provide further evidence for substrate mechanics affecting NSPC fate although the stiffness range in our experiments is quite high compared to previous studies in the literature and was not meant to mimic a physiological range. We find increased differentiation of mNSPCs into oligodendrocytes and potentially neurons on membranes with stiffness ~1.6 MPa compared to

membranes of stiffness ~10 kPa. In contrast, there was no significant effect on astrocyte generation in this stiffness range. Increasing substrate stiffness has been associated with decreased neuronal differentiation of adult rat hippocampal NSPCs, but within the stiffness range of 0.01-10 kPa[5, 7] which is well outside the range used in our model. Previous studies investigating NSPC differentiation into oligodendrocytes on substrates of varying stiffness have yielded conflicting results and used stiffness ranges outside those employed here. Oligodendrocyte differentiation from rodent NSPCs has been shown to increase with increasing substrate stiffness from 0.1-10 kPa, a range that does not reach the stiffness of the pre-stretched membrane in our studies[6]. However, a separate group reported decreases in oligodendrocyte differentiation from NSPCs in this same substrate stiffness range[7]. These discrepancies in differentiation pattern are likely due to varying substrate materials (polyacrylamide vs. methacrylamide chitosan) or cell source (hippocampus vs. forebrain SVZ NSPCs) in these studies. Additional studies with fewer variables will be needed to clarify the effects of stiffness on oligodendrocyte generation and the responses of NSPCs to a wide range of stiffnesses. Our data provide further evidence for mechanical factors affecting neural stem cell fate, showing substrates with stiffness in the ~1 MPa range can alter the differentiation of mNSPCs.

Our stiffness data were generated on pre-stretched membranes that were a control for the stiffness increase inherent in our stretched membranes. However, on pre-stretched membranes the laminin density may differ from that on unstretched membranes since cells are seeded on membranes after they are stretched and the laminin molecules coated on the membranes may be farther apart from each other after the application of the stretch. In order to control for this, we included the pre-stretched-then-coated condition, in which laminin is coated on the membrane after stretch to avoid perturbation by stretch. We assumed stretching the membrane prior to

coating would not alter the binding affinity of laminin to the membrane surface. In support of this, we did not observe any difference in the total number of cells on the pre-stretched and pre-stretched-then-coated membranes, suggesting similar cell adhesion, proliferation, and survival on these two membranes and consistent with comparable laminin coating. The fact that oligodendrocyte differentiation did not differ between cells on the pre-stretched and pre-stretched-then-coated membranes showed that the stiffness effects attributed to the pre-stretched membranes were not due to a reduction in laminin density.

Specific ECMs clearly impact the response of NSPCs to mechanical stresses. Thus, these warrant attention when designing biomaterial scaffolds for NSPC transplantation into the CNS. Scaffolds in the tissue will also transmit mechanical forces, which our data suggest will affect differentiation of the embedded cells. For this reason, materials for CNS applications should be designed with consideration of the mechanical environment that takes into account stiffness of the material, the mechanical stresses transplanted cells may encounter, and the ECM or integrin ligating component of the material.

Our findings identify the significant role active mechanical forces such as tensile strain play in NSPC lineage decisions and the involvement of ECMs in these choices. Knowledge of the impact of these forces on NSPC differentiation allows for better understanding of NSPC responses to physiological and pathological manipulations of CNS tissue.

2.5 MATERIALS AND METHODS

J-Flex device to apply equibiaxial stretch

The J-Flex device utilizes rubber corks with circular Teflon disks adhered to their centers and applies a 10% static equibiaxial stretch to the membrane in the same manner as the Flexcell Tension System (Flexcell International Corporation) except instead of a negative pressure

pulling down the membrane against the loading posts, the J-Flex device pushes the posts up against the membrane (Fig. 2.2a,b). The height of the Teflon disks regulates the percentage of applied strain to the membrane and it was determined that a disk height of 10.32 mm strains the membrane 10%. Measurements were made by applying markings to the membrane and quantitating their distance increase relative to one another using calipers once the device was in place. A 10% strain value was chosen as a relevant mechanical stimulus since this strain level has been applied to neural cells cultured on pliable membranes *in vitro* to model trauma and strains in this range were measured in models of surrogate brain material in human skulls subjected to rotational forces used to predict strain fields *in vivo*[39].

Cell culture and application of stretch

For the stretch experiments, NSPCs were isolated from the cerebral cortices of embryonic day 12.5 (E12.5) mice and passaged as non-adherent spheres for at least 1 passage before use. Cortical tissue from multiple embryos from each E12.5 litter was pooled, and separate litters and subsequently cultured cells were considered a biological repeat. Cells were seeded at 150,000 cells per membrane and 25,000 cells per 12 mm cover slip onto laminin (20 µg/mL) or fibronectin (10 µg/mL) coated Bioflex plates and glass cover slips as previously described[18]. Cells were left for 18 hours in proliferation conditions prior to differentiation for 3 days (neurons) or 7 days (astrocytes and oligodendrocytes). Proliferation media for E12.5 NSPCs is DMEM, 1x B27, 1x N2, 1mM sodium pyruvate, 2mM L-glutamine, 1mM N-acetylcysteine, and growth factors 20 ng/mL EGF, 10 ng/mL FGF, and the cofactor 2 µg/mL heparin. Differentiation conditions utilize the same media without the inclusion of EGF, FGF, and heparin. Adult rat hippocampal NSPCs were cultured as previously described[40]. NSPCs were cultured on unstretched, stretched, and pre-stretched membranes. Unstretched membranes

contained cells that had no applied stretch stimulus, and stretched membranes had a 10% equibiaxial stretch applied 18 hours after cell seeding at the start of differentiation following the removal of growth factors or in mixed differentiation media (adult rat hippocampal NSPCs). The rate of equibiaxial strain application by the J-Flex device on the membranes in units of strain/sec was 20% (10% strain was reached in 0.5 ± 0.1s). In the pre-stretched treatment, NSPCs were seeded onto membranes already experiencing a 10% equibiaxial stretch (applied after ECM coating), effectively eliminating any stretch stimulus to the cells. This group was included in order to distinguish substrate stiffness and stretch effects. In order to determine whether laminin on the pre-stretched membrane was altered by the stretch and thus contributing to the results observed on pre-stretched membranes, control membranes were stretched then coated with laminin to avoid perturbation of the laminin molecules (prestretched-then-coated treatment). In this condition, membranes were placed under stretch and then coated with laminin followed by cell seeding. The stiffness of the unstretched membrane is around 10 kPa while the stiffness of a membrane experiencing 10% equibiaxial stretch is close to 1.6 MPa as previously shown[41]. The elastic modulus of the membrane at 10% strain was measured using an Instron materials testing system at the University of California, Irvine and was found to be equal to 1.864 MPa. The slight discrepancy in stiffness between the Instron measurement and the value obtained in [41] can be attributed to the fact that the Instron system imposes a uniaxial strain as opposed to an equibiaxial strain. Cells were immunostained for the neuronal markers MAP2/DCX at 3 days differentiation and the astrocyte and oligodendrocyte markers GFAP and PDGFR-α/O4, respectively at 5-7 days differentiation since these time points provide quantifiable fields of cells for analysis as previously described[42, 43]. PDGFR-α was used at 5 days on E12.5 cells since it is a marker for oligodendrocytes at an earlier stage in development.

For adult rat hippocampal NSPCs, immunostaining for oligodendrocytes using O4 was done at 5 days since these cells displayed a higher propensity for oligodendrocyte differentiation than the E12.5 mNSPCs.

Immunostaining and cell quantitation

Cells were fixed with 4% paraformaldehyde for 10 min as described previously[44]. Cells immunostained for cytoskeletal markers of neurons and astrocytes were treated with 0.3% Triton X-100 in PBS for 5 minutes prior to blocking for 1 hour in 5% bovine serum albumin (BSA) in phosphate saline buffer (PBS). Cells to be stained for surface markers of oligodendrocytes (O4 and PDGFR-α) were not treated with Triton X-100 prior to blocking. Prior to primary antibody staining, the silicone elastomer membranes from the Bioflex plates were cut out using a scalpel for easier manipulation. The region of the membrane used for analysis specifically excluded the edges where the teflon disk would create a bend in the membrane since this may represent a confounding topographical cue for the cells. Cells were then immunostained at 4^{o}C overnight for neurons with mouse anti-MAP2 (Sigma M9942) and anti-DCX (Santa Cruz Biotechnology SC-8066 (c-18)) at 1:200, astrocytes with mouse anti-GFAP (Sigma G3893) at 1:200, and oligodendrocytes with mouse anti-O4 (R&D Systems MAB1326) at 1:100 and rabbit anti-PDGFR-α (Genetex GTX25460) at 1:200. Secondary antibodies (Alexa 488 and 555, Invitrogen A21206, A31570, A21432, A21426) were used at 1:200 at room temperature in the dark for 2 hours. Both primary and secondary antibodies were diluted in 1% BSA in PBS. Cell nuclei were counterstained for 1 minute with Hoechst 33342 at 1:500 in PBS. Coverslips and membranes with fixed cells were mounted with Vectashield (Vector Labs) and imaged using a Nikon Eclipse Ti microscope with a 10x or 20x objective and images were acquired using NIS element AR3.10 software.

The percentages of cells that had differentiated into neurons, astrocytes, and oligodendrocytes were calculated from 3-5 randomly selected fields per experiment. At least 3 independent experiments were performed with separate sets of cells (biological repeats), with more than 1500 cells quantitated and analyzed for each group. Total cell number was determined by counting all Hoechst-stained nuclei on membranes and glass. In order to assess generation of neurons, astrocytes, and oligodendrocytes from mNSPCs, strict criteria were applied. For neurons, cells expressing the neuronal markers MAP2 or DCX with neurites at least three times the length of the cell body were counted as neurons. For astrocytes, cells exhibiting a filamentous and cytoskeletal pattern of GFAP expression in the cytoplasm were counted as positive. In the case of E12.5 cortex derived mNSPCs, undifferentiated cells do not express GFAP, allowing for an accurate quantitation of astrocyte generation[44]. Oligodendrocytes were counted by clear expression of the extracellular markers O4 or PDGFR-α on cellular processes surrounding a cell nucleus. ImageJ was used to quantitate positively stained cells.

Integrin blocking during migration

E12.5 mNSPCs spheres were allowed to adhere to coverslips that were pre-coated with laminin and pre-blocked with BSA (1% BSA in PBS) for 1 hour. Spheres were subsequently incubated with rat IgG2A isotype control antibody (clone 54447, 10µg/mL; R&D Systems MAB006) or a function-blocking α6 integrin antibody (clone GoH3, 10µg/mL; AbD Serotec MCA699EL) in proliferation medium. Spheres incubated in proliferation medium without antibody were also used as negative controls. The spheres were imaged at the time point of initial addition of integrin blocker or control and at 20, 90 minutes, 4, 16, and 24 hours. Radial migration of individual cells outward from the edge of the sphere was monitored and the distance traveled was measured at each time point.

Integrin blocking during differentiation

E12.5 mNSPCs were plated onto laminin-coated unstretched or stretched membranes or glass coverslips that were pre-blocked with 1% BSA for 1 hour in order to reduce non-specific binding of antibody. Cells were seeded into the wells in proliferation media and allowed to adhere for 18 hours prior to switching to differentiation media. Adhered cells were incubated in α6 blocking antibody (clone GoH3, 10µg/mL, AbD Serotec MCA699EL), IgG2A isotype control antibody (clone 54447, 10µg/mL, R&D Systems MAB006), or no antibody for 2 hours in differentiation media to allow for antibody infiltration onto the ventral surface of the cells, followed by the application of 10% equibiaxial stretch in the respective stretch groups. Membranes were fixed and immunostained for the oligodendrocyte marker O4 after 7 days of differentiation, with a 100% differentiation media replacement done at 3 days.

Statistical Analysis

All statistical analyses utilized a one-way single factor ANOVA to compare two samples and utilized data from three or more independent biological repeats.

2.6 ACKNOWLEDGMENTS

The authors would like to thank the National Institute of Neurological Disorders and Stroke (NS082174) and the National Science Foundation CAREER Award (IOS-1254060) for funding these studies and Dr. Wendy Liu and Frances McWhorter from University of California, Irvine for their assistance in developing the J-Flex device. The authors would also like to thank Dr. David Schaffer for the gift of adult rat hippocampal NSPCs.

2.7 AUTHOR CONTRIBUTIONS

J.A., M.M.P., J.L.N., F.T., and L.A.F designed experiments; J.A. performed experiments and assays; L.P.M. performed dissections to obtain cells used in experiments; J.A. and J.C.E. designed and built J-Flex device; J.A. analyzed data; J.A. and L.A.F. wrote the manuscript; L.A.F. supervised the project; All authors edited and approved the final manuscript.

2.8 SUPPLEMENTAL MATERIAL

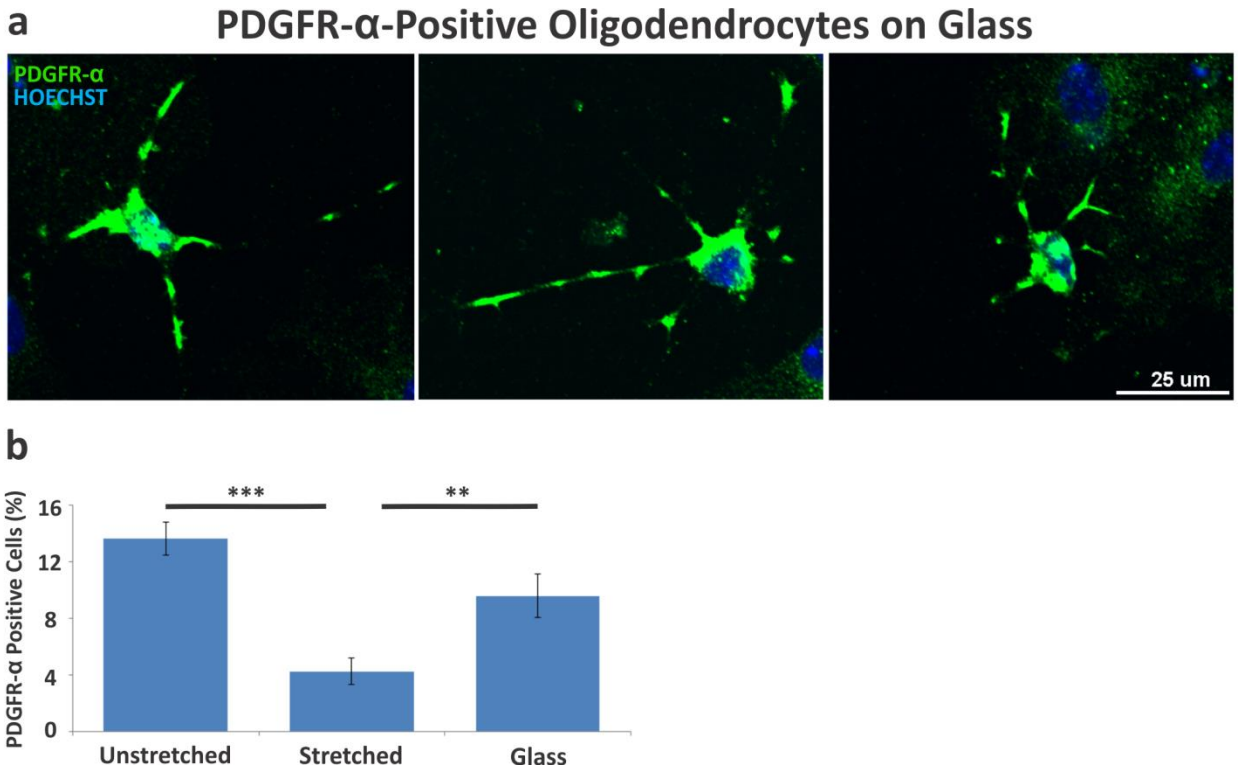

Figure 2.S1. Stretch inhibits mNSPC differentiation into PDGFR-α-positive oligodendrocytes. (a) Images of E12 mNSPCs differentiated on glass showing cell surface oligodendrocyte marker PDGFR-α co-stained with nuclear DNA marker Hoechst. (b) Static stretch reduces oligodendrocyte differentiation (cells on stretched compared to unstretched membranes). PDGFR-α recognizes oligodendrocytes at an earlier stage of differentiation than O4, so the percentage of cells identified with this marker is higher than that recognized by the more mature marker O4 as shown in Figure 3a. P = 1.15E-06 (unstretched vs. stretched). P = 0.005 (glass vs. stretched). **P < 0.01, ***P < 0.001. Error bars represent SEM. N=3 independent biological repeats.

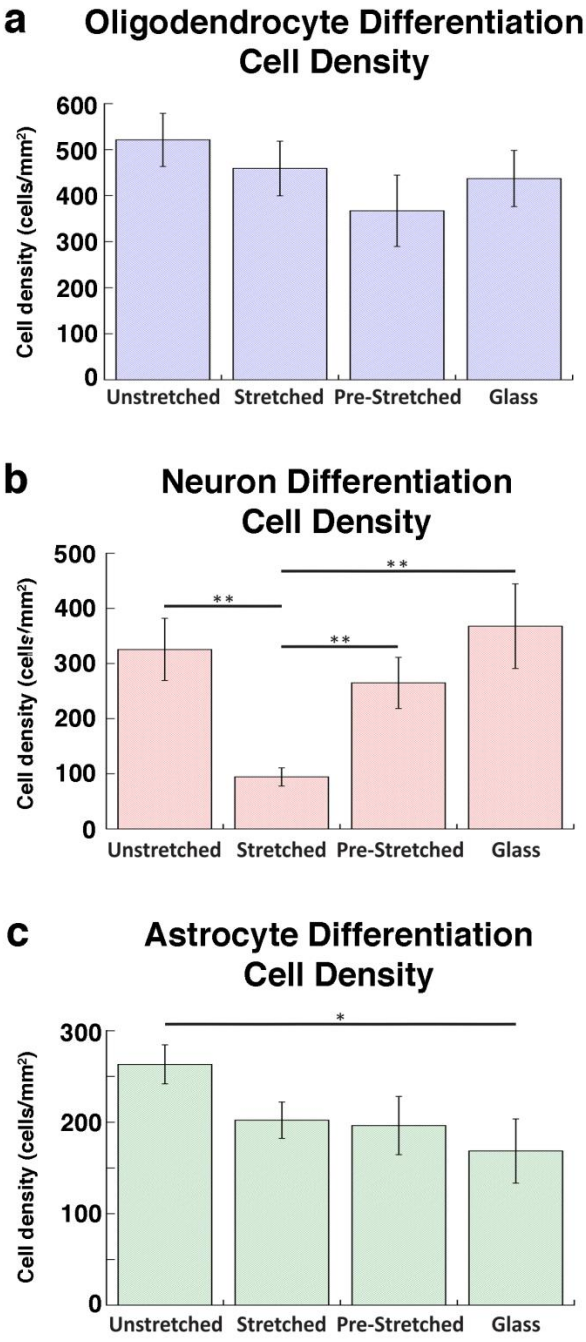

Figure 2.S2. Cell density quantitation of differentiated mNSPCs. The average cell density in cells/mm^2 is shown for cells on unstretched, stretched, and pre-stretched membranes and glass for (a) oligodendrocyte (b) neuron, and (c) astrocyte cell differentiation experiments matching those shown in Figure 5. *P < 0.05, **P < 0.01. Error bars represent SEM. N=3 independent biological repeats.

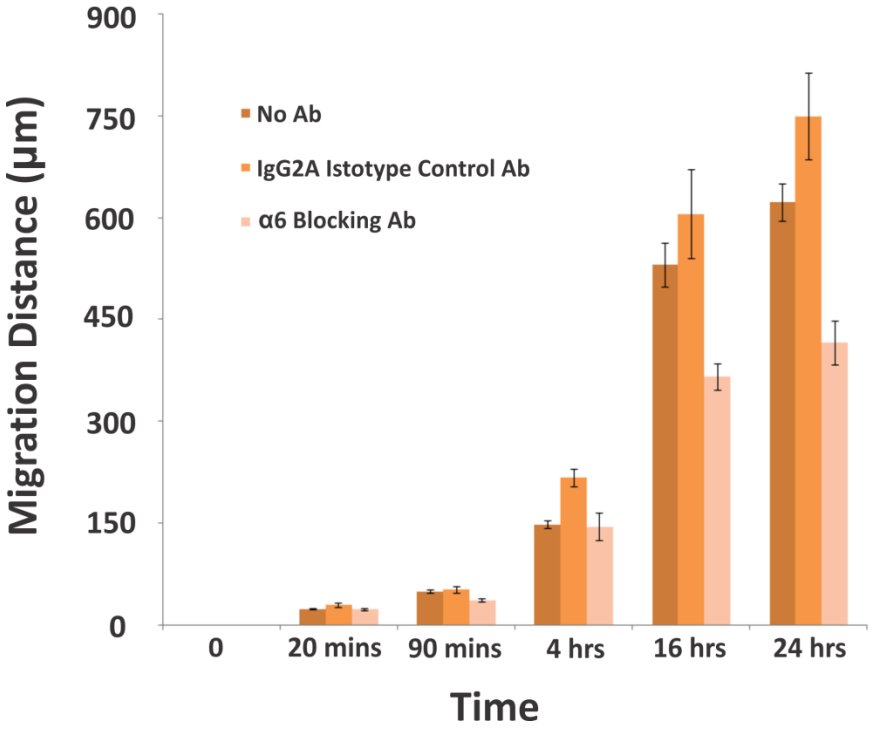

Figure 2.S3. E12 mNSPCs express functional α6 integrin. mNSPC migration out of spheres over 24 hours during incubation with no antibody (No Ab), IgG2A isotype control antibody, or α6 integrin function-blocking antibody. Perturbing α6 integrin using a function-blocking antibody decreases migration of mNSPCs on laminin substrates, indicating these cells express functional cell surface α6 integrin. Error bars represent SEM.

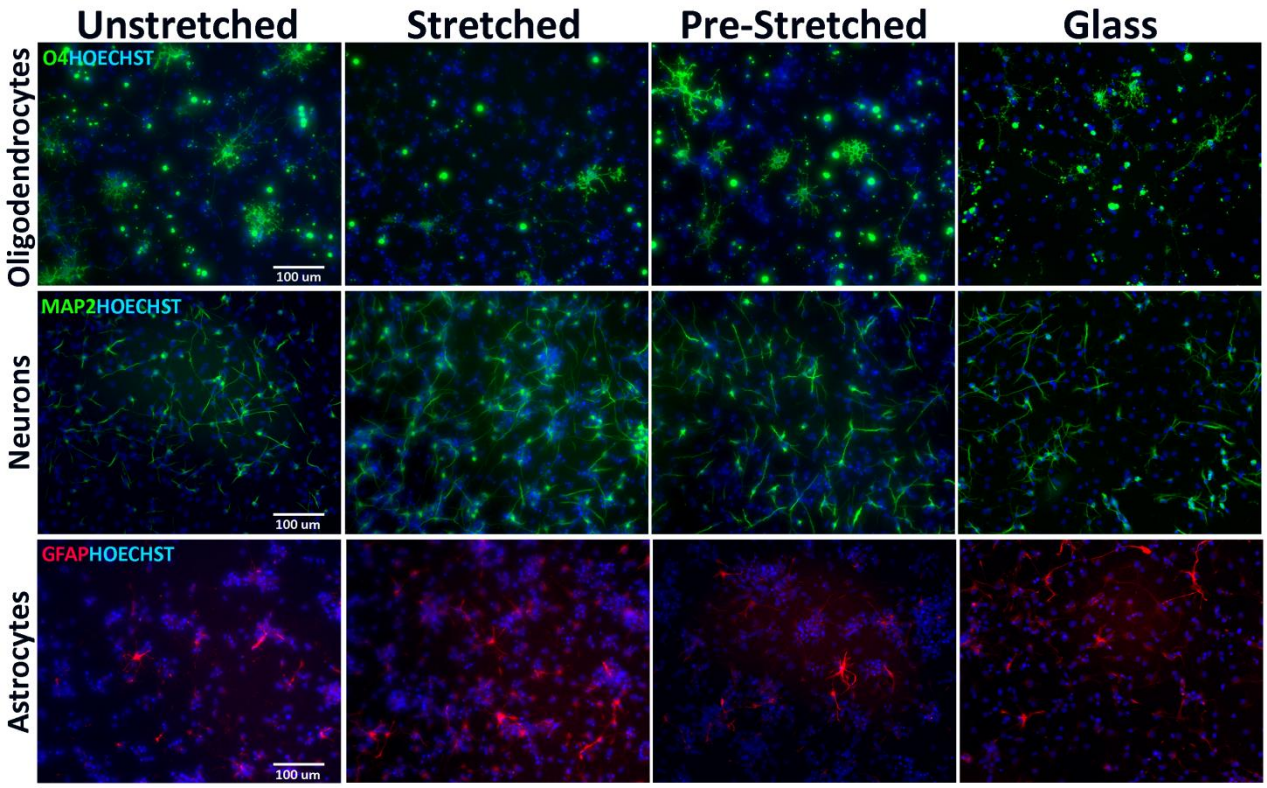

Figure 2.S4. Immunocytochemistry of mNSPC differentiation. Images of E12 mNSPCs differentiated on unstretched, stretched, and pre-stretched membranes and glass showing nuclear DNA marker Hoechst co-stained with cell surface oligodendroglial marker O4 (top), cytoskeletal neuronal marker MAP2 (middle), and cytoskeletal astrocytic marker GFAP (bottom).

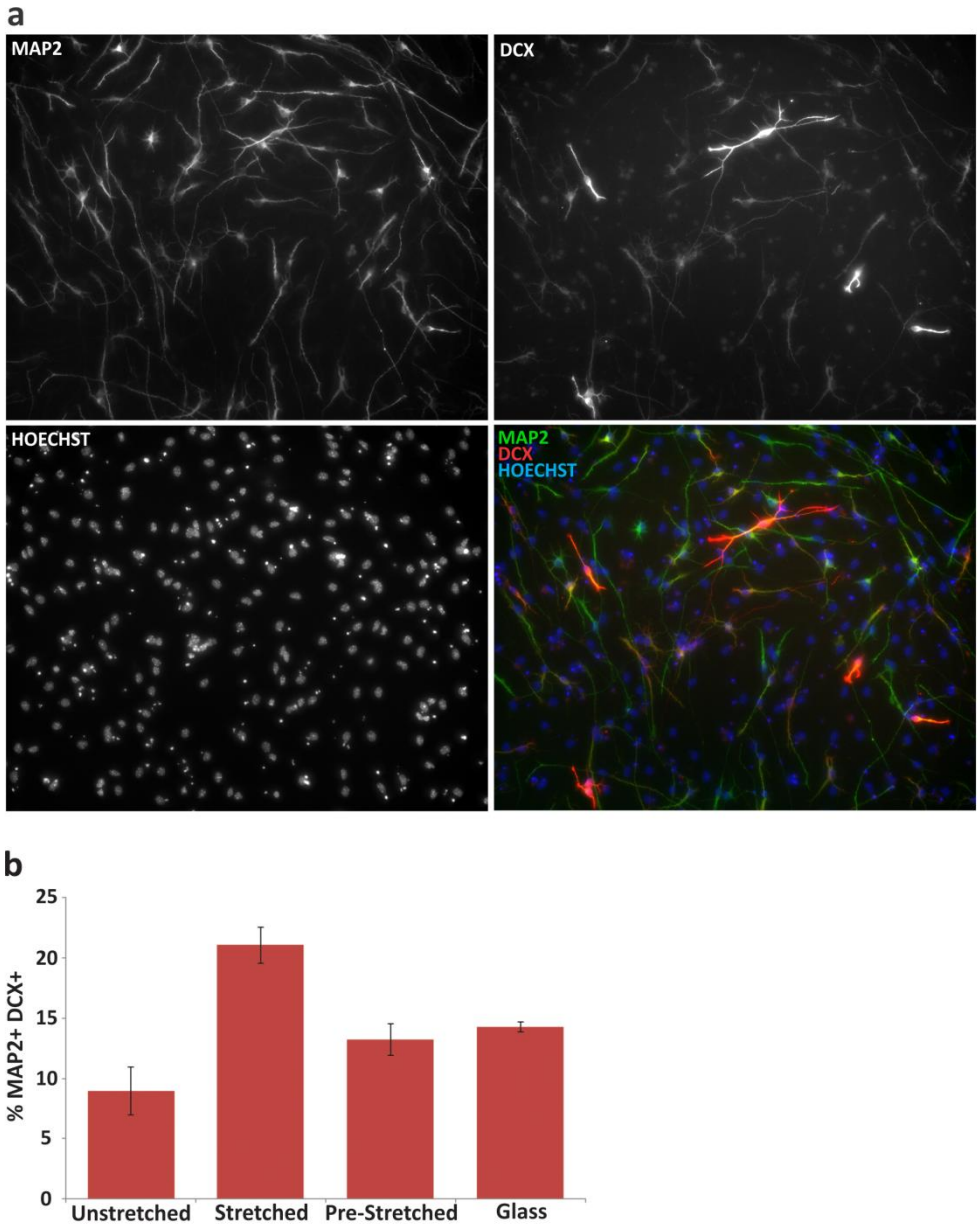

Figure 2.S5. Immunocytochemistry of neurons differentiated from mNSPCs using multiple markers. (a) Images of E12 mNSPCs differentiated on an unstretched membrane showing neuronal markers MAP2 (top left) and DCX (top right) with nuclear DNA marker Hoechst (bottom left) and the co-stain (bottom right). (b) Quantitation of neurons using two markers (MAP2 and DCX) shows a pattern similar to that presented in Figure 5 with MAP2 alone; more neurons are generated from mNSPCs on stretched or pre-stretched membranes and glass than those on unstretched membranes. There was no statistical analyses performed since N=1 independent biological repeat for these data. Error bars represent SEM of multiple quantified fields.

2.9 REFERENCES

1. Gage, F.H. Mammalian neural stem cells. *Science* **287**, 1433-1438 (2000).
2. Kshitiz et al. Control of stem cell fate and function by engineering physical microenvironments. *Integr Biol* **4**, 1008-1018 (2012).
3. Engler, A., Sen, S., Sweeney, H. & Discher, D. Matrix elasticity directs stem cell lineage specification. *Cell* **126**, 677-689 (2006).
4. Tyler, W.J. The mechanobiology of brain function. *Nat Rev Neurosci* **13**, 867-878 (2012).
5. Saha, K. et al. Substrate modulus directs neural stem cell behavior. *Biophys J* **95**, 4426-4438 (2008).
6. Leipzig, N. & Shoichet, M. The effect of substrate stiffness on adult neural stem cell behavior. *Biomaterials* **30**, 6867-6878 (2009).
7. Keung, A., de Juan-Pardo, E., Schaffer, D. & Kumar, S. Rho GTPases mediate the mechanosensitive lineage commitment of neural stem cells. *Stem cells* **29**, 1886-1897 (2011).
8. Kurpinski, K., Chu, J., Hashi, C. & Li, S. Anisotropic mechanosensing by mesenchymal stem cells. *Proc Natl Acad Sci U S A* **103**, 16095-16100 (2006).
9. Park, J.S. et al. Differential effects of equiaxial and uniaxial strain on mesenchymal stem cells. *Biotechnol Bioeng* **88**, 359-368 (2004).
10. Kurpinski, K., Chu, J., Wang, D. & Li, S. Proteomic profiling of mesenchymal stem cell responses to mechanical strain and TGF-beta1. *Cell Mol Bioeng* **2**, 606-614 (2009).
11. Kim, I.S., Song, Y.M. & Hwang, S.J. Osteogenic responses of human mesenchymal stromal cells to static stretch. *J Dent Res* **89**, 1129-1134 (2010).
12. Chowdhury, F. et al. Material properties of the cell dictate stress-induced spreading and differentiation in embryonic stem cells. *Nat Mater* **9**, 82-88 (2010).
13. Heisenberg, C.-P.P. & Bellaïche, Y. Forces in tissue morphogenesis and patterning. *Cell* **153**, 948-962 (2013).
14. Nishimura, T., Honda, H. & Takeichi, M. Planar cell polarity links axes of spatial dynamics in neural-tube closure. *Cell* **149**, 1084-1097 (2012).
15. Suzuki, M., Morita, H. & Ueno, N. Molecular mechanisms of cell shape changes that contribute to vertebrate neural tube closure. *Dev Growth & Differ* **54**, 266-276 (2012).
16. Chen, Y.C., Smith, D.H. & Meaney, D.F. In-vitro approaches for studying blast-induced traumatic brain injury. *J Neurotrauma* **26**, 861-876 (2009).
17. Chang, Y.-J.J., Tsai, C.-J.J., Tseng, F.-G.G., Chen, T.-J.J. & Wang, T.-W.W. Micropatterned stretching system for the investigation of mechanical tension on neural stem cells behavior. *Nanomed-nanotechnol biol med e* **9**, 345-355 (2013).
18. Flanagan, L., Rebaza, L., Derzic, S., Schwartz, P. & Monuki, E. Regulation of human neural precursor cells by laminin and integrins. *J Neurosci Res* **83**, 845-856 (2006).
19. Blaschuk, K., Frost, E. & ffrench-Constant, C. The regulation of proliferation and differentiation in oligodendrocyte progenitor cells by alphaV integrins. *Development* **127**, 1961-1969 (2000).
20. Colognato, H., Ramachandrappa, S., Olsen, I. & ffrench-Constant, C. Integrins direct Src family kinases to regulate distinct phases of oligodendrocyte development. *J Cell Biol* **167**, 365-375 (2004).
21. Relucio, J., Tzvetanova, I.D., Ao, W., Lindquist, S. & Colognato, H. Laminin alters fyn regulatory mechanisms and promotes oligodendrocyte development. *J Neurosci* **29**, 11794-11806 (2009).
22. D'Angelo, F. et al. Mechanotransduction: tuning stem cells fate. *J Funct Biomater* **2**, 67-87 (2011).
23. Milner, R. & Campbell, I. The integrin family of cell adhesion molecules has multiple functions within the CNS. *J Neurosci Res* **69**, 286-291 (2002).
24. O'Meara, R.W., Michalski, J.P. & Kothary, R. Integrin signaling in oligodendrocytes and its importance in CNS myelination. *J Signal Transduct* **2011**, 354091 (2011).
25. Lathia, J.D. et al. Patterns of laminins and integrins in the embryonic ventricular zone of the CNS. *J Comp Neurol* **505**, 630-643 (2007).
26. Chen, Z.-L.L., Indyk, J.A. & Strickland, S. The hippocampal laminin matrix is dynamic and critical for neuronal survival. *Mol Biol Cell* **14**, 2665-2676 (2003).

27. Relucio, J., Menezes, M.J., Miyagoe-Suzuki, Y., Takeda, S. & Colognato, H. Laminin regulates postnatal oligodendrocyte production by promoting oligodendrocyte progenitor survival in the subventricular zone. *Glia* **60**, 1451-1467 (2012).
28. Zheng, W., Christensen, L.P. & Tomanek, R.J. Differential effects of cyclic and static stretch on coronary microvascular endothelial cell receptors and vasculogenic/angiogenic responses. *Am J Physiol Heart Circ Physiol* **295**, H794-800 (2008).
29. Foster, C.D., Varghese, L.S., Gonzales, L.W., Margulies, S.S. & Guttentag, S.H. The Rho pathway mediates transition to an alveolar type I cell phenotype during static stretch of alveolar type II cells. *Pediatr Res* **67**, 585-590 (2010).
30. Cavalcanti-Adam, E.A. et al. Cell spreading and focal adhesion dynamics are regulated by spacing of integrin ligands. *Biophys J* **92**, 2964-2974 (2007).
31. Arnold, M. et al. Activation of integrin function by nanopatterned adhesive interfaces. *Chemphyschem* **5**, 383-388 (2004).
32. Maheshwari, G., Brown, G., Lauffenburger, D.A., Wells, A. & Griffith, L.G. Cell adhesion and motility depend on nanoscale RGD clustering. *J Cell Sci* **113 (Pt 10)**, 1677-1686 (2000).
33. Milner, R. & Ffrench-Constant, C. A developmental analysis of oligodendroglial integrins in primary cells: changes in alpha v-associated beta subunits during differentiation. *Development* **120**, 3497-3506 (1994).
34. Milner, R. et al. Expression of alpha vbeta3 and alpha vbeta8 integrins during oligodendrocyte precursor differentiation in the presence and absence of axons. *Glia* **21**, 350-360 (1997).
35. Roca-Cusachs, P., Gauthier, N.C., Del Rio, A. & Sheetz, M.P. Clustering of alpha(5)beta(1) integrins determines adhesion strength whereas alpha(v)beta(3) and talin enable mechanotransduction. *Proc Natl Acad Sci U S A* **106**, 16245-16250 (2009).
36. Colognato, H. et al. CNS integrins switch growth factor signalling to promote target-dependent survival. *Nat Cell Biol* **4**, 833-841 (2002).
37. Geddes, D.M., Cargill, R.S. & LaPlaca, M.C. Mechanical stretch to neurons results in a strain rate and magnitude-dependent increase in plasma membrane permeability. *J Neurotrauma* **20**, 1039-1049 (2003).
38. Geddes-Klein, D.M., Schiffman, K.B. & Meaney, D.F. Mechanisms and consequences of neuronal stretch injury in vitro differ with the model of trauma. *J Neurotrauma* **23**, 193-204 (2006).
39. Margulies, S.S., Thibault, L.E. & Gennarelli, T.A. Physical model simulations of brain injury in the primate. *J Biomech* **23**, 823-836 (1990).
40. Peltier, J., Agrawal, S., Robertson, M.J. & Schaffer, D.V. In vitro culture and analysis of adult hippocampal neural progenitors. *Methods Mol Biol* **621**, 65-87 (2010).
41. Colombo, A., Cahill, P.A. & Lally, C. An analysis of the strain field in biaxial Flexcell membranes for different waveforms and frequencies. *Proc Inst Mech Eng H* **222**, 1235-1245 (2008).
42. Labeed, F.H. et al. Biophysical characteristics reveal neural stem cell differentiation potential. *PLoS One* **6**, e25458 (2011).
43. Nourse, J.L. et al. Membrane biophysics define neuron and astrocyte progenitors in the neural lineage. *Stem Cells* **32**, 706-716 (2014).
44. Flanagan, L. et al. Unique dielectric properties distinguish stem cells and their differentiated progeny. *Stem cells* **26**, 656-665 (2008).

CHAPTER 3

THE STRETCH-ACTIVATED ION CHANNEL PIEZO1 DIRECTS LINEAGE CHOICE IN HUMAN NEURAL STEM CELLS

Authors: Medha M. Pathak[1], Jamison L. Nourse[2,3], Truc Tran[1], Jennifer Hwe[1], **Janahan Arulmoli**[3,4], Dai Trang T. Le[1], Elena Bernardis[5], Lisa A. Flanagan[2,3,4], Francesco Tombola[1]

Author Affiliations:

[1] Department of Physiology & Biophysics

[2]Department of Neurology

[3]Sue & Bill Gross Stem Cell Research Center

[4]Department of Biomedical Engineering

[5]Department of Pediatrics, Section of Dermatology, Children's Hospital of Philadelphia, Philadelphia, PA, 19104, USA

[1-4]University of California, Irvine, Irvine, CA, 92697, USA

Keywords: calcium signaling, matrix mechanics, myosin II, Yap/Taz, blebbistatin

3.1 ABSTRACT

Neural stem cells are multipotent cells with the ability to differentiate into neurons, astrocytes and oligodendrocytes. Lineage specification is strongly sensitive to the mechanical properties of the cellular environment. However, molecular pathways transducing matrix mechanical cues to intracellular signaling pathways linked to lineage specification remain unclear. We found that the mechanically-gated ion channel, Piezo1, is expressed by brain-derived human neural stem/progenitor cells and is responsible for a mechanically-induced ionic current. Piezo1 activity triggered by traction forces elicited influx of Ca^{2+}, a known modulator of differentiation, in a substrate-stiffness dependent manner. Inhibition of channel activity by the pharmacological inhibitor GsMTx-4 or by siRNA-mediated Piezo1 knockdown suppressed neurogenesis and enhanced astrogenesis. Piezo1 knockdown also reduced the nuclear localization of the mechanoreactive transcriptional co-activator Yap. We propose that the mechanically-gated ion channel Piezo1 is an important determinant of mechanosensitive lineage choice in neural stem cells and may play similar roles in other multipotent stem cells.

3.2 INTRODUCTION

Mechanical properties of the cellular environment are powerful modulators of stem cell behavior. For instance, local mechanical cues such as extracellular matrix elasticity and nanotopology affect stem cell lineage choice[1, 2]. Mechanical effects on fate are particularly relevant for stem cell transplant therapy, since stem cells encounter diverse mechanical signals upon engraftment[3, 4]. Moreover, before transplantation, stem cells are grown *in vitro*, where the mechanical properties of culture conditions affect their behavior. Recent studies show that stem cells may possess a memory of past mechanical environments[5], and that mechanical properties of the culturing environment prior to transplantation can influence the outcome of *in vivo* stem cell transplants[6]. Hence, a molecular and mechanistic understanding of how stem cells process mechanical cues and how this results in downstream signaling events and ultimately in fate decisions is needed for greater control over the fate of transplanted cells.

Studies in mesenchymal and neural stem cells have revealed the involvement of focal adhesion zones and cytoskeletal proteins that participate in the generation of cellular traction forces such as integrins, non-muscle myosin II[7], Rho GTPases[8-10] and vinculin[11]. Recent work has also identified the nucleoskeletal protein lamin-A[12] and the transcription factors Yap and Taz[13] in mechanotransduction in mesenchymal stem cells. However, the mechanisms by which mechanical cues detected by cellular traction forces are transduced to downstream intracellular pathways of differentiation remain unclear.

Ion channels are involved, directly or indirectly, in the transduction of all forms of physical stimuli – including sound, light, temperature, mechanical force, and even gravity – into intracellular signaling pathways. Hence, we wondered whether ion channels could be involved in transducing matrix mechanical cues to intracellular signaling pathways linked to lineage

specification. In particular, we focused here on cationic stretch-activated channels (SACs) since they are known to detect mechanical forces with high sensitivity and broad dynamic range, and because they are permeable to Ca^{2+}, an important second messenger implicated in cell fate[14, 15]. We examined the role of SACs in neural stem cells, for which mechanical cues influence specification along the neuronal-glial lineage[8, 16, 17]. We find that human neural stem/progenitor cells (hNSPCs) express the SAC Piezo1, and that the activity of the channel is mediated by cell-generated traction forces. Piezo1 activation elicits transient Ca^{2+} influx in a substrate-stiffness-dependent manner, favors nuclear localization of the mechanoreactive transcription co-activator Yap, and influences neuronal vs. glial specification.

3.3 RESULTS

We used cultures of human neural stem/progenitor cells, SC23 and SC27, derived from the cerebral cortices of two separate postmortem fetal brains[18, 19] to test the role of SACs in mechanical modulation of stem cell behavior. Both cultures express standard neural stem cell markers, including Sox2, nestin, and the cell surface marker CD133, and have the potential to differentiate into the three major neural cell types: astrocytes, neurons and oligodendrocytes[18-22]. When transplanted into a mouse model of Sandhoff disease, these hNSPCs stably integrated into the host brain and delayed disease onset, reflecting their functional and therapeutic potential[23]. Similar fetal brain-derived hNSPCs have also been shown to differentiate into neurons, astrocytes and oligodendrocytes upon transplantation into the central nervous system[24], and are currently in clinical trials for multiple neurological conditions[25, 26].

3.3.1 hNPSCs exhibit stretch-activated ionic currents

To test whether SC23 and SC27 cells possess SAC activity, we mechanically stimulated their plasma membranes using a piezoelectric actuator while simultaneously measuring ionic

currents with whole-cell patch clamp. We consistently observed ionic currents in response to mechanical stimuli (Fig. 3.1a). Peak amplitude increased with stimulus intensity along a Boltzmann curve as expected for a SAC (Fig. 3.1b). We obtained confirmation of this result using a different patch clamp assay, which measures currents from a small patch of membrane rather than from the whole cell. In this cell-attached configuration, the membrane is stretched by negative suction pulses applied with a high-speed pressure clamp (Fig. 3.1c, d, and Fig. 3.S1). We measured ionic currents in response to mechanical stimulation in 91 out of 107 cells (85%) using this technique.

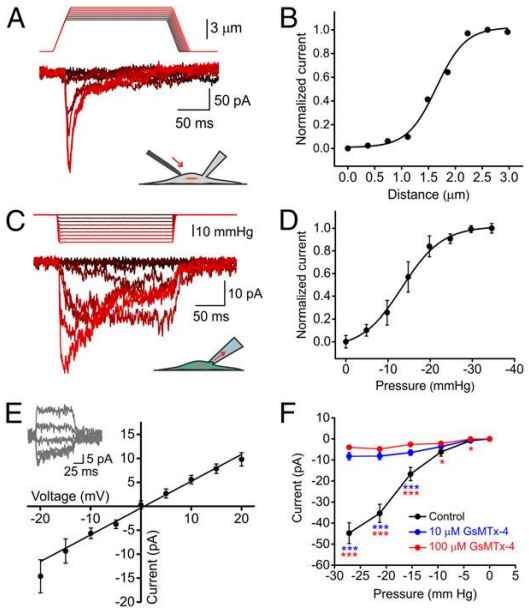

Figure 3.1. Mechanically-induced currents in hNSPCs. (a) Representative traces of mechanically-induced inward currents from by SC23 hNSPC cells. Cells were subjected to a series of mechanical stimuli by indenting the plasma membrane with a stimulation probe. The probe was moved in steps of 0.4 μm while recording in the whole-cell patch configuration and a holding potential of −80 mV. Representative of n = 6 cells. (b) Current amplitude in response to indentation by probe displacement from traces shown in A. (c) Representative currents in an SC27 hNSPC cell induced by negative pipette pressure (0 to −30 mm Hg in steps of 5 mm Hg) administered by a pressure clamp. Holding potential: −80 mV. (d) Normalized current-pressure relationship of stretch-activated currents at a holding potential of −80 mV fitted with a Boltzmann equation with P_{50} = -13.4 mmHg, s = 4.75 mmHg (n = 8 cells, mean ± SEM). (e) Average current-voltage relationships of stretch-activated channels in SC27 hNSPC cells (n = 7 cells, mean ± SEM). Inset shows current traces in response to voltage steps from -40 mV to 40 mV in steps of 20 mV, applied 250 ms before a negative pressure pulse of -30 mmHg. (f) Mean

current amplitudes elicited by membrane stretch in cell-attached patch clamp mode in the absence (black, n = 29 cells) and presence of 10 □M (blue, n = 69 cells) and 100 □M extracellular GsMTx-4 (red, n = 42 cells). Error bars indicate SEM and are smaller than data points in some cases. *p < 0.05, **p < 0.01, ***p < 0.001 by two-sample t-test. See also Fig. 3.S1.

Ionic currents measured by both techniques displayed hallmarks of SACs: in standard extracellular and intracellular solutions (see Methods) and at a holding potential of -80 mV, the currents were inward in direction and reduced in magnitude exponentially when presented with a persisting mechanical stimulus (Fig. 3.1a and c). Ionic currents reversed direction near 0 mV (reversal potential = -0.75 ± 0.67 mV, Fig. 3.1e), consistent with activity of a nonspecific cation channel. We next tested the susceptibility of hNSPC SAC currents to GsMTx-4, a peptide isolated from the venom of the Chilean rose tarantula spider, *Grammostola rosea*. GsMTx-4 is the only known drug to specifically inhibit cationic SACs without inhibiting other ion channel families such as voltage-gated sodium, potassium, and calcium channels[27] or potassium-selective SACs[28]. It acts as a gating modifier by partitioning into the cell membrane and affecting force transfer to the channel protein [29]. hNSPC SAC currents were inhibited by extracellular GsMTx-4 (Fig. 3.1f), consistent with their generation by a stretch-activated cationic channel.

3.3.2 Molecular identification of SAC

We next asked which ion channel(s) could be responsible for the measured mechanically gated currents. Based on the electrophysiological properties of the ionic currents, we examined 9 known cationic mechanosensitive channels for expression in SC27 hNSPCs using quantitative real time polymerase chain reaction (qRT-PCR) (Fig. 3.S2). Of these, Piezo1 was expressed at much greater levels than the other channels. The Piezo channels were recently shown to mediate physiologically relevant mechanically-activated and non-selective cationic currents in mammals[30-34]. Like the endogenous hNSPC SAC, Piezo1 displays inactivation to persisting

mechanical stimuli[31] and is sensitive to GsMTx-4[35]. While Piezo1 was highly expressed in SC23 and SC27 cells, its paralogue, Piezo2, was not (Fig. 3.2a).

To determine whether Piezo1 underlies the hNSPC mechanically-induced currents, we tested the effect of small interfering RNA (siRNA) mediated gene knockdown on the ionic current. We transfected SC27 hNSPCs with a pool of four siRNAs against Piezo1. We performed qRT-PCR to assess transcript levels and cell-attached patch clamp recordings to examine ionic current amplitude 36-72 hours after transfection. Treatment with Piezo1 siRNAs reduced Piezo1 transcripts and caused an attenuation of ionic currents (Fig. 3.2). Pools of non-targeting control siRNAs or GAPDH siRNAs and the fluorescent reporter of transfection (siGlo) alone did not show a significant reduction of the Piezo1 RNA or of mechanotransduction currents (Fig. 3.2, Fig. 3.S3). Among the Piezo1-siRNA transfected cells, Piezo1 transcripts were reduced by 76.2 ± 0.9% and mean maximal current amplitude was reduced by 89% relative to untransfected cells, with 27 out of 42 cells (64%) showing no measurable current. The near-complete loss of mechanically-evoked currents in response to Piezo1 siRNA indicates that Piezo1 underlies mechanotransduction currents in hNSPCs.

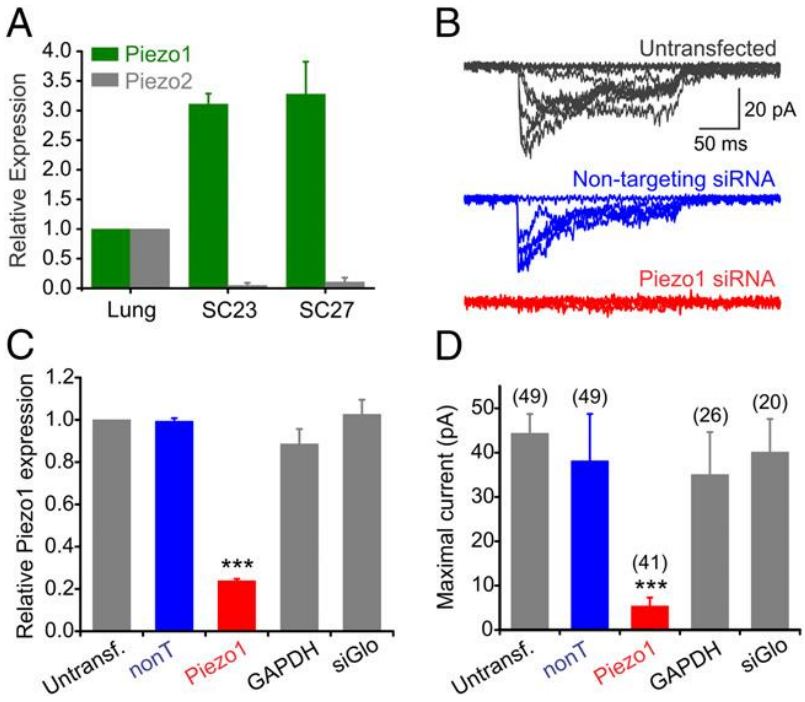

Figure 3.2. Piezo1 is essential for mechanically-induced currents in hNSPCs. (a) mRNA expression of *Piezo1* (green) and *Piezo2* (gray) in SC23 and SC27 hNSPCs determined by qRT-PCR with 18S as the reference gene. Human lung was used as the tissue calibrator by the $2^{-\Delta\Delta CT}$ method, since it was previously shown to express both channels[31]. n = 6 independent experiments for Piezo1 and n = 4 independent experiments for Piezo2. Data are mean ± SEM. (b) Representative mechanotransduction currents from an untransfected (top, gray; same cell as in Fig. 3.1c), a cell transfected with a control non-targeting pool of siRNAs (middle, blue) and a cell transfected with four siRNAs against Piezo1 (bottom, red). Holding potential = -80 mV. (c) Quantification of Piezo1 transcripts by qRT-PCR from three independent transfection experiments. Parallel samples were used for patch clamp measurements in panel D. ***$p < 0.001$ by ANOVA. (d) Mean maximal mechanotransduction currents recorded from untransfected cells, from cells transfected with a non-targeting pool of four siRNAs (20 nM, blue), siGlo transfection marker alone (20 nM) or with a pool of four siRNAs against Piezo1 (20 nM, red) or GAPDH (25 nM). Numbers in parentheses refer to the numbers of cells patched for each condition. Data are from three independent transfection experiments, as in panel C. ***$p < 0.001$ with Kruskalwallis test. See also Fig. 3.S2, 3.S3 and 3.S10.

3.3.3 Piezo1 activity elicits spontaneous Ca^{2+} transients

Piezo1 has been implicated in cellular processes in which cells respond to an external mechanical force, for instance, when cells respond to a stretch stimulus, osmotic pressure, or shear stress[31, 33, 34, 36-38]. We asked whether cell-generated forces, such as traction forces, can activate Piezo1. Our patch clamp assays described above preferentially stimulate cells on the

dorsal surface of the cell, while traction forces are more prominently generated at the cell's ventral surface, where the cell contacts the substrate through focal adhesion zones. To assay the activity of Piezo1 at the ventral surface we utilized the fact that the channel displays a preference for conducting Ca^{2+} over other cations[31]. We imaged spontaneous Ca^{2+} dynamics of hNSPCs grown on glass coverslips and loaded with the fluorescent Ca^{2+} indicator Fluo-4AM. We selectively imaged plasma membrane events in the absence of intracellular background fluorescence by using Total Internal Reflection Fluorescence Microscopy (TIRFM). We observed many spontaneous Ca^{2+} transients over a time scale of seconds (Fig. 3.3a, b). Spontaneous Ca^{2+} signals were reversibly abolished by chelating external Ca^{2+} with EGTA, indicating that Ca^{2+} influx through the plasma membrane is required for the generation of the signals (Fig. 3.3c, d). We quantified the spontaneous Ca^{2+} transients by computing the amplitude of the transients, their frequency, and the area under the fluorescence curve. All three measures showed reversible and statistically significant reduction in the presence of EGTA.

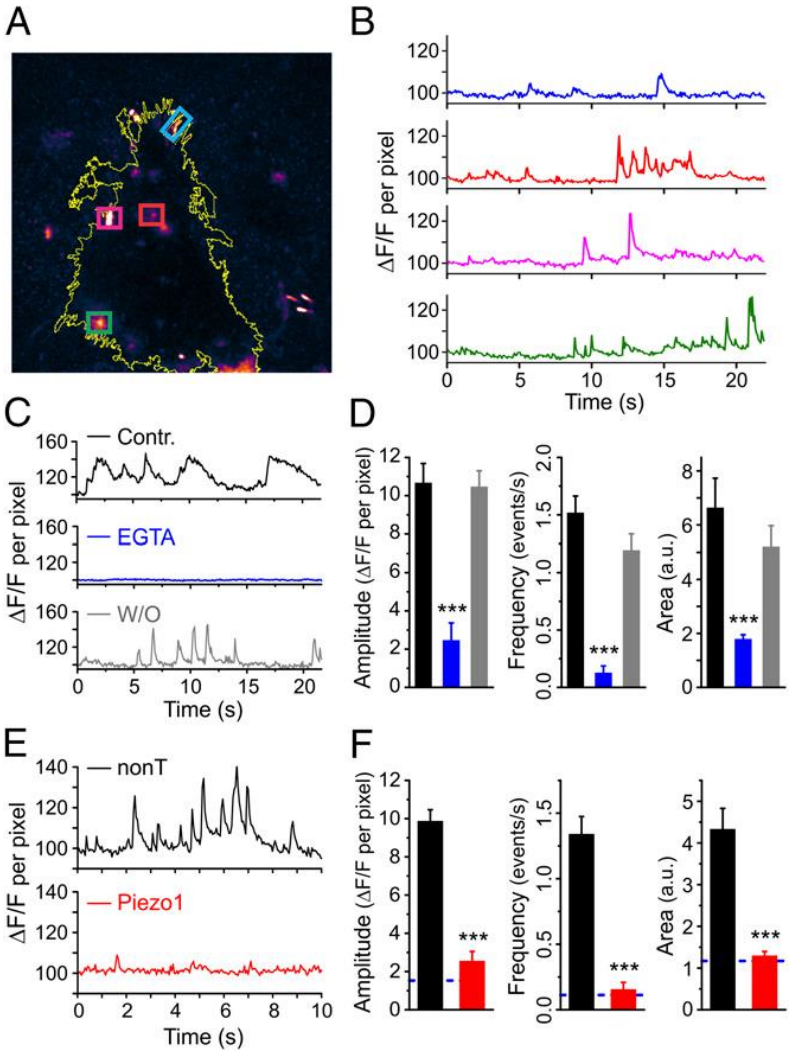

Figure 3.3 Piezo1 activity elicits spontaneous Ca^{2+} signals. (a) A maximum projection TIRFM image an hNSPC cell loaded with Fluo4-AM from a 600-frame video showing hotspots of Ca^{2+} activity. Four regions of interest (ROI) are marked by colored boxes. Yellow line depicts the outline of the cell. See also Supplementary Movie 1. (b) Plots of fluorescence intensity over time of the hotspots highlighted in panel A. Color of the traces matches the corresponding box color in panel A. Data are shown as signal/pixel with the fluorescence intensity at the start of the recording normalized to 100 (see Methods). (c,d) Spontaneous Ca^{2+} transients are reversibly inhibited by addition of 6 mM EGTA to the bath solution. n = 22 for Control, 28 for EGTA and 27 for Wash. (e,f) hNSPC transfected with Piezo1 siRNA show fewer and smaller spontaneous Ca^{2+} transients than cells transfected with non-targeting siRNA. Blue line in panel f represents levels expected in the absence of external calcium (based on Fig. 3.3d). n = 44 for non-targeting siRNA and 53 for Piezo1 siRNA. Error bars represent SEM. *p< 0.05, **p < 0.01, ***p < 0.001 by two-sample t-test.

To test whether spontaneous Ca^{2+} transients arise from Piezo1 activity we examined the effect of Piezo1 knockdown on spontaneous Ca^{2+} transients. Cells transfected with Piezo1

siRNA showed a strong reduction in Ca^{2+} transients compared to control-transfected cells, as evidenced by analysis of amplitude and frequency of events, as well as the area under the curve (Fig. 3.3e, f). The residual calcium signals measured in Piezo1 knockdown cells were of similar magnitude to those measured in EGTA-treated cells. Significant reduction in spontaneous Ca^{2+} transients was also obtained with extracellular application of the SAC inhibitor GsMTx-4 (Fig. 3.S4). Taken together, these observations carried out in the absence of an externally applied mechanical force indicate that Piezo1 activity generates spontaneous Ca^{2+} transients in hNSPCs.

3.3.4 Piezo1 is activated by traction forces

Traction forces allow cells to actively sense the stiffness, geometry and topography of their environment, and play an important role in cell adhesion, migration, extracellular matrix reorganization and differentiation[39]. These forces are generated in an ATP-dependent process by non-muscle myosin II along actin fibers, and are transmitted to the substrate through focal adhesion zones. Blebbistatin is known to specifically inhibit myosin II[40] and as a result, traction forces[7]. To determine whether Piezo1 is activated by traction forces, we examined whether blebbistatin inhibits the spontaneous Ca^{2+} transients generated by it. We found that blebbistatin treatment abolishes spontaneous Ca^{2+} transients to a similar extent as EGTA (Fig. 3.4a, b). These results indicate that Piezo1 can be activated by cell-generated forces such as traction forces, without application of an external mechanical force.

Since traction forces are known to vary with substrate stiffness, an important modulator of differentiation in several different stem cell types[7, 8], we asked whether Piezo1 activity varies with substrate stiffness. We performed TIRFM imaging of spontaneous Ca^{2+} transients of hNSPCs grown on high-refractive index Qgel silicone elastomers of varying stiffness[41], fabricated as described in the Methods section. We found that spontaneous Ca^{2+} activity scaled

with substrate stiffness, with minimal or no transients on soft substrates (0.4 and 0.7 kPa) and increasing activity on stiffer substrates (3.7 kPa and 750 kPa and glass) (Fig. 3.4c, d). Thus, Piezo1 activity varies with substrate stiffness.

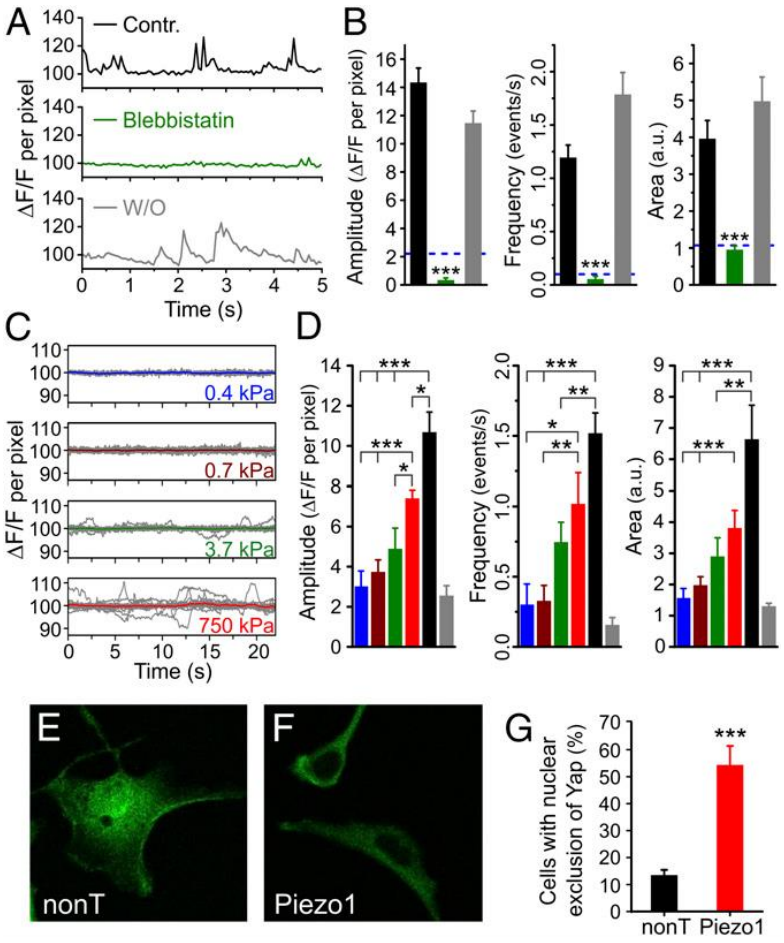

Figure 3.4. Piezo1 activity is linked to traction forces, substrate stiffness, and Yap localization. (a, b) Spontaneous Ca^{2+} transients are reversibly inhibited by the traction force inhibitor, blebbistatin (50 μM), which acts by blocking the ATPase activity of myosin II. n = 57 for control, 49 for blebbistatin; 28 for washout. Blue line in panel B represents levels expected in the absence of external calcium (based on Fig. 3.3d). (c,d) Spontaneous Ca^{2+} transients measured from hNSPCs grown on high-refractive index silicone elastomers scale with substrate stiffness. n = 14 for 0.4 kPa, 26 for 0.7 kPa, 15 for 3.7 kPa, 14 for 750 kPa and 22 for glass. Colors of columns in panel d are matched to the traces in panel c:*blue*, 0.4 kPa; *brown*, 0.7 kPa; *green*, 3.7 kPa; *red*, 750 kPa; *black*, Glass; *gray*, data from Piezo1 siRNA-transfected cells from Fig. 3.3f (reproduced for comparison). (e-g) hNSPCs grown on glass coverslips show nuclear exclusion of Yap at a higher frequency when transfected with Piezo1 siRNA as compared to non-targeting siRNA. Error bars represent SEM. *p< 0.05, **p < 0.01, ***p < 0.001 by two-sample t-test.

3.3.5 Piezo1 knockdown evokes nuclear exclusion of the mechanoreactive transcriptional co-activator, Yap

Since Piezo1 activity varies with substrate stiffness, we asked whether it affects a molecule known to relay substrate stiffness information to the nucleus. The transcriptional co-activators, Yap (Yes-associated protein) and Taz (transcriptional coactivator with PDZ-binding motif, a.k.a. WWTR1) were first identified as part of the Hippo pathway that controls organ size[42]. Recent findings in epithelial cells and in mesenchymal stem cells show that Yap and Taz localize to the nucleus on stiff substrates, while on soft substrates they are shuttled to the cytoplasm[13]. The same study also showed that Yap and Taz influence mechanosensitive lineage specification in mesenchymal stem cells. The molecular mechanism by which matrix stiffness regulates Yap/Taz localization remains unknown.

We first examined Yap localization in hNSPCs on soft (0.7 kPa) and stiff (750 kPa) substrates using immunostaining. As seen for other cell types, hNSPCs grown on soft substrates display exclusion of the Yap protein from the nucleus (Fig. 3.S5). Next, we examined Yap localization in hNSPCs grown on glass coverslips and transfected with either non-targeting or Piezo1 siRNA. Glass has stiffness in the GPa range, where Yap is expected to localize to the nucleus. We observed that cells transfected with Piezo1 siRNA displayed nuclear exclusion to a greater frequency than cells transfected with non-targeting siRNA. This suggests that Piezo1 knockdown can override the mechanical cue for localizing Yap to the nucleus, and that Yap could be a downstream effector of Piezo1 activity.

3.3.6 Effect of substrate stiffness on hNSPC differentiation

Earlier studies on rodent neural stem cells have shown the importance of matrix elasticity in lineage specification[8, 16, 17]. However, the effect of substrate stiffness on hNSPC differentiation

has not been previously investigated. When we differentiated hNSPCs on substrates of different stiffness (0.7 kPa vs. 750 kPa), we observed a greater number of MAP2-positive neuronal cells on the stiffer substrate (Fig. 3.S6). In rodent neural stem cells, substrate stiffness was found to have the opposite effect, with soft substrates (<1 kPa) supporting more neurogenesis than stiffer substrates (>5 kPa)[8, 16, 17]. Since we performed our differentiation assays on Qgel-based substrates, while earlier studies used polyacrylamide or methacrylamide chitosan as supporting material[8, 16, 17], we wondered whether this difference could be responsible for the discrepant results. However, when we differentiated rat adult hippocampal neural stem cells (rahNSCs, which generated more neurons on soft polyacrylamide substrates[17]) on Qgels (0.7 kPa vs. 750 kPa), we similarly observed more neurogenesis on softer substrates (Fig. 3.S7). Hence, we conclude that the difference in mechanosensitive differentiation between hNSPCs and rahNSCs is likely due to the different origin of the two types of cells (human vs. rat, fetal vs. adult, cortical vs. hippocampal).

3.3.7 Piezo1 directs neuronal-glial lineage choice of hNSPCs

The results presented in Fig. 3.4 show that Piezo1-mediated Ca^{2+} transients increase on stiffer substrates. We also found that stiffer substrates favor neuronal differentiation of hNSPCs (Fig. 3.S6). Hence, we asked whether Piezo1 activity influences hNSPC lineage choice. We used two different approaches in testing this. We first determined whether pharmacological inhibition of Piezo1 by extracellular application of GsMTx-4 alters hNSPC lineage choice. hNSPCs were differentiated in the presence and absence of extracellular GsMTx-4 and differentiation was assayed using Map2 and Dcx as neuronal markers and GFAP as astrocytic marker (see Methods). In the presence of GsMTx-4, SC23 hNSPCs showed an increase in astrocyte formation, as evidenced by the percentage of GFAP-positive cells, from 48.2 ± 2.9 to 63.5 ± 2.7

(35% increase relative to control)(Fig. 3.5a). We showed earlier that SC27 hNSPCs generate neurons at higher percentages than SC23s[21]; hence tests on neurogenesis were performed with the SC27 hNSPCs. These hNSPCs showed a reduction in neuron formation from 6.4 ± 0.3 to 2.8 ± 0.3 (54% decrease relative to control) when differentiated in the presence of GsMTx-4, as evidenced by the percentage of Map2-positive cells (Fig. 5B). Similar results were also obtained for Dcx-positive cells (Fig. 3.S8). Thus, pharmacological inhibition of SACs appears to promote astrocyte formation and reduce neuron formation.

To determine whether this effect on lineage choice specifically involved Piezo1 we examined differentiation in the context of siRNA-mediated knockdown of Piezo1. SC27 hNSPCs were transfected with either Piezo1 siRNA or non-targeting siRNA and differentiated into neurons or astrocytes after allowing 24 hours for siRNA action. qRT-PCR analysis indicated that Piezo1 knockdown is 78-86% at 1-4 days post transfection and 71% at 7 days. Immunological analysis of the differentiated progeny showed that Piezo1 knockdown increased astrocyte formation from 9.8 ± 0.5 to 14.2 ± 0.7 (48% increase relative to control) (Fig. 3.5c), while reducing neuron formation from 5.2 ± 0.3 to 3.2 ± 0.3 (42% decrease relative to control) (Fig. 3.5d, Fig. 3.S9). SC23 hNSPCs also showed an increase in astrogenesis with Piezo1 knockdown (Fig. 3.S10). These results recapitulate the effect of pharmacological SAC inhibition on lineage choice and demonstrate that Piezo1 activity is involved in neuronal-glial specification of hNSPCs.

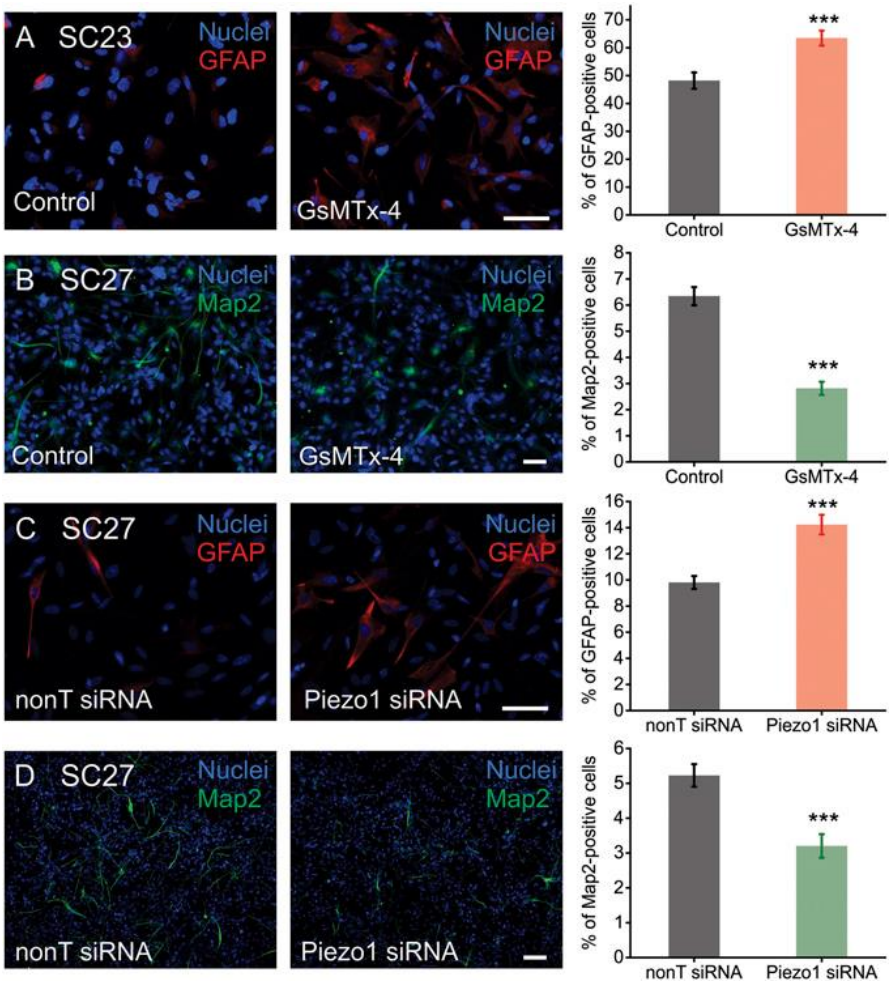

Figure 3.5. Piezo1 directs neuronal-glial lineage choice in human neural stem cells. (a) SC23 hNSPCs display an increase in astrogenesis (GFAP-positive cells) in the presence of 5 □M free GsMTx-4 (see Methods). n = 3 independent experiments. (b) SC27 hNSPCs display a reduction in the percentage of Map2-positive cells when differentiated in the presence of 5 □M free GsMTx-4. n = 4 biological repeats from three independent experiments. (c) SC27 hNSPCs transfected with 20 nM Piezo1 siRNA differentiate into astrocytes at a higher efficiency than SC27 hNSPCs transfected with 20 nM control non-targeting siRNA. n = 3 biological repeats from 2 independent transfection experiments. (d) SC27 hNSPCs transfected with 20 nM Piezo1 siRNA show a reduction in neurogenesis compared to cells transfected with 20 nM control non-targeting siRNA. n = 3 biological repeats from two independent transfection experiments. Scale bar = 20 um. ***$p < 0.001$ with two-sample t-test. See also Fig. 3.S8-3.S10.

3.4 DISCUSSION

Matrix mechanics is a strong determinant of stem cell behavior with important implications for regenerative medicine and stem cell therapy. Using a multi-disciplinary approach, we have uncovered a new molecular player, the SAC Piezo1, which detects matrix

mechanics and directs lineage specification of hNSPCs. The Piezo1 protein was discovered recently and shown to be the pore-forming subunit of a nonspecific cation channel that is intrinsically gated by membrane tension[31, 32]. Recent studies demonstrate a role for Piezo1 in regulating erythrocyte volume[43], epithelial crowding and homeostasis[36], cell migration[44] and detection of blood flow[33, 34]. Our results suggest a new role for Piezo1 in detecting matrix elasticity and determining lineage choice. In addition, we find that Piezo1 activation can be triggered by cell-generated forces in the absence of an external mechanical force, thus bringing to light a new way to regulate Piezo1 gating.

Piezo1 is also identified in public gene expression databases from human embryonic stem (hES) cells[45], mesenchymal stem cells[46] and neural stem cells[47, 48]. Of particular interest, van de Leemput *et al.* (2014) differentiated hES cells into brain organoids to study gene expression changes accompanying human corticogenesis. Their RNA-seq database (http://cortecon.neuralsci.org) shows Piezo1 expression throughout the differentiation process. Temporal analysis of Piezo1 expression especially correlated with the periods of pluripotency (day 0 of the differentiation protocol) and of upper layer neuron generation during corticogenesis (day 63 onwards). These findings are consistent with our observations in fetal, cortical hNSPCs that Piezo1 activity supports neuron formation.

Identification of mechanosensors and transducers involved in stem cell fate has been an area of intense investigation since the discovery that mechanical cues can direct differentiation outcomes. Most of the molecules discovered to date are cytoskeletal proteins such as myosin II[7], Rho/ROCK system[8, 10], vinculin[11]. While cytoskeletal proteins and cellular contractility regulators are essential for generating traction forces and sensing environmental mechanics, molecular mechanisms connecting these signaling molecules to intracellular pathways that

influence differentiation have remained elusive. Spontaneous and evoked Ca^{2+} transients are known to regulate gene expression and differentiation in several types of stem cells (for recent reviews of Ca^{2+} signaling in stem cells see[14, 15]). In this context, a stretch-activated ion channel that is activated by traction forces and elicits Ca^{2+} influx is an attractive candidate for transducing mechanosensitive lineage specification. Supporting this role for Piezo1, we find that stiff substrates increase Piezo1 activity and favor neuronal specification of hNSPCs, while inhibition of Piezo1, either by genetic knockdown or by pharmacological inhibition, has the opposite effect and reduces neuronal specification (Figs. 3.S6 and 3.5).

We also find that Piezo1 activity influences nucleo-cytoplasmic localization of the mechano-reactive transcriptional co-activator Yap. Yap and its partner Taz have been studied in mesenchymal stem cells, where their nucleo-cytoplasmic localization governs lineage choice[13]. However, similar roles of Yap and Taz in neural stem cells have not been yet investigated. Our observations lay the foundation for further mechanistic elucidation of the Piezo1-Yap/Taz connection in the context of hNSPC differentiation.

The identification of an ion channel involved in mechanosensitive lineage specification of neural stem cells raises the question of whether Piezo1 may play a similar role in other multipotent stem cells. Interestingly, mesenchymal stem cells, which also display strongly mechanosensitive differentiation, express Piezo1 as well (Fig. 3.S11), suggesting that Piezo1 could have a similar role in multiple types of stem cells.

The role of Piezo1 in lineage specification has potential therapeutic implications for neural stem cell transplant therapy. One of the bottle-necks of this therapeutic approach, which is currently under investigation for the treatment of neurological disorders such as Alzheimer's disease, Parkinson’s disease, stroke, and spinal cord injury, is directing cell fate after injection.

Pharmacological agents aimed at modulating Piezo1 activity may be useful in directing lineage choice during neural stem cell transplant therapy.

In conclusion, we propose that myosin-II-dependent traction forces involved in the detection of matrix elasticity generate local membrane tension that triggers the activation of Piezo1. Channel activation results in transient Ca^{2+} influx through the plasma membrane, nuclear localization of Yap, and altered neuronal-glial specification of hNSPCs (Fig. 3.S12). Our findings point to Piezo1 as an important determinant of mechanosensitive lineage choice in neural stem cells and possibly other multipotent stem cells, providing a link between extracellular matrix mechanics and intracellular signaling pathways. Future work will determine the mechanism by which Piezo1 activity regulates mechanosensitive lineage commitment in the stem cell niche and how these results translate to the *in vivo* environment.

3.5 MATERIALS AND METHODS

Patch clamp measurements, TIRFM Ca^{2+} imaging, differentiation assays were performed on two brain-derived human fetal hNSPC cultures (SC23 and SC27) isolated from the cerebral cortices of two separate fetuses of 23 weeks gestational age[18-21]. Further details on cell culture conditions, siRNA knockdown experiments, electrophysiological measurements, calcium imaging, Qgel substrate fabrication and data analysis are presented below.

Ethics statement

Informed written consent was obtained for all human subjects, and all human cell research involves cells with no patient identifiers and has been approved by the University of California, Irvine Institutional Review Board and Human Stem Cell Research Oversight Committee.

Human neural stem/progenitor cell culture

Two brain-derived human fetal neural stem/progenitor cell (hNSPC) cultures (SC23 and SC27) were isolated from the cerebral cortices of two separate fetuses of 23 weeks gestational age and maintained as previously described [20, 21]. Briefly, undifferentiated cells were grown as adherent cultures on fibronectin (Fisher Scientific, Pittsburgh PA) coated flasks in basal medium containing DMEM/F12 (Invitrogen, Carlsbad CA), 20% (v/v) BIT-9500 (Stem Cell Technologies, Vancouver BC), 1% (v/v) antibiotic/antimycotic (Invitrogen, Carlsbad CA), supplemented with the following growth factors: 40 ng/ml EGF (BD Biosciences, Bedford MA), 40 ng/ml FGF (BD Biosciences, Bedford MA), and 40 ng/ml PDGF (Peprotech, Rocky Hill NJ). hNSPCs were passaged approximately every 7 days using Cell Dissociation Buffer (Invitrogen, Carlsbad CA) and split 1:2. Cells were used at passages P10-20.

For neuronal differentiation, hNSPCs were plated on laminin (Invitrogen, Carlsbad CA) coated coverslips [20, 21] in 1:1 basal medium and Neurobasal medium (Invitrogen, Carlsbad CA) supplemented with 1× B27 (Invitrogen, Carlsbad CA), 1% heat inactivated fetal bovine serum (Invitrogen, Carlsbad CA), 20 ng/ml BDNF (Peprotech, Rocky Hill NJ), 20 ng/ml NT3 (Peprotech, Rocky Hill NJ), 2.5 ng/ml FGF (BD Biosciences, Bedford, MA), and 0.1 μM retinoic acid (Sigma, St. Louis MO) for 14 days. To induce astrocyte differentiation, hNSPCs on laminin-coated coverslips were incubated in DMEM/F12 (Invitrogen, Carlsbad CA), 20% (v/v) heat-inactivated FBS (Invitrogen, Carlsbad CA) and 1% (v/v) antibiotic-antimycotic (Invitrogen, Carlsbad CA) for 5-7 days.

For differentiation experiments in which GsMTx-4 (Peptide International Inc, Louisville KY) was added to cell culture media, we adjusted the peptide concentration to account for sequestration by serum proteins. The concentration of free GsMTx-4 was previously shown to be

reduced 20-fold per 10% increase in serum concentration [49]. Based on the amount of serum proteins in our neuronal differentiation medium and astrocyte differentiation medium, we used 100 mM and 200 mM GsMTx-4 respectively, which affords 5 mM free peptide. Concentrations in the text refer to free concentrations. Media was replaced every 12 hours to replenish any peptide lost due to hydrolysis.

For differentiation experiments that involved Piezo1 knockdown, hNSPCs were transfected with 20 nM Piezo1 or non-targeting siRNA as described below. After allowing 24 hours for siRNA action, the proliferation medium was replaced by the specified differentiation medium. Differentiation and assessment of differentiated progeny were performed as described. While siRNA effects are expected to be reduced with cell division, differentiation involves an integration of signals over time and may reflect the effect of the initial gene knockdown. In addition, neurons are post-mitotic once committed, reducing siRNA dilution effects. qRT-PCR analysis indicated that Piezo1 knockdown is 82-86% at 2-4 days post transfection and 71% at 7 days.

Culture of adult rat hippocampal neural stem cells.

Adult rat hippocampal neural stem cells were a kind gift from Dr. David V. Schaffer, UC Berkeley, and were cultured as per protocols published from the Schaffer lab (ref Peltier et al 2010). Differentiation on Qgel substrates (see section "Preparation of high-refractive index substrates of varying stiffness" for details) utilized mixed differentiation conditions (1 μM RA, 1% (v/v) FBS, 1% N-2 in DMEM/F-12).

Electrophysiology

Patch-clamp experiments were performed in standard whole-cell or cell-attached configurations using an Axopatch 200B amplifier (Molecular Devices, Sunnyvale CA). Currents

were filtered at 5 kHz and sampled at 20 kHz. All experiments were performed at room temperature. Leak subtraction was performed off-line.

For whole-cell patch clamp, pipettes were pulled from standard-walled borosilicate glass capillaries (Warner Instruments, Hamden CT) and filled with an internal solution consisting of (in mM) 137 KCl, 9 NaCl, 1 $MgCl_2$, 5 EGTA, 0.4 GTP, 10 HEPES, pH 7.3 with KOH. The extracellular solution consisted of (in mM) 148 NaCl, 2 $MgCl_2$, 3 KCl, 3 $CaCl_2$, 8 glucose, 10 HEPES, pH 7.3 with NaOH. In these solutions pipettes had a resistance of 2-3 MΩ.

For cell attached recordings, pipettes prepared from thin-walled borosilicate glass capillaries (Warner Instruments, Hamden CT) were filled with a solution consisting of (in mM) 130 NaCl, 5 KCl, 10 HEPES, 1 $CaCl_2$, 1 $MgCl_2$, 10 TEA-Cl (pH 7.3 with NaOH). An external solution comprising of (in mM) 140 KCl, 10 HEPES, 1 $MgCl_2$, 10 glucose (pH 7.3 with KOH) was used to zero the membrane potential. Pipettes had a resistance of 0.6-0.9 MΩ in these solutions.

Effect of GsMTx-4 on stretch-activated currents was examined in cell-attached patch clamp mode with either 10 mM or 100 mM GsMTx-4 in the bath and pipette solutions.

Mechanical stimulation

Mechanical stimulation in whole-cell recordings was performed using a fire-polished glass pipette positioned at an angle of 60° to the cell being recorded. The glass probe was mounted on a piezoelectric stack (P-841.10, Physik Instrumente, Irvine CA) driven by a controller (E-625.SR Physik Instrumente, Irvine CA) controlled via Clampex (Molecular Devices, Sunnyvale, CA). The tip of probe was typically positioned about 1.5 μm from the cell. The probe had a velocity of 0.4 μm/ms during stimulus onset and offset and was moved in steps

of 0.4 μm increment every 20s to allow for recovery of mechanosensitive currents. Membrane potential was held at -80 mV.

Mechanical stimulation during cell-attached recordings utilized a high-speed pressure clamp, HSPC-1 from ALA Scientific (Farmingdale, NY), controlled by Clampex. Suction pulses were administered to the membrane patch through the patch pipette connected to the HSPC-1. Membrane potential was held at -80 mV. Normalized current-pressure relationships were fitted with a Boltzmann equation of the form: $I(P) = 1/[1 + \exp(-(P-P_{50})/s)]$, where I is the peak of the stretch-activated current at pressure P, P_{50} is pressure that elicits 50% of the maximal current and s is slope, a measure of the channel's sensitivity to pressure. For I-V analysis, voltage steps were applied from a holding potential of -80mV, 250 ms before a pressure pulse of 100 ms duration.

Quantitative real-time polymerase chain reaction (qRT-PCR)

hNSPC total RNA was isolated using Aurum total RNA isolation kit (Bio-Rad Laboratories, Hercules, CA). RNA from adult human bone marrow mesenchymal stem cells was purchased from ScienCell Research Laboratories (Carlsbad, CA) and human lung RNA was purchased from Ambion (Life Technologies, Grand Island, NY). Complementary DNA (cDNA) was synthesized using M-MLV reverse transcriptase from Promega (Madison WI) in a S100 Thermal Cycler (BioRAd, Hercules CA). The enzyme was heat inactivated at 95°C for 5 min and cDNA was used in qRT-PCR assays. qRT-PCR was performed with an ABI Viia7 using TaqMan probe-based gene expression assays and Taqman universal PCR master mix (Applied Biosystems, Grand Island NY). Data was collected using Applied Biosystems ViiA 7 software v 1.2 and analyzed by comparative C_T method using 18S to normalize C_T values. Gene expression assays included human Piezo1 (Hs00207230), Piezo2 (Hs00401026), GAPDH (Hs02758991) and 18S (Hs03928985), all from Life Technologies (Grand Island NY).

siRNA knockdown

siRNA experiments used On-TARGETplus siRNA pools (Thermo Scientific, Pittsburgh PA) that utilize a dual-strand modification pattern to effectively reduce off-target effects and enhance specificity towards the target gene. siGlo red fluorescent transfection marker (Thermo Scientific, Pittsburgh PA) was used to identify transfected cells. Total siRNA concentrations for transfection experiments were 20 nM for Piezo1, 25 nM for GAPDH and 20 nM of non-targeting control siRNA. 20 nM of siGlo was co-transfected along with the siRNA. The sequences in the Piezo1 siRNA pool were: GCAGCAUGACAGACGACAU, UGGGUAUGCCAACGAGAA, UGGCUGAUGUUGUCGACUU, GCGCAUCAGUCAUCGUUUU. The sequences in the pool of non-targeting control siRNA were: UGGUUUACAUGUCGACUAA, UGGUUUACAUGUUGUGUGA, UGGUUUACAUGUUUUCUGA, UGGUUUACAUGUUUUCCUA and the sequences in the GAPDH siRNA pool were: GUCAACGGAUUUGGUCGUA, CAACGGAUUUGGUCGUAUU, GACCUCAACUACAUGGUUU, UGGUUUACAUGUUCCAAUA. siRNA was introduced into cells using 1ul/ml Dharmafect 1 transfection reagent (Thermo Scientific, Pittsburgh PA) as per manufacturer's instructions. Knockdown was assessed by qRT-PCR for every transfection experiment.

TIRFM imaging of spontaneous Ca^{2+} transients

We used an Olympus IX71 microscope equipped with an Ixon EMCCD camera (Andor, Windsor, CT) a 488 nm solid-state laser (Melles Griot, Rochester NY) and an Olympus 100x, 1.49 numerical aperture objective lens. Images were taken with an exposure time of 0.04081 seconds at 13.7 Hz. Cells were loaded with 1 μM Fluo-4/AM in phenol red-free DMEM/F12 (Invitrogen, Carlsbad CA) for 10 min at 37°C, washed 3 times, incubated at 37C for 10-15 min

to allow cleavage of the AM ester and then imaged. Imaging was performed at room temperature in a bath solution comprising 148 mM NaCl, 3 mM KCl, 3 mM $CaCl_2$, 2 mM $MgCl_2$, 8 mM glucose, 10 mM HEPES, pH adjusted to 7.3 with NaOH. Experiments designed for testing the effect of extracellular Ca^{2+} chelation included 6 mM ethylene glycol tetraacetic acid (EGTA) in the bath solution. When testing the effect of GsMTx-4 on Ca^{2+} dynamics with TIRFM, we found that it took several minutes for the 34-amino acid peptide, to diffuse under the cell. Hence we performed these measurements on hNSPCs that had been plated in medium containing 100 mM GsMTx-4 and the peptide was maintained throughout Fluo4-AM labeling and imaging. hNSPCs from parallel wells plated in medium without GsMTx-4 were used as controls. SC23 and SC27 hNSPCs behaved similarly under all the conditions reported. Fluorescence signals are reported as a ratio ($\Delta F/F$) of the mean change in fluorescence (ΔF) at each pixel in a region of interest relative to the baseline fluorescence (F) obtained from the first 10 frames. Baseline fluorescence was normalized to 100.

We found that hNSPCs treated with transfection reagent or 50 mM blebbistatin (Cayman Chemicals, Ann Arbor MI) displayed photosensitivity as evidenced by an increase in global cytosolic Ca^{2+} over a period of seconds. Blebbistatin has been documented to compromise cell viability in widefield blue-light illumination over a time course of minutes (Mikulich, Juzenas 2012, Kolega 2004). Kolega (2004) found that blebbistatin's effect on cell health could be prevented by using lower illumination intensity. Hence we made the following experimental changes for TIRF imaging on siRNA-transfected and blebbistatin-treated cells: (i) reduced laser excitation intensity; (iii) reduced the duration of imaging to 100 frames (blebbistatin experiments) or 200 frames (siRNA experiments); (iv) reduced camera exposure time to 20 ms. Under these conditions we did not observe any evidence of photosensitivity.

Preparation of high-refractive index substrates of varying stiffness

To test Ca^{2+} dynamics on substrates of varying stiffness using TIRFM we used a high refractive index silicone elastomer, Qgel 920 from Quantum Silicones (Richmond, VA) as described by Gutierrez *et al.*[41]. Qgel 920 has a refractive index of 1.49 after curing. Parts A and B of Qgel 920 were mixed in varying proportions as per recipes from Gutierrez *et al.* for substrates of 0.4, 0.7 and 3.7 kPa stiffness, while the 750 kPa Qgel was made according to manufacturer instructions using parts A and B in a 1:1 ratio with a hardening additive 88104EX added to part B at 4% v/v (Quantum Silicones). After mixing the components of Qgel 920, the elastomer was coated on to 18 mm No. 1 cover slips using a spin coater (Chemat Scientific, Northridge CA) at 2000 rpm and then baked at 70°C for 2 hours. To functionalize the surface of the Qgel with fibronectin, the substrates were treated with 3-aminopropyl trimethoxysilane (Acros Organics, New Jersey NJ) for 1 minute, washed with methanol and then with distilled water. Fibronectin was covalently linked to the surface by incubating the substrates with 30µg/ml fibronectin and 100 µg/ml 1-Ethyl-3-(3-dimethylaminopropyl) carbodiimide (Acros Organics, New Jersey NJ) in phosphate-buffered saline, pH 7.4 for 30 min at room temperature. The substrates were washed several times with PBS and used within 2 days. Control experiments performed with fluorescently-labeled fibronectin indicated uniform distribution of fibronectin across substrates of different stiffnesses by this procedure. Substrates were stored at 4C until use. Qgels used in differentiation experiments were prepared as described above. Their surface was then funzionalized via crosslinking to laminin (30mg/ml).

Immunofluorescence staining

Neurons and astrocytes were generated by differentiating hNSPCs as described above (Human neural stem/progenitor cell culture) and detected by immunocytochemistry. Immunostaining was performed as previously described [20, 21] using the following antibodies: anti-doublecortin (C-18) polyclonal, 1:200 (Santa Cruz Biotechnology, Santa Cruz, CA); anti-GFAP (clone G5A) monoclonal, 1:200 (Sigma, St. Louis, MO); anti-MAP2 (microtubule-associated protein 2) (clone HM2) monoclonal, 1:200 (Sigma, St. Louis, MO). The secondary antibodies used were donkey anti-mouse Alexa-555, donkey anti-goat Alexa-488, at 1:200 (Molecular Probes/Invitrogen, Carlsbad, CA). Percentages of cells that differentiated into neurons or astrocytes were calculated from images of 3-5 randomly selected fields for each cell population; total cell number in a field was counted using nuclei stained by Hoechst 33342 (4 µg/ml in phosphate-buffered saline, Molecular Probes, Eugene, OR).

Quantitation of immunostained images

To automatically count the nuclei in each image we applied an extension of the "Finding Dots" computational imaging tool presented in[50, 51] i.e. an unsupervised machine learning algorithm that automatically extracts, or 'segments', all nuclei. Given each individual acquired image, the software outputs a segmentation mask of all the nuclei, along with the coordinates of the nuclei centers, without requiring any prior knowledge about the nuclei aside from the fact they have a brighter intensity when compared to their common background. Running Matlab on a standard desktop, each image, resized to have the longest side of 350 pixels, took approximately 75 seconds to be processed. Accuracy of the automatic counting was above 93%. Following automatic segmentation of nuclei, each image was manually inspected to correct any omissions or false positives.

Once we had the correct nuclei count and corresponding segmentation mask for each image, we computed the nuclei associated with astrocytes. This was done in two steps: first the astrocytes images were thresholded to obtain an approximate mask of the astrocyte staining. Second, we overlaid the astrocyte mask and the nuclei mask and computed the percentage of area overlap for each nucleus. For most experimental settings, nuclei that overlapped by more than 25% with astrocyte staining were labeled as astrocytes. This procedure was followed by a visual inspection of the images to correct any errors and to produce the final astrocyte count. Neuron counting was performed manually on blinded images. We only counted cells that stained positive for the specified neuronal marker and also extended processes at least 2x the length of the cell body. Quantitation of Yap localization was performed manually on blinded images.

Confocal imaging of Yap localization

hNSPCs immuno-stained by the anti-Yap (63.7) monoclonal, 1:200 dilution (Santa Cruz Biotechnology, Santa Cruz, CA) were imaged on a Zeiss LSM 700 confocal microscope with a Plan-Apochromat 20x objective with 0.8 numeric aperture. Alexa 488 secondary signals were imaged with 488 nm excitation and Hoechst nuclear stain was imaged with 405 nm excitation.

Data analysis

Image analysis was performed with ImageJ (US National Institutes of Health). All statistical tests were run in Origin 8 (OriginLab Corporation, Northamptom MA). Data in all figures are shown as mean ± SEM. Unless otherwise stated, statistical significance was evaluated using unpaired two-tailed Student's t-test for comparing difference between two samples. Significance values and sample sizes are reported for each analysis in the text or figure legends.

3.6 ACKNOWLEDGMENTS

We thank Dr. Stephen White for the use of his spin coater, Drs. Ian Parker and Joseph Dynes for advice with TIRF experiments, Ms. Lisa McDonnell for technical assistance, and Drs. Peter Donovan and Mathew Blurton-Jones for comments on the manuscript. This work was supported by a CORCL Award from UCI and NIH grant GM098973 to F.T., Undergraduate Research Opportunities Program funding to T.T., a seed grant from the UCI Center for Autism Research and Treatment to L.A.F. and F.T., and by NSF CAREER Award IOS-1254060, Grant UL1 TR000153 from NCRR and NCATS, and a gift by Pearl Tze Hosfiel and Keith Hosfiel to L.A.F. This work was made possible, in part, through access to the Optical Biology Shared Resource of the Cancer Center Support Grant (CA-62203) at the UCI. We are also grateful for the support received from the Sue & Bill Gross Stem Cell Research Center at UCI. M.M.P. was supported in part by a postdoctoral research fellowship from the Helen Hay Whitney Foundation.

3.7 SUPPLEMENTAL MATERIAL

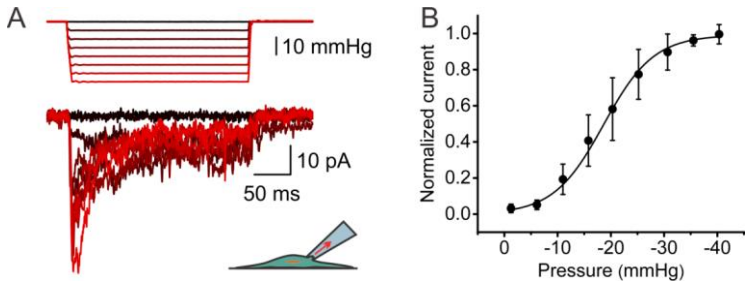

Figure 3.S1. (a) Representative currents induced by negative pipette pressure (0 to -35 mm Hg, Δ 5 mm Hg) administered by a pressure clamp in an SC23 hNSPC cell. *Inset*, schematics of patch clamp configuration. (b) Normalized current-pressure relationship of stretch-activated currents at a holding potential of −80 mV fitted with a Boltzmann equation with P_{50} = -18.6mmHg, s = 4.7 mmHg (n = 5 cells, mean ± SEM).

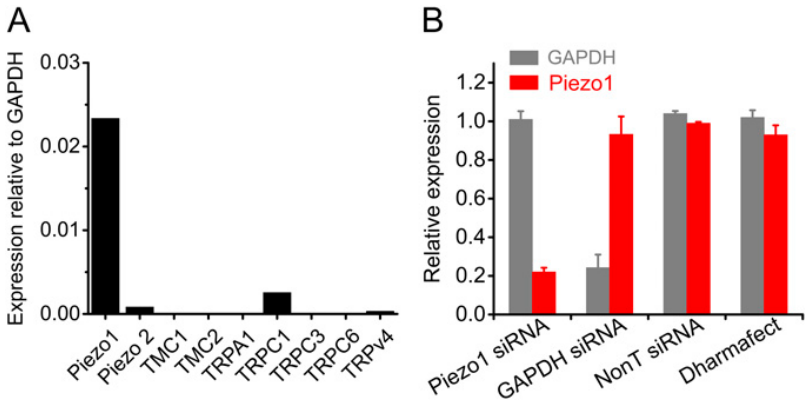

Figure 3.S2. (a) Determination of expression levels of known mechanosensitive channels in SC27 hNSPCs by qRT-PCR. (b) hNSPCs transfected with Piezo1 siRNA, GAPDH siRNA, or nontargetting control (nonT) siRNA or treated with DharmaFECT reagent alone were assayed by qRT-PCR for Piezo1 and GAPDH transcript levels using 18S as a reference gene. Piezo1 and GAPDH transcript levels were reduced only when transfected by the corresponding siRNA and not in response to nontargeting control siRNA or transfection reagent alone. Errors bars represent SEM. N=10 for Piezo1 siRNA and nontargeting control siRNA; n=3 for GAPDH siRNA; and n=7 for DharmaFECT.

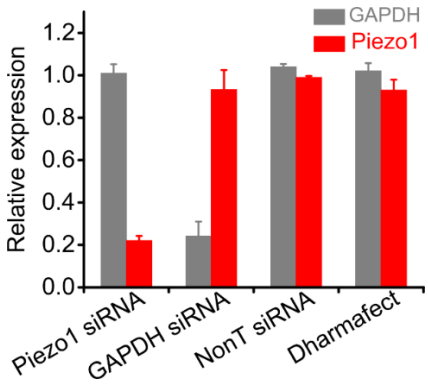

Figure 3.S3. hNSPCs transfected with GAPDH siRNA, non-targeting control siRNA or treated with Dharmafect reagent alone were assayed by qRT-PCR for Piezo1 and GAPDH transcript levels using 18S as a reference gene. Piezo1 and GAPDH transcript levels were only reduced when transfected by the corresponding siRNA, and not in response to non-targeting control siRNA or transfection reagent alone. Data are Mean ± SEM. n = 10 for Piezo1 siRNA and nonT siRNA, n = 3 for GAPDH siRNA and n = 7 for Dharmafect.

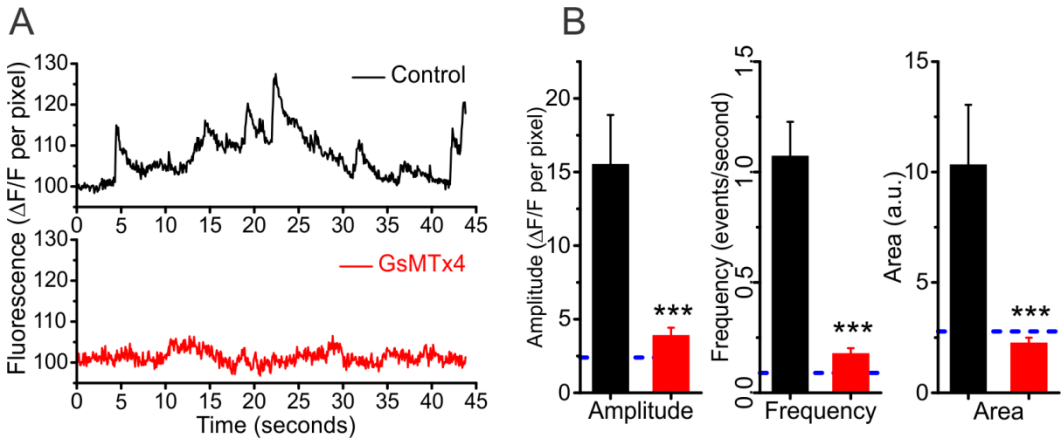

Figure 3.S4. (a, b) hNSPC show fewer and smaller spontaneous Ca^{2+} transients in the presence of 100 μM extracellular GsMTx-4 than cells in control conditions. Blue dotted lines in panel b represent levels expected in the absence of external calcium. n = 39 for control and 42 for GsMTx-4.

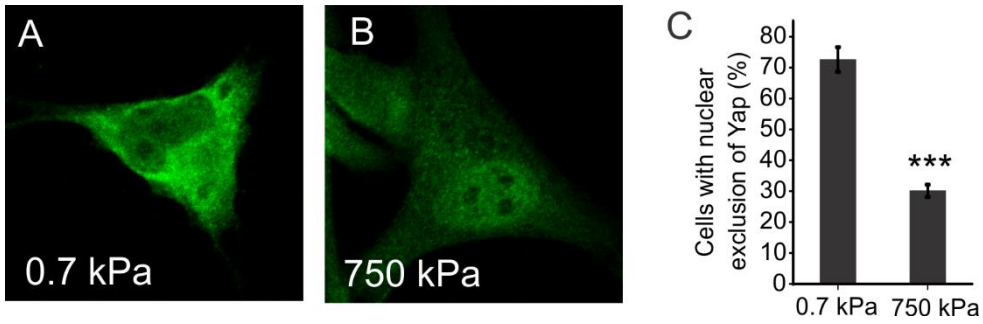

Figure 3.S5. hNSPCs grown on silicone elastomers of 0.7 kPa (a) display nuclear exclusion of Yap, while hNSPCs grown on 750 kPa (b) display Yap signal in the nucleus as well as the cytoplasm. Panel c shows the percentage of cells exhibiting nuclear exclusion on the two stiffnesses. ***$p < 0.001$.

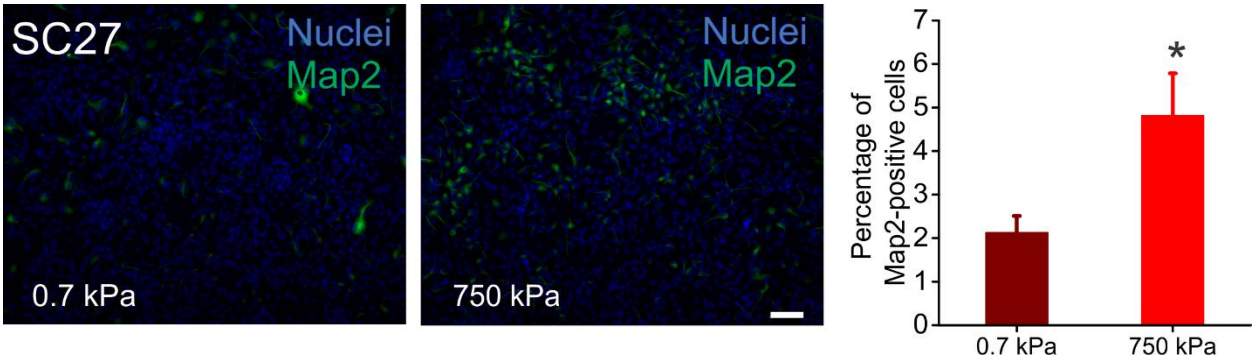

Figure 3.S6. SC27 hNSPCs show increased neurogenesis when differentiated on Qgel substrates of 0.7 kPa and 750 kPa stiffness and immune-stained for Map2. *$p < 0.05$ with two-sample t-test.

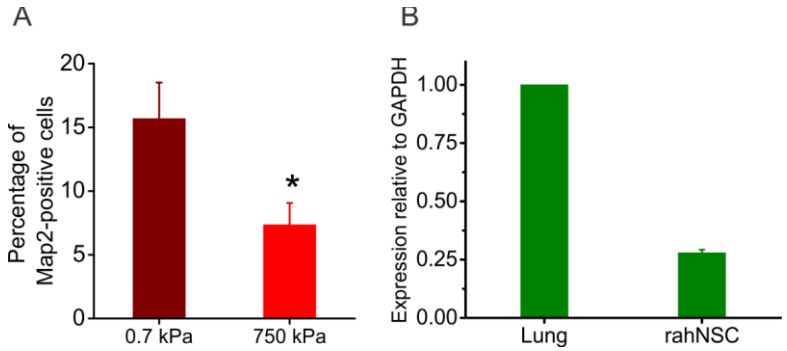

Figure 3.S7. (a) Adult rat hippocampal neural stem cells (rahNSCs) show reduced neurogenesis on stiffer (750 kPa) Qgel substrates than on softer (0.7 kPa) substrates when differentiated in mixed differentiation conditions and stained for the neuronal marker Map2. *$p < 0.05$ with two-sample t-test. (b) Expression of Piezo1 in rahNSCs determined by qRT-PCR from total RNA extracted from rahNSCs with 18S as the reference gene. Rat lung was used as the tissue calibrator by the $2^{-\Delta\Delta CT}$ method. Data are from two biological repeats. See Figs. 3.2a and 3.S10 for Piezo1 expression data in hNSPCs and human mesenchymal stem cells, respectively. Data are mean ± SEM.

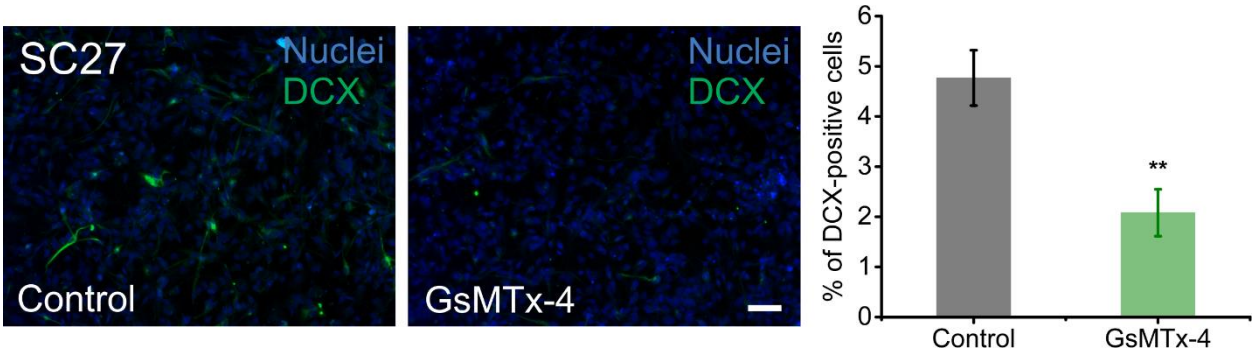

Figure 3.S8. SC27 hNSPCs display a reduction in the percentage of DCX-positive cells when differentiated in the presence of 5 μM free GsMTx-4. Scale bar = 20 μm. **p < 0.01 with two-sample t-test.

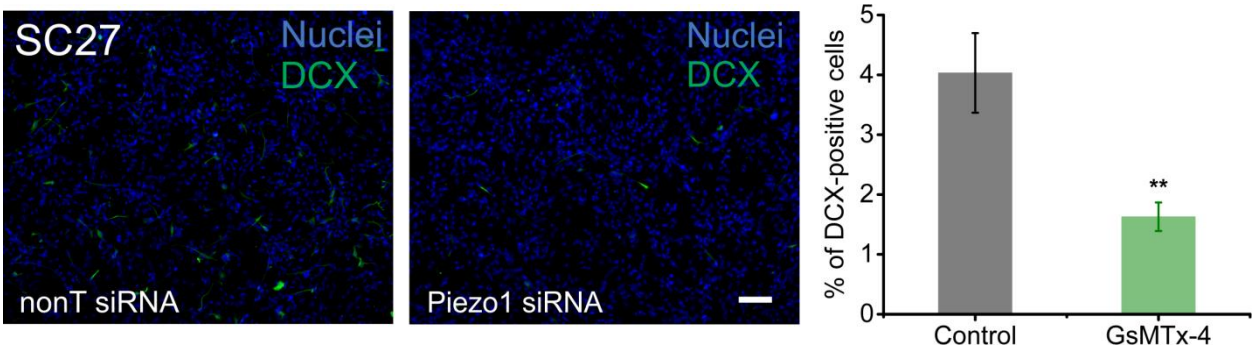

Figure 3.S9. SC27 hNSPCs transfected with 20 nM Piezo1 siRNA show a reduction in DCX-positive cells compared to hNSPCs transfected with 20 nM control non-targeting siRNA. Scale bar = 20 μm. **p < 0.01 with two-sample t-test.

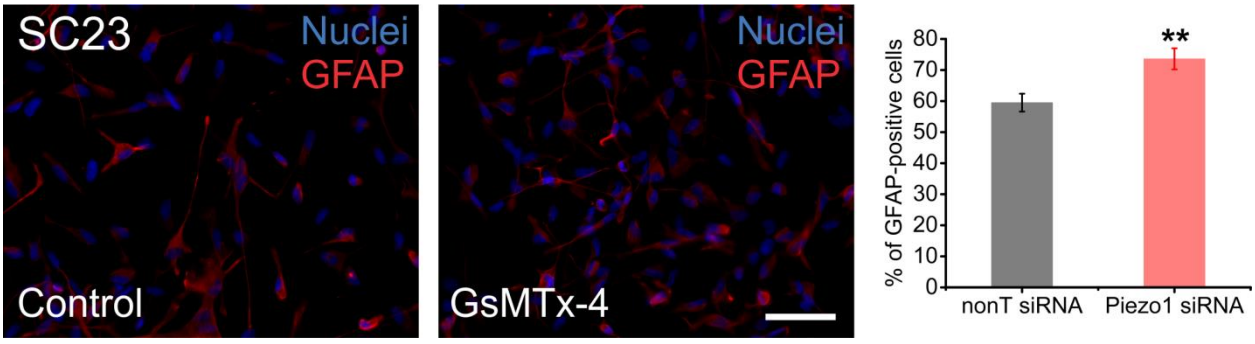

Figure 3.S10. SC23 hNSPCs transfected with 20 nM Piezo1 siRNA differentiate into astrocytes at a higher efficiency than SC23 hNSPCs transfected with 20 nM control non-targeting siRNA. n = 2 biological repeats. Scale bar = 20 μm. **p < 0.01

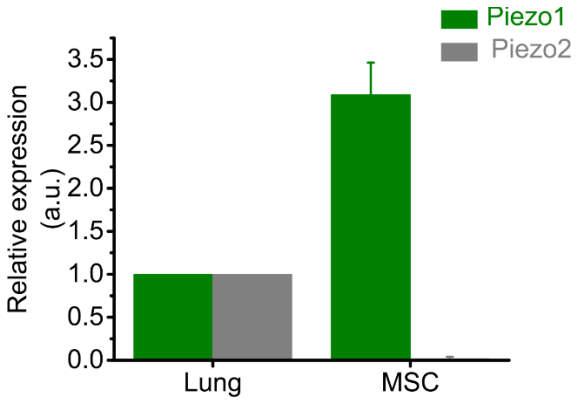

Figure 3.S11. Piezo1 transcripts are present in mesenchymal stem cells. mRNA expression profiles of *Piezo1* and *Piezo2* determined by qRT-PCR from total RNA extracted from adult human mesenchymal stem cells. 18S was used as the reference gene and human lung was used as the tissue calibrator. n = 4 technical repeats. Data are mean ± SEM.

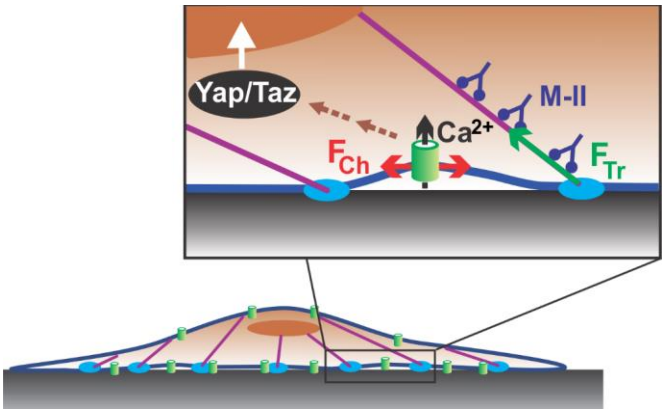

Figure 3.S12. Working model of Piezo1 activity in hNSPCs. Myosin-II-dependent traction forces generate local membrane tension that triggers the activation of Piezo1. Channel activation results in transient Ca^{2+} influx and, through a hitherto unknown mechanisms, in nuclear localization of Yap, and ultimately in altered neuronal-glial specification of hNSPCs. Piezo1 in green, myosin IIa molecules in dark blue (M-II), focal adhesion zones are shown in light blue, actin fibers in purple, and the nucleus in brown. F_{Tr} represents the traction force and F_{Ch} represents the force on Piezo1.

3.8 REFERENCES

1. Sun, Y., Chen, C. & Fu, J. Forcing stem cells to behave: a biophysical perspective of the cellular microenvironment. *Annual review of biophysics* **41**, 519-542 (2012).
2. Watt, F.M. & Huck, W.T. Role of the extracellular matrix in regulating stem cell fate. *Nature reviews. Molecular cell biology* **14**, 467-473 (2013).
3. Jones, D.L. & Wagers, A.J. No place like home: anatomy and function of the stem cell niche. *Nature reviews. Molecular cell biology* **9**, 11-21 (2008).
4. Tyler, W.J. The mechanobiology of brain function. *Nature reviews. Neuroscience* **13**, 867-878 (2012).
5. Yang, C., Tibbitt, M.W., Basta, L. & Anseth, K.S. Mechanical memory and dosing influence stem cell fate. *Nature materials* **13**, 645-652 (2014).
6. Gilbert, P. et al. Substrate elasticity regulates skeletal muscle stem cell self-renewal in culture. *Science (New York, N.Y.)* **329**, 1078-1081 (2010).
7. Engler, A., Sen, S., Sweeney, H. & Discher, D. Matrix elasticity directs stem cell lineage specification. *Cell* **126**, 677-689 (2006).
8. Keung, A., de Juan-Pardo, E., Schaffer, D. & Kumar, S. Rho GTPases mediate the mechanosensitive lineage commitment of neural stem cells. *Stem cells (Dayton, Ohio)* **29**, 1886-1897 (2011).
9. Kim, T.-J. et al. Substrate rigidity regulates Ca2+ oscillation via RhoA pathway in stem cells. *Journal of cellular physiology* **218**, 285-293 (2009).
10. McBeath, R., Pirone, D.M., Nelson, C.M., Bhadriraju, K. & Chen, C.S. Cell shape, cytoskeletal tension, and RhoA regulate stem cell lineage commitment. *Dev Cell* **6**, 483-495 (2004).
11. Holle, A. et al. In situ mechanotransduction via vinculin regulates stem cell differentiation. *Stem cells (Dayton, Ohio)* **31**, 2467-2477 (2013).
12. Swift, J. et al. Nuclear lamin-A scales with tissue stiffness and enhances matrix-directed differentiation. *Science (New York, N.Y.)* **341**, 1240104 (2013).
13. Dupont, S. et al. Role of YAP/TAZ in mechanotransduction. *Nature* **474**, 179-183 (2011).
14. Leclerc, C., Neant, I. & Moreau, M. The calcium: an early signal that initiates the formation of the nervous system during embryogenesis. *Frontiers in molecular neuroscience* **5**, 3 (2012).
15. Tonelli, F.M. et al. Stem cells and calcium signaling. *Advances in experimental medicine and biology* **740**, 891-916 (2012).
16. Leipzig, N. & Shoichet, M. The effect of substrate stiffness on adult neural stem cell behavior. *Biomaterials* **30**, 6867-6878 (2009).
17. Saha, K. et al. Substrate modulus directs neural stem cell behavior. *Biophysical journal* **95**, 4426-4438 (2008).
18. Palmer, T. et al. Cell culture. Progenitor cells from human brain after death. *Nature* **411**, 42-43 (2001).
19. Schwartz, P. et al. Isolation and characterization of neural progenitor cells from post-mortem human cortex. *Journal of neuroscience research* **74**, 838-851 (2003).
20. Flanagan, L., Rebaza, L., Derzic, S., Schwartz, P. & Monuki, E. Regulation of human neural precursor cells by laminin and integrins. *Journal of neuroscience research* **83**, 845-856 (2006).
21. Labeed, F. et al. Biophysical characteristics reveal neural stem cell differentiation potential. *PloS one* **6** (2011).
22. Pistollato, F., Chen, H.-L., Schwartz, P., Basso, G. & Panchision, D. Oxygen tension controls the expansion of human CNS precursors and the generation of astrocytes and oligodendrocytes. *Molecular and cellular neurosciences* **35**, 424-435 (2007).
23. Lee, J.-P. et al. Stem cells act through multiple mechanisms to benefit mice with neurodegenerative metabolic disease. *Nature medicine* **13**, 439-447 (2007).
24. Salazar, D.L., Uchida, N., Hamers, F.P., Cummings, B.J. & Anderson, A.J. Human neural stem cells differentiate and promote locomotor recovery in an early chronic spinal cord injury NOD-scid mouse model. *PLoS One* **5**, e12272 (2010).
25. Gupta, N. et al. Neural stem cell engraftment and myelination in the human brain. *Science translational medicine* **4**, 155ra137 (2012).
26. Tsukamoto, A., Uchida, N., Capela, A., Gorba, T. & Huhn, S. Clinical translation of human neural stem cells. *Stem cell research & therapy* **4**, 102 (2013).

27. Suchyna, T.M. et al. Identification of a peptide toxin from Grammostola spatulata spider venom that blocks cation-selective stretch-activated channels. *J Gen Physiol* **115**, 583-598 (2000).
28. Bowman, C., Gottlieb, P., Suchyna, T., Murphy, Y. & Sachs, F. Mechanosensitive ion channels and the peptide inhibitor GsMTx-4: history, properties, mechanisms and pharmacology. *Toxicon : official journal of the International Society on Toxinology* **49**, 249-270 (2007).
29. Suchyna, T. et al. Bilayer-dependent inhibition of mechanosensitive channels by neuroactive peptide enantiomers. *Nature* **430**, 235-240 (2004).
30. Kim, S.E., Coste, B., Chadha, A., Cook, B. & Patapoutian, A. The role of Drosophila Piezo in mechanical nociception. *Nature* **483**, 209-212 (2012).
31. Coste, B. et al. Piezo1 and Piezo2 are essential components of distinct mechanically activated cation channels. *Science (New York, N.Y.)* **330**, 55-60 (2010).
32. Coste, B. et al. Piezo proteins are pore-forming subunits of mechanically activated channels. *Nature* **483**, 176-181 (2012).
33. Li, J. et al. Piezo1 integration of vascular architecture with physiological force. *Nature* (2014).
34. Ranade, S.S. et al. Piezo1, a mechanically activated ion channel, is required for vascular development in mice. *Proc Natl Acad Sci U S A* **111**, 10347-10352 (2014).
35. Bae, C., Sachs, F. & Gottlieb, P. The mechanosensitive ion channel Piezo1 is inhibited by the peptide GsMTx4. *Biochemistry* **50**, 6295-6300 (2011).
36. Eisenhoffer, G.T. et al. Crowding induces live cell extrusion to maintain homeostatic cell numbers in epithelia. *Nature* **484**, 546-549 (2012).
37. Faucherre, A., Kissa, K., Nargeot, J., Mangoni, M.E. & Jopling, C. Piezo1 plays a role in erythrocyte volume homeostasis. *Haematologica* **99**, 70-75 (2014).
38. Miyamoto, T. et al. Functional role for Piezo1 in stretch-evoked Ca(2)(+) influx and ATP release in urothelial cell cultures. *The Journal of biological chemistry* **289**, 16565-16575 (2014).
39. Discher, D.E., Janmey, P. & Wang, Y.L. Tissue cells feel and respond to the stiffness of their substrate. *Science* **310**, 1139-1143 (2005).
40. Straight, A.F. et al. Dissecting temporal and spatial control of cytokinesis with a myosin II Inhibitor. *Science* **299**, 1743-1747 (2003).
41. Gutierrez, E. et al. High refractive index silicone gels for simultaneous total internal reflection fluorescence and traction force microscopy of adherent cells. *PloS one* **6** (2011).
42. Zhao, B., Li, L., Lei, Q. & Guan, K.L. The Hippo-YAP pathway in organ size control and tumorigenesis: an updated version. *Genes & development* **24**, 862-874 (2010).
43. Zarychanski, R. et al. Mutations in the mechanotransduction protein PIEZO1 are associated with hereditary xerocytosis. *Blood* **120**, 1908-1915 (2012).
44. McHugh, B.J., Murdoch, A., Haslett, C. & Sethi, T. Loss of the integrin-activating transmembrane protein Fam38A (Piezo1) promotes a switch to a reduced integrin-dependent mode of cell migration. *PLoS One* **7**, e40346 (2012).
45. Theunissen, T.W. et al. Systematic Identification of Culture Conditions for Induction and Maintenance of Naive Human Pluripotency. *Cell stem cell* (2014).
46. Barberi, T., Willis, L.M., Socci, N.D. & Studer, L. Derivation of multipotent mesenchymal precursors from human embryonic stem cells. *PLoS medicine* **2**, e161 (2005).
47. Fathi, A. et al. Comprehensive gene expression analysis of human embryonic stem cells during differentiation into neural cells. *PLoS One* **6**, e22856 (2011).
48. van de Leemput, J. et al. CORTECON: a temporal transcriptome analysis of in vitro human cerebral cortex development from human embryonic stem cells. *Neuron* **83**, 51-68 (2014).
49. Gottlieb, P., Barone, T., Sachs, F. & Plunkett, R. Neurite outgrowth from PC12 cells is enhanced by an inhibitor of mechanical channels. *Neuroscience letters* **481**, 115-119 (2010).

CHAPTER 4

COMBINATION SCAFFOLDS OF SALMON FIBRIN, HYALURONIC ACID, AND LAMININ FOR HUMAN NEURAL STEM CELL AND VASCULAR TISSUE ENGINEERING

Authors: **Janahan Arulmoli**[1,2], Heather J. Wright[2,3], Duc T.T. Phan[3], Urmi Sheth[2], Richard A. Que[1], Giovanni A. Botten[4], Mark Keating[1], Elliot L. Botvinick[1,8], Medha M. Pathak[2,5], Thomas I. Zarembinski[6], Daniel S. Yanni[7], Olga V. Razorenova[2,3], Christopher C.W. Hughes[1,3,8], Lisa A. Flanagan[1,2,9*]

Author Affiliations:

[1]Department of Biomedical Engineering

[2]Sue & Bill Gross Stem Cell Research Center

[3]Department of Molecular Biology and Biochemistry

[4]Department of Microbiology, Immunology, & Molecular Genetics

[5]Department of Physiology & Biophysics

[6]BioTime, Inc.

[7]Disc Comfort, Inc.

[8]The Edwards Lifesciences Center for Advanced Cardiovascular Technology

[9]Department of Neurology

[1-3, 5,8,9]University of California, Irvine, Irvine, CA, 92697, USA

[4]University of California, Los Angeles, Los Angeles, CA, 90095, USA

[6]BioTime, Inc., 1301 Harbor Parkway, Alameda, CA, 94502, USA

[7]Disc Comfort, Inc. 351 Hospital Road, Suite 202, Newport Beach, CA, 92663, USA

Keywords: neural stem cell; biomaterial scaffold; hydrogel; neural tissue engineering; integrin; co-culture; salmon fibrin; hyaluronic acid; laminin; neurovascular niche

4.1 ABSTRACT

Human neural stem/progenitor cells (hNSPCs) are good candidates for treating central nervous system (CNS) trauma since they secrete beneficial trophic factors and differentiate into mature CNS cells; however, many cells die after transplantation. This cell death can be ameliorated by inclusion of a biomaterial scaffold, making identification of optimal scaffolds for hNSPCs a critical research focus. We investigated the properties of fibrin-based scaffolds and their effects on hNSPCs and found that fibrin generated from salmon fibrinogen and thrombin stimulates greater hNSPC proliferation than mammalian fibrin. Fibrin scaffolds degrade over the course of a few days *in vivo*, so we sought to develop a novel scaffold that would retain the beneficial properties of fibrin but degrade more slowly to provide longer support for hNSPCs. We found combination scaffolds of salmon fibrin with interpenetrating networks (IPNs) of hyaluronic acid (HA) with and without laminin polymerize more effectively than fibrin alone and generate compliant hydrogels matching the physical properties of brain tissue. Furthermore, combination scaffolds support hNSPC proliferation and differentiation while significantly attenuating the cell-mediated degradation seen with fibrin alone. HNSPCs express two fibrinogen-binding integrins, αVβ1 and α5β1, and several laminin binding integrins (α7β1, α6β1, α3β1) that can mediate interaction with the scaffold. Lastly, to test the ability of scaffolds to support vascularization, we analyzed human cord blood-derived endothelial cells alone and in co-culture with hNSPCs and found enhanced vessel formation and complexity in co-cultures within combination scaffolds. Overall, combination scaffolds of fibrin, HA, and laminin are excellent biomaterials for hNSPCs.

4.2 INTRODUCTION

Stem cells are an important component of tissue engineering and regenerative medicine approaches since they provide beneficial secreted molecules to stimulate repair and can replace lost cells[1]. CNS neural stem cells are multipotent stem cells capable of self-renewal and differentiation into more committed progenitors that can generate neurons, astrocytes, and oligodendrocytes [2]. Transplanted neural stem and progenitor cells (NSPCs) migrate to areas of injury, actively respond to the microenvironment, secrete neuroprotective compounds, generate differentiated cells, and improve functional recovery[3-7]. However, a significant limitation of stem cell transplantation into the damaged CNS is that most cells die upon injection, with reports of surviving cells ranging from 0-30% at 4 weeks post-transplant for non-immortalized human NSPCs (hNSPCs) in rodent models of ischemic stroke[8]. The incorporation of NSPCs into a biocompatible scaffold, which is a 3-dimensional structure that supports tissue formation, can alleviate low cell survival post-transplant. For example, inclusion of a scaffold increases survival of NSPCs transplanted into rodent models of stroke[9] and traumatic brain injury (TBI)[10]. Scaffolds provide a 2-fold increase in mouse NSPC survival 2 weeks post-transplant into the infarct core of a mouse stroke model[9]. Furthermore, scaffolds increase survival of mouse NSPCs in a rodent model of TBI up to 5.6 fold at 8 weeks post-transplant and induce significant improvements in cognitive function[10]. Thus identifying beneficial scaffolds for hNSPCs is critical for realizing their therapeutic potential.

Three-dimensional scaffolds provide stem cells with an appropriate microenvironment and recapitulate the functions of native tissue[11-13]. Thorough scaffold characterization in an *in vitro* setting is essential for optimizing key parameters that support NSPC function. This must be done prior to implementation in animal models of injury in which the *in vivo* niche is quite

complex. Critical scaffold attributes for NSPC transplantation into CNS tissue[14] include non-toxic polymerization, biocompatibility with both transplanted NSPCs and host tissue, the ability to be injected as a liquid and polymerize in situ to form a tight apposition with the host tissue, and mechanical properties that match that of the CNS. The scaffold must also support vascularization to provide nutrient delivery to cells within the scaffold, have non-toxic degradation by-products and a degradation rate that allows sufficient time for cellular integration. Extracellular matrix (ECM) components such as proteins and polysaccharides are attractive candidates for scaffolds since they are biocompatible, contain sites for cellular adhesion, and provide suitable substrates for stem cell survival, growth, and function.

Fibrin is an ECM protein involved in blood clotting during the coagulation cascade that is non-toxic and biocompatible. Fibrin hydrogels are formed when fibrinogen is cleaved by thrombin to generate fibrin monomers that are covalently crosslinked by Factor XIIIa to create a mesh, which can be degraded by the enzyme plasmin. By varying the concentrations of fibrinogen and thrombin, the mechanical properties and polymerization time of the hydrogel can be modulated[15]. Fibrin contains multiple adhesive sites including RGD sequences that engage integrins on the cell surface. Fibrin has been used as a scaffold for mouse and human NSPCs and growth factor delivery vehicle in rodent spinal cord injury models[16-19]. Intriguingly, the source of fibrin can play an integral role in its effectiveness as a scaffold. Salmon fibrin, as opposed to human and bovine fibrin, encourages greater neurite outgrowth of rodent CNS neurons and better resists degradation by cellular proteases[20, 21]. Salmon fibrin matches the mechanical characteristics of CNS tissue[20, 22] and when used to treat rats with dorsal hemisection spinal cord injuries promotes greater locomotor functional recovery, density of serotonergic fibers caudal to the lesion site, and recovery of bladder function than mammalian fibrin [23]. Salmon fibrin has

been developed as a human therapeutic and has passed numerous toxicity and immunogenicity tests[24, 25]. Although salmon fibrin is an effective scaffold to treat CNS injury[23], it degrades rapidly *in vivo* (~7 days) and thus is unlikely to provide long-term support for transplanted hNSPCs.

In order to mitigate this rapid degradation, we designed combination scaffolds of fibrin and a material commonly found in the NSPC niche within the brain, hyaluronic acid (HA)[26], which has been shown to persist for at least 2 months when transplanted into the CNS[27, 28]. HA is a naturally occurring polysaccharide present in the ECM that is high in the developing brain and in the postnatal brain in regions adjacent to the lateral ventricles where stem cells reside[26, 29]. HA has been developed as a biomaterial for NSPC applications[30] including tissue repair after acute ischemic stroke[27, 28]. HA scaffolds increase the survival of transplanted mouse NSPCs two-fold, promote the differentiation of human induced pluripotent stem cell (iPS)-derived NSPCs into immature neurons, and reduce the host inflammatory response when transplanted into the infarct stroke cavity of a mouse model[9, 31]. HA has advantages as a scaffold material but is not always sufficient to promote cell adhesion[32, 33], so can be combined with adhesive peptides or another ECM component to provide cell attachment. Thus, combination scaffolds of fibrin and HA may benefit from the cell adhesive properties of fibrin and degradation rate of HA.

Another ECM component beneficial for neural cells that can be incorporated into scaffolds is laminin. Laminin stimulates hNSPC expansion, migration, and differentiation[34] and can be used to functionalize various biomaterials to encourage neural cell adhesion in neural tissue engineering applications[35, 36]. Laminin-containing collagen-based scaffolds significantly improve the survival of mouse NSPCs 8 weeks after transplant into the traumatically injured mouse brain and animals treated with laminin-containing scaffolds and NSPCs perform better in

behavioral tests than untreated controls[10]. Matrigel scaffolds, which are predominantly collagen and laminin, seeded with embryonic stem cell-derived hNSPCs decrease infarct volume after focal cerebral ischemia in rats compared to cell transplants alone[37].HA-laminin scaffolds enhance NSPC migration in response to stromal cell-derived factor-1α (SDF-1α) gradients, which arise from injured brain tissue[38]. Interestingly, HA in the scaffolds leads to upregulation of the SDF-1α receptor, CXCR4, on NSPCs while enhanced migration is dependent on both HA and laminin in the scaffolds. Since laminin has beneficial effects on NSPCs and hNSPCs express laminin-binding integrins[34, 39], we tested laminin in our combination scaffolds with fibrin and HA.

The biomaterial composition of the scaffold affects its vascularization *in vivo*, which is critical for bringing nutrients to transplanted cells. Crosstalk between endothelial cells and NSPCs also impacts NSPC function and has inspired interest in the *in vivo* neurovascular niche. Endothelial cells promote proliferation and neuronal differentiation of rodent NSPCs in culture and slice models, mediated at least in part through VEGF produced by endothelial cells acting on NSPC VEGF receptors and upregulation of genes in the Notch pathway in NSPCs[40-43]. NSPCs and endothelial cells/vessels are closely associated *in vivo*, creating neurovascular niches that can be mimicked by including both cell types in scaffold constructs[44]. Co-transplantation of mouse NSPCs and either mouse or bovine endothelial cells without a scaffold into rodent stroke models leads to greater numbers of integrated NSPCs, greater NSPC proliferation, more neuronal differentiation, and improved functional recovery[45, 46]. A poly(ethylene glycol)-based scaffold containing mouse NSPCs and mouse endothelial cells transplanted subcutaneously formed better vessels than transplants of endothelial cells alone in the scaffold[47]. In order to test scaffold and NSPC effects on vasculogenesis and to incorporate components of the human neurovascular

niche, we added human endothelial colony-forming cell-derived endothelial cells (hECFC-ECs) to the scaffolds. Determining optimal scaffold and cell conditions to encourage vascularization *in vitro* may accelerate the formation of functional vasculature after transplantation[48-50].

While fibrin and HA have been tested individually as scaffolds, they each have limitations that may be overcome by incorporating them into a combination scaffold. The goal of our study was to compare fibrin and combination scaffolds to determine their material properties, effects on hNSPCs, and potential for vascularization. The polymerization kinetics and mechanical properties of the scaffolds were tested to determine whether they could be used as injectable scaffolds and match the stiffness of CNS tissue. HNSPCs were seeded in scaffolds to test cell proliferation and differentiation and hNSPC cell surface integrins for scaffold binding were identified. Since degradation of fibrin only scaffolds occurred rapidly *in vivo*[23], the degradation of fibrin and combination scaffolds seeded with hNSPCs was assessed over time and at multiple cell concentrations. Co-cultures of hNSPCs and hECFC-ECs in the scaffolds were utilized to measure vasculogenesis as a function of scaffold biomaterial and cellular composition to assess potential for vascularization. These studies enabled crosstalk between vascular endothelial cells and neural cells, creating a neurovascular niche that affects NSPC function[42, 44, 51] as well as endothelial cell behavior and vasculogenesis[47, 52, 53]. A comparison of fibrin only and combination scaffolds across multiple parameters allowed a thorough analysis of their potential use as scaffolds for hNSPCs.

4.3 MATERIALS AND METHODS

Cell Culture

Fetal-derived hNSPCs (SC27 and SC23) were isolated from the cerebral cortices of two separate brains by the National Human Neural Stem Cell Resource and were grown as adherent cultures on 6-well plates coated with 10 μg/mL fibronectin (human; Fisher Scientific, Hampton, NH, USA)[54]. HNSPC basal medium included DMEM/F12 (Fisher Scientific, Hampton, NH, USA), 20% BIT 9500 (bovine serum albumin, insulin, and transferrin; Stem Cell Technologies, Vancouver, CA), and 1% antibiotic/antimycotic (penicillin/streptomycin/amphotericin; Thermo Fisher Scientific, Waltham, MA, USA). Proliferation media was prepared from basal media via addition of 40 ng/mL epidermal growth factor (EGF; PeproTech, Rocky Hill, NJ, USA), 40 ng/mL basic-fibroblast growth factor (bFGF; PeproTech), and 20 ng/mL platelet-derived growth factor (PDGF-AB; PeproTech,). Proliferation was measured at 3, 6, or 7 days post cell-seeding in proliferation media. Astrocyte differentiation media consisted of DMEM/F12, 20% fetal bovine serum (FBS; Gibco, Waltham, MA, USA), and 1% antibiotic/antimycotic. Neuronal differentiation media consisted of 96% Neurobasal (Thermo Fisher Scientific, Waltham, MA, USA), 2% B-27 (Thermo Fisher Scientific), 1% GlutaMAX (Thermo Fisher Scientific), and 1% pen/strep (penicillin/streptomycin; Thermo Fisher Scientific) with 20 ng/mL brain-derived neurotrophic factor (BDNF; PeproTech), 20 ng/mL glial-derived neurotrophic factor (GDNF; PeproTech), and 0.5 μM dibutyryl cyclic AMP (cAMP; Sigma-Aldrich, St. Louis, MO, USA) (modified from[55]). HNSPCs were differentiated for 5 days in astrocyte differentiation media and 14 days in neuronal differentiation. Cells were routinely passaged 1:2 or 1:3 and seeded at $5x10^4$ – $1x10^6$ hNSPCs per 100 μL hydrogel for experiments and equal numbers of viable cells (Trypan Blue staining) were used for each experimental group. Proliferation media was refreshed every

day (50%) for passaging and every other day (100%) for scaffold proliferation assays to minimize mechanical disruption of the gels with daily media changes. Differentiation media was refreshed (100%) every other day. For co-culture experiments, hNSPCs were tagged with CellTracker Green (Thermo Fisher Scientific; C2925) at 10 μM for 45 minutes prior to seeding into scaffolds.

HECFC-ECs were isolated from cord blood as previously described with approval from UC Irvine's Institutional Review Board[56]. After isolation, cells were expanded on flasks coated with 10 μg/mL fibronectin (human; Fisher Scientific) in EGM-2 media supplemented with a growth factor bullet kit (Lonza, Basel, SUI; CC-3162). HECFC-EC were transduced with lentivirus to express mCherry fluorescence. Lentiviral constructs to express fluorescence (LeGO-C2) were gifts from Boris Fehse (Addgene plasmids, Cambridge, MA, USA; 27339). Cells were used for experiments between passages 4 and 8. All cell types were cultured in a 37^{o}C, 5% CO_2 humidified incubator.

Hydrogel/scaffold formulation

Fibrin gels were formulated by cleaving 5 mg/mL salmon fibrinogen (SeaRun Holdings, Inc.) with 2 U/mL salmon thrombin (SeaRun Holdings, Inc.) in Minimal Essential Media (MEM; Thermo Fisher Scientific). For combination hydrogels, 1 mg/mL thiolated Hyaluronic Acid (HA) (Glycosil®; BioTime, Inc.) (average molecular weight (MW) ~250 kDa) with or without 100 μg/mL laminin (Thermo Fisher Scientific) was included in the hydrogel mixture prior to addition of thrombin. HA of 250 kDa MW was chosen for these studies since HA of this size has a lower viscosity and is readily modified in a reaction vessel via thiol addition to carboxylic acid groups on the repeating HA disaccharide chain[57, 58] This thiol modification allows for the

straightforward addition of cell adhesion peptides or cross-linking sites to the HA hydrogel. The MW of this HA is within the range of sizes of HA used successfully as scaffolds for transplantation (60 kDa – 1.6 MDa)[28, 31, 59] and 250 kDa HA increases survival of transplanted NSPCs[9, 60]. Bovine and human fibrinogen and thrombin were obtained from Calbiochem or Sigma as lyophilized proteins and had endotoxin levels less than 0.5 EU/mL. HNSPC and/or hECFC-EC cell solution was added at a volume of 50 μL and mixed with 50 μL of hydrogel solution to create 100 μL scaffolds, cultured on 18 mm diameter cover slips in 12-well plates.

Cell proliferation assay

The Click-iT EdU kit (Thermo Fisher Scientific) was used to identify hNSPCs entering S-phase of the cell cycle. HNSPCs were seeded at $1x10^5$ cells per 100 μL hydrogel and cultured in proliferation medium supplemented with 10 μM EdU nucleoside analog at 37 ^oC for 6 hours. The scaffold constructs were fixed, permeabilized, and blocked as previously described[34]. A copper ion (Cu^{1+}) catalyzes a covalent bond between an Alexa Fluor azide and an alkyne in the EdU in the Click-iT reaction. All cell nuclei were stained with 4 μg/mL Hoechst 33342 in PBS. The percentage of EdU-positive cells was determined by quantifying 3-5 randomly selected fields from each scaffold group imaged using a Zeiss Spinning Disc Confocal Microscope (Zeiss, Oberkochen, DEU).

Scaffold degradation and assessment of soluble fibrinogen

Fibrin scaffold degradation and amount of soluble fibrinogen in the media was determined using Western Blot. Briefly, $1x10^5$, $3x10^5$, $6x10^5$, $1x10^6$, or no cells were seeded in fibrin only, fibrin/HA, or fibrin/HA/laminin scaffolds. Proliferation media was added 30 minutes after initial polymerization was induced with thrombin. In order to assess the amount of soluble

fibrinogen released from hydrogels not seeded with cells, media samples for Western Blot were taken immediately after adding media to polymerized hydrogels lacking cells. These were used as control samples to determine fold changes in degradation in comparison to cell-seeded hydrogels. After 7 or 30 days in culture in a 37^{o}C, 5% CO_2 humidified incubator, 1 – 5 μL of conditioned media was removed from the well and mixed with SDS loading buffer (312 mM Tris HCl pH 6.8, 10% SDS, 0.05% bromophenol blue, 50% glycerol, 10% beta-mercapto ethanol). Samples were loaded in each lane of 10% bis-acrylamide gels and transferred onto 0.2 μm nitrocellulose membranes (BioRad). Within a single experiment, an equal amount of media was withdrawn from each sample for analysis. Blots were stained with Ponceau S to detect total protein. Ponceau S staining and mouse anti-transferrin were used to verify equal loading and transfer of each lane since transferrin is a component of the cell culture media. The primary antibodies used were 1:50,000 dilution of rabbit anti-salmon fibrinogen[23] and 1:1,000 dilution of mouse anti-transferrin (Abcam, Cambridge, UK; ab10208). Membranes were incubated with primary antibodies overnight at 4 °C with gentle agitation. The following secondary antibodies were used: goat anti-mouse HRP conjugate (Thermo Fisher Scientific; # 31430), goat anti-rabbit HRP conjugate (Pierce #31460), horse anti-mouse AP (Vector Labs, Burlingame, CA, USA; #AP-2000). Membranes were incubated with secondary antibodies for 1 hour at room temperature with gentle agitation and the signal was developed using Amersham ECL Prime western blotting substrate (GE Healthcare, Scottsdale, AZ, #RPN2236) or SigmaFast BCIP/NBT substrate (Sigma Aldrich; #B5655) for HRP or AP conjugates, respectively. Standard curves were generated by loading a range of 1 – 1000 ng of salmon fibrinogen for every experiment to accurately assess linearity of protein detection and degradation within experimental groups. ImageJ software was used to obtain quantitative measurements of band intensity for comparison

between groups through the integrated density function, which sums the values of the pixels for a given band. The integrated density values for the bands in the standard curve for each experiment was used to correlate the specific amount of fibrinogen released in the experimental groups. It should be noted that fold change in fibrinogen detection across conditions was used for some analyses rather than total amount (μg) in order to control for minor variations in scaffold degradation across experiments.

Mechanical characterization of hydrogels

Bulk rheology was used to obtain the viscoelastic properties of the hydrogels. Elastic and viscous moduli were quantified using a stress-controlled rheometer (Anton Paar; MCR 301, Graz, Austria) with a 25 mm diameter parallel plate geometry. Samples containing salmon fibrinogen (5 mg/mL) alone or with HA (1 mg/mL) were diluted in MEM and mixed with salmon thrombin (2 U/mL). The hydrogels were prepared at a total volume of 140 μL and immediately loaded onto the rheometer upon addition of thrombin. A humidified chamber was created via a solvent trap filled with deionized H_2O in order to prevent hydrogel evaporation during analysis. Oscillatory measurements were taken at a frequency of f = 1 Hz and strain of γ = 1% with a height gap of 200 μm. A Peltier temperature control system kept the chamber at 22.5 ^{o}C. The elastic (G') and viscous (G'') moduli were recorded over a time sweep until there was no longer a change in G'. The time sweep was subsequently followed by a frequency sweep performed at γ = 1% from f = 0.01 to 100 Hz. At the conclusion of the frequency sweep, a strain sweep was successively performed at f = 1 Hz from γ = 1 to 10,000%.

Gel point of the hydrogels was analyzed by reducing the concentration of thrombin in the hydrogels to 0.15 U/mL in order to capture polymerization kinetics. Samples were prepared as

described above and oscillatory measurements were performed at f = 1 Hz and γ = 1%. Measurements were obtained every 1 s in order to capture the time required to transition from liquid to viscoelastic solid (G' = G'').

Immunostaining and Imaging

For the purposes of immunocytochemistry, scaffold constructs were fixed with 4% paraformaldehyde for 20 minutes. After 4x15 minute PBS washes, cells were treated with 0.3% Triton X-100 (Sigma) in PBS for 15 minutes followed by 4x15 minute PBS washes. Constructs were then blocked using 10% donkey serum, 5% BSA, 0.1% Triton X-100 in PBS overnight at 4 ^{o}C on a rocker. Primary antibodies were diluted in 10% donkey serum, 5% BSA, 0.1% Triton X-100 in PBS and were incubated overnight at 4 ^{o}C on a rocker. The following primary antibodies were used: rabbit anti-Ki67 (Leica Biosystems, Wetzlar, DEU; KI67P-CE) diluted 1:500, mouse anti-GFAP (Sigma Aldrich; G3893) diluted 1:200, mouse anti-MAP2 (Sigma Aldrich; M4403) diluted 1:200, goat anti-doublecortin (Santa Cruz Biotechnology, Dallas, TX, USA; SC-8066 (c-18)) diluted 1:200. Following primary antibody incubation, scaffold constructs underwent 4x15 minute PBS washes. Secondary antibodies were diluted in 10% donkey serum, 5% BSA, 0.1% Triton X-100 in PBS and were incubated with cells for 2 hours in the dark at room temperature on a rocker. The following secondary antibodies were used at 1:200 dilutions: donkey anti-rabbit 555 (Thermo Fisher Scientific; A-31572), donkey anti-mouse 555 (Thermo Fisher Scientific; A-31570), donkey anti-goat 488 (Thermo Fisher Scientific; A-11055). Secondary antibody incubation was followed by 4x15 minute PBS washes. Cell nuclei were counterstained with 4 μg/mL Hoechst 3342 in PBS for 5 minutes, followed by 1x15 minute PBS wash. Scaffolds were mounted with 20 μL Vectashield (Vector Labs; H-1000) onto cover glass and imaged using a Zeiss Spinning Disc Confocal Microscope (Zeiss) using a 20X or 40X objective with numerical

apertures 0.8 and 0.75, respectively. Images were acquired using AxioVision Rel 4.8 software. Each individual image stack was 80 μm thick using 1.3 μm slice thickness. ImageJ was used to quantitate positively stained cell nuclei for proliferation.

For confocal reflection microscopy, samples of the combination and fibrin scaffolds were prepared as described in section 1.2.2 on 35 mm glass bottom dishes (MatTek) and then imaged using a reflection confocal system as previously used[61], with some modifications, to image the 3D architecture of non-labeled fibrin hydrogels[62]. Samples were imaged on an IX81 inverted microscope (Olympus) equipped with a FluoView 1200 laser scanning confocal unit (Olympus) using a 60X oil objective (PlanApo TIRFM 1.45 NA, Olympus) and 488 nm laser (Olympus). For each sample (n = 3 per hydrogel), 7 μm z-stacks of each hydrogel were taken with a step size of 100 nm. Presented images were contrast enhanced for viewing purposes.

Flow Cytometry

Samples from proliferating, confluent cultures were dissociated from the culture surface as previously described[54]. Briefly, hNSPCs were harvested as a single cell suspension with Cell Dissociation Buffer (Thermo Fisher Scientific), incubated and labeled with primary antibodies for 30 minutes in the dark, and analyzed on an LSR II Flow Cytometer (BD Biosciences, Franklin Lakes, NJ, USA) using a 488 nm laser. Primary antibodies used were: FITC-labeled anti-human CD51 (anti-αV integrin, Biolegend, San Diego, CA, USA; 327907) and isotype control FITC-labeled mouse IgG2a (Biolegend; 400209) at 1:100 dilution in 5% BSA. An unstained control was included alongside the stained samples and propidium iodide was used to discern live from dead cells. Up to 10,000 events were collected and stored electronically on the

BD FACSDIVA software. FLOWJO software was used to quantitate the percentage of hNSPCs expressing CD51.

Vascular Analysis

Quantitative analysis of vascular formation was performed using AngioTool[63]. Images were taken with a 20X objective with numerical aperture 0.8 on a Zeiss Spinning Disc Confocal Microscope (Zeiss) on day 5 post-seeding and analyzed for vessel percentage area, total number of branch points, and total vessel length. Five randomly selected fields were obtained from each condition for analysis.

RNA Sequencing

RNA was isolated from SC27 passage 12, 15, and 17 hNSPCs grown to confluency in single wells of 6 well plates (1-2x10^6 cells) using the Bio-Rad RNA Isolation Kit (Genicity, Irvine, CA, USA; G00065). Genomic DNA contamination of all RNA samples was assessed by using qRT-PCR for human 18S and GAPDH with and without reverse transcriptase and found to be insignificant. cDNA for qRT-PCR was synthesized using M-MLV reverse transcriptase (Promega). qRT-PCR was performed using TaqMan primers on an Abi ViiA7 qPCR machine (Applied Biosystems, Foster City, CA, USA).

Total RNA was further monitored for quality control using the Agilent Bioanalyzer Nano RNA chip and Nanodrop absorbance ratios for 260/280nm and 260/230nm. RNA library preparation and sequencing was performed at the UCI Genomics Core. Library construction was performed according to the Illumina TruSeq mRNA stranded protocol. The input quantity for total RNA was 250ng and mRNA was enriched using oligo dT magnetic beads. The enriched mRNA was chemically fragmented for five minutes. First strand synthesis used random primers

and reverse transcriptase to make cDNA. After second strand synthesis the double-stranded cDNA was cleaned using AMPure XP beads and the cDNA was end repaired and the 3' ends were adenylated. Illumina barcoded adapters were ligated on the ends and the adapter ligated fragments were enriched by nine cycles of PCR. The resulting libraries were validated by qPCR and sized by Agilent Bioanalyzer DNA high sensitivity chip. The concentrations for the libraries were normalized and the libraries were multiplexed together. The concentration for clustering on the flowcell was 12.5pM. The multiplexed libraries were sequenced on one lane using single read 100 cycles chemistry for the HiSeq 2500. The version of HiSeq control software was HCS 2.2.58 with real time analysis software, RTA 1.18.64.

For sequence mapping and bioinformatic analysis, RNA-Seq data was processed as described previously[64]. All bioinformatics analyses were conducted using the Galaxy platform[65]. Reads were aligned to the human GRCh37/hg19 reference genome with the TopHat program[66] using most default parameters. Alignments were restricted to uniquely mapping reads with two possible mismatches permitted. RPKM (reads per kilobase pair per million mapped reads) were calculated as described [67] for hg19 RefSeq genes using the SeqMonk program (http://www.bioinformatics.babraham.ac.uk/projects/seqmonk/). MRNA RPKMs were derived by counting exonic reads and dividing by mRNA length. Since all samples were from a single cell type (hNSPCs), we designated RPKM value cutoffs of above 10 (high), 1-10 (moderate), and below 1 (low) to denote expression levels of genes of interest. As validation, highly expressed transcripts such as beta-actin and GAPDH fall into the high category (beta-actin 2247.6 ± 255.6, GAPDH 886.3 ± 105.6), as does the FGFR1 (57.45 ± 4.6) known to function in NSPCs, while FGFR2 is in the moderate category (2.36 ± 0.7), and the muscle marker MyoD is in the low category (0.023 ± 0.003). Factors listed as being involved in angiogenesis were

obtained from a commercial human angiogenesis PCR array (Qiagen, Hilden, DEU) and combined with factors previously identified by the Hughes Lab at UCI.

Statistical Analysis

All statistical analyses utilized a one-way single factor ANOVA with Tukey post-hoc tests for multiple comparisons.

4.4 RESULTS

4.4.1 hNSPC proliferation in scaffolds is dependent on the species of fibrin

Tissue engineered scaffolds for transplantation of stem cells to aid CNS regeneration should inherently support stem cell survival and growth. We investigated whether fibrin source influences the proliferative capacity of cerebral cortical hNSPCs since fibrin source significantly affects the extension of neurites from mammalian neurons, with longer neurites formed in salmon fibrin than human or bovine fibrin[20].

Greater numbers of hNSPCs were present in salmon fibrin scaffolds than in bovine or human fibrin scaffolds after 6 days in culture, as illustrated by Hoechst-stained nuclei within each scaffold (Fig. 4.1a). Proliferation, quantified as the percentage of cells in S-phase of the cell cycle detected by EdU incorporation, was significantly greater for hNSPCs in salmon fibrin than cells in mammalian fibrin (Fig. 4.1b). A similar trend of more proliferating hNSPCs in salmon fibrin was detected by immunostaining for the proliferation marker phospho-histone H3, which labels mitotic cells in M-phase of the cell cycle (number of phospho-histone H3-positive cells per field: salmon fibrin 15.6 ± 1.7; bovine fibrin 6.8 ± 1.0; human fibrin 9.4 ± 2.1).

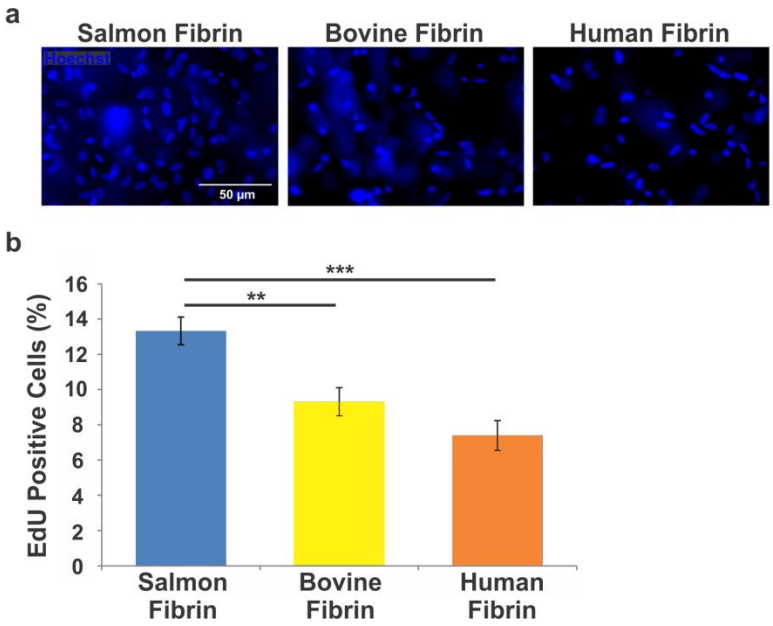

Figure 4.1. Salmon fibrin encourages greater hNSPC proliferation than bovine or human fibrin. HNSPCs ($5x10^4$) were seeded into scaffolds of salmon, bovine, or human fibrin and cells were analyzed after 6 days. (a) More hNSPCs are present in salmon fibrin than mammalian fibrin scaffolds (nuclei detected by Hoechst staining). (b) EdU-incorporation reveals a higher percentage of cells in S-phase of the cell cycle in salmon fibrin scaffolds than mammalian fibrin. P = 0.0023 (salmon vs. bovine), P = 2.5E-05 (salmon vs. human). **P < 0.01, ***P < 0.001. Error bars represent SEM. N = 3 independent biological repeats.

4.4.2 Inclusion of HA increases polymerization efficiency and stiffness of salmon fibrin scaffolds

Polymerization kinetics and mechanical strength of injectable scaffolds are essential components of biomaterial design that can determine the outcome of a cellular therapeutic[68]. Salmon fibrin as a scaffold biomaterial improves locomotor functional recovery, serotonergic innervation, and bladder recovery in spinal cord injured rats[23], but the scaffold degrades within 1 week, which would allow little time to support hNSPCs post-transplant. We thus created combination scaffolds of salmon fibrin and an interpenetrating network (IPN) of thiolated hyaluronic acid, which has been used previously as a scaffold for CNS transplantation[31, 60], to test whether the combined biomaterial would have different degradation and mechanical

properties than fibrin hydrogels. We incorporated laminin in combination scaffolds due to its prominent role as an ECM in the NSPC niche and because it stimulates hNSPC expansion, migration, and differentiation[34, 69-71].

A conventional rheometer was used to characterize the polymerization time of the single and combination hydrogels. The polymerization time, or gel point, is defined here as the time required for the hydrogel's storage modulus (G') and loss modulus (G'') to be equal. The time sweeps for the hydrogels show that fibrin/HA reaches gel point significantly faster than fibrin alone (Fib. 2 a,b). To analyze the extent of polymerization, the amount of non-polymerized fibrinogen associated with the different hydrogels was assessed by collecting media for Western Blot analysis of fibrinogen after hydrogel gelation. Initial experiments clarified linear detection of soluble fibrinogen using this approach (Fig. 4.S1). After polymerization was complete, significantly more non-polymerized fibrinogen was released from fibrin hydrogels than hydrogels with HA included, while the presence of laminin in the hydrogels had no additional effect (Fig. 4.2c). While there is significantly less soluble fibrinogen remaining after polymerization of the combination hydrogels, the vast majority of the 500 μg fibrinogen in the polymerization reaction is incorporated into the hydrogels in all cases. Polymerization of combination hydrogels is more rapid and complete than fibrin hydrogels.

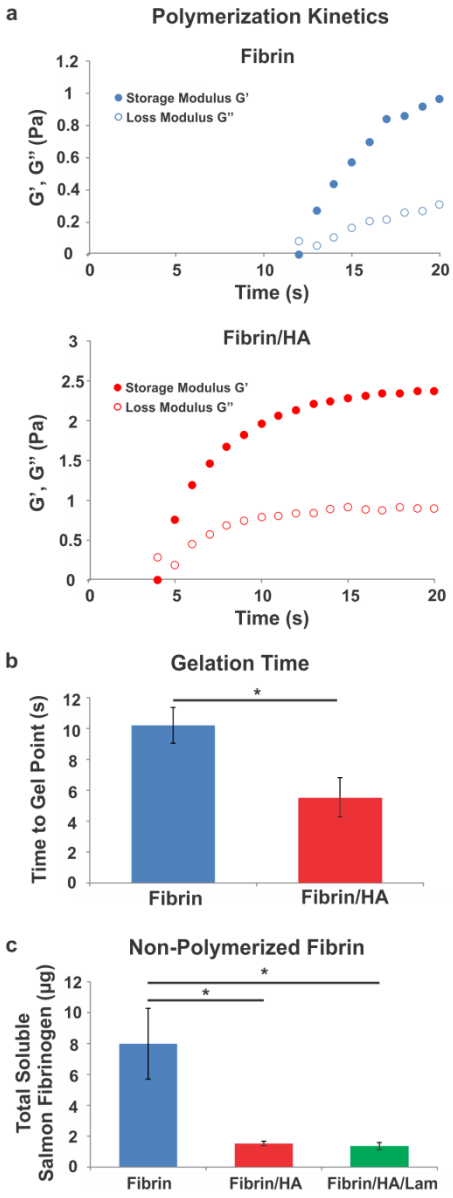

Figure 4.2. Increased gelation efficiency of combination hydrogels. (a) Polymerization of fibrin hydrogels (blue) and combination fibrin/HA hydrogels (red) was measured by oscillatory rheology. Storage modulus G' (closed circles) and loss modulus G'' (open circles) over time illustrate the transition of the scaffold from a liquid to gel state. The transition occurs much more rapidly for fibrin/HA combination hydrogels. (b) The time to gel point, defined as the time at which G'=G'' for each hydrogel, is approximately twice as long for fibrin (blue bar) as fibrin/HA hydrogels (red bar). P=0.048. (c) The amount of soluble, non-polymerized fibrinogen released into the media approximately 30 minutes after the onset of polymerization of hydrogels not seeded with cells is significantly higher for fibrin (blue bar) than combination hydrogels (red and green bars), revealing more complete polymerization of combination hydrogels. P = 0.048 (fibrin vs. fibrin/HA), P = 0.044 (fibrin vs. fibrin/HA/lam). *P < 0.05. Error bars represent SEM. N = 3 independent biological repeats.

Since mechanical properties of the microenvironment affect stem cells[72, 73], the mechanical properties of each hydrogel were measured using bulk rheology. The viscoelastic properties of fibrin and fibrin/HA scaffolds were independently characterized using conventional rheology, until G' and G'' remained relatively stable (Fig. 4.3a top). The hydrogels were initially more viscous at early time points near polymerization (G''>G'), but demonstrated more elastic behavior as gelation progressed (G'>G''). Both G' and G'' remained relatively independent of frequency (Fig. 4.3a middle) and strain (Fig. 4.3a bottom), which are hallmark characteristics of viscoelastic materials[74, 75]. Hydrogels with HA were significantly stiffer than those of fibrin alone, but both hydrogels were less than 250 Pa (fibrin 119.23 ± 16.48 Pa, fibrin/HA 202.3 ± 17.33 Pa; Fig. 4.3b). These findings indicate that the bulk mechanical properties of fibrin and combination scaffolds are within the optimal stiffness range (100-1,000 Pa) for CNS tissue and for supporting NSPC proliferation and neuronal differentiation[76, 77].

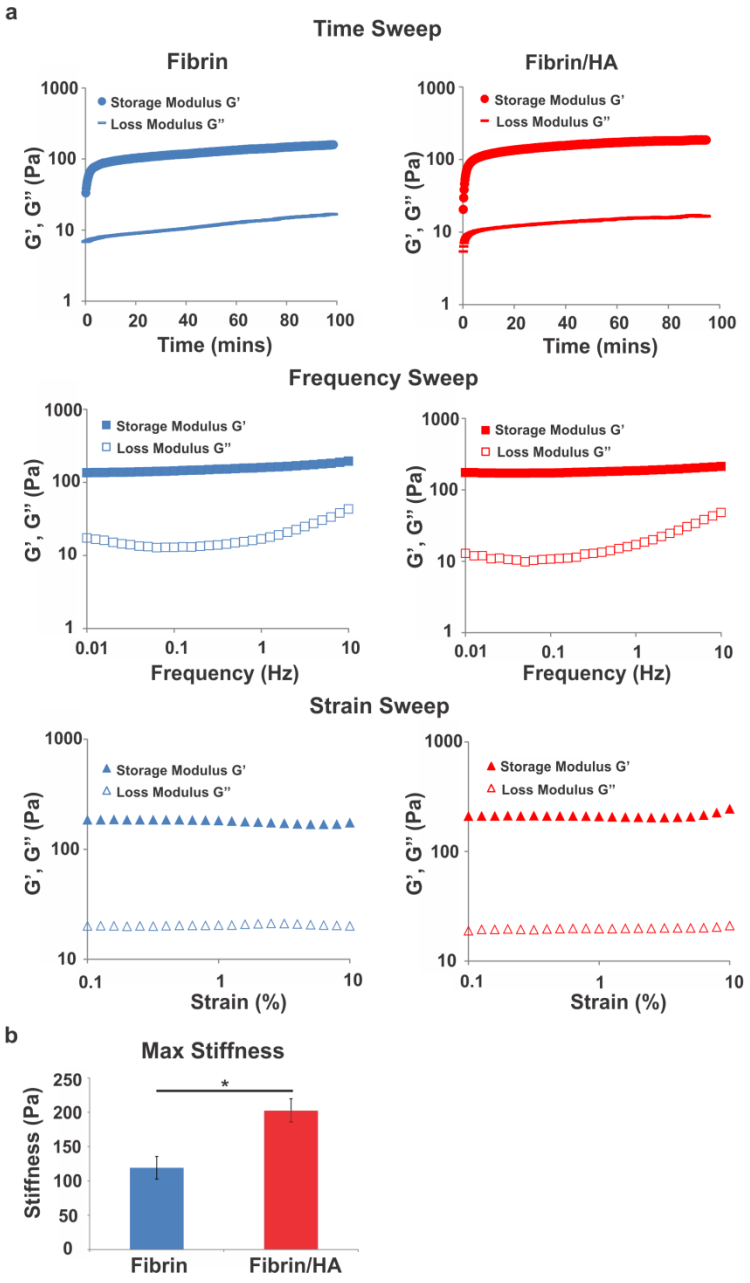

Figure 4.3. Combination scaffolds are stiffer than fibrin scaffolds but both are in the stiffness range of CNS tissue. (a) Oscillatory rheology was used to gather bulk mechanical properties of fibrin and fibrin/HA hydrogels. Storage modulus G' (closed circles) and loss modulus G'' (closed dashes) over time illustrate the transition of the scaffold from a liquid to gel-like state for fibrin (blue) and fibrin/HA (red) hydrogels. Storage modulus G' (closed squares and triangles) remains greater than the loss modulus G'' (open squares and triangles) over a broad range of frequencies and strains for both hydrogels (middle and bottom plots). (b) The maximum hydrogel stiffness measured by the storage modulus G' at 90 minutes indicates scaffolds with fibrin and HA (red bar) are significantly stiffer than those with fibrin alone (blue

bar) although both are within 100-250 Pa. P = 0.026. *P < 0.05. Error bars represent SEM. N = 3 independent biological repeats.

Confocal reflection microscopy was used to assess the micro-architecture of the fibrin and combination hydrogels since the hydrogel remains fully hydrated without fixation in this method, thus preserving native structure[61, 62]. The fibrin network was visualized with a confocal microscope by scanning with a 488 nm laser and collecting the light reflected back from the hydrogel. We found fibrin fibers easier to visualize in fibrin hydrogels, while the fibrin in combination hydrogels appeared intermixed with less reflective material (Fig. 4.S2). HA has high water content and thus may have a low reflective signal in confocal reflection microscopy since a large difference in refractive index between the material and water is required to obtain a strong signal with this method. Hydrated HA may surround fibrin fibers in the combination hydrogels, partially masking reflection and inhibiting clear visualization of individual fibers.

4.4.3 HNSPCs proliferate and differentiate within combination scaffolds

The proliferative capacity of hNSPCs within fibrin and combination scaffolds was assessed to gauge scaffold ability to support hNSPC function. HNSPCs proliferate similarly well in fibrin and combination scaffolds with HA and HA/laminin, as evaluated by Ki-67 immunostaining, to detect cycling cells not in G_0-phase of the cell cycle (Fig. 4.4). There was a slight but not significant trend of increased hNSPC proliferation within scaffolds that included HA and laminin over scaffolds of fibrin alone, indicating that at a minimum HA and laminin do not inhibit cell proliferation. EdU-incorporation to mark proliferating cells in S-phase revealed a matching trend in that more proliferating hNSPCs were present in combination scaffolds than fibrin scaffolds after 7 days of culture (EdU-positive cells in fibrin 10.74 ± 1.54 %, fibrin/HA

14.55 ± 1.52 %, fibrin/HA/lam 14.62 ± 4.04 %). These values are similar to those of cells cultured on laminin-coated glass, indicating that scaffolds enable hNSPC proliferation[78].

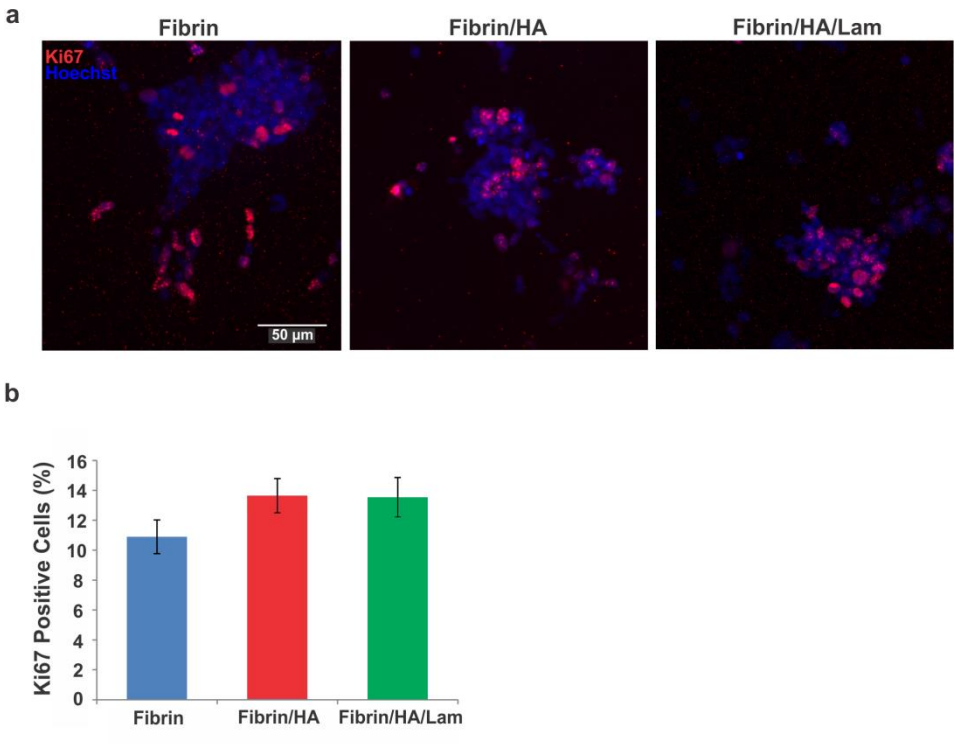

Figure 4.4. HNSPCs proliferate within combination scaffolds. (a) HNSPCs ($1x10^5$) were seeded into fibrin or combination scaffolds and proliferating cells not in G0 of the cell cycle were detected by immunostaining for Ki67. (b) Ki67-positive nuclei were quantified after 3 days in proliferating conditions and indicate that inclusion of HA (red bar) and HA with laminin (green bar) is not detrimental to the hNSPCs as shown by similar proliferation of the cells in combination and fibrin scaffolds (blue bars). Error bars represent SEM. N = 3 independent biological repeats.

An important characteristic of scaffolds is the ability to promote differentiation of transplanted stem cells since differentiated cells may stimulate repair of the host tissue. For this reason, we investigated differentiation of hNSPCs into neurons and astrocytes within the various scaffolds. We observed differentiation of hNSPCs into astrocytes within fibrin, fibrin/HA, and fibrin/HA/lam scaffolds, as assessed by immunostaining for the astrocyte marker glial fibrillary acidic protein (GFAP) (Fig. 4.5a). HNSPCs also formed neurons positive for the early neuronal

marker doublecortin within all three scaffolds (Fig. 4.5b). Immunostaining is not uniform throughout the gels, making quantitative analysis of differentiated cells impractical. Interestingly, neurite outgrowth from differentiated neurons was most robust in combination scaffolds containing laminin (Fig. 4.5b right). Some differentiated neurons within the combination scaffolds were double positive for doublecortin and the more mature neuronal marker, microtubule-associated protein 2 (MAP2) (Fig. 4.S3). These data indicate that combination scaffolds can support hNSPC proliferation and differentiation, providing rationale for their use as transplant constructs to restore injured CNS tissue.

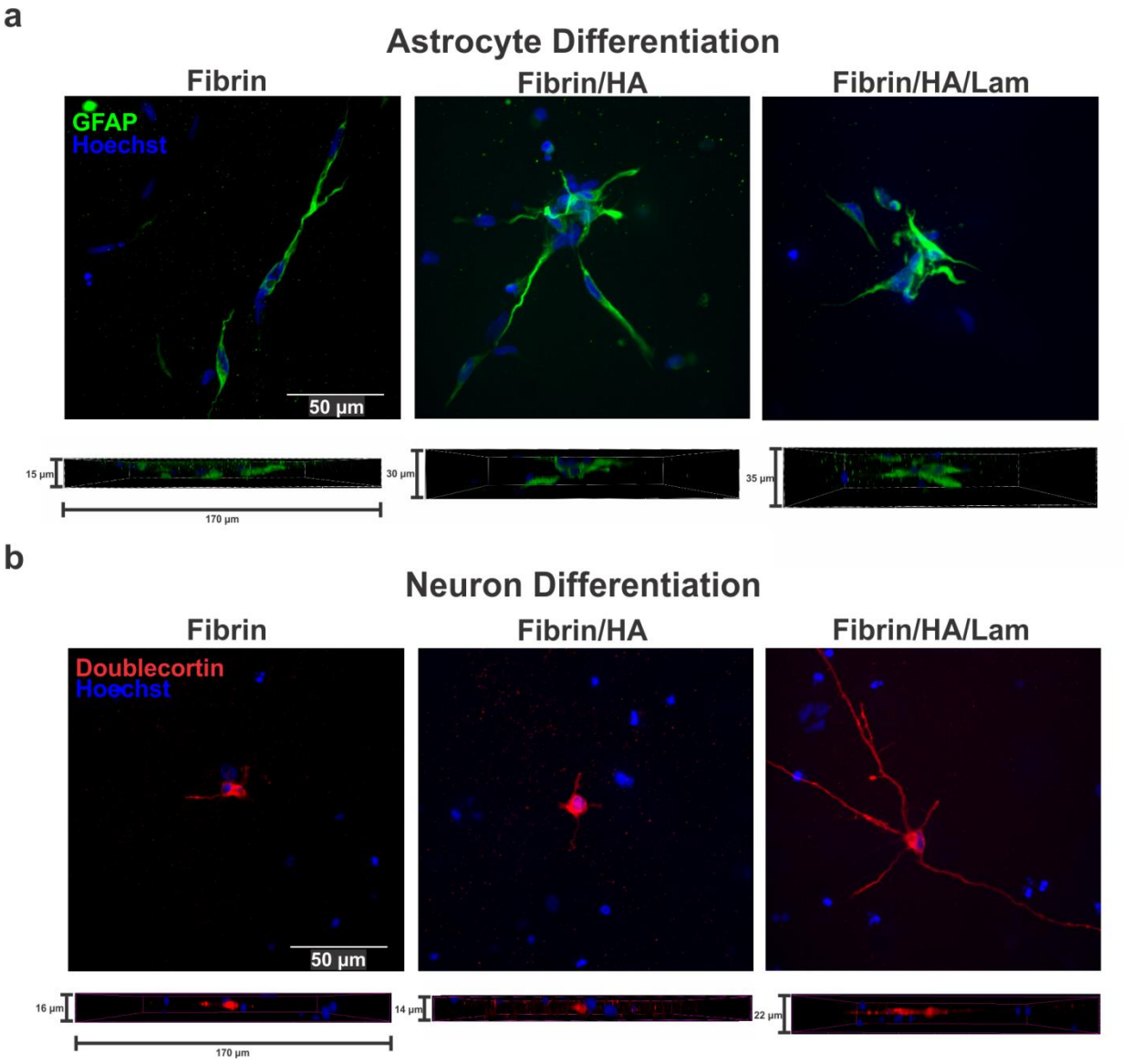

Figure 4.5. HNSPCs differentiate in combination scaffolds. hNSPCs ($1x10^5$) were differentiated in scaffolds for (a) 5 days to assess astrocytes using the marker GFAP or (b) 14 days for neurons using the marker doublecortin. Lower images in (a) and (b) reveal side view reconstructions to illustrate the three-dimensional nature of the scaffolds and the cell extensions. HNSPCs formed astrocytes and neurons in all scaffolds, but neurite outgrowth was most pronounced in combination scaffolds containing laminin.

4.4.4 hNSPCs express fibrinogen- and laminin-binding integrins

The proliferation, differentiation, and elongation of hNSPCs within scaffolds containing fibrin and laminin ECM suggest these cells express ECM-binding integrin α and β subunits. RNA Sequencing (RNA-Seq) was utilized to determine the types of integrins expressed by hNSPCs and indicated high levels of mRNA for β1, α7, α3, α6, β5, αV, α5, and α9 integrins (Fig. 4.6a, b). These integrins primarily bind fibrinogen (Fig. 4.6c), laminin, fibronectin, tenascin, osteopontin, and vitronectin[79-81]. The only fibrinogen-binding integrins expressed by hNSPCs at high or moderate levels in the RNA-Seq data are αVβ1 and α5β1 (Fig. 4.6c). In agreement with the RNA data presented here, we previously found by flow cytometry that hNSPCs express the α5 integrin subunit (~56% positive), and also the laminin-binding integrins β1, α7, α6, and α3[34]. However, our previous analysis did not include αV, so flow cytometry was used to determine that ~54% of the hNSPC population expresses cell surface αV (Fig. 4.6d). Therefore, after using RNA-Seq to assess expression levels of all integrins and flow cytometry to determine cell surface expression, we conclude that hNSPCs likely interact with fibrinogen in scaffolds through αVβ1 and α5β1 integrins and with laminin via α7β1, α6β1, α6β4, and α3β1.

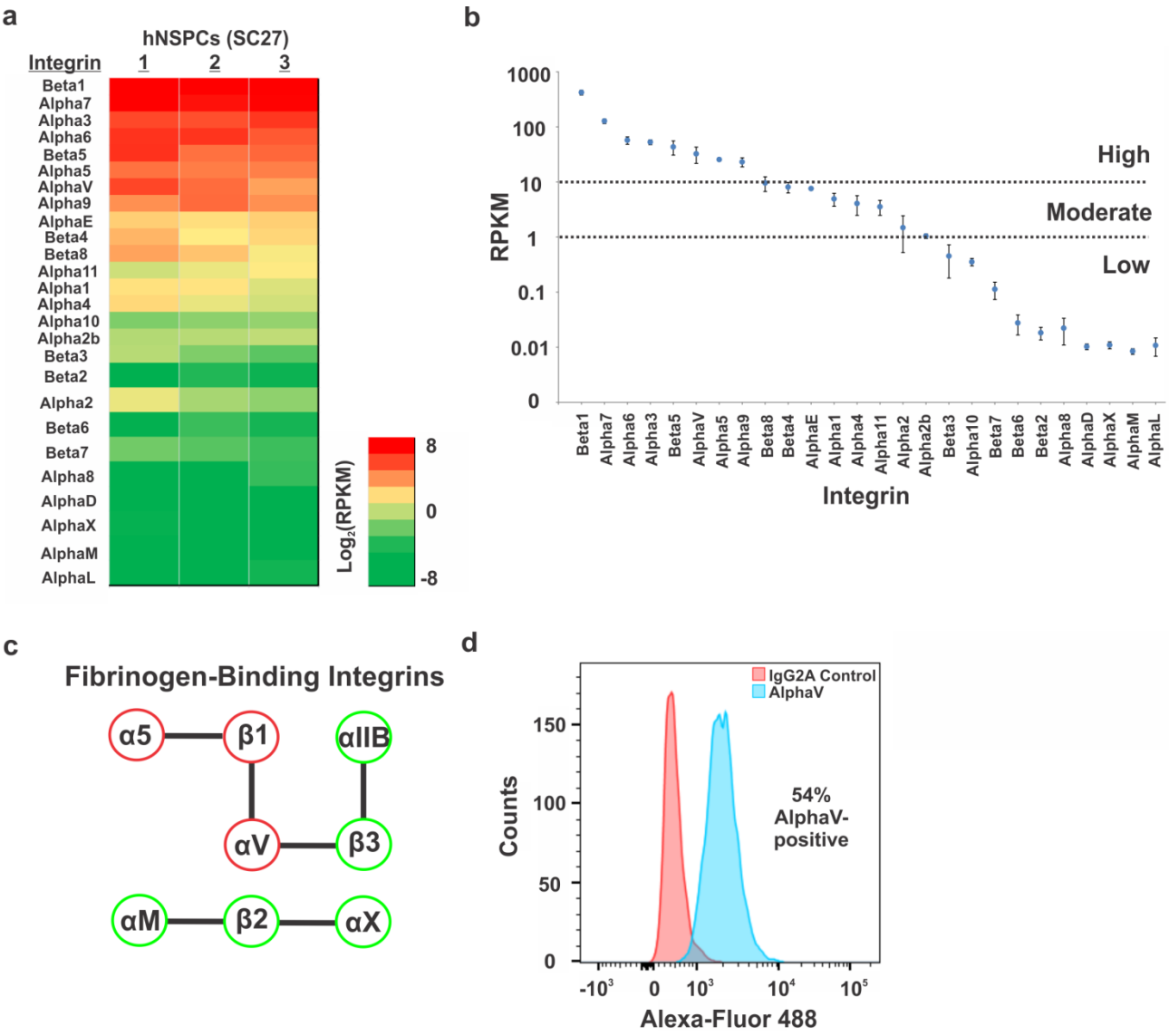

Figure 4.6. HNSPCs express ECM-binding integrins. (a) RNA-seq analysis indicates hNSPC integrin gene expression levels from three biological replicates. Colors indicate the log_2RPKM (reads per kilobase of transcript per million mapped reads) value for each α or β integrin, with red indicating higher expression and green lower expression. (b) The scatterplot displays average RPKM values for each integrin generated from the three replicates of hNSPCs organized from high to low expressers (error is SEM). Genes are clustered into three categories: high (>10 RPKM), moderate (1-10 RPKM), and low (<1 RPKM) expression. Dotted lines indicate 10 RPKM and 1 RPKM boundaries. For comparison, beta-actin, GAPDH, and FGFR1 fall in the highly expressed category, while FGFR2 is moderately expressed, and the muscle marker MyoD shows low to no expression. (c) Integrin binding schematic illustrating α and β integrins identified as fibrinogen-binding heterodimers; lines between α and β pairs indicate heterodimers. Red outlines denote integrins highly expressed by hNSPCs and green indicates lack of expression by hNSPCs[77]. (d) Flow cytometric analysis indicates hNSPC cell surface αV integrin

expression. Histogram of Alexa-Fluor 488-positive cells reveals a shift (~54% positive cells) in hNSPCs labeled with an antibody against αV integrin compared to IgG2A isotype control.

Interaction of HA with cells is mediated by several receptors, including CD44[82], RHAMM[83], and ICAM1[84]. However, HA is not always sufficient for cell adhesion[32, 33], and in our study hNSPCs do not bind to HA alone but require addition of a cell adhesion molecule or peptide to mediate binding (Fig. 4.S4). We assessed HA receptors by RNA-Seq and found the following levels of expression: CD44 (high, Avg. RPKM 316.7), TLR4 (high, Avg. RPKM 69.13), RHAMM (high, Avg. RPKM 16.8), layilin (low-moderate, Avg. RPKM 1.69), ICAM1 (low-moderate, Avg. RPKM 1.57), TLR2 (none, Avg. RPKM 0.02), lymphatic vessel endothelial hyaluronan receptor 1 (none, Avg. RPKM 0.02). Thus, hNSPCs express several receptors known to bind HA though they are not sufficient to mediate adhesion of these cells.

4.4.5 Hyaluronic acid slows hNSPC-mediated degradation of salmon fibrin *in vitro*

Degradation kinetics is another pivotal component of biomaterial design that can determine the efficacy of scaffolds for transplanted cells[68]. The inclusion of HA increased the polymerization efficiency and mechanical strength of the hydrogels as mentioned previously, so we tested whether it would affect hNSPC-mediated scaffold degradation. Since the scaffolds are formed by fibrinogen polymerization, whether as fibrin or fibrin/HA scaffolds, degradation was assessed by measuring the release of soluble fibrinogen from the cell-seeded scaffold after a period of time in culture. HNSPCs were cultured in proliferating conditions within fibrin, fibrin/HA, fibrin/HA/lam scaffolds and degradation was measured using Western blot analysis of salmon fibrinogen released from the scaffold into the culture media over time (Fig. 4.7a).

The inclusion of HA in the scaffolds significantly reduced hNSPC-mediated scaffold degradation (Fig. 4.7). After 7 days in culture, there was approximately 7-fold more soluble

fibrinogen present in the media of the fibrin compared to fibrin/HA scaffolds relative to hydrogels without cells seeded (Fig. 4.7b). Additionally, as the concentration of cells seeded within the fibrin scaffolds increased, there was an increase in the amount of fibrinogen released into the culture media after 7 days. In contrast, higher cell concentrations did not stimulate a significant increase in the amount of soluble fibrinogen released from fibrin/HA scaffolds (Fig. 4.7c). The same amount of conditioned media was loaded for each sample and equal loading was confirmed by Ponceau S staining of all proteins in each sample and immunoblotting for transferrin, a major protein component of the media (Fig. 4.7c and Fig. 4.S5). The inclusion of laminin did not alter the degradation kinetics of the combination scaffolds at 7 days (Fig. 4.7d). We examined whether cell-mediated degradation would be exacerbated at longer time points such as 30 days, which is sufficient time for initial hNSPC differentiation *in vivo*[85]. The release of soluble fibrinogen is increased nearly 20-fold from fibrin scaffolds after 30 days relative to hydrogels without cells seeded, while the combination scaffolds released less than 3 fold as much fibrinogen (Fig. 4.7d and Fig. 4.S6a). There was a significant increase in degradation of the fibrin scaffolds from the 7 day to 30 day time points, but strikingly this was not the case for scaffolds including HA or HA and laminin (Fig. 4.7d). Ponceau S confirmed approximately equal protein loading across all samples (Fig. 4.S6b).

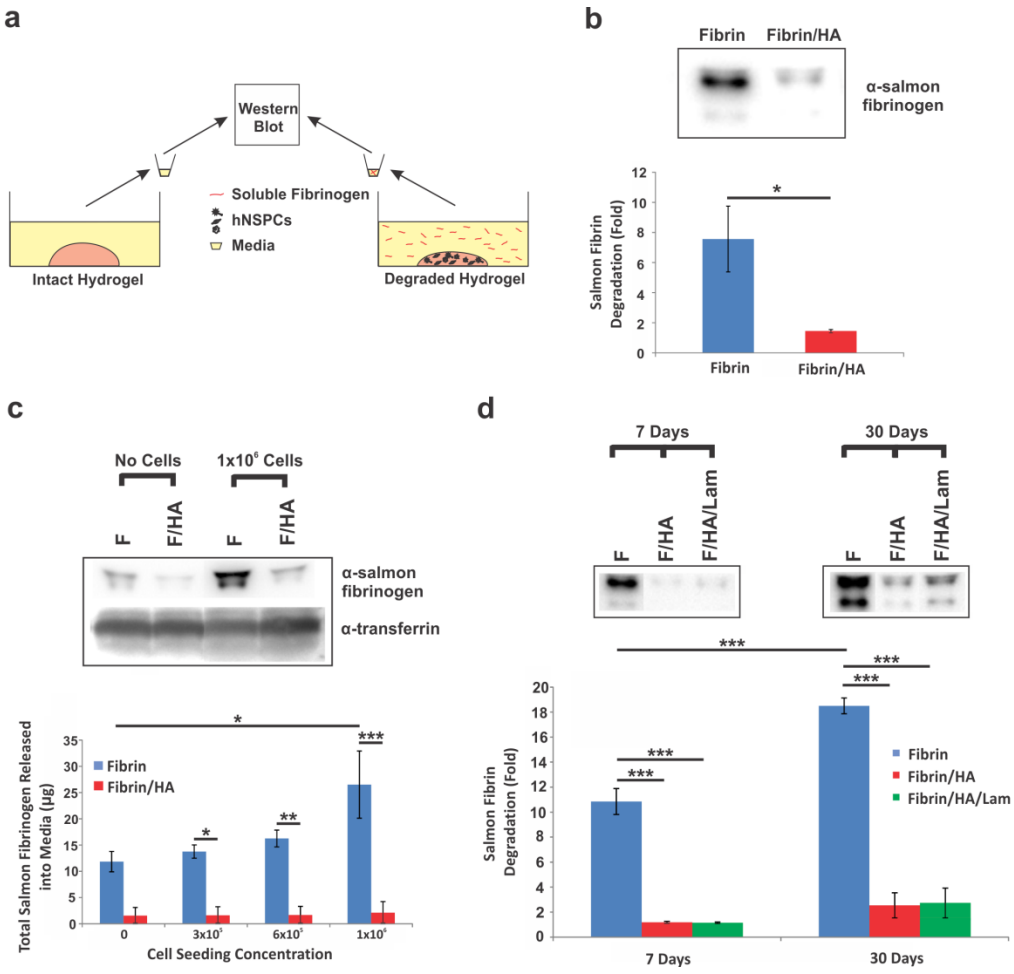

Figure 4.7. Combination scaffolds seeded with hNSPCs degrade more slowly than fibrin scaffolds. (a) HNSPCs were seeded into salmon fibrin only or combination scaffolds with salmon fibrin and HA or salmon fibrin, HA, and laminin and degradation was assessed by measuring release of fibrinogen from the scaffold into the media by Western Blot. Intact hydrogels without cells seeded were used as controls. (b) Fibrinogen released into the media was detected by an anti-salmon fibrinogen antibody[24.] HNSPCs ($1x10^5$) cause significantly greater degradation of fibrin than combination scaffolds after 7 days in culture. Values are fold change in amount of fibrinogen released into the media relative to that from fibrin/HA hydrogels without seeded cells. P = 0.032. *P < 0.05. (c) Seeding scaffolds with higher numbers of cells ($1x10^6$) leads to greater release of fibrinogen from fibrin (F) than from fibrin/HA (F/HA) scaffolds after 7 days as detected by Western blot. Transferrin, which is a component of the media, demonstrates approximately equal loading of media per lane. Total salmon fibrinogen released into the media after 7 days increases when scaffolds are seeded with increasing numbers of hNSPC in fibrin scaffolds (blue bars), but is substantially reduced by the presence of HA (red bars). Cells were seeded at $3x10^5$, $6x10^5$, and $1x10^6$ cells per scaffold. P = 0.027 (fibrin vs. fibrin/HA, $3x10^5$), P = 0.007 (fibrin vs. fibrin/HA, $6x10^5$), P < 0.0001 (fibrin vs. fibrin/HA, $1x10^6$), P = 0.029 (fibrin no cells vs. fibrin $1x10^6$). *P < 0.05, **P < 0.01, ***P < 0.001. (d) Degradation induced by hNSPCs ($1x10^5$) seeded in fibrin scaffolds (F, blue bars) increases with increasing time in culture (7 days vs. 30 days), as shown by fold change in fibrinogen released

into the media relative to that from fibrin/HA hydrogels without cells seeded. Fibrin degradation is attenuated drastically by the presence of HA (F/HA, red bars) and HA with laminin (F/HA/Lam, green bars). P = 0.0002 (fibrin 7 days vs. fibrin 30 days), P < 0.0001 (fibrin 7 days vs. fibrin/HA 7 days), P < 0.0001 (fibrin 7 days vs. fibrin/HA/lam 7 days), P < 0.0001 (fibrin 30 days vs. fibrin/HA 30 days), P < 0.0001 (fibrin 30 days vs. fibrin/HA/lam 30 days). ***P < 0.001. Error bars represent SEM. N = 3 independent biological repeats.

4.4.6 hNSPCs and combination scaffolds increase human endothelial cell-derived vasculogenesis

In order to create a scaffold construct that mimics the neurovascular niche, promotes vascularization, and encourages synergistic cross-talk between neural and endothelial cells, we used fibrin alone or in combination with HA and laminin to co-culture hNSPCs with hECFC-ECs. Scaffolds of fibrin, HA, and laminin with hNSPCs significantly bolstered vessel formation. HECFC-EC-derived vessels were easily visible in the scaffolds with and without hNSPCs after 5 days in culture (Fig. 4.8a). Quantitative analysis included vessel area percentage and total vessel length to indicate vessel growth, and the number of branch points as a reflection of vessel network complexity. Fibrin/HA/lam scaffolds with both hECFC-ECs and hNSPCs yielded the highest vessel area percentage, defined as the area of a given field occupied by vessels (Fig. 4.8b). These scaffolds contained a significantly higher vessel area than fibrin with hECFC-ECs, fibrin with co-cultured hNSPCs and hECFC-ECs, or combination scaffolds with hECFC-ECs only. However, inclusion of hNSPCs with hECFC-ECs in fibrin scaffolds showed a significantly greater vessel area percentage than hECFC-ECs alone in fibrin, demonstrating the marked effect of hNSPCs on vascular network formation within the scaffolds.

Examination of total vessel length, defined as the length of the vessels per imaged field, further confirmed the findings from vessel area percentage. Fibrin/HA/lam and the inclusion of co-cultured hNSPCs and hECFC-ECs significantly enhanced total vessel length in comparison to

hECFC-ECs cultured alone within fibrin or combination scaffolds (Fig. 4.8c). There was a significant increase in the vessel length of co-cultured hECFC-ECs in fibrin scaffolds compared to hECFC-ECs cultured alone in fibrin, suggesting that hNSPCs substantially affect the length of hECFC-EC-derived vessels, regardless of biomaterial composition.

The number of vessel branch points within the scaffolds was measured as an indicator of vascular complexity. We found that the fibrin/HA/lam scaffolds with co-cultured hNSPCs and hECFC-ECs contained significantly more branch points than those with hECFC-ECs only and fibrin scaffolds with hECFC-ECs (Fig. 4.8d). Indeed, there was a nearly 2-fold increase in vessel branch points in co-cultures within combination scaffolds compared to the hECFC-ECs cultured alone in fibrin, highlighting the synergistic effect of both HA and laminin with hNSPCs on vascular network complexity.

Since hNSPCs are likely affecting vasculogenesis through secretion of pro-angiogenic factors, we analyzed our RNA-Seq data for known angiogenic factors. We found that hNSPCs express high mRNA levels of several angiogenic factors likely to contribute to increased vasculogenesis of hECFC-ECs (Fig. 4.8e). We grouped the angiogenic factors into functional classes (growth factors, cytokines/chemokines, adhesion molecules/ECM, and proteases/inhibitors) and designated cutoffs for high, moderate, and low expression. Interestingly, a larger majority of the adhesion molecule/ECM angiogenic factors and proteases and inhibitors that modify the ECM screened for in hNSPCs were highly expressed (71% and 55%, respectively), while only 32% of the growth factors and 13% of the cytokines/chemokines were highly expressed (Fig. 4.8f-i), emphasizing the influence the matrix has on promoting angiogenesis. The Hughes lab previously identified SPARC, IGFBP7, collagen type 1 alpha 1, TGF-βI (transforming growth factor β-induced protein ig-h3, Big-h3), fibronectin 1, HGF, and

PCOLCE as being essential for sprouting or lumen formation from endothelial cells when secreted by stromal cells *in vitro*[86, 87], and these factors are also highly expressed by hNSPCs (Fig. 4.8). In sum, we studied the effect of scaffold composition and the presence of hNSPCs on the ability of hECFC-ECs to form complex vessel networks and found that both play an integral role in promoting formation of new vessels. RNA-Seq revealed that hNSPCs express several factors involved in angiogenesis, many of which are constituents of the ECM, that likely facilitate increased vasculogenesis by hECFC-ECs.

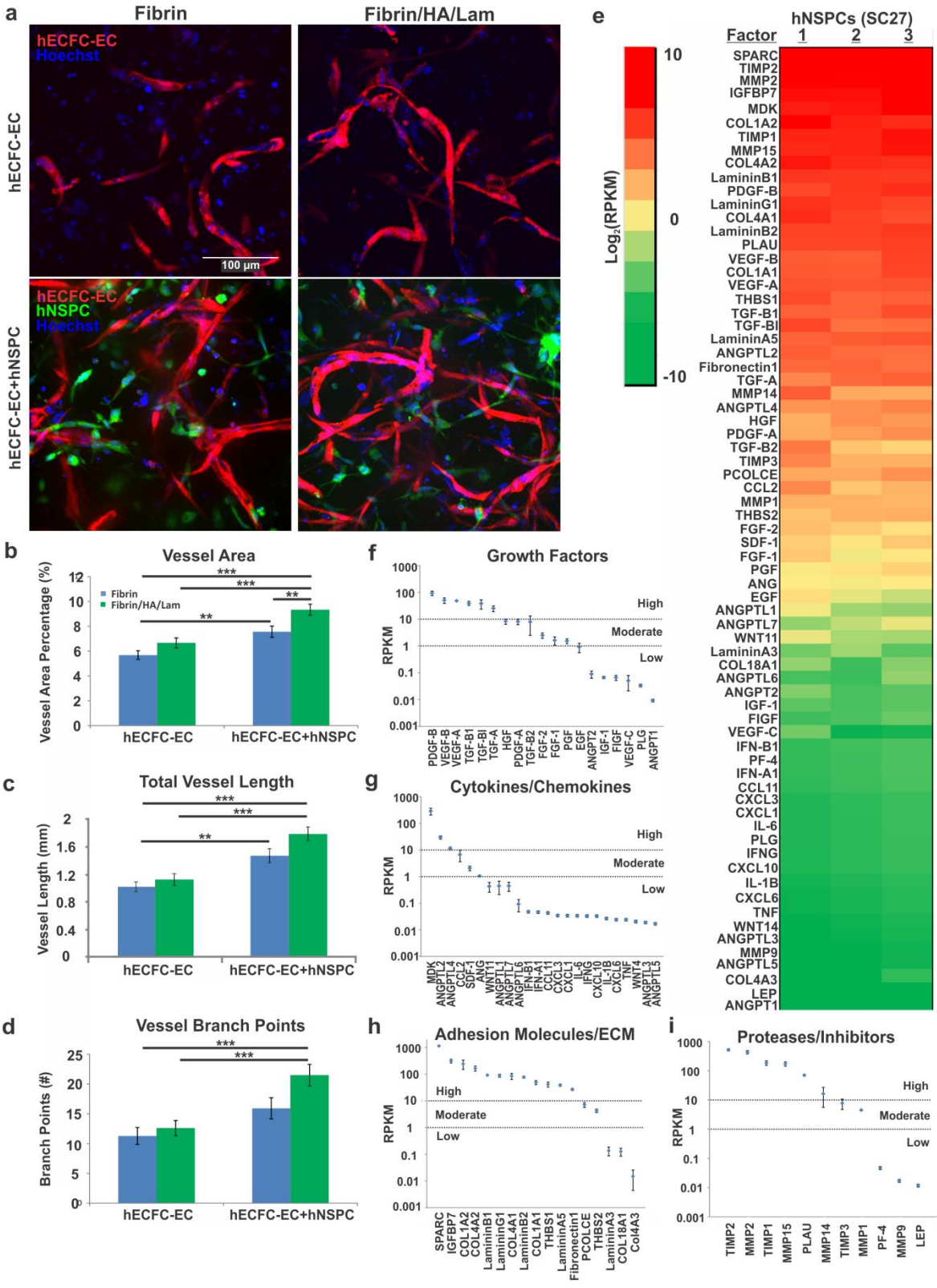

Figure 4.8. Emulation of the human neurovascular niche within scaffolds. (a) HECFC-ECs expressing mCherry were plated at $2.5x10^5$ cells per scaffold with or without hNSPCs labeled

with Cell Tracker Green at $5x10^4$ cells per scaffold. All cell nuclei were detected with Hoechst (blue). Neural and vascular cells interact *in vitro* in the scaffolds and hECFC-ECs form early vessels after 5 days in culture. (b) Quantitative analysis of vessel area indicates a positive effect of hNSPCs on vessel formation with additional increases in vessel formation present in combination scaffolds of fibrin/HA/laminin (green bars) when compared to fibrin scaffolds (blue bars). P = 1.26E-07 (fibrin/HA/lam – ECFC-EC+NSPC vs. fibrin – ECFC-EC), P = 7.64E-05 (fibrin/HA/lam – ECFC-EC+NSPC vs. fibrin/HA/lam – ECFC-EC), P=0.0032 (fibrin – ECFC-EC+NSPC vs. fibrin – ECFC-EC), P = 0.0068 (fibrin/HA/lam – ECFC-EC+NSPC vs. fibrin – ECFC-EC+NSPC). (c) Total vessel length is significantly greater in the presence of hNSPCs in both combination and fibrin scaffolds and is highest in combination scaffolds containing both cell types. P = 2.04E-06 (fibrin/HA/lam – ECFC-EC+NSPC vs. fibrin – ECFC-EC), P = 4.97E-05 (fibrin/HA/lam – ECFC-EC+NSPC vs. fibrin/HA/lam – ECFC-EC), P = 0.004 (fibrin – ECFC-EC+NSPC vs. fibrin – ECFC-EC). (d) The number of vessel branch points is significantly enhanced by the presence of hNSPCs and is greatest in combination scaffolds (green bars). P = 1.09E-04 (fibrin/HA/lam – ECFC-EC+NSPC vs. fibrin – ECFC-EC), P = 4.63E-04 (fibrin/HA/lam – ECFC-EC+NSPC vs. fibrin/HA/lam – ECFC-EC). **P < 0.01, ***P < 0.001. Error bars represent SEM. N = 3 independent biological repeats. (e) RNA-seq analysis indicates angiogenic factor gene expression from three biological replicates of hNSPCs. Colors indicate the $\log_2$RPKM value for each factor, with red indicating higher expression and green lower expression (see inset for scale). (f) A scatterplot displays average RPKM values for angiogenic growth factors generated from the three replicates of hNSPCs organized from high to low expressers (error is SEM). Genes are clustered into three categories: high (>10 RPKM), moderate (1-10 RPKM), and low (<1 RPKM) expression. Dotted lines indicate 10 RPKM and 1 RPKM boundaries. For comparison, beta-actin, GAPDH, and FGFR1 fall in the highly expressed category, while FGFR2 is moderately expressed, and the muscle marker MyoD shows low to no expression. (g) Scatterplot of average RPKM values for cytokines and chemokines from the three hNSPC replicates. (h) Scatterplot of average RPKM values for adhesion molecules and ECM from the three hNSPC replicates. (i) Scatterplot of average RPKM values for proteases and inhibitors from the three hNSPC replicates.

4.5 DISCUSSION

The development of biomaterial scaffolds that provide maximal support for hNSPC survival and function will likely improve the ability of these cells to successfully treat the damaged CNS. We report here on the establishment of a novel combination scaffold incorporating salmon fibrin, HA, and laminin and the results of multiple tests showing that the scaffold material properties, effects on hNSPCs, degradation rate after seeding with hNSPCs, and potential for vascularization make it a viable material for these cells. Initial studies demonstrated the benefits of including salmon fibrin in the scaffolds since it stimulates greater

hNSPC proliferation than mammalian fibrin. The incorporation of HA and laminin with salmon fibrin yields hydrogels that polymerize more effectively and are slightly stiffer than fibrin alone, but ideally match the mechanical characteristics of CNS tissue. Combination scaffolds support the proliferation and differentiation of hNSPCs, which express integrins that moderate binding to fibrin and laminin, indicating the advantages of these materials as substrates for hNSPCs. Combination scaffolds have a significantly slower hNSPC-mediated degradation profile than fibrin, thus overcoming a limitation of fibrin as a single component scaffold. Co-cultures of hNSPCs and hECFC-ECs revealed that vessel formation and branching complexity were enhanced in combination scaffolds containing both cell types, indicating the ability of these scaffolds to support vascularization. Combination scaffolds thus fulfill key criteria for hNSPC scaffolds, including non-toxic polymerization, biocompatibility with hNSPCs, ability to be injected as a liquid then polymerize *in situ*, match the stiffness of the surrounding CNS tissue, reasonable degradation rate, and support for vascularization.

Salmon fibrin is a more effective biomaterial than mammalian fibrin for neuronal process extension, sprouting of human umbilical vein endothelial cells (HUVECs), functional recovery in a dorsal hemisection spinal cord injury model, and as shown here proliferation of hNSPCs[20, 21, 23]. The differences between salmon and mammalian fibrin may be attributed to species-specific variations in the fibrinogen sequence. Fibrinogen is a large glycoprotein containing pairs of three subunit chains Aα, Bβ, and γ. Fibrinogen chains are heavily glycosylated, and differences in carbohydrate modifications between salmon and mammalian fibrinogens may underlie some of the discrepancies between species, including variations in charge and solubility[20, 24]. The salmon genome has recently been sequenced and comparison of the predicted amino acid sequences of salmon and mammalian (human and bovine) fibrinogen reveals discrepancies in the location of

RGD sequences within the chains. The salmon fibrinogen Aα and γ chains each contain one RGD sequence while both human and bovine Aα chains encode two RGDs with none in the γ chains. The salmon fibrinogen sequence is much more similar in this regard to the zebrafish fibrinogen sequence. The location differences in RGD sequences between salmon and mammalian fibrinogen might affect binding to cell surface integrins and in turn could be involved in differential integrin activation, which could influence a variety of cellular processes and explain the species-specific effects of salmon fibrin compared to mammalian fibrin.

Critical material properties for CNS scaffolds include polymerization kinetics that allow the scaffold and cells to be injected as a liquid and polymerize completely in the tissue and mechanical properties that match the soft tissue of the brain and spinal cord. The polymerization characteristics of the fibrin and combination scaffolds are similar since both are controlled by thrombin and the rate of polymerization can be modulated by adjusting the thrombin concentration, making fibrin-based scaffolds useful for CNS applications[16, 23]. The combination scaffolds described in this study have polymerization kinetics suitable for cell transplantation. We are currently using these scaffolds with hNSPCs in an *in vivo* rodent model of ischemic stroke. We previously injected salmon fibrin as a hydrogel for spinal cord injury[23] and are now injecting the combination scaffold through a 30 gauge blunt tip needle into naïve and infarcted rat striatum. By utilizing thrombin at a concentration of 0.1 U/mL, we can inject 3 μL of scaffold/hNSPC solution at 1 μL/min without experiencing premature polymerization within the transplantation syringe. Thus, the polymerization kinetics of both fibrin and combination scaffolds are suitable for transplantation.

There was significantly less non-polymerized fibrinogen released from the combination hydrogels than the fibrin hydrogels 30 minutes after the onset of polymerization, suggesting

more complete polymerization of the combination hydrogels (Fig. 4.2c). This may relate to differences between the two types of hydrogels in cross-link density and subsequent polymer trapping. An estimation of the distance between cross-links within the hydrogels can be obtained by employing the equation $G_o = \gamma kT$, where G_o is the low frequency elastic modulus and γ represents the number of polymeric network strands per unit volume[88]. For fibrin hydrogels the distance between cross-links is estimated to be 32.5 nm, while for the combination hydrogels the distance is lower at 27.3 nm due to the IPN of HA. The reduced distance between cross links in the combination scaffolds suggest there may be increased trapping of fibrinogen that prevents its escape during polymerization. This finding is similar to previous work illustrating decreased length between fiber nodes of collagen-fibrin IPN combination scaffolds compared to those of pure collagen[89].

The reduced cross-link distance in the combination scaffolds may be tied to substrate mechanics, which can affect NSPC differentiation and thus is an important parameter to consider for NSPC transplantation scaffolds[90]. NSPC differentiation is strongly influenced by substrate stiffness in ranges physiologically relevant for CNS tissue[91], such that soft substrates support neuronal differentiation while stiffer substrates induce generation of glia[72, 73, 92]. A mechanical stretch stimulus decreases NSPC differentiation into oligodendrocytes when the substrate is laminin, but not fibronectin, highlighting the importance of integrin signaling to substrate sensing[93]. HNSPCs also express a stretch-activated ion channel, Piezo1, that responds to a variety of mechanical stimuli and guides lineage choice towards neurons or astrocytes based on substrate stiffness[94]. The stiffness of the fibrin and combination hydrogels used here (~100-300 Pa) falls within the optimal range for supporting neurite branching[95], NSPC differentiation[72, 73, 92], and matches the compliance of human brain tissue (~100 – 1000 Pa)[25, 91, 96]. The scaffolds that

include HA are slightly stiffer than those without HA, which may be due to a combination of factors including the increased cross-link density, potential cross-linking of thiols on the HA with cysteine residues on fibrinogen via disulfide bonding, and an increase in polymer mass from the HA. The polymerization kinetics and mechanical properties of combination scaffolds of fibrin and HA are optimal for hNSPCs and CNS tissue applications.

The rate of scaffold degradation to allow for proper cellular integration has been highlighted as an important component of scaffold design[97]. Although there is no consensus on the ideal residence time for an implanted scaffold, it is crucial for the scaffold to remain intact long enough to promote transplanted cell survival and incorporation into the host. It should be noted that as the scaffold degrades over time *in vivo*, its mechanical properties will change, and the microenvironment of the transplanted cells will be dominated by the host tissue rather than the scaffold. *In vitro*, salmon fibrin scaffolds seeded with mouse spinal cord neurons persist intact much longer than bovine fibrin or human fibrin scaffolds seeded with cells as measured by gross observation of the scaffolds[20]. Similarly, HUVECs degrade human fibrin more swiftly than salmon fibrin *in vitro*[21]. Despite salmon fibrin's reduced degradation in these *in vitro* studies, it degraded on the order of 7 days in the more complex *in vivo* environment of the injured rodent spinal cord[23], which would be too short to support the differentiation of hNSPCs *in vivo*, requiring a minimum of one month. Integration of HA with salmon fibrin to create combination scaffolds significantly attenuated cell-mediated fibrin degradation while the inclusion of laminin did not further affect degradation (Fig. 4.7). These findings suggest that the IPN created by HA slows fibrin degradation and this may occur by several different mechanisms. The thiols on the HA may cross-link with cysteines on fibrinogen via disulfide bridges, rendering the combination scaffold less susceptible to degradation. HA may also bind plasmin and thus limit its diffusion.

Plasmin is formed from plasminogen via enzymes termed plasminogen activators. Plasminogen activator expression by hNSPCs may also be reduced within the combination scaffolds due to the presence of HA, as HA can inhibit expression of plasminogen activator in human synovial fibroblasts[98]. Based on our RNA-Seq data, hNSPCs express the plasminogen activators, urokinase and tissue plasminogen activator, but do not express plasminogen. Plasminogen is present in the fibrin hydrogels since it co-purifies with fibrinogen[20, 99]. Combining fibrin and HA to create a composite scaffold ameliorates the rapid cell-mediated degradation occurring with fibrin alone.

Scaffolds for hNSPCs should support basic cell functions, such as proliferation and differentiation, which in many cases will be mediated by binding to integrins on the cell surface. Each of the individual scaffold components (fibrin, HA, and laminin) have been demonstrated to encourage rodent and human NSPC proliferation *in vitro* and *in vivo*[16, 34, 39, 60]. Thus it is not surprising that hNSPCs proliferate when cultured in combination scaffolds of these biomaterials (Fig. 4.4), suggesting these scaffolds may aid cell survival and expansion post transplantation. Although laminin stimulated expansion of hNSPCs in a two-dimensional system[34, 39], the addition of laminin to the combination scaffolds did not further increase hNSPC proliferation. However, laminin may have more of an effect on neurite outgrowth of neurons differentiated from hNSPCs (Fig. 4.5b), which would fit with laminin's long-recognized role in the promotion of neurite outgrowth[34, 100, 101]. Fibrin and HA promote differentiation in other systems as scaffolds with growth factors support the differentiation of mouse and human NSPCs into neurons and glia *in vivo*[19] and HA/polylysine multilayer films encourage rat NSPC differentiation into neurons and glia *in vitro*[102].

Interactions between cells and ECM scaffolds are mediated by cell surface integrins[79] and hNSPCs express integrins to bind fibrin (αVβ1 and α5β1) and laminin (α7β1, α6β1, and α3β1) as shown by RNA-Seq analysis and flow cytometry (Fig. 4.6)[34 80, 81]. Combination scaffolds of fibrin and HA support hNSPCs and these cells have cell surface fibrinogen and laminin-binding integrins necessary for adhesion to the scaffolds.

An important characteristic of scaffolds is the ability to support vascularization and our data indicate combination scaffolds of fibrin, HA, and laminin encourage the formation of vessels from hECFC-ECs. Adding human NSPCs to hECFC-ECs within salmon fibrin-HA-laminin scaffolds significantly increases the formation of vascular structures (Fig. 4.8). Since for most measures of vessel formation there were not significant differences between the fibrin or combination scaffolds with hECFC-ECs alone, we conclude that the hNSPCs have a more dominant effect on vessel generation than the biomaterial composition. The vessels we observed from hECFC-ECs are not fully developed vascular structures. Further vessel maturation and stabilization would require the addition of perivascular cells to facilitate anastomosis and increase survival of networks, which we plan to explore in future work. Overall, our data indicate a strong synergistic effect of human neural stem cells and biomaterials on the formation of human vessels.

Similar effects of NSPCs on formation of vessels from endothelial cells have been described for rodent cells, but not for human cells to our knowledge. Co-transplantation of mouse NSPCs and mouse ES-derived vascular progenitor cells without a scaffold into rodent stroke models leads to enhanced vessel formation in the infarct area[46]. Mouse NSPCs induce more vessel/cord formation from mouse brain periventricular endothelial cells when both cell types are co-cultured on Matrigel[41]. Co-transplants of mouse NSPCs and mouse endothelial cells

in a synthetic poly(ethylene glycol)-based scaffold implanted subcutaneously generated better vessel formation than transplants of endothelial cells alone in the scaffolds[47]. Using the same scaffold and cells in a rat model of spinal cord injury, the greatest degree of vessel formation occurred in the scaffold containing both mouse NSPCs and endothelial cells[53]. Our data now add to this literature by demonstrating similar effects of human NSPCs on human endothelial cell vessel formation.

The effect of hNSPCs on vasculogenesis by hECFC-ECs may be due to neural cell secreted factors acting on the hECFC-ECs. RNA-seq analysis of the hNSPCs shows high expression of multiple genes relevant for vasculogenesis (Fig. 4.8). The vasculogenic factors assessed in the RNA-seq data comprise a broad class of growth factors, cytokines/chemokines, adhesion molecules and ECM, and proteases and inhibitors. A large percentage of the factors in the adhesion molecule/ECM and proteases/inhibitors categories were highly expressed (71% and 55%, respectively), suggesting that a significant component of the effect of hNSPCs on vasculogenesis may be mediated by modifying the ECM. In particular, hNSPCs produce collagen I and IV, laminin, and fibronectin as well as the proteases MMP2, MMP15, plasminogen activator (PLAU), MMP14, and the protease inhibitors TIMP2 and TIMP1 (Fig. 4.8). In addition to factors that modify the ECM, hNSPCs express high levels of the growth factors VEGF, PDGF, and TGF-β1 (Fig. 4.8), all of which are factors essential for angiogenesis[103-105]. Rodent NSPCs express VEGF-A *in vitro*, and *in vivo* production of VEGF-A has been demonstrated for mouse hippocampal NSPCs[106-108]. Human NSPCs transplanted into a rodent stroke model promote behavioral recovery and neovascularization, and both of these effects are lost if VEGF is blocked with a human VEGF-specific antibody[109]. Here, we add to these findings by providing direct evidence of VEGF-A and VEGF-B mRNA production by

hNSPCs. We showed previously that the growth factors TGF-α, HGF, and the ECM molecule fibronectin, all of which are expressed by hNSPCs, are secreted by fibroblasts and contribute to angiogenic sprouting from endothelial cells[86, 87]. Intriguingly, hNSPCs also express elevated levels of SPARC (secreted protein acidic and rich in cysteine), IGFBP7 (insulin-like growth factor binding protein 7), collagen I, TGF-βI (transforming growth factor β-induced protein ig-h3, βig-h3), and moderate levels of PCOLCE (procollagen C-endopeptidase enhancer 1), each of which we found to be required for endothelial cell lumen formation, which relates to vessel formation and maturation[86]. These data suggest that factors produced by the hNSPCs are likely playing a key role in increasing vasculogenesis in co-cultures with hECFC-ECs, highlighting the relevance of crosstalk between neural and endothelial cells for vascularization.

Interest in the use of scaffolds containing multiple components is growing in the fields of tissue engineering and regenerative medicine. Scaffolds combining fibrin and hyaluronic acid induce greater chondrogenesis of human bone marrow-derived mesenchymal stem cells (BMSCs) *in vitro* than fibrin scaffolds[110]. Human MSCs and human umbilical vein endothelial cells (HUVECs) were plated in scaffolds of fibrin or collagen/fibrin combinations at different mass ratios to assess vascularization[111]. In this case, the ratio of components in the combination scaffold played a key role in its effect on cells. Vessel formation was best in either fibrin or combination scaffolds at a mass ratio of 40/60 (collagen/fibrin); notably the individual and combinations scaffolds were of similar stiffness with combination scaffolds having more robust polymerization kinetics than those of fibrin. MSCs coalesced along vessels in the 40/60 combination scaffolds, but specific effects of the scaffold on MSCs were not assessed. Combination scaffolds have been utilized to provide a localized source of therapeutic molecules, as fibrin-HA IPNs loaded with SDF-1α promote homing of chondrogenic progenitor cells and

subsequent functional repair of bovine cartilage[112]. In regards to NSPCs, HA-collagen scaffolds increase mouse NSPC survival when transplanted into the infarct core of stroke-injured mice[9]. Our study now identifies combination scaffolds of fibrin-HA-laminin as beneficial scaffolds for human NSPCs since they resist rapid degradation, enhance vascularization by hECFC-ECs, and support hNSPC proliferation and differentiation. Based on the promising results to date with combination scaffolds, more research is clearly warranted, to test the effects of a variety of combination scaffolds on human NSPCs as these cells move toward use in clinical applications.

4.6 CONCLUSIONS

Our data indicate that combination scaffolds consisting of salmon fibrin with HA and laminin possess material properties that enable polymerization with cells, mimic native brain tissue, support hNSPC function, and better resist degradation than fibrin alone. Furthermore, hNSPCs work synergistically with combination scaffolds to enhance vasculogenesis from hECFC-ECs, thus providing motivation for their use to create vascularized transplant scaffold constructs to treat human disease. Our findings offer implications for the use of more complex neural tissue engineering strategies utilizing multiple human cell types and scaffold biomaterials to enhance cellular function *in vitro* and *in vivo*. Employment of more sophisticated methods such as combination scaffolds to increase stem cell survival and function post-transplant will be critical for their use as cellular therapeutics.

4.7 ACKNOWLEDGMENTS

The authors would like to thank Dr. Evelyn Sawyer and Sea Run Holdings Inc. for the gift of salmon fibrinogen and thrombin; Dr. Phillip Schwartz for providing hNSPCs; the laboratories of Drs. Szu Wang and Nancy Da Silva for assistance in obtaining rheological measurements; Rylan

Kautz and Andrew Yale for assistance in designing the graphical abstract; UCI Genomics Core for running RNA Sequencing. This work was supported by the National Institute of Neurological Disorders and Stroke (T32 NS082174, predoctoral fellowship to JA), the California Institute for Regenerative Medicine (RB5-07254, LAF), the Craig H. Neilsen Foundation (SCIRTS-296387, LAF), and the National Center for Research Resources and the National Center for Advancing Translational Sciences, National Institutes of Health, through Grant UL1 TR001414 (Pilot Grant to LAF), and the National Institute of Health (R01 PQD5-CA180122, CCWH). CCWH also receives support from the Chao Family Comprehensive Cancer Center through a National Cancer Institute Center Grant (P30A062203).

4.8 SUPPLEMENTAL MATERIAL

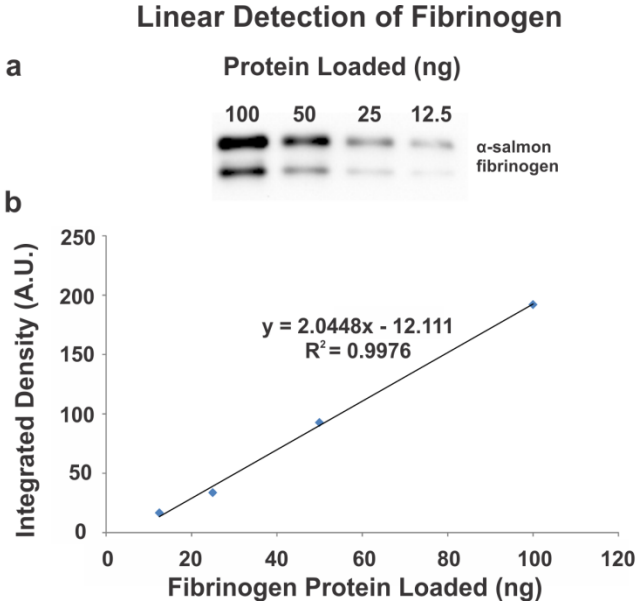

Figure 4.S1. Detection of fibrinogen by Western Blot is linear. (a) An anti-salmon fibrinogen antibody was used to detect set amounts of salmon fibrinogen loaded into each lane [21]. (b) Band intensity of detected fibrinogen increases linearly with the amount of protein loaded per lane ensuring accurate measurements of released fibrinogen into the media in hNSPC-seeded samples.

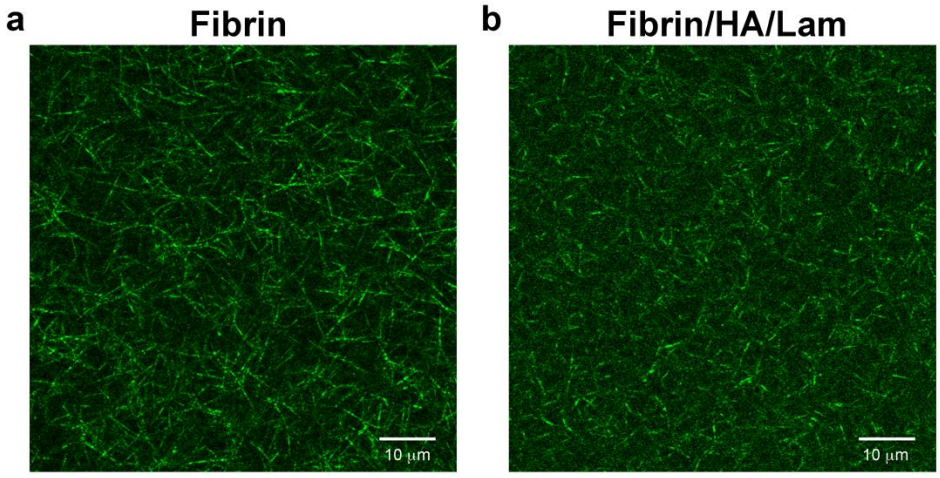

Figure 4.S2. Confocal reflection imaging of hydrogels. Confocal reflection microscopy was used to obtain z-stacks of the (a) fibrin and (b) fibrin/HA/lam hydrogels. Representative images of backscattered light display fibers from each hydrogel, with images taken at a plane 20 μm from the surface of the glass bottom culture dish. Each z-stack is 7 μm with 100 nm step.

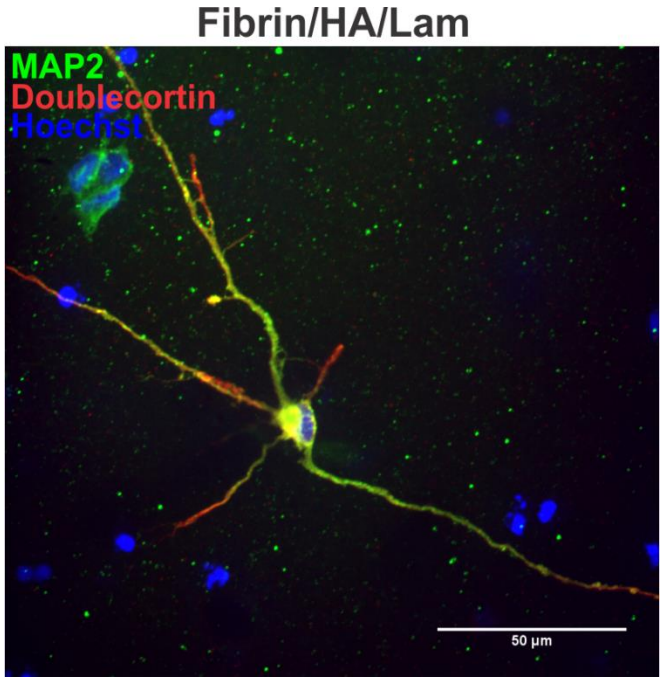

Figure 4.S3. Neurons differentiated from hNSPCs in scaffolds express multiple neuronal markers. Image of a neuron differentiated from hNSPCs in fibrin/HA/lam scaffold co-stained by neuronal markers MAP2 (green) and doublecortin (red). All nuclei are stained with Hoechst (blue).

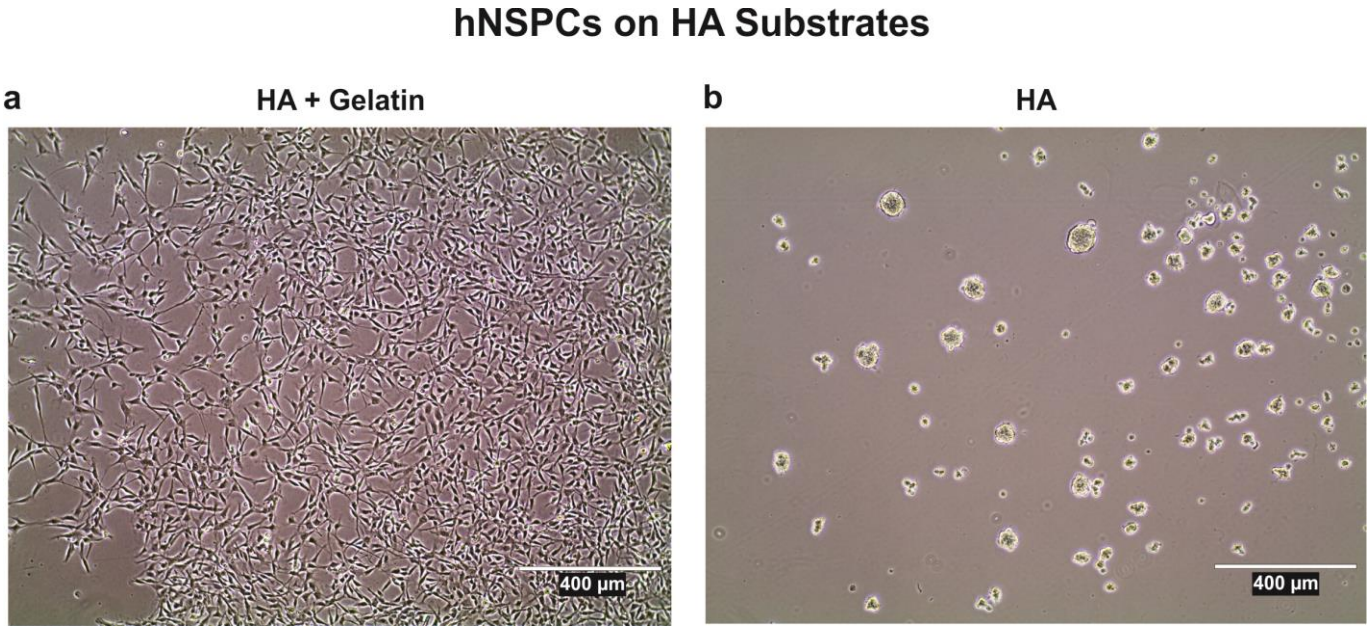

Figure 4.S4. HA requires the inclusion of adhesion sites in order to bind hNSPCs. (a) hNSPCs bind and elaborate processes when seeded onto glass coverslips coated with HA that includes cross-linked gelatin peptides. (b) hNSPCs form spheres and don't bind to the substrate when seeded onto HA without the inclusion of adhesion peptides.

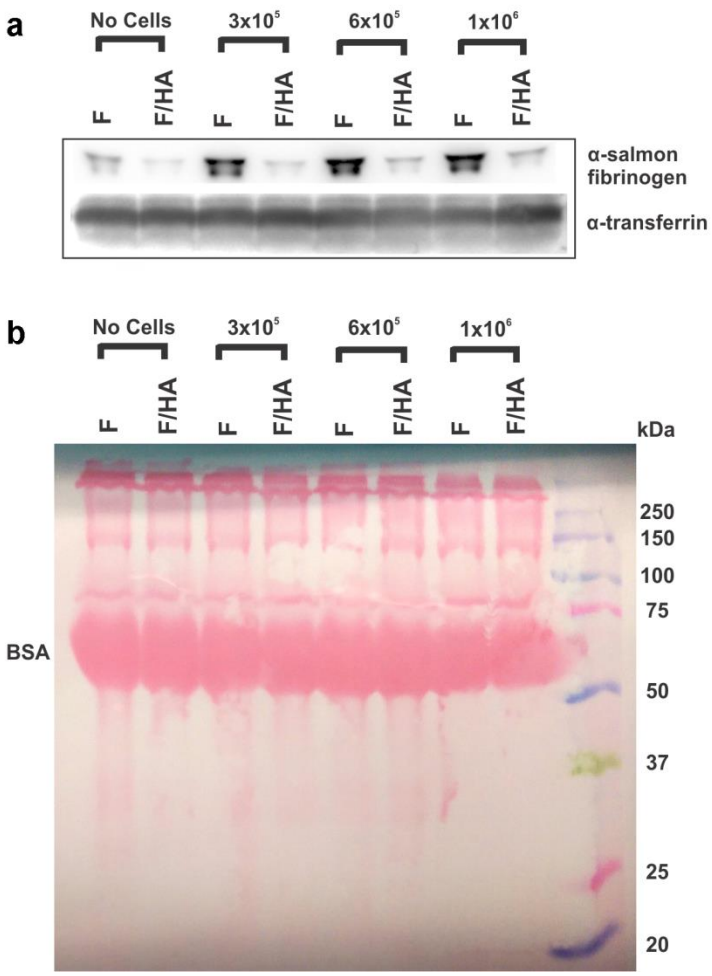

Figure 4.S5. Equivalent loading of protein per lane detected by Ponceau S stain for cell titration fibrin degradation studies. (a) Total salmon fibrinogen released into the media increases with increasing hNSPC concentration in salmon fibrin hydrogels (F), but is substantially reduced by the presence of HA (F/HA). Cells were seeded at $3x10^5$, $6x10^5$, and $1x10^6$ cells per hydrogel. Detection of transferrin in the media demonstrates approximately equal loading of media per lane. (b) Total protein detected by Ponceau S demonstrates approximately equal protein loading per lane for both fibrin and combination hydrogels. The thick red band near 66.5 kDa is BSA, which is a major component of the media. F denotes fibrin only, F/HA correlates to fibrin with HA, and F/HA/Lam signifies fibrin with HA and laminin.

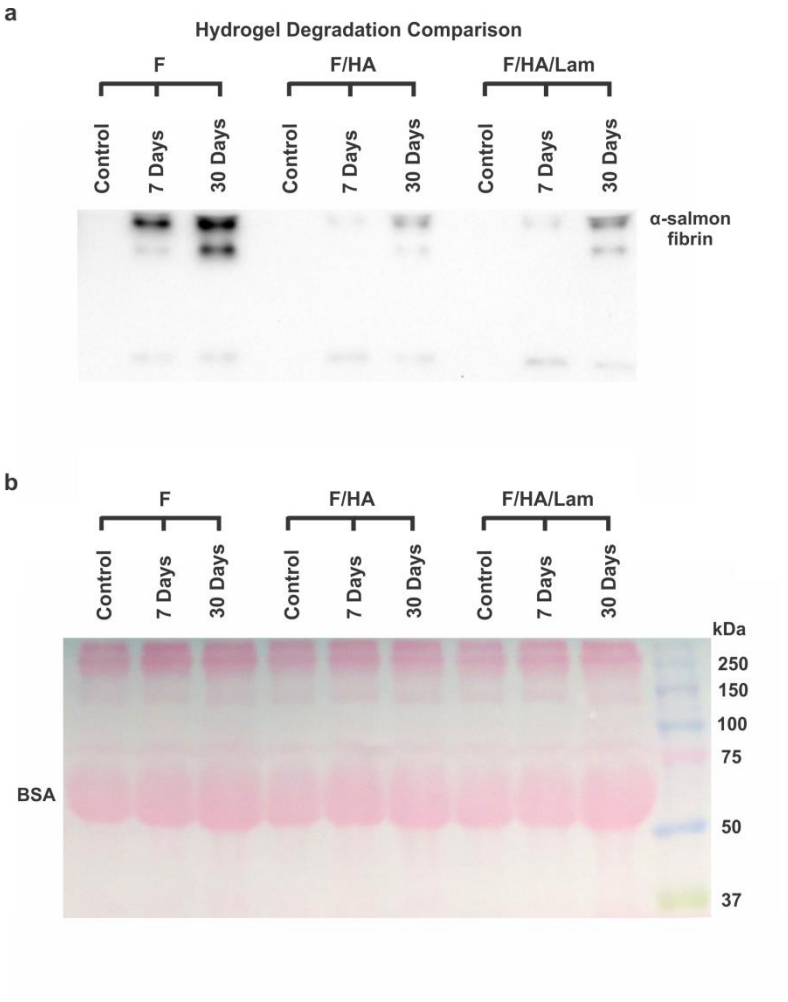

Figure 4.S6. Reduced degradation of fibrin in combination scaffolds over time. (a) Western Blot detection of salmon fibrinogen released into the media at 7 or 30 days reveals increased degradation of fibrin only hydrogels compared to combination scaffolds when both are seeded with hNSPCs ($1x10^5$). The media from the no cells control group was analyzed immediately after addition of media to the hydrogel (~30 minutes after induction of polymerization). (b) Total protein detected by Ponceau S demonstrates approximately equal loading per lane for both fibrin only and combination hydrogels. The thick band near 66.5 kDa is BSA, which is a major component of the media. F denotes fibrin only, F/HA correlates to fibrin with HA, and F/HA/Lam signifies fibrin with HA and laminin.

4.9 REFERENCES

1. Lindvall, O. & Kokaia, Z. Stem cells for the treatment of neurological disorders. *Nature* **441**, 1094-1096 (2006).
2. Gage, F.H. Mammalian neural stem cells. *Science* **287**, 1433-1438 (2000).
4. Kelly, S. et al. Transplanted human fetal neural stem cells survive, migrate, and differentiate in ischemic rat cerebral cortex. *Proc Natl Acad Sci U S A* **101**, 11839-11844 (2004).
4. Hayashi, J. et al. Primate embryonic stem cell-derived neuronal progenitors transplanted into ischemic brain. *Journal of cerebral blood flow and metabolism : official journal of the International Society of Cerebral Blood Flow and Metabolism* **26**, 906-914 (2006).
5. Ikeda, R. et al. Transplantation of neural cells derived from retinoic acid-treated cynomolgus monkey embryonic stem cells successfully improved motor function of hemiplegic mice with experimental brain injury. *Neurobiology of disease* **20**, 38-48 (2005).
6. McCreedy, D.A. et al. Survival, Differentiation, and Migration of High-Purity Mouse Embryonic Stem Cell-derived Progenitor Motor Neurons in Fibrin Scaffolds after Sub-Acute Spinal Cord Injury. *Biomater Sci* **2**, 1672-1682 (2014).
7. Burns, T., Verfaillie, C. & Low, W. Stem cells for ischemic brain injury: a critical review. *The Journal of comparative neurology* **515**, 125-144 (2009).
8. Bliss, T., Guzman, R., Daadi, M. & Steinberg, G. Cell transplantation therapy for stroke. *Stroke; a journal of cerebral circulation* **38**, 817-826 (2007).
9. Zhong, J. et al. Hydrogel matrix to support stem cell survival after brain transplantation in stroke. *Neurorehabilitation and neural repair* **24**, 636-644 (2010).
10. Tate, C.C. et al. Laminin and fibronectin scaffolds enhance neural stem cell transplantation into the injured brain. *J Tissue Eng Regen Med* **3**, 208-217 (2009).
11. Evans, N., Gentleman, E. & Polak, J. Scaffolds for stem cells. *Materials Today* **9**, 26-33 (2006).
12. Zhang, J. et al. Physically associated synthetic hydrogels with long-term covalent stabilization for cell culture and stem cell transplantation. *Advanced materials (Deerfield Beach, Fla.)* **23**, 5098-5103 (2011).
14. Willerth, S.M. & Sakiyama-Elbert, S.E. Combining stem cells and biomaterial scaffolds for constructing tissues and cell delivery. (2008).
14. Skop, N.B., Calderon, F., Cho, C.H., Gandhi, C.D. & Levison, S.W. Improvements in biomaterial matrices for neural precursor cell transplantation. *Mol Cell Ther* **2**, 19 (2014).
15. Li, X., Katsanevakis, E., Liu, X., Zhang, N. & Wen, X. Engineering neural stem cell fates with hydrogel design for central nervous system regeneration. *Progress in Polymer Science* **37**, 1105-1129 (2012).
16. Johnson, P., Tatara, A., McCreedy, D., Shiu, A. & Sakiyama-Elbert, S. Tissue-engineered fibrin scaffolds containing neural progenitors enhance functional recovery in a subacute model of SCI. *Soft matter* **6**, 5127-5137 (2010).
17. Johnson, P.J., Tatara, A., Shiu, A. & Sakiyama-Elbert, S.E. Controlled release of neurotrophin-3 and platelet-derived growth factor from fibrin scaffolds containing neural progenitor cells enhances survival and differentiation into neurons in a subacute model of SCI. *Cell Transplant* **19**, 89-101 (2010).
18. Wilems, T.S., Pardieck, J., Iyer, N. & Sakiyama-Elbert, S.E. Combination therapy of stem cell derived neural progenitors and drug delivery of anti-inhibitory molecules for spinal cord injury. *Acta Biomater* **28**, 23-32 (2015).
19. Lu, P. et al. Long-distance growth and connectivity of neural stem cells after severe spinal cord injury. *Cell* **150**, 1264-1273 (2012).
20. Ju, Y.-E., Janmey, P., McCormick, M., Sawyer, E. & Flanagan, L. Enhanced neurite growth from mammalian neurons in three-dimensional salmon fibrin gels. *Biomaterials* **28**, 2097-2108 (2007).
21. Sieminski, A.L. & Gooch, K.J. Salmon fibrin supports an increased number of sprouts and decreased degradation while maintaining sprout length relative to human fibrin in an in vitro angiogenesis model. *J Biomater Sci Polym Ed* **15**, 237-242 (2004).

22. Prange, M.T. & Margulies, S.S. Regional, directional, and age-dependent properties of the brain undergoing large deformation. *J Biomech Eng* **124**, 244-252 (2002).
24. Sharp, K. et al. Salmon fibrin treatment of spinal cord injury promotes functional recovery and density of serotonergic innervation. *Experimental neurology* **235**, 345-356 (2012).
24. Laidmäe, I. et al. Stability, sterility, coagulation, and immunologic studies of salmon coagulation proteins with potential use for mammalian wound healing and cell engineering. *Biomaterials* **27**, 5771-5779 (2006).
25. Uibo, R. et al. Soft materials to treat central nervous system injuries: evaluation of the suitability of non-mammalian fibrin gels. *Biochimica et biophysica acta* **1793**, 924-930 (2009).
26. Preston, M. & Sherman, L.S. Neural stem cell niches: roles for the hyaluronan-based extracellular matrix. *Front Biosci (Schol Ed)* **3**, 1165-1179 (2011).
27. Moshayedi, P. & Carmichael, S.T. Hyaluronan, neural stem cells and tissue reconstruction after acute ischemic stroke. *Biomatter* **3**, e23863 (2013).
28. Khaing, Z.Z. et al. High molecular weight hyaluronic acid limits astrocyte activation and scar formation after spinal cord injury. *J Neural Eng* **8**, 046033 (2011).
29. Margolis, R.U., Margolis, R.K., Chang, L.B. & Preti, C. Glycosaminoglycans of brain during development. *Biochemistry* **14**, 85-88 (1975).
30. Khaing, Z.Z. & Seidlits, S.K. Hyaluronic acid and neural stem cells: implications for biomaterial design. *Journal of Materials Chemistry B* **3**, 7850-7866 (2015).
31. Lam, J., Lowry, W.E., Carmichael, S.T. & Segura, T. Delivery of iPS-NPCs to the Stroke Cavity within a Hyaluronic Acid Matrix Promotes the Differentiation of Transplanted Cells. *Adv Funct Mater* **24**, 7053-7062 (2014).
32. Chopra, A. et al. Reprogramming cardiomyocyte mechanosensing by crosstalk between integrins and hyaluronic acid receptors. *J Biomech* **45**, 824-831 (2012).
34. Chopra, A. et al. Augmentation of integrin-mediated mechanotransduction by hyaluronic acid. *Biomaterials* **35**, 71-82 (2014).
34. Flanagan, L., Rebaza, L., Derzic, S., Schwartz, P. & Monuki, E. Regulation of human neural precursor cells by laminin and integrins. *Journal of neuroscience research* **83**, 845-856 (2006).
35. Stabenfeldt, S.E., García, A.J. & LaPlaca, M.C. Thermoreversible laminin-functionalized hydrogel for neural tissue engineering. *J Biomed Mater Res A* **77**, 718-725 (2006).
36. Junka, R., Valmikinathan, C.M., Kalyon, D.M. & Yu, X. Laminin Functionalized Biomimetic Nanofibers For Nerve Tissue Engineering. *J Biomater Tissue Eng* **3**, 494-502 (2013).
37. Jin, K. et al. Transplantation of human neural precursor cells in Matrigel scaffolding improves outcome from focal cerebral ischemia after delayed postischemic treatment in rats. *J Cereb Blood Flow Metab* **30**, 534-544 (2010).
38. Addington, C.P. et al. Enhancing neural stem cell response to SDF-1α gradients through hyaluronic acid-laminin hydrogels. *Biomaterials* **72**, 11-19 (2015).
39. Hall, P.E., Lathia, J.D., Caldwell, M.A. & Ffrench-Constant, C. Laminin enhances the growth of human neural stem cells in defined culture media. *BMC Neurosci* **9**, 71 (2008).
40. Calvo, C.F. et al. Vascular endothelial growth factor receptor 3 directly regulates murine neurogenesis. *Genes Dev* **25**, 831-844 (2011).
41. Vissapragada, R. et al. Bidirectional crosstalk between periventricular endothelial cells and neural progenitor cells promotes the formation of a neurovascular unit. *Brain Res* **1565**, 8-17 (2014).
42. Shen, Q. et al. Endothelial cells stimulate self-renewal and expand neurogenesis of neural stem cells. *Science* **304**, 1338-1340 (2004).
44. Sun, J., Zhou, W., Ma, D. & Yang, Y. Endothelial cells promote neural stem cell proliferation and differentiation associated with VEGF activated Notch and Pten signaling. *Dev Dyn* **239**, 2345-2353 (2010).
44. Tavazoie, M. et al. A specialized vascular niche for adult neural stem cells. *Cell Stem Cell* **3**, 279-288 (2008).
45. Nakagomi, N. et al. Endothelial cells support survival, proliferation, and neuronal differentiation of transplanted adult ischemia-induced neural stem/progenitor cells after cerebral infarction. *Stem Cells* **27**, 2185-2195 (2009).

46. Li, J. et al. Neurovascular recovery via co-transplanted neural and vascular progenitors leads to improved functional restoration after ischemic stroke in rats. *Stem Cell Reports* **3**, 101-114 (2014).
47. Ford, M.C. et al. A macroporous hydrogel for the coculture of neural progenitor and endothelial cells to form functional vascular networks in vivo. *Proc Natl Acad Sci U S A* **103**, 2512-2517 (2006).
48. Chen, X. et al. Rapid anastomosis of endothelial progenitor cell-derived vessels with host vasculature is promoted by a high density of cotransplanted fibroblasts. *Tissue Eng Part A* **16**, 585-594 (2010).
49. Chen, X. et al. Prevascularization of a fibrin-based tissue construct accelerates the formation of functional anastomosis with host vasculature. *Tissue Eng Part A* **15**, 1363-1371 (2009).
50. White, S.M. et al. Longitudinal in vivo imaging to assess blood flow and oxygenation in implantable engineered tissues. *Tissue Eng Part C Methods* **18**, 697-709 (2012).
51. Shen, Q. et al. Adult SVZ stem cells lie in a vascular niche: a quantitative analysis of niche cell-cell interactions. *Cell Stem Cell* **3**, 289-300 (2008).
52. Li, Q., Ford, M.C., Lavik, E.B. & Madri, J.A. Modeling the neurovascular niche: VEGF- and BDNF-mediated cross-talk between neural stem cells and endothelial cells: an in vitro study. *J Neurosci Res* **84**, 1656-1668 (2006).
54. Rauch, M.F. et al. Engineering angiogenesis following spinal cord injury: a coculture of neural progenitor and endothelial cells in a degradable polymer implant leads to an increase in vessel density and formation of the blood-spinal cord barrier. *Eur J Neurosci* **29**, 132-145 (2009).
54. Schwartz, P.H. et al. Isolation and characterization of neural progenitor cells from post-mortem human cortex. *J Neurosci Res* **74**, 838-851 (2003).
55. Yuan, S.H. et al. Cell-surface marker signatures for the isolation of neural stem cells, glia and neurons derived from human pluripotent stem cells. *PLoS One* **6**, e17540 (2011).
56. Melero-Martin, J.M. et al. In vivo vasculogenic potential of human blood-derived endothelial progenitor cells. *Blood* **109**, 4761-4768 (2007).
57. Shu, X.Z., Liu, Y., Luo, Y., Roberts, M.C. & Prestwich, G.D. Disulfide cross-linked hyaluronan hydrogels. *Biomacromolecules* **3**, 1304-1311 (2002).
58. Zheng Shu, X., Liu, Y., Palumbo, F.S., Luo, Y. & Prestwich, G.D. In situ crosslinkable hyaluronan hydrogels for tissue engineering. *Biomaterials* **25**, 1339-1348 (2004).
59. Struve, J. et al. Disruption of the hyaluronan-based extracellular matrix in spinal cord promotes astrocyte proliferation. *Glia* **52**, 16-24 (2005).
60. Liang, Y., Walczak, P. & Bulte, J. The survival of engrafted neural stem cells within hyaluronic acid hydrogels. *Biomaterials* **34**, 5521-5529 (2013).
61. Kotlarchyk, M.A., Botvinick, E.L. & Putnam, A.J. Characterization of hydrogel microstructure using laser tweezers particle tracking and confocal reflection imaging. *J Phys Condens Matter* **22**, 194121 (2010).
62. Hartmann, A., Boukamp, P. & Friedl, P. Confocal reflection imaging of 3D fibrin polymers. *Blood Cells Mol Dis* **36**, 191-193 (2006).
64. Zudaire, E., Gambardella, L., Kurcz, C. & Vermeren, S. A computational tool for quantitative analysis of vascular networks. *PLoS One* **6**, e27385 (2011).
64. Lissner, M.M. et al. Age-Related Gene Expression Differences in Monocytes from Human Neonates, Young Adults, and Older Adults. *PLoS One* **10**, e0132061 (2015).
65. Goecks, J., Nekrutenko, A., Taylor, J. & Team, G. Galaxy: a comprehensive approach for supporting accessible, reproducible, and transparent computational research in the life sciences. *Genome Biol* **11**, R86 (2010).
66. Trapnell, C. et al. Transcript assembly and quantification by RNA-Seq reveals unannotated transcripts and isoform switching during cell differentiation. *Nat Biotechnol* **28**, 511-515 (2010).
67. Mortazavi, A., Williams, B.A., McCue, K., Schaeffer, L. & Wold, B. Mapping and quantifying mammalian transcriptomes by RNA-Seq. *Nat Methods* **5**, 621-628 (2008).
68. Straley, K.S., Foo, C.W. & Heilshorn, S.C. Biomaterial design strategies for the treatment of spinal cord injuries. *J Neurotrauma* **27**, 1-19 (2010).
69. Anlar, B. et al. Expression of adhesion and extracellular matrix molecules in the developing human brain. *J Child Neurol* **17**, 707-713 (2002).

70. Georges-Labouesse, E., Mark, M., Messaddeq, N. & Gansmüller, A. Essential role of alpha 6 integrins in cortical and retinal lamination. *Curr Biol* **8**, 983-986 (1998).
71. Kazanis, I. & ffrench-Constant, C. Extracellular matrix and the neural stem cell niche. *Dev Neurobiol* **71**, 1006-1017 (2011).
72. Saha, K. et al. Substrate modulus directs neural stem cell behavior. *Biophysical journal* **95**, 4426-4438 (2008).
74. Leipzig, N. & Shoichet, M. The effect of substrate stiffness on adult neural stem cell behavior. *Biomaterials* **30**, 6867-6878 (2009).
74. Winter, H.H. & Chambon, F. Analysis of linear viscoelasticity of a crosslinking polymer at the gel point. *Journal of Rheology (1978-present)* **30**, 367-382 (1986).
75. Calvet, D., Wong, J.Y. & Giasson, S. Rheological monitoring of polyacrylamide gelation: Importance of cross-link density and temperature. *Macromolecules* **37**, 7762-7771 (2004).
76. Banerjee, A. et al. The influence of hydrogel modulus on the proliferation and differentiation of encapsulated neural stem cells. *Biomaterials* **30**, 4695-4699 (2009).
77. Aurand, E.R., Wagner, J., Lanning, C. & Bjugstad, K.B. Building biocompatible hydrogels for tissue engineering of the brain and spinal cord. *J Funct Biomater* **3**, 839-863 (2012).
78. Lu, J. et al. Advancing practical usage of microtechnology: a study of the functional consequences of dielectrophoresis on neural stem cells. *Integrative biology : quantitative biosciences from nano to macro* **4**, 1223-1236 (2012).
79. Milner, R. & Campbell, I. The integrin family of cell adhesion molecules has multiple functions within the CNS. *Journal of neuroscience research* **69**, 286-291 (2002).
80. Marshall, J.F. et al. Alpha v beta 1 is a receptor for vitronectin and fibrinogen, and acts with alpha 5 beta 1 to mediate spreading on fibronectin. *J Cell Sci* **108 (Pt 3)**, 1227-1238 (1995).
81. Suehiro, K. et al. Fibrinogen binds to integrin alpha(5)beta(1) via the carboxyl-terminal RGD site of the Aalpha-chain. *J Biochem* **128**, 705-710 (2000).
82. Lesley, J., Hyman, R. & Kincade, P.W. CD44 and its interaction with extracellular matrix. *Adv Immunol* **54**, 271-335 (1993).
84. Turley, E.A., Austen, L., Vandeligt, K. & Clary, C. Hyaluronan and a cell-associated hyaluronan binding protein regulate the locomotion of ras-transformed cells. *J Cell Biol* **112**, 1041-1047 (1991).
84. McCourt, P.A., Ek, B., Forsberg, N. & Gustafson, S. Intercellular adhesion molecule-1 is a cell surface receptor for hyaluronan. *J Biol Chem* **269**, 30081-30084 (1994).
85. Tennstaedt, A. et al. Human neural stem cell intracerebral grafts show spontaneous early neuronal differentiation after several weeks. *Biomaterials* **44**, 143-154 (2015).
86. Newman, A.C., Nakatsu, M.N., Chou, W., Gershon, P.D. & Hughes, C.C. The requirement for fibroblasts in angiogenesis: fibroblast-derived matrix proteins are essential for endothelial cell lumen formation. *Mol Biol Cell* **22**, 3791-3800 (2011).
87. Newman, A.C. et al. Analysis of stromal cell secretomes reveals a critical role for stromal cell-derived hepatocyte growth factor and fibronectin in angiogenesis. *Arterioscler Thromb Vasc Biol* **33**, 513-522 (2013).
88. Larson, R.G. The structure and rheology of complex fluids, Vol. 34. (Oxford university press New York, 1999).
89. Rowe, S.L. & Stegemann, J.P. Microstructure and mechanics of collagen-fibrin matrices polymerized using ancrod snake venom enzyme. *J Biomech Eng* **131**, 061012 (2009).
90. D'Angelo, F. et al. Mechanotransduction: tuning stem cells fate. *J Funct Biomater* **2**, 67-87 (2011).
91. Tyler, W.J. The mechanobiology of brain function. *Nat Rev Neurosci* **13**, 867-878 (2012).
92. Keung, A., de Juan-Pardo, E., Schaffer, D. & Kumar, S. Rho GTPases mediate the mechanosensitive lineage commitment of neural stem cells. *Stem cells (Dayton, Ohio)* **29**, 1886-1897 (2011).
94. Arulmoli, J. et al. Static stretch affects neural stem cell differentiation in an extracellular matrix-dependent manner. *Sci Rep* **5**, 8499 (2015).
94. Pathak, M.M. et al. Stretch-activated ion channel Piezo1 directs lineage choice in human neural stem cells. *Proc Natl Acad Sci U S A* **111**, 16148-16153 (2014).
95. Georges, P. et al., Vol. 897 0897-J0802 (Cambridge Univ Press.

96. Levental, I., Georges, P.C. & Janmey, P.A. Soft biological materials and their impact on cell function. *Soft Matter* **3**, 299-306 (2007).
97. Dhandayuthapani, B., Yoshida, Y., Maekawa, T. & Kumar, D.S. Polymeric scaffolds in tissue engineering application: a review. *International Journal of Polymer Science* **2011** (2011).
98. Nonaka, T. et al. Comparison of the inhibitory effects of two types (90 kDa and 190 kDa) of hyaluronic acid on the expression of fibrinolytic factors in human synovial fibroblasts. *Modern Rheumatology* **12**, 160-166 (2002).
99. Wang, L.Z. et al. Purification of salmon clotting factors and their use as tissue sealants. *Thromb Res* **100**, 537-548 (2000).
100. Lander, A.D., Fujii, D.K. & Reichardt, L.F. Laminin is associated with the "neurite outgrowth-promoting factors" found in conditioned media. *Proc Natl Acad Sci U S A* **82**, 2183-2187 (1985).
101. Hantaz-Ambroise, D., Vigny, M. & Koenig, J. Heparan sulfate proteoglycan and laminin mediate two different types of neurite outgrowth. *J Neurosci* **7**, 2293-2304 (1987).
102. Lee, I.C., Wu, Y.C., Cheng, E.M. & Yang, W.T. Biomimetic niche for neural stem cell differentiation using poly-L-lysine/hyaluronic acid multilayer films. *J Biomater Appl* **29**, 1418-1427 (2015).
104. Ferrara, N. Role of vascular endothelial growth factor in regulation of physiological angiogenesis. *Am J Physiol Cell Physiol* **280**, C1358-1366 (2001).
104. Battegay, E.J., Rupp, J., Iruela-Arispe, L., Sage, E.H. & Pech, M. PDGF-BB modulates endothelial proliferation and angiogenesis in vitro via PDGF beta-receptors. *J Cell Biol* **125**, 917-928 (1994).
105. Ferrari, G., Cook, B.D., Terushkin, V., Pintucci, G. & Mignatti, P. Transforming growth factor-beta 1 (TGF-beta1) induces angiogenesis through vascular endothelial growth factor (VEGF)-mediated apoptosis. *J Cell Physiol* **219**, 449-458 (2009).
106. Kirby, E.D., Kuwahara, A.A., Messer, R.L. & Wyss-Coray, T. Adult hippocampal neural stem and progenitor cells regulate the neurogenic niche by secreting VEGF. *Proc Natl Acad Sci U S A* **112**, 4128-4133 (2015).
107. Maurer, M.H., Tripps, W.K., Feldmann, R.E. & Kuschinsky, W. Expression of vascular endothelial growth factor and its receptors in rat neural stem cells. *Neurosci Lett* **344**, 165-168 (2003).
108. Mosher, K.I. et al. Neural progenitor cells regulate microglia functions and activity. *Nat Neurosci* **15**, 1485-1487 (2012).
109. Horie, N. et al. Transplanted stem cell-secreted vascular endothelial growth factor effects poststroke recovery, inflammation, and vascular repair. *Stem Cells* **29**, 274-285 (2011).
110. Snyder, T.N., Madhavan, K., Intrator, M., Dregalla, R.C. & Park, D. A fibrin/hyaluronic acid hydrogel for the delivery of mesenchymal stem cells and potential for articular cartilage repair. *J Biol Eng* **8**, 10 (2014).
111. Rao, R.R., Peterson, A.W., Ceccarelli, J., Putnam, A.J. & Stegemann, J.P. Matrix composition regulates three-dimensional network formation by endothelial cells and mesenchymal stem cells in collagen/fibrin materials. *Angiogenesis* **15**, 253-264 (2012).
112. Yu, Y. et al. Use of Recombinant Human Stromal Cell–Derived Factor 1α–Loaded Fibrin/Hyaluronic Acid Hydrogel Networks to Achieve Functional Repair of Full-Thickness Bovine Articular Cartilage Via Homing of Chondrogenic Progenitor Cells. *Arthritis & Rheumatology* **67**, 1274-1285 (2015).

CHAPTER 5

HUMAN NEURAL STEM CELL TISSUE ENGINEERING TO TREAT STROKE IN A RAT MODEL OF TRANSIENT MIDDLE CEREBRAL ARTERY OCCLUSION

Authors: Janahan Arulmoli[1,2], Clarissa C. Ro[2,6], Cynthia C.H. Bee[3], Victor B. Pham[2,4], Wenbin Liao[2,4], Daniel L. Haus[2,5], Eric M. Gold[2,5], Rebecca A. Nishi[2,5], Oswald Steward[5], Aileen J. Anderson[2,5], Ron Frostig[3], Brian J. Cummings[2,5], Lisa A. Flanagan[1,2,6]

Author Affiliations:

[1]Department of Biomedical Engineering

[2]Sue & Bill Gross Stem Cell Research Center

[3]Department of Neurobiology and Behavior

[4]Department of Pharmaceutical Sciences

[5]Department of Anatomy and Neurobiology

[6]Department of Neurology

[1-6]University of California, Irvine, Irvine, CA, 92697, USA

5.1 INTRODUCTION

Stroke is a leading cause of death and long-term disability nationwide[1], imposing direct economic costs of over $70 billion annually[2]. An ischemic stroke occurs when an artery becomes blocked and inhibits blood circulation to the brain, and ischemic strokes account for 87% of all stroke occurrences in the United States[1]. Despite comprehensive efforts from the medical research community, most stroke sufferers do not qualify for current FDA-approved treatment options. Current treatments include tissue plasminogen activator (tPA) and stent-based clot removal systems, all of which must be administered within 6 hours of stroke onset in order to be effective, thus creating a substantial unmet clinical need that could be ameliorated by identifying novel stroke therapies.

Stem cell transplantation stands as a promising therapy for those battling to regain normal daily function after stroke. Neural stem/progenitor cells (NSPCs) are good therapeutic candidates since they can secret trophic factors beneficial to central nervous system (CNS) cells and differentiate into CNS neurons, astrocytes, and oligodendrocytes. However, many NSPCs die after transplantation, creating a significant bottleneck in the field. Tissue engineering via the inclusion of a biomaterial scaffold can taper transplanted cell death and improve stem cell-mediated recovery[3]. Our work has demonstrated that easily deformable, injectable, non-toxic scaffolds are a good match for CNS tissue, which is one of the softest in the body. Injectable scaffolds that polymerize *in vivo* can form tight appositions with the spared tissue and promote recovery without further damaging surrounding regions. These scaffolds may also provide an optimal niche for transplanted NSPCs.

Biomaterials used as scaffolds for NSPC transplants should be optimized to support these cells. We found that fibrin, a natural material generated during the blood clotting cascade, sourced from Atlantic salmon supports CNS cells and matches the stiffness of CNS tissue[4, 5]. However, implantation of salmon fibrin in a rodent model of acute spinal cord injury revealed rapid scaffold degradation *in vivo* (~7 days), thus suggesting fibrin is unlikely to provide long-term support for the differentiation of transplanted NSPCs which requires 1 month or longer.

In order to mitigate this rapid degradation, we designed combination scaffolds that include materials commonly found in the NSPC niche within the brain, hyaluronic acid (HA) and laminin, in addition to salmon fibrin (See Chapter 3). HA is a glycosaminoglycan utilized as an injectable transplant biomaterial that when coupled with collagen promotes NSPC survival in the stroke-injured brain and persists for at least 2 months *in vivo*[6, 7]. *In vitro* studies of 3D scaffolds embedded with human NSPCs (hNSPCs) reveal significantly slower degradation of combination scaffolds (fibrin/HA/laminin) while retaining favorable polymerization kinetics, deformability, and support of hNSPC growth and differentiation (See Chapter 3). Furthermore, hNSPCs co-cultured with human endothelial colony-forming cell-derived endothelial cells (hECFC-ECs) promote increased vascularization of the combination scaffold (See Chapter 3) and may potentially encourage cross-talk between the two cell types and *in vivo* scaffold vascularization. Our *in vitro* data demonstrate the beneficial effects of the combination scaffold on hNSPCs, validating the transition of this tissue engineered construct into an *in vivo* system to test the ability to treat CNS damage such as stroke.

The most commonly used model in experimental stroke research is filamentous occlusion of the middle cerebral artery (MCA), developed initially for studies in rats[8]. A nylon filament is inserted into the internal carotid artery (ICA) via the common carotid artery (CCA) and advanced

intracranially to occlude blood flow in the MCA (Fig. 5.1). The suture is advanced 20-22 mm from the external carotid artery (ECA) and ICA bifurcation in rats, occluding collateral circulation from the anterior communicating arteries. After varying durations of the MCAO (transient MCAO, tMCAO), the filament can be removed to obtain reperfusion, mimicking a clinically relevant stroke as seen in humans. Alternatively, the suture can be left in place indefinitely to obtain a permanent MCAO (pMCAO), which results in a more severe ischemic lesion within the brain. This model provides a valuable platform for investigating the utility of hNSPCs and biomaterial scaffolds as transplant therapeutics for stroke. The main parameters to be investigated are the survival, proliferation, differentiation, and migration of transplanted hNSPCs as well as degradation kinetics of the scaffold within the lesion site.

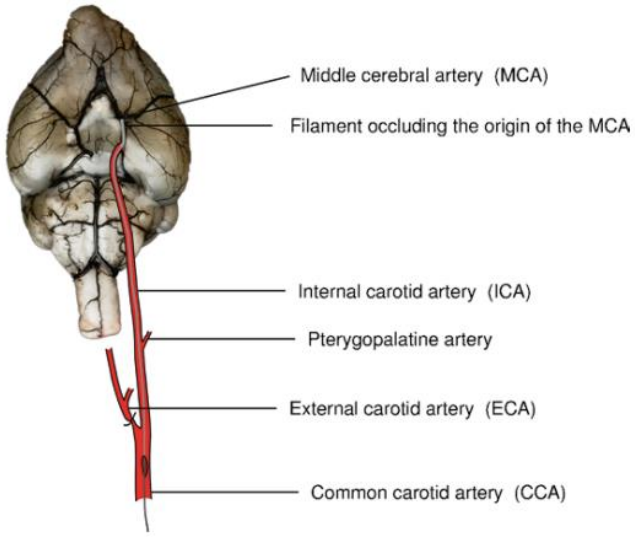

Figure 5.1. Filamentous occlusion of the MCA. Reprinted by permission from Dr. Nils Hecht, Department of Neurosurgery, Charité-Unversitätsmedizin Berlin[9].

5.2 MATERIALS AND METHODS

Cell Culture

Fetal-derived hNSPCs (SC27) were isolated from the cerebral cortices of brain by the National Human Neural Stem Cell Resource and were grown as adherent cultures on 6-well plates coated with 10 μg/mL fibronectin (human; Fisher Scientific, Hampton, NH, USA) (54 Scaffold paper). HNSPC basal medium included DMEM/F12 (Fisher Scientific, Hampton, NH, USA), 20% BIT 9500 (bovine serum albumin, insulin, and transferrin; Stem Cell Technologies, Vancouver, CA), and 1% antibiotic/antimycotic (penicillin/streptomycin/amphotericin; Thermo Fisher Scientific, Waltham, MA, USA). Proliferation media was prepared from basal media via addition of 40 ng/mL epidermal growth factor (EGF; PeproTech, Rocky Hill, NJ, USA), 40 ng/mL basic-fibroblast growth factor (bFGF; PeproTech), and 40 ng/mL platelet-derived growth factor (PDGF-AB; PeproTech,). Cells were dissociated using Cell Dissociation Buffer (Invitrogen) and prepared for transplantation.

Scaffold Formulation and Transplant Construct Preparation

Fibrin scaffolds were used for transplantation with 5 mg/mL salmon fibrinogen (lot 1478, SeaRun Holdings, Inc.) and 0.1 U/mL salmon thrombin (lot 194, SeaRun Holdings, Inc.) final concentrations in Minimum Essential Media (MEM). For combination scaffolds, 1 mg/mL thiolated Hyaluronic Acid (HA) (Glycosil®; BioTime, Inc.) (average molecular weight (MW) ~250 kDa) and 100 μg/mL laminin (Thermo Fisher Scientific) was included in the hydrogel mixture with salmon fibrinogen and thrombin. Human fibrin scaffolds consisted of 5 mg/mL human fibrinogen (lot 2681834, EMD Millipore) and 0.1 U/mL human thrombin (lot 2688037, EMD Millipore) final concentrations in MEM. Table 5.1 highlights the concentrations and

volumes of scaffold constructs prepared for transplantation with 3 µL of solution used per injection. A 5X volume of each treatment group was made to ensure ample solution was available for multiple transplants during a day of surgeries.

Table 5.1 Formulation of scaffold constructs used in transplants

Treatment Group	Components	Final Concentrations for transplant (per 3 µL injection)	Final Volumes (5X)
Salmon fibrin + hNSPCs (6 rats)	Salmon fibrinogen (50 mg/mL stock)	5 mg/mL	1.5 µL
	Salmon thrombin (2 U/mL stock)	0.1 U/mL	0.75 µL
	hNSPCs ($1x10^8$/mL stock)	$1x10^5$ cells	5 µL
	MEM	-	7.75 µL
			Total = 15 µL
Salmon fibrin/HA/Laminin + hNSPCs (6 rats)	Salmon fibrinogen (50 mg/mL stock)	5 mg/mL	1.5 µL
	Salmon thrombin (2 U/mL stock)	0.1 U/mL	0.75 µL
	HA (10 mg/mL stock)	1 mg/mL	1.5 µL
	Laminin (1 mg/mL stock)	100 µg/mL	1.5 µL
	hNSPCs ($1x10^8$/mL stock)	$1x10^5$ cells	5 µL
	MEM	-	5.75 µL
			Total = 15 µL
Human fibrin + hNSPCs (6 rats)	Human fibrinogen (50 mg/mL stock)	5 mg/mL	1.5 µL
	Human thrombin (2 U/mL stock)	0.1 U/mL	0.75 µL
	hNSPCs ($1x10^8$/mL stock)	$1x10^5$ cells	5 µL
	MEM	-	7.75 µL
			Total = 15 µL
Cells only (5 rats)	hNSPCs ($1x10^8$/mL stock)	$1x10^5$ cells	5 µL
	MEM	-	10 µL
			15 µL

Rat Middle Cerebral Artery Occlusion Model

Adult male Sprague-Dawley rats weighing 300-400 g were used for stroke experiments and the well-established intraluminal vascular occlusion method was used to induce tMCAO[10, 11]. Briefly, to achieve tMCAO, rats were anesthetized via Ketamine-Xylazine IP injection (100 mg/kg-10 mg/kg) and placed in a supine position. Upon confirmation of insensitivity to pain, the surgical procedure was initiated. Fur in the ventral neck region was shaved with electric clippers to expose the skin and disinfected with Betadine (Thermo Fisher Scientific). A 1 cm midline incision was made on the neck and the skin was retracted with retractors to expose the right common carotid artery (CCA), external carotid artery (ECA), and the internal carotid artery (ICA). Arteries were carefully dissociated from surrounding nerves and fascia. Two 8-0 silk sutures were tied: 1 around the ECA and the other distal to the ECA/ICA bifurcation on the CCA. After tightening the sutures, a third silk suture was loosely tied proximally on the CCA near the ECA/ICA bifurcation. A vascular clamp was then applied at the bifurcation of the ECA/ICA bifurcation and a small incision into the CCA was made using microscissors. An intraluminal monofilament suture with a silicon rubber-coated tip (Doccol Corporation) was inserted into the incision and advanced to the clamp. The third suture was then tightened to secure the vessel to the suture without inhibiting the mobility of the intraluminal monofilament suture. The clamp was then removed from the bifurcation and the monofilament suture advanced into the ICA for a distance 25-29 mm beyond the bifurcation. This resulted in occlusion of the origin of the middle cerebral artery (MCA). The suture was maintained in this position for 90 minutes to model a transient MCAO. Rats were supplemented with 1% isoflurane by nosecone if pain sensitivity was detected during the 90 minute occlusion period. After occlusion, the suture

was then withdrawn back into the CCA and the third suture tightened to ensure no hemorrhaging and the incision was closed using autoclips.

Transplantation

For naïve intracranial injections, female Sprague Dawley rats weighing 200-250 g were used. For stroke experiments, all animals were injected subcutaneously with Tacrolimus (Prograf, 1 mg/kg) 1 day before transplantation and once daily post-transplant until the animals were sacrificed for analysis to ensure suppression of the innate immune reaction elicited by the transplantation of human cells. Briefly, at 7 days post-stroke induction, rats were anesthetized with 2% isoflurane and positioned in a stereotaxic holder (Leica Microsystems, Inc.). A midline incision was made exposing the skull and a 5 μL Hamilton syringe (87930) with a 0.5'' 30G blunt tip needle was mounted into a UMP-3 (World Precision Instruments) injector attached to a SYS-Micro4 Controller. For stroke experiments, the transplant needle was positioned to 0.96 mm anterior to bregma and 3 mm lateral to midline on the right hemisphere. For naïve brain transplants, the needle was positioned at bregma then moved 5.5 mm lateral to midline on the left hemisphere. A spot was marked on the skull to indicate the exact position. The needle was subsequently moved and a burr hole was drilled using a Dremel rotary tool at 5,000 rpm. Cell or cell/scaffold solution (3 μL) was mixed thoroughly and loaded slowly into the transplant needle over a duration of ~10 s. In stroke animals, the needle was repositioned at the marked coordinates and lowered slowly to 5 mm ventral relative to bregma to create a small pocket within the brain tissue for the solution, then raised to 5.5 mm. For naïve transplants, the needle was lowered to 5.5 mm ventral relative to bregma and raised to 3.5 mm. The solution was injected at a rate of 1 μL/min and the needle was left in the brain for 2 minutes after completion of transplant before slow retraction of the needle. The remaining scaffold solution was monitored

for polymerization over the duration of injection to ensure the scaffold did not polymerize prematurely. Bone wax was then applied to close the burr hole, and the midline incision was sealed using autoclips.

Behavioral Analysis

For locomotor functional analysis, the rotarod test was used as previously described (Li et al. J Biol Chem 2014). Briefly, at 10 days post-transplant, each rat was placed on the rotarod for seven trials (Economex, Columbus Instruments). The cylinder rotates at 6 rpm and when the trial begins, accelerates at a rate of 0.2 rpm/s. The elapsed time before a rat falls off of the rotating cylinder is recorded. The first two trials were used as training and the remaining five trial times were averaged for each animal.

Tissue Collection

At the end of experimentation, all animals were anesthetized with a lethal IP dose of Euthasol (100 mg/kg) and transcardially perfused with 50 mL of PBS, followed by 400-500 mL of 4% paraformaldehyde. Brains were carefully dissected and post-fixed and sank for 2 days in a solution of 4% paraformaldehyde/20% sucrose in PBS at 4^{o}C, flash frozen at -60^{o}C in isopentane (2-methyl butane), and stored at -80^{o}C.

Immunohistochemistry

Frozen brains were embedded in Colorless Neg-50 (Thermo Fisher Scientific) compound with 4 brains per block. Slices 35-40 μm in thickness to maintain scaffold integrity were cut using a cryostat and mounted onto microscope slides using a UV-based CryoJane Sectioning Aid System (Electron Microscope Sciences). Slides were collected in a 12 set series for the purposes

of unbiased stereology. Immunostaining was performed as previously described[12]. Briefly, sections were washed in PBS and incubated in 0.3% Triton X-100 for 5 minutes. After 3x5 minute PBS washes, sections were blocked for 1 hour in 10% donkey serum, 5% bovine serum albumin (BSA), and 0.1% Triton X-100. Sections were then incubated overnight at room temperature in primary antibody within a humidified chamber. Primary antibodies used were: mouse anti-SC121 (1:1000, Stem Cells, Inc.), rabbit anti-salmon fibrinogen (1:6000), and goat anti-human fibrinogen (1:4000, Abcam). Following 3x5 minute PBS washes, sections were then incubated with donkey anti-mouse 488 (1:200, Thermo Fisher Scientific), donkey anti-rabbit 555 (1:200, Thermo Fisher Scientific) or donkey anti-goat 594 (1:200, Jackson ImmunoResearch) for 2 hours at room temperature. After 3x5 minute PBS washes sections were counterstained for 5 minutes with Hoechst 33342 (1:500, Life Technologies) in PBS. Following 1x5 minute PBS wash, slides were mounted onto cover glass using Vectashield (Vector Labs) and imaged using a Nikon Eclipse Ti microscope. Images were acquired using NIS element AR3.10 software.

5.3 RESULTS AND DISCUSSION

5.3.1 Scaffolds and hNSPCs can be detected in transplants into naïve rat brain

In order to validate the ability of scaffold constructs to be detected *in vivo*, we injected healthy rats with hNSPCs alone, salmon fibrin alone, salmon fibrin with hNSPCs, or combination scaffolds with hNSPCs. The goal was to detect human cells and salmon fibrin via immunostaining 24 hours after transplant into the cerebral cortex as justification for utilizing this method in the larger stroke study. We found human cells can be detected with the human cytoplasmic marker SC121 and the fibrin scaffold with a salmon fibrinogen antibody[4] (Fig. 5.2). This preliminary study confirmed that the tissue engineered construct could be transplanted and

followed by sectioning and immunostaining of the brain tissue for subsequent detection and analysis.

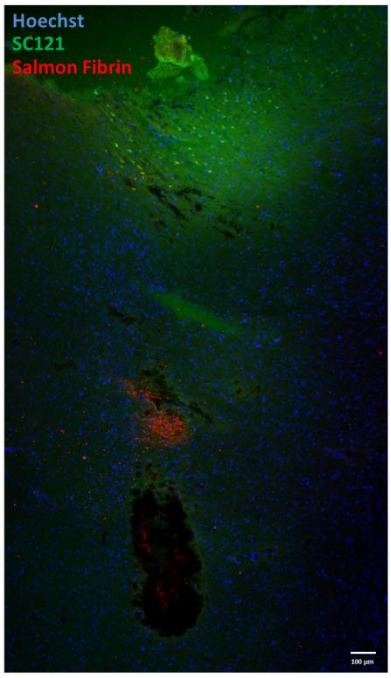

Figure 5.2. Detection of transplanted hNSPCs and salmon fibrin in rat cortical tissue. (a) hNSPCs injected into the cerebral cortex of naïve rats with salmon fibrin can be detected 24 hours after transplant with the human cytoplasmic marker SC121. Salmon fibrin is detected with a salmon fibrinogen antibody and all nuclei are counterstained with Hoechst.

5.3.2 Increasing the time of tMCAO increases cerebral infarct size and severity in rats

The ability of the intraluminal suture-based tMCAO model to produce a consistent lesion within the rat brain is critical for the purposes of investigating the ability of hNSPC/scaffold transplantations to be an effective therapeutic for stroke. 2,3,5-triphenyltetrazolium chloride (TTC) is a stain that detects infarction in stroke-injured rats[13]. TTC staining differentiates healthy from ischemic tissue since it is reduced by enzymes in healthy tissue to a red, light-sensitive compound (formazan). This allows simple delineation of healthy tissue appearing deep red from injured tissue which is white in color. We performed TTC staining on rats that underwent permanent or transient MCAO for 30, 60, and 90 minutes (Fig. 5.3).

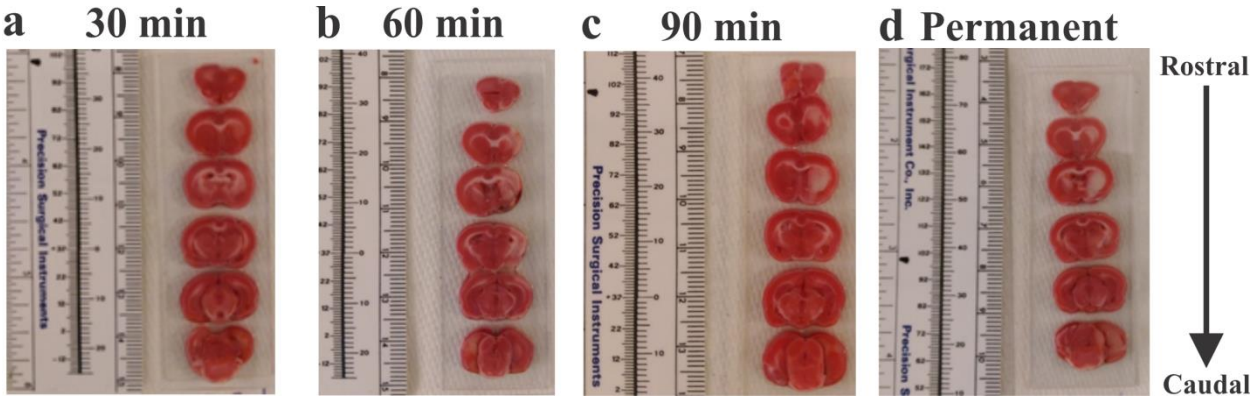

Figure 5.3. TTC staining of rat brain following MCAO. TTC staining exposes healthy (red) and infarcted (white) tissue. The severity of the lesion increases with time as shown by (a) 30 minute, (b) 60 minute, (c) 90 minute, and (d) permanent MCAO. Brains shown are in 3 mm slices each with the caudal side facing upward in each image. The 6 slices are displayed from top to bottom representing the rostral to caudal ends of the brains.

We found that with a 30 minute occlusion, most of the brain tissue remains intact without a noticeable infarct region (Fig. 5.3a). For the 60 minute occlusion, there is a prevalent infarct in the outer cortical region (Fig. 5.3b). We obtain a large subcortical infarct within the striatal region in the 90 minute transient occlusion (Fig. 5.3c). A more severe subcortical striatal lesion can be obtained with a permanent MCAO (Fig. 5.3d), but due to the increased physiological and clinical relevance of a 90 minute occlusion in addition to its track record as an established *in vivo* model[14, 15], we decided to proceed with a transient model for the transplantation study.

5.3.3 Scaffolds improve hNSPC-mediated functional recovery of stroke-injured rats

Based on assessment of the lesion by TTC staining, a 90 minute tMCAO model was chosen to assess scaffold and hNSPC transplants. Rats were given a 90 minute transient MCAO and hNSPC alone or with scaffolds (salmon fibrin, combination, or human fibrin) were transplanted 7 days after onset of stroke. The 7 day time point was chosen since partial liquefaction of the necrotic tissue at this time provides an area devoid of normal brain structure and it allows the aggressive initial immune response due to the insult to subside. The primary goal of any stroke treatment is to attain recovery of lost function post-insult. Several tests are

used to assess simple and complex task completion in stroke-injured rats. These include evaluations of a variety of functions such as motor, sensory, reflex, balance, learning, memory, and coordination[16]. At 10 days post-transplant we examined motor coordination and balance alterations in the rats via the accelerated rotarod, which has been established as a method to assess functional levels in rodents after stroke[17, 18]. Furthermore, many human stroke survivors suffer from motor and coordination impairments, suggesting the clinical relevance of this type of behavioral assessment. The rotarod apparatus has a cylinder that can rotate at a variable speed and as the rod accelerates over time, the duration the animal remains on the cylinder is documented. We found that uninjured rats performed better overall than all rats that received an MCAO, which is in congruence with prior studies[19] (Fig. 5.4). Interestingly, rats that received a scaffold along with hNSPCs performed better than those that received hNSPCs only regardless of the scaffold used, suggesting the importance of the biomaterial in promoting hNSPC-mediated recovery. Since this was a pilot study, there is a need for additional controls and repeats of the test in order to obtain a more confident idea of the efficacy of the tissue engineered construct in encouraging functional recovery. These controls include a 90 minute MCAO untreated and sham transplanted animals.

After 14 days, cardiac perfusion was performed on all rats and brains were removed for sectioning and analysis of hNSPC survival and scaffold degradation. The two most critical outcomes from the study are transplanted cell survival and scaffold degradation. Humans cells can be detected by the human cytoplasmic marker SC121 or nuclear marker Ku80, while scaffolds can be labeled using antibodies against salmon and human fibrinogen. Since it remains to be known whether transplanted cells migrate out of the scaffold to regions of the brain away from the transplantation site, brains must be sectioned completely rather than only near the

region of transplant. By assessing which scaffolds resist degradation and support hNSPC survival the greatest, a follow-up 2 month study can be implemented to assess long-term efficacy of the transplant construct as a treatment for stroke.

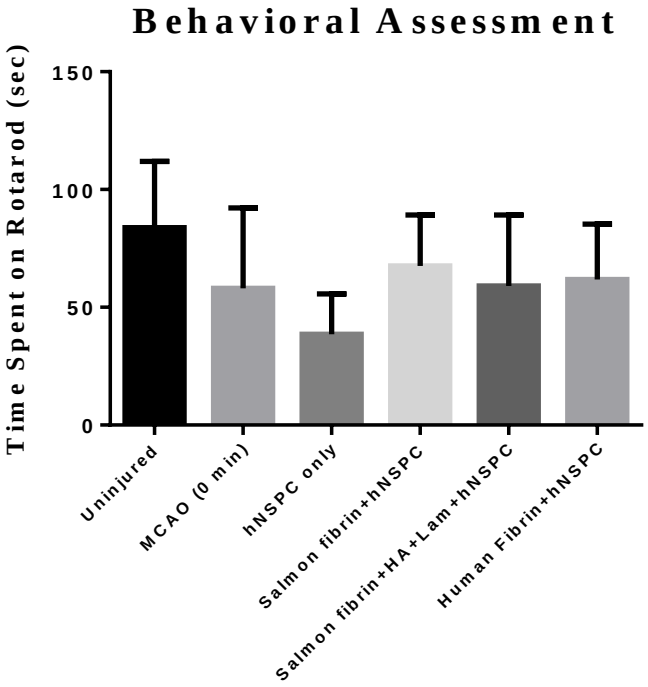

Figure 5.4. Functional assessment of stroke-injured rats via rotarod. Rats were transplanted with hNSPCs alone or with salmon fibrin, combination (salmon fibrin/HA/laminin), or human fibrin scaffolds and assessed at 10 days post-transplant on the rotarod. Rats that received hNSPCs alone performed the worst while uninjured control animals performed better than all other groups. Animals that received a short MCAO (immediate removal of intraluminal suture) performed similarly to those that had the scaffold and hNSPC treatment. Error bars represent SEM of different animals that received the same treatment.

5.4 CONCLUSIONS AND FUTURE DIRECTIONS

This study utilized a tMCAO model in rats to transplant hNSPCs via the combination scaffolds developed in Chapter 3 as a therapy for stroke. A 90 minute occlusion was identified as the optimal time frame to obtain a sizable subcortical infarct as assessed by TTC staining. Cells and scaffolds can be visualized by immunofluorescence staining when transplanted into naïve rat

brain. When transplanted into stroke-injured brain, scaffolds improve motor function of rats better than transplants of cells only. Analysis of the surviving human cells and degradation of scaffolds after 2 weeks motivates a 2 month long-term transplantation study. The long-term study would include the scaffold that best resisted degradation and promoted transplanted cell survival from the 2 week study. HNSPC proliferation and differentiation into neurons, astrocytes, and oligodendrocytes will be analyzed and the ability of hECFC-ECs to vascularize and provide nutrients to the scaffold construct will be measured in co-transplants with hNSPCs. Finally, immune response to the transplant construct can be studied through microglia and reactive astrocyte staining adjacent to the lesion and transplantation site. The long-term study would provide a valuable stride in the development of novel preclinical scaffold and cell-based stroke therapeutics.

5.5 REFERENCES

1. Roger, V. et al. Heart disease and stroke statistics--2012 update: a report from the American Heart Association. *Circulation* **125** (2012).
2. Lloyd-Jones, D. et al. Heart disease and stroke statistics--2009 update: a report from the American Heart Association Statistics Committee and Stroke Statistics Subcommittee. *Circulation* **119**, 181 (2009).
3. Willerth, S.M. & Sakiyama-Elbert, S.E. Combining stem cells and biomaterial scaffolds for constructing tissues and cell delivery. (2008).
5. Sharp, K. et al. Salmon fibrin treatment of spinal cord injury promotes functional recovery and density of serotonergic innervation. *Experimental neurology* **235**, 345-356 (2012).
5. Ju, Y.-E., Janmey, P., McCormick, M., Sawyer, E. & Flanagan, L. Enhanced neurite growth from mammalian neurons in three-dimensional salmon fibrin gels. *Biomaterials* **28**, 2097-2108 (2007).
6. Moshayedi, P. & Carmichael, S.T. Hyaluronan, neural stem cells and tissue reconstruction after acute ischemic stroke. *Biomatter* **3** (2013).
7. Zhong, J. et al. Hydrogel matrix to support stem cell survival after brain transplantation in stroke. *Neurorehabilitation and neural repair* **24**, 636-644 (2010).
8. Koizumi, J., Yoshida, Y., Nakazawa, T. & Ooneda, G. Experimental studies of ischemic brain edema, I: a new experimental model of cerebral embolism in rats in which recirculation can be introduced in the ischemic area. *Jnp J Stroke* **8** (1986).
9. Belayev, L., Endres, M. & Prinz, V. Focal cerebral ischemia in the mouse and rat using the intraluminal suture–filament model. *Rodent Models of Stroke*, 29-40 (2010).
10. Chen, J. et al. Therapeutic benefit of intracerebral transplantation of bone marrow stromal cells after cerebral ischemia in rats. *J Neurol Sci* **189**, 49-57 (2001).
11. Iihoshi, S., Honmou, O., Houkin, K., Hashi, K. & Kocsis, J.D. A therapeutic window for intravenous administration of autologous bone marrow after cerebral ischemia in adult rats. *Brain Res* **1007**, 1-9 (2004).
12. Haus, D.L. et al. CD133-enriched Xeno-Free human embryonic-derived neural stem cells expand rapidly in culture and do not form teratomas in immunodeficient mice. *Stem Cell Res* **13**, 214-226 (2014).
13. Bederson, J.B. et al. Evaluation of 2,3,5-triphenyltetrazolium chloride as a stain for detection and quantification of experimental cerebral infarction in rats. *Stroke* **17**, 1304-1308 (1986).
15. Calloni, R.L. et al. Transient middle cerebral artery occlusion in rats as an experimental model of brain ischemia. *Acta Cir Bras* **25**, 428-433 (2010).
15. Chen, Q., Chopp, M., Bodzin, G. & Chen, H. Temperature modulation of cerebral depolarization during focal cerebral ischemia in rats: correlation with ischemic injury. *J Cereb Blood Flow Metab* **13**, 389-394 (1993).
16. Schaar, K.L., Brenneman, M.M. & Savitz, S.I. Functional assessments in the rodent stroke model. *Exp Transl Stroke Med* **2**, 13 (2010).
17. Chen, J. et al. Intravenous administration of human umbilical cord blood reduces behavioral deficits after stroke in rats. *Stroke* **32**, 2682-2688 (2001).
18. Jones, B.J. & Roberts, D.J. The quantitative measurement of motor inco-ordination in naive mice using an accelerating rotarod. *Journal of Pharmacy and Pharmacology* **20**, 302-304 (1968).
19. Rogers, D.C., Campbell, C.A., Stretton, J.L. & Mackay, K.B. Correlation between motor impairment and infarct volume after permanent and transient middle cerebral artery occlusion in the rat. *Stroke* **28**, 2060-2065; discussion 2066 (1997).

CHAPTER 6

EFFECTS OF ADHESION PEPTIDE-CONJUGATED HYALURONIC ACID SCAFFOLDS ON HUMAN NEURAL STEM CELL BEHAVIOR

Authors: **Janahan Arulmoli**[1,2*], Urmi Sheth[2*], Michael Onorato[3], Thomas I. Zareminski[3], Lisa A. Flanagan[1,2,4]

Author Affiliations:

[1]Department of Biomedical Engineering

[2]Sue & Bill Gross Stem Cell Research Center

[3]BioTime, Inc.

[4]Department of Neurology

*Denotes equal contribution to this work

[1,2,4]University of California, Irvine, Irvine, CA, 92697, USA

[3]BioTime, Inc., 1010 Atlantic Avenue, Suite 102, Alameda, CA, 94501, USA

6.1 INTRODUCTION

Each year, approximately 2.5 million Americans suffer from brain trauma in the form of traumatic brain injuries or strokes[1]. Much of the damage sustained from these events is irreversible. Ancillary to the initial insult, debris and signals released by dying cells evoke a secondary inflammatory response that results in additional cell death, followed by the formation of a glial scar[1, 2]. While the glial scar prevents the spread of tissue damage, it also secretes molecules such as chondroitin sulfate proteoglycans into the extracellular matrix (ECM) that inhibit axonal regeneration[2]. Thus, the damaged area and surrounding tissue degenerate into an inhospitable environment with few nutrients and an abnormal ECM.

One therapeutic approach to improve recovery from brain trauma involves transplanting neural stem and progenitor cells (NSPCs) to the injury site. NSPCs have the ability to differentiate into the three main cell types in the central nervous system (CNS): neurons, astrocytes, and oligodendrocytes[1]. The adult brain houses endogenous NSPCs in the subventricular zone (SVZ) and the dentate gyrus (DG), but too few of these cells contribute to recovery of neurological function in the damaged areas[3]. It was estimated that approximately 0.2% of the neurons destroyed by stroke in the striatum were replaced by endogenous NSPCs[4]. Therefore, exogenous cells are likely needed to make up for the neuronal loss and transplanted, exogenous NSPCs can lead to functional recovery in rodent stroke models[5, 6]. However, due to the hostile environment within a CNS lesion site, cells undergo cell death through multiple mechanisms and cell survival is very low, in the 0.2-10% range[7-9]. One study reported that an impressive 58% of exogenous NSPCs survived five weeks after transplant, but only 1% of these cells retained proliferative capacity[10].

In order to support grafted cells and ensure that they survive and proliferate, scaffold biomaterials can be transplanted in conjunction with NSPCs. Properties of the scaffolds, such as injectability, polymerization and degradation rate, chemical and physical characteristics, and biocompatibility affect the success of the cell-scaffold transplant construct in the injured CNS. Scaffolds can be composed of a variety of materials, both natural (such as alginate, collagen, fibrin, or hyaluronic acid) and synthetic (such as poly(ethylene glycol), poly(lactic acid), or poly(lactic-co-glycolic acid))[11]. Human fibrin scaffolds containing growth factors increased the survival of mouse neural progenitor cells in a rat spinal cord injury model over cells transplanted without fibrin, possibly by localizing cells and growth factors at the lesion site in addition to acting as a neuroprotective entity[12]. Additionally, human neural stem cells containing an enhanced firefly luciferase gene were transplanted into a corticectomized rat model both with and without a poly-L-lactic acid (PLLA) scaffold. The cells embedded within the PLLA scaffold continued to produce an intense luciferase signal at 14 days and proliferate up to 8 days post-transplant, while the luciferase signal and the proliferation rate of the cells transplanted alone began to decrease at 8 and 5 days, respectively[13]. This is likely due to the dramatic decrease in cell survival in non-scaffold transplants compared to those including scaffolds. Matrigel, a gelatinous mixture of proteins produced by mouse sarcoma cells cells that forms a scaffold, increased survival of human neural progenitor cells and decreased the size of the lesion when transplanted with cells into a rat middle cerebral artery occlusion model of stroke[14]. NSPCs also retained proliferative capacity *in vivo* when transplanted in a urinary bladder matrix (UBM), while NSPCs transplanted without the matrix displayed low viability[15]. This may be attributed to the UBM's intrinsic anti-inflammatory properties, which shielded the NSPCs from the inhospitable environment created after injury.

Hyaluronic acid (HA) was chosen as the scaffold for this study since it is a glycosaminoglycan naturally found in the brain. Its slow degradation rate, high water retention, porosity, and anti-inflammatory properties make it a viable candidate as a scaffold for neural stem cells[16]. HA increases proliferation of human neural stem cells *in vitro* and when transplanted into the mouse striatum in an HA/gelatin/PEGDA (PEG diacrylate) scaffold demonstrated higher rates of survival than cells transplanted in a phosphate buffered saline vehicle[17]. PEGDA is a cross-linking agent that forms a hydrogel when acrylates on PEGDA react with sulfhydryl groups on thiolated HA[18]. Gelatin allows the cells to bind to and interact with the matrix, as HA has no native integrin-mediated binding sites for NSPCs. HA plays a role in NSPC migration by interacting with CD44 and the receptor for hyaluronic acid-mediated motility (RHAMM)[19]. However, these receptors are not present in all cells. In addition, integrin-mediated binding has been shown to direct cell proliferation and differentiation, which is an important consideration for biomaterial scaffolds[20]. A variety of other large biomolecules have been incorporated into HA, including collagen and fibrinogen to promote cell adhesion[21, 22]. Though they effectively allow cells to bind in 3D scaffolds, full length non-recombinant biomolecules that must be purified from biological materials can be difficult to obtain FDA-approval for since they may be contaminated with other biologically active constituents. Conversely, short peptide sequences known to have cell adhesion properties, such as the IKVAV and YIGSR sequences derived from laminin, are chemically synthesized, easy to purify, and more straightforward in obtaining FDA-approval as a device to compliment a cellular therapeutic. These peptides can be added to HA to promote cell binding and differentiation into neurons[23]. In this study, thiolated HA modified with various peptide sequences at different concentrations was cross-linked with a PEGDA cross-linker and human neural stem and progenitor cells (hNSPCs) were embedded into

these scaffolds. Proliferation and process extension of hNSPCs in HA-peptide scaffolds was compared to that in control salmon fibrin scaffolds since we found these cells to exhibit robust proliferation and extension in salmon fibrin (See Chapter 4). The primary objective of this study was to identify an optimized scaffold for hNSPCs that would be easier to translate into clinical applications for CNS injury due to the simplicity of utilizing peptides for cell adhesion rather than full length biomolecules.

6.2 MATERIALS AND METHODS

Cell Culture

Fetal brain-derived cortical human NSPCs (SC27) were grown as adherent cultures on fibronectin (Fisher Scientific) for several passages before use. The proliferation media used to grow the cells consisted of DMEM/F12 (Invitrogen), 20% BIT 9500 (v/v, Stem Cell Technologies), 1% antibiotic/antimycotic (Thermo Fisher Scientific), and 40 ng/mL each of FGF (BD Biosciences), EGF (BD Biosciences), and PDGF-AB (Peprotech). The hNSPCs were passaged once confluent, usually every 4-6 days, using Cell Dissociation Buffer (Invitrogen). Cells ranging from passage 11-25 were used for these studies.

Two-Dimensional Substrates

Two-dimensional (2D) layers of HA-peptide matrices were prepared on glass coverslips. Glycosil® (thiolated HA, HyStem), Gelin® (gelatin peptide), and Extralink® (PEGDA) (BioTime, Inc.) were dissolved in degassed water to achieve a total concentration of 10 mg/mL each. The mechanism of cross-linking is shown in Figure 6.1.

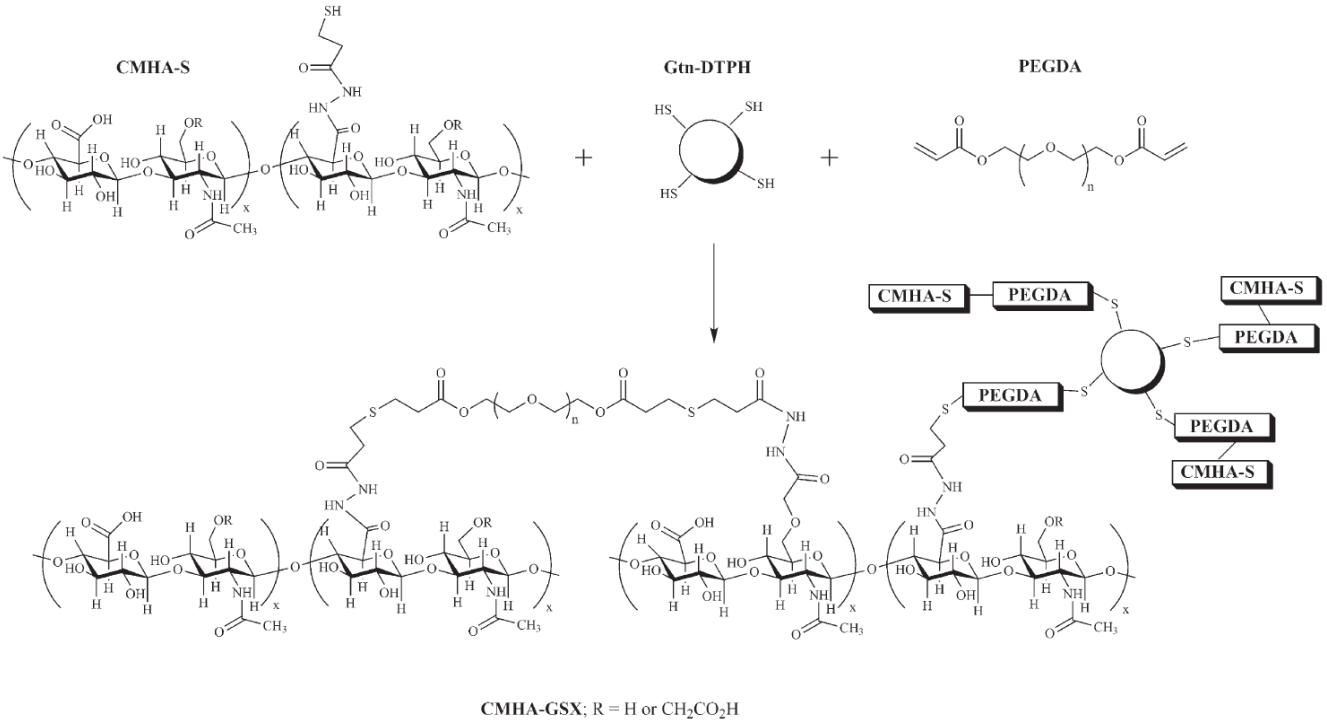

Figure 6.1. Hydrogel synthesis via chemical cross-linking of thiolated HA (CMHA-S) with PEG-diacrylate (PEGDA) and thiolated-Gelatin (Gtn-DTPH). Reprinted by permission from John Wiley and Sons: Macromolecular Bioscience[18], copyright 2009.

Coverslips were coated with a solution of 0.71% Glycosil®, 0.2% Extralink®, and 880 mM of various maleimide-conjugated peptides (Table 6.1, Fig. 6.2). 0.8% Glycosil® with 0.2% Extralink®, 0.4% Glycosil®/0.4% Gelin® with 0.2% Extralink® (Hystem C), laminin, and fibronectin coated coverslips were used as controls. Glycosil® was allowed to react with either the peptides or with Gelin® for five minutes before Extralink® was added. 20,000 hNSPCs were plated on each coverslip and incubated in proliferation media for two days. The degree of adhesion was assessed as being 'good', 'fair', or 'poor' based on cell spreading and extension on each substrate. The results of this adhesion study were used to determine which peptides would be used in 3D hydrogels.

Table 6.1 Peptides (highlighted) provided by BioTime, Inc. used in combination with HA and the biomolecules from which the peptides originate. MPA- denotes a maleimide group and –OH a hydroxide group.

Peptide	Origin
MPA-PHSRN-OH	Fibronectin
MPA-VKNEED-OH	Fibronectin
MPA-LHGPEILDVPST-OH	Fibronectin
MPA-DGEA-OH	Collagen
MPA-IKVAV-OH	Laminin
MPA-REDVY-OH	Fibronectin
MPA-YIGSR-OH	Laminin
MPA-RGD-OH	Fibronectin
MPA-RDG-OH	Inert

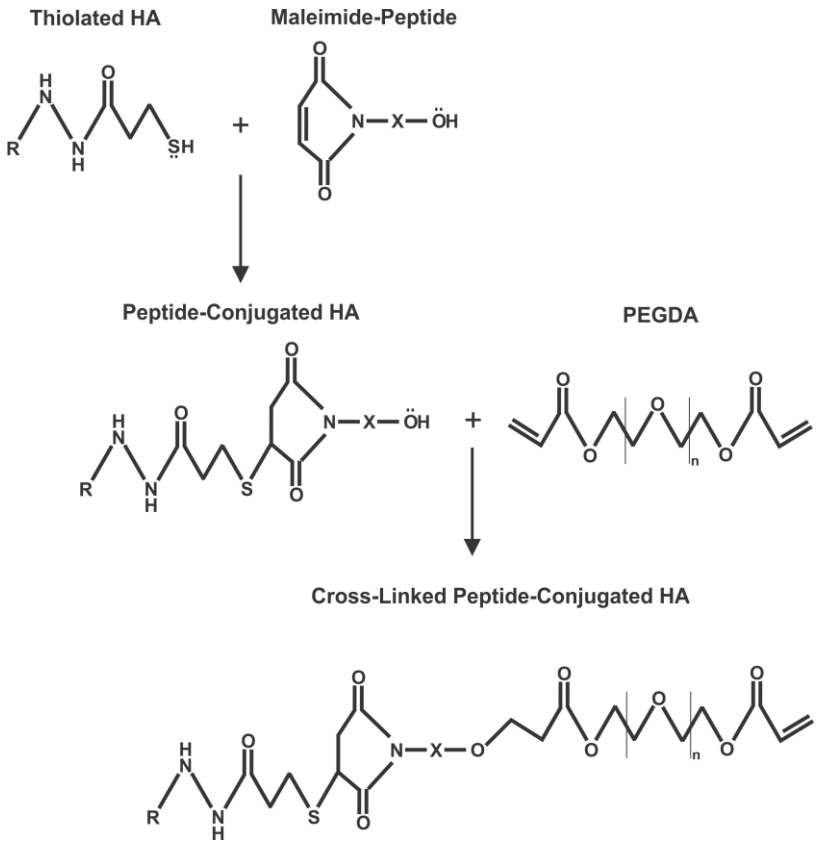

Figure 6.2. Chemical cross-linking of thiolated HA with maleimide-conjugated adhesion peptides. Thiolated HA is initially conjugated to the peptide followed by cross-linking with PEGDA to form the hydrogel. R signifies the repeating disaccharide units of HA and X denotes the peptide sequences as highlighted in Table 6.1.

Three-Dimensional Scaffolds

To make 3D hydrogels, 0.71% Glycosil® (w/v) was mixed with 880 mM of peptide solution. Peptides used included REDVY, RGD, and RDG (inert peptide to keep the total peptide concentration constant). Cells were counted with a hemocytometer and 100,000 hNSPCs were added to each solution. 0.2% Extralink® (w/v) was reacted with each solution to induce polymerization, which usually occurred between 5 to 20 minutes. Immediately before polymerization, the solution was pipetted onto an 18 mm coverslip.

Proliferation

The hydrogels were kept in proliferation medium for three days, with a media change on day 2. On day 3, they were fixed in 4% paraformaldehyde for 15 minutes, washed 3 times for 10 minutes each (3x10 minutes) in PBS, and stored in 0.05% sodium azide. Phase contrast images of live cells on or in hydrogels were taken each day on a digital microscope (EVOS).

Process Extension

Hydrogels made for observation of cell process extension differed slightly from those for proliferation conditions. For one experiment, an equal concentration of an MMP-degradable cross-linker (with a cleavable KGGPQGIWGQK region) was used instead of Extralink. A REDVY 200 mM scaffold was made with this cross linker, and was fixed in 4% paraformaldehyde after three days in proliferation conditions (as above). A second experiment studied the effects of titrating the Glycosil and Extralink concentrations on cell extension. One scaffold was made using the proliferation condition formulation of 0.71% (w/v) Glycosil, 880

mM REDVY, and 0.2% (w/v) Extralink, while others had decreased concentrations of Glycosil (0.4%, 0.2%) or Extralink (0.15%, 0.1%). These five matrices were kept in proliferation conditions for one day and then switched to astrocyte differentiation medium (ADM): DMEM/F12 (Invitrogen), 20% HI FBS (Invitrogen), and 1% antibiotic/antimycotic (Thermo Fisher Scientific). After eight days, the scaffolds were fixed in 4% paraformaldehyde for 15 minutes. After 3x10 minute washes with PBS, the hydrogels were stored in 0.05% sodium azide. Images were taken daily on a digital microscope (EVOS).

Immunocytochemistry

All steps for staining scaffolds were done on a rocker at room temperature unless otherwise specified. Scaffolds were washed 3x10 minutes in PBS and then permeablized with 0.3% Triton X-100 for 15 minutes (Sigma). After 3x10 minute washes in PBS, they were blocked for one hour in 10% donkey serum, 5% BSA, and 0.1% Triton X-100 in PBS. The scaffolds were then incubated with primary antibodies diluted in blocking solution overnight at 4^{o}C. The primary antibodies included the proliferation markers rabbit anti-Ki67, diluted 1:500 (Leica Biosystems) and mouse anti-phospho-histone H3 (PH3), diluted 1:200 (Cell Signaling Technology), as well as the astrocyte marker GFAP, diluted 1:200 (Sigma-Aldrich). After 3x10 minute washes, the scaffolds were incubated for one hour with goat anti-rabbit 555 secondary antibody (Life Technologies) and/or donkey anti-mouse 488 secondary antibody (Jackson ImmunoResearch) diluted 1:200 in blocking solution. Alternatively, FITC phalloidin (Sigma-Aldrich), which stains F-actin was diluted 1:500 in blocking solution and used without a primary antibody. The scaffolds were washed 3x10 minutes and then incubated with 4 µg/mL Hoechst 3342 in PBS for 5 minutes. They were washed once for 10 minutes in PBS and then mounted onto a cover glass with 15 µL Vectashield (Vector Labs). Three images of 40 µm Z-stacks in

each hydrogel were acquired using a Zeiss Spinning Disk Confocal microscope (Zeiss). Three independent biological repeats were performed in the REDVY 50 mM/RDG 830 mM, REDVY 200 mM/RDG 680 mM, REDVY 880 mM, and REDVY 440 mM/RGD 440 mM gels, as well as the controls (salmon fibrin lot 1479, Hystem, and Hystem C (Glycosil+Gelin)). Percent cells staining positive for each marker was determined using ImageJ.

Statistical Analysis

A one-way ANOVA with a Tukey HSD post-hoc test was used to determine if significant differences existed between cells in the different hydrogel types.

6.3 RESULTS

Initially, hNSPCs were plated on a 2D layer of HA-peptide matrix to determine their ability to adhere to HA when various peptide sequences were incorporated. Since there are several HA receptors that hNSPCs possess, we assessed HA receptor mRNA levels by RNA-Seq (See Chapter 4) (Table 6.2). Though there are high expression levels of various receptors, none of these are sufficient to promote hNSPC adhesion to HA in the absence of an incorporated amino acid peptide sequence. The peptide sequences used in this study are shown in Table 6.1 and the peptide combinations and HA concentrations used in 2D experiments are presented in Table 6.3. The degree of cell binding was assessed by observation of cell attachment and spreading by phase contrast microscopy. Experimental coatings that allowed similar cell attachment as the positive controls (Hystem C, fibronectin, or laminin) were given a 'good' rating. These included REDVY 880 mM and REDVY 440 mM. A 'fair' rating was given to experimental coatings that allowed attachment of a significant proportion of the cells. The coatings that received this rating were REDVY 220 mM, REDVY 110 mM, and REDVY 440 mM/RGD 440 mM. REDVY 50 mM, IKVAV 440 mM/YIGSR 440 mM, and the seven peptide

combination received a ‘poor’ rating for their inability to bind the vast majority of cells (Fig. 6.3).

Table 6.2 Expression levels of HA receptors in hNSPCs by RNA-Seq analysis. Expression levels are categorized as high (>10 RPKM), moderate (1-10 RPKM), or low-none (<<1 RPKM).

HA receptor	RPKM (reads per kilobase per million mapped reads)	Relative Expression Level
CD44	316.7	High
TLR4	69.13	High
RHAMM	16.8	High
Layilin	1.69	Moderate
ICAM1	1.57	Moderate
TLR2	0.02	None
Lymphatic vessel endothelial hyaluronan receptor 1	0.02	None

Table 6.3 Composition of coatings used in 2D experiments.

Scaffold	Content
Hystem	0.8% (w/v) Glycosil, 0.2% (w/v) Extralink
Hystem C	0.4% (w/v) Glycosil, 0.4% (w/v) Gelin, 0.2% (w/v) Extralink
REDVY 880 mM	0.71% (w/v) Glycosil, 880 mM REDVY, 0.2% (w/v) Extralink
REDVY 440 mM	0.71% (w/v) Glycosil, 440 mM REDVY, 440 mM RDG (inert), 0.2% (w/v) Extralink
REDVY 220 mM	0.71% (w/v) Glycosil, 220 mM REDVY, 660 mM RDG (inert), 0.2% (w/v) Extralink
REDVY 110 mM	0.71% (w/v) Glycosil, 110 mM REDVY, 770 mM RDG (inert), 0.2% (w/v) Extralink
REDVY 50 mM	0.71% (w/v) Glycosil, 50 mM REDVY, 830 mM RDG (inert), 0.2% (w/v) Extralink
REDVY 440 mM/RGD 440 mM	0.71% (w/v) Glycosil, 440 mM REDVY, 440 mM RGD (active), 0.2% (w/v) Extralink

IKVAV 440 mM/ YIGSR 440 mM	0.71% (w/v) Glycosil, 440 mM IKVAV, 440 mM YIGSR, 0.2% (w/v) Extralink
Seven peptide cocktail	0.71% (w/v) Glycosil, 126.7 mM each of PHSRN, VKNEED, LHGPEILDVPST, DGEA, IKVAV, YIGSR, and RGD, 0.2% (w/v) Extralink

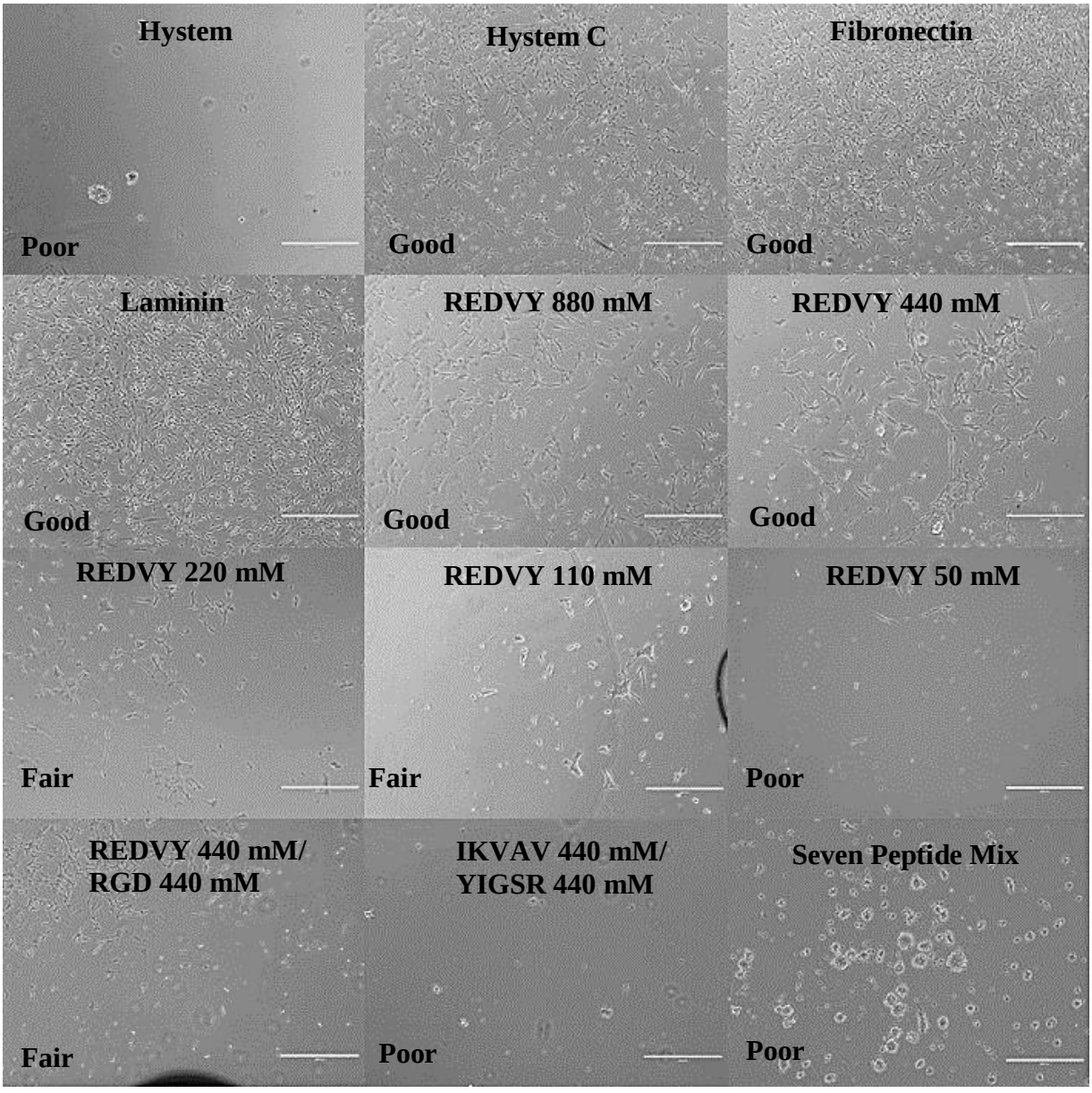

Figure 6.3. Binding of hNSPCs to hyaluronic acid/peptide coated coverslips. Peptides were added to Glycosil at a concentration of 880 mM. Cell binding to REDVY 880 mM and REDVY

440 mM was rated as ‘good’. Cell binding to REDVY 220 mM, REDVY 110 mM, and REDVY 440 mM/RGD 440 mM was ‘fair’. Binding to the other combinations of peptides (REDVY 50 mM, IKVAV 440 mM/YIGSR 440 mM, and the seven peptide combination) was ‘poor’. HyStem served as a negative control since there are no adhesion sites included. Hystem C, fibronectin, and laminin were positive controls. Scale bar is 400 um.

The results from the 2D experiments determined which peptides and concentrations to use in the 3D scaffolds. REDVY 880, REDVY 200, and REDVY 50 mM were chosen to use in the scaffolds as they covered a range of REDVY concentrations. REDVY 440 mM/RGD 440 mM was also used to see the effect of a combination of peptides in 3D. The cells were observed over the course of the three day proliferation period for the extension of processes that would indicate adhesion to the scaffold. However, no extending processes were present in the proliferation-condition HA hydrogels (Fig 6.4).

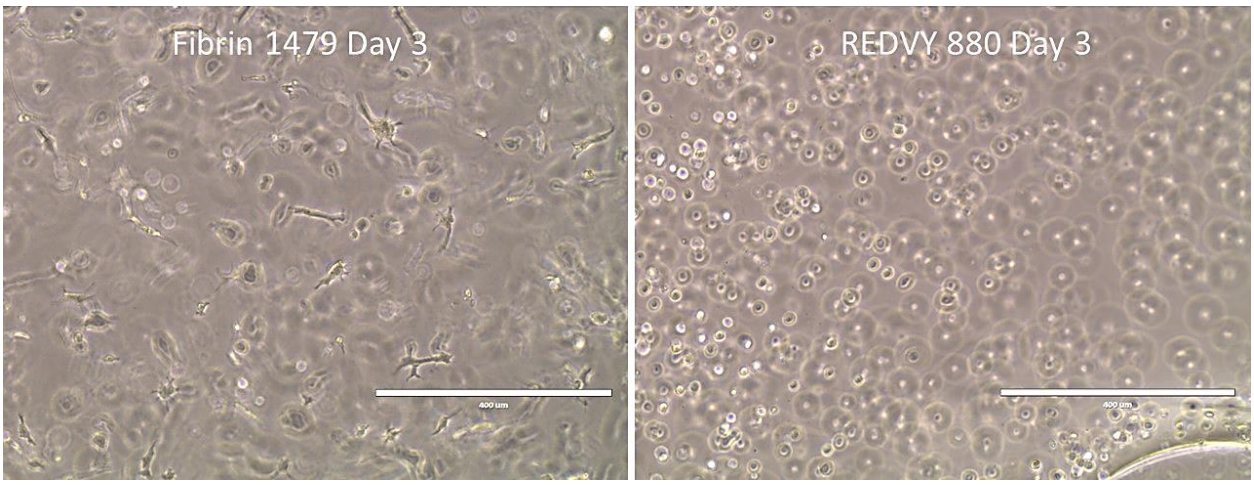

Figure 6.4. Comparison of hNSPC morphology in fibrin vs. HA scaffolds in proliferation conditions. HNSPCs in the salmon fibrin scaffold have extended processes into the matrix. However, in the representative image of the HA scaffolds, cells remain rounded. Scale bar is 400 μm.

To test whether cells were proliferating in the hydrogels but unable to extend, cells were stained with the proliferation markers Ki67 and phosphohistone H3 (PH3). The Ki67 antibody labels cells that are not in G0, and therefore are actively going through the cell cycle, while PH3 antibody labels cells in S phase at the time of fixing. Two markers were chosen in order to

confirm the observed pattern of proliferation in each individual stain. Staining with Ki67 and PH3 showed that the cells were still undergoing proliferation despite the irregular morphology (Fig. 6.5).

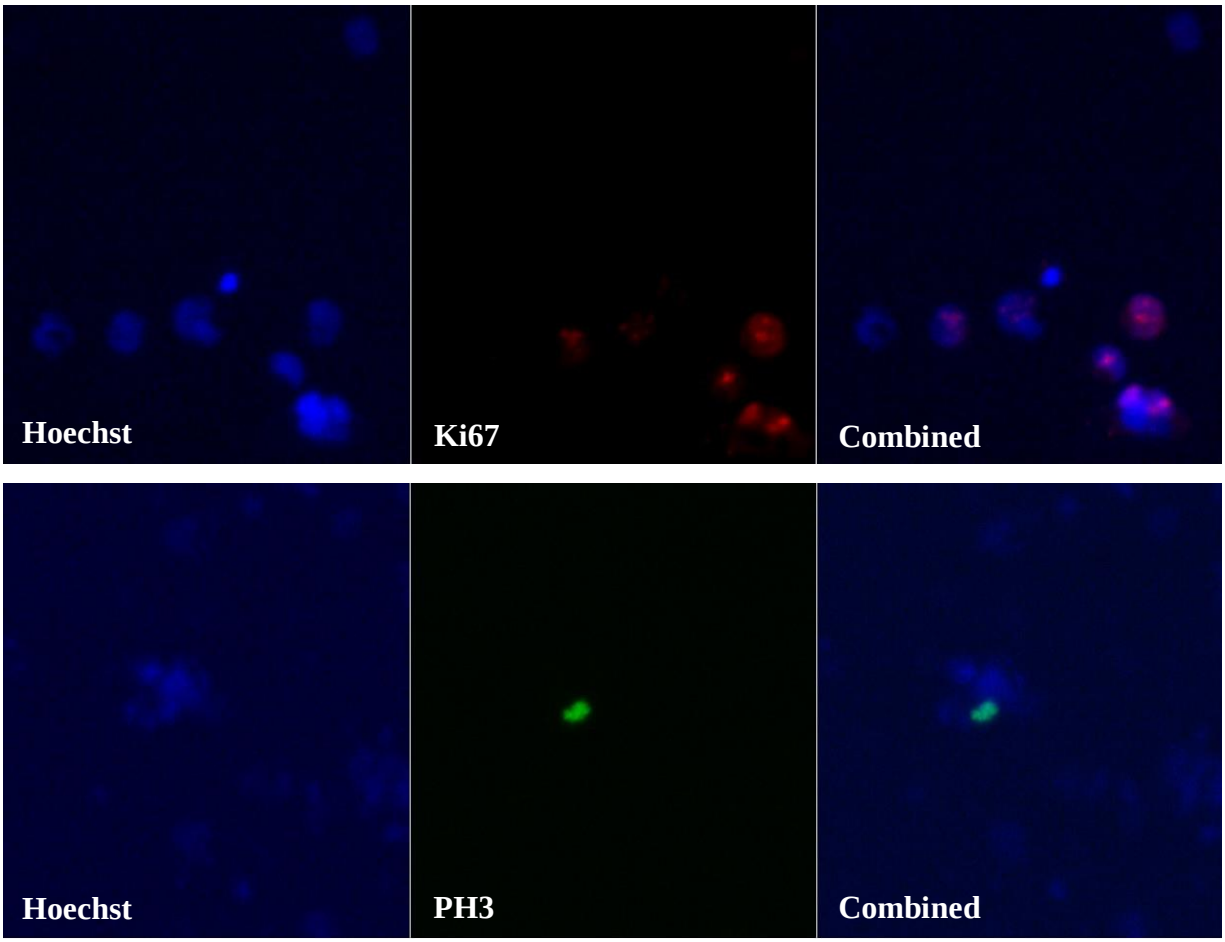

Figure 6.5. Representative immunostaining of proliferating hNSPCs in REDVY/RGD (top row) and REDVY-200 mM scaffolds (bottom row). Far more cells stained when using the Ki67 antibody than when using PH3, as Ki67 stains cells during the entire active cell cycle and PH3 stains mitotic cells during S phase only.

Salmon fibrin scaffolds, which support proliferation of hNSPCs (See Chapter 4), were used to compare proliferation between cells in salmon fibrin and cells in the various HA scaffolds. Staining of hNSPCs by Ki67 was not significantly different between any of the HA

scaffolds and salmon fibrin (Fig. 6.6). PH3 staining of hNSPCs between the different types of scaffolds was significantly different, with cells in both salmon fibrin and REDVY 440 mM/RGD 440 mM displaying a higher percentage of proliferating cells than those in the Hystem C scaffold (Fig 6.7).

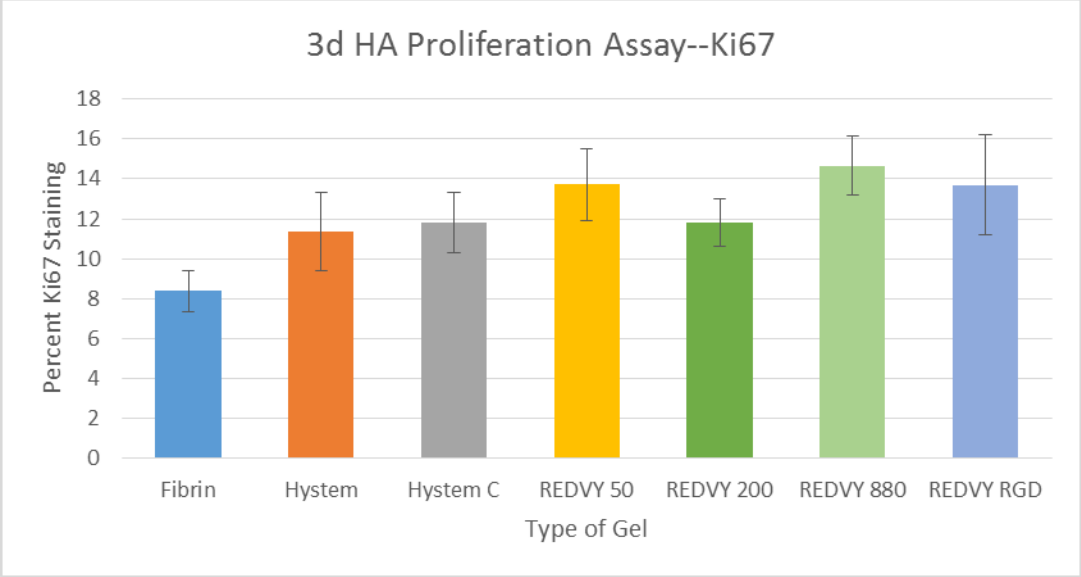

Figure 6.6. Percentage of cells in HA scaffolds stained for the proliferation marker Ki67. There were no significant differences between the percentages of proliferating hNSPCs in any groups after 3 days in culture in proliferation conditions (P = 0.19). Error bars represent SEM. N=3 independent biological repeats.

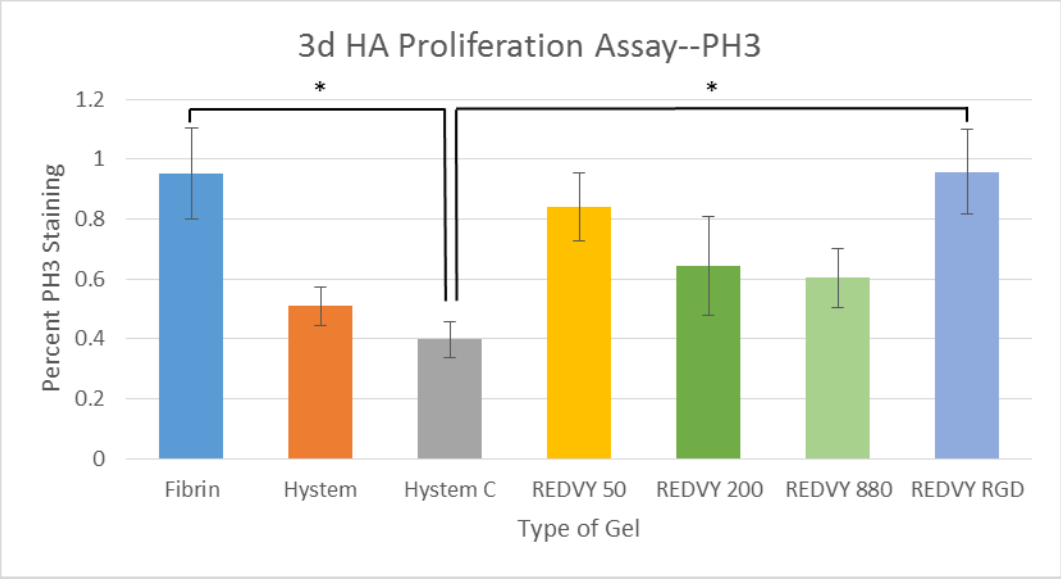

Figure 6.7. Percentage of cells in HA scaffolds stained for the proliferation marker phosphohistone H3 (PH3). HNSPCs in the Hystem C scaffold exhibited a significantly lower proliferation than the cells in the salmon fibrin scaffold (P = 0.011) and in the REDVY 440 mM/RGD 440 mM scaffold (P = 0.016). Error bars represent SEM. N=3 independent biological repeats.

As mentioned previously, extension of cellular processes was not observed in proliferation conditions. We hypothesized that the lack of extension was due to the dense network of Extralink (PEGDA) cross-links that remains intact over time, allowing minimal rearrangement by cells. To test this we replaced Extralink with an MMP-degradable crosslinker than would allow for gradual breakdown of the matrix and manipulation by hNSPC processes. However, the replacement of Extralink with the MMP-degradable cross linker also failed to produce any noticeable hNSPC process extension, as assessed by phalloidin staining of F-actin throughout the cytoskeleton of the cell (Fig. 6.8). This suggests that another mechanism such as substrate stiffness may be playing a role in inhibiting cell spreading in these scaffolds.

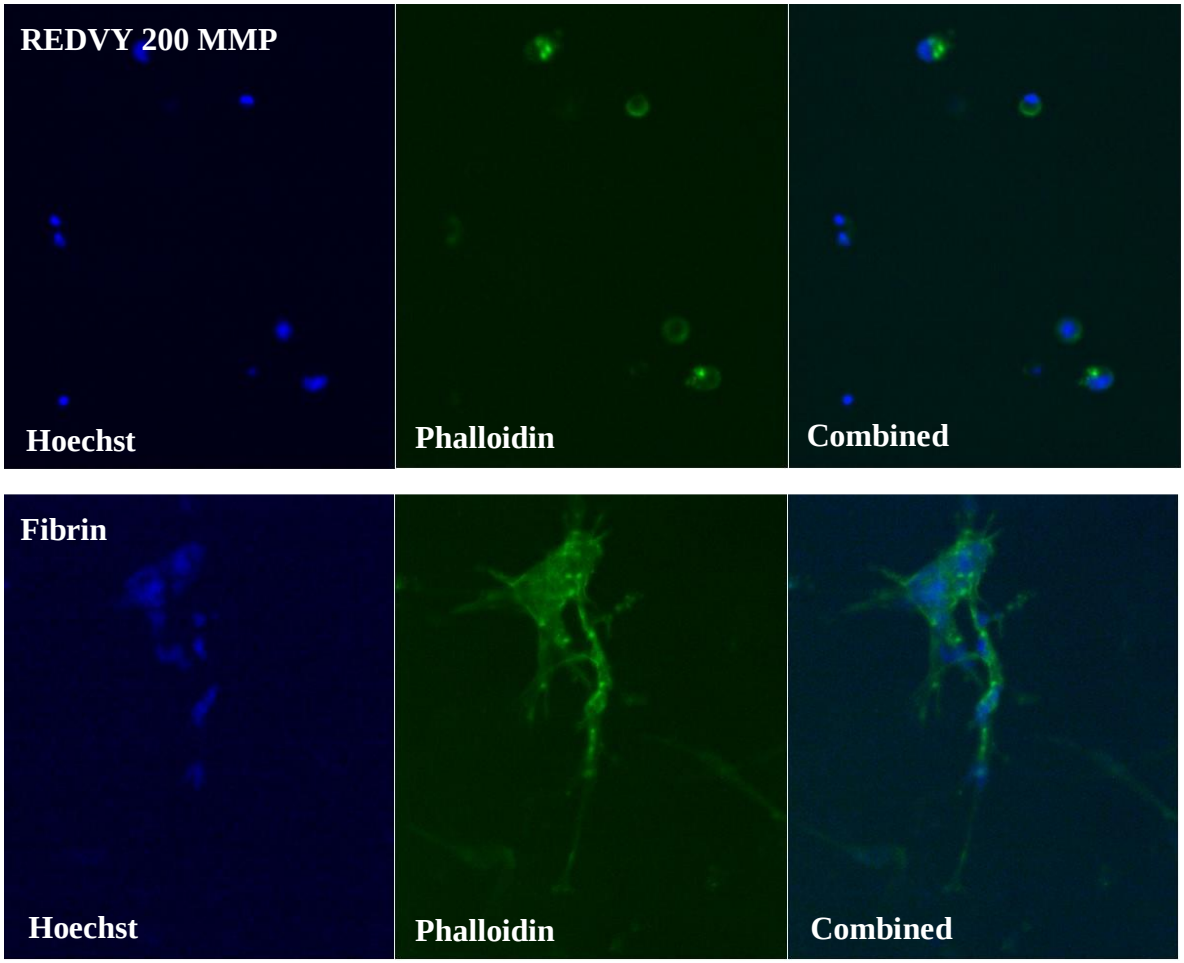

Figure 6.8. Scaffolds composed of 0.71% (w/v) Glycosil, 200 mM REDVY, and 0.2% (w/v) MMP-degradable cross-linker show no observable process extension via phalloidin staining. F-actin staining by phalloidin (green) shows visible process extension in salmon fibrin scaffolds (bottom) and very little extension in HA scaffolds with an MMP-degradable cross-linker (top). The ability of the hNSPCs to cleave the cross-linker with MMP2 did not seem to effect any changes in cellular morphology.

Process extension in these experiments was assessed by phase-contrast imaging as well. The phase-contrast images appeared similar to the HA+REDVY 880 mM image seen in Figure 6.2. However, the titration of Glycosil and Extralink produced hydrogels with fewer HA molecules in which hNSPC extension could be seen. Astrocyte differentiation conditions were used in this experiment since these hNSPCs readily differentiate into neurons and astrocytes, with astrocytes forming as early as 5 days from initiation of differentiation. The HA hydrogels are stiffer (~340

Pa)[18] than the fibrin-based scaffolds introduced in Chapter 3 (< 200 Pa), and were therefore hypothesized to more readily support astrocyte over hNSPC or neuronal process extension based on previous work demonstrating astrocytes favoring stiffer substrates[24, 25]. When 0.4% (w/v) Glycosil and 0.2% (w/v) Extralink were used instead of 0.71% (w/v) Glycosil and 0.2% (w/v) Extralink, a small number hNSPCs produced elongated processes from the cell body. This is likely due to the stiffness of this scaffold being below 100 Pa[18]. Extension could be observed by F-actin staining with phalloidin and astrocyte staining via glial fibrillary acidic protein (GFAP) (Fig. 6.9).

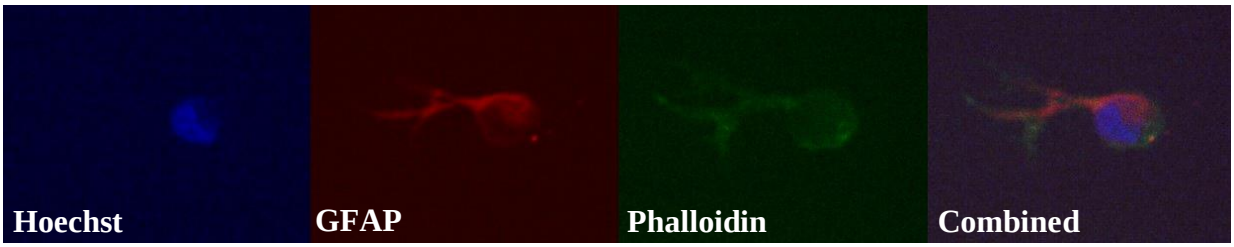

Figure 6.9. Scaffolds composed of 0.4% (w/v) Glycosil, 0.2% (w/v) Extralink, and 880 mM REDVY supported process extension of several hNSPCs in 3D. GFAP is associated with intermediate filaments of astrocytes and phalloidin with actin, so phalloidin staining extends beyond the GFAP staining.

In the 0.2% (w/v) Glycosil and 0.2% (w/v) Extralink scaffold, polymerization was slow to occur and the cells sank onto the coverslip, forming a two-dimensional layer that provided little information about the ability of cells to extend processes in three dimensions. Decreasing the concentration of Extralink to 0.15% (w/v) and 0.1% (w/v) while keeping Glycosil at 0.71% (w/v) had no effect on extension (data not shown). This mimicked what was seen by phase-contrast imaging, in which a single cell was found to have extended a process in the 0.4% (w/v) Glycosil/0.2% (w/v) Extralink scaffold (Fig. 6.10), while many cells extended processes in the 0.2% (w/v) Glycosil/0.2% (w/v) Extralink scaffold though they were all in the same plane (Fig. 6.11).

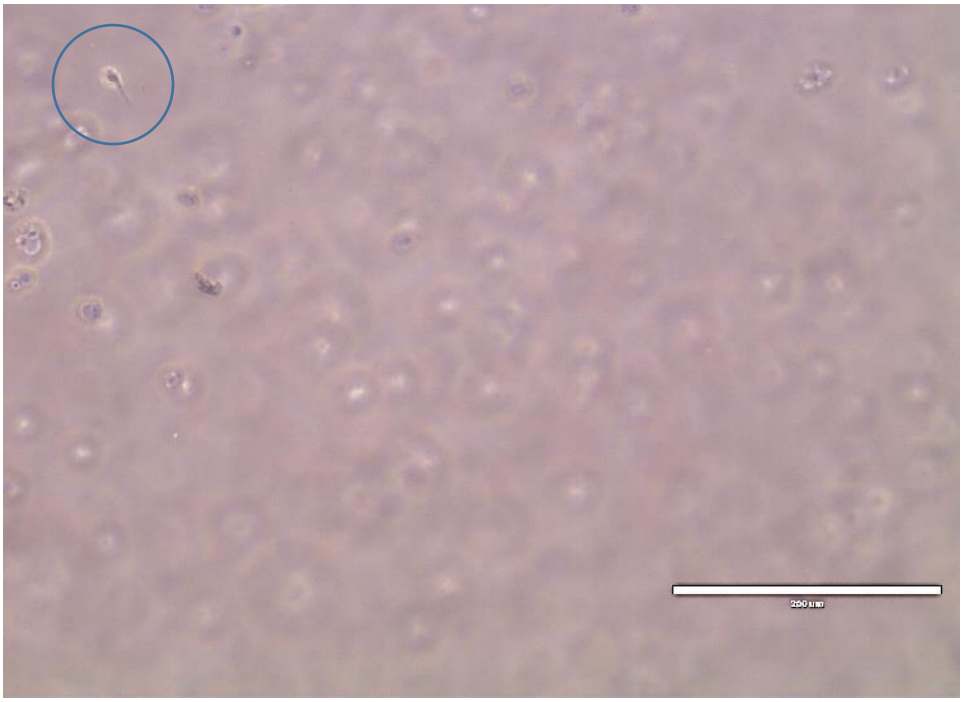

Figure 6.10. Phase contrast image of hNSPCs at day 6 in astrocyte differentiation conditions in a 0.4% (w/v) Glycosil and 0.2% (w/v) Extralink scaffold. One cell with an extended process (blue circle) was found at this lower concentration of HA. Scale bar is 200 µm.

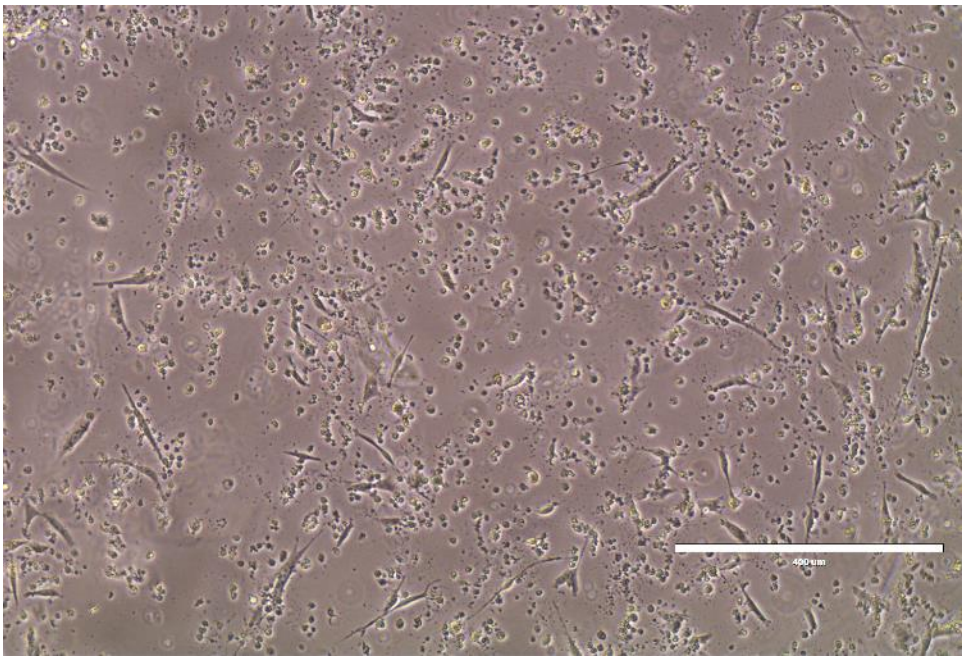

Figure 6.11. Phase contrast image of hNSPCs at day 6 in astrocyte differentiation conditions in a 0.2% (w/v) Glycosil and 0.2% (w/v) Extralink scaffold. HNSPCs sank through to the bottom of the scaffold to form a single layer. Many were able to extend processes,

but a large amount of debris and cells with rounded morphologies were seen in this condition. Scale bar is 400 μm.

6.4 DISCUSSION

The utilization of hyaluronic acid bound to short peptide sequences as an effective scaffold for NSPCs has drawn increasing attention and interest[23]. This combination of materials may also obtain FDA approval more quickly in conjunction with a cellular therapeutic than alternate scaffold candidates. In this study, the peptide REDVY allowed adhesion of hNSPCs to the HA matrix. In 2D studies, a REDVY concentration of 880 mM in a Glycosil/Extralink coating allowed attachment of the greatest number of NSPCs to the coated surface. A majority of cells also attached to surfaces coated with 440 mM REDVY, 440 mM REDVY/440 mM RGD, and 220 mM REDVY. Notably, neither of the laminin-derived sequences, YIGSR or IKVAV, promoted binding of hNSPCs at 440 mM or 127.5 mM. This result diverges from literature that claims these specific laminin sequences allow cells to adhere to HA[23]. The observed difference in outcome could be attributed to the different concentrations used or to the addition of flanking amino acid residues that may allow for better presentation of the peptide's binding site to the cell[23, 26].

Four experimental 3D scaffolds and three controls were stained with the proliferation markers PH3 and Ki67. The percentage of cells stained for Ki67 was much higher than the percentage of cells stained for PH3, as the Ki67 antibody labels cells in all phases of the cell cycle except G0, while the PH3 antibody only stains cells in S phase. The Ki67 staining did not reveal a significant difference in the proliferation of the SC27 cells in scaffolds, while PH3 staining did. The differences were between the fibrin and the Hystem C scaffolds as well as the REDVY 440 mM/RGD 440 mM and the Hystem C scaffolds. Though not a significant difference, a higher degree of cell proliferation was observed in the Ki67 stained REDVY 440

mM/RGD 440 mM hydrogel compared to the other scaffolds. These results suggest that the peptide combination of REDVY and RGD is more effective at promoting proliferation in HA scaffolds than gelatin. It is possible that the lack of significance in Ki67 staining is due to the fact that it is a more promiscuous marker, labeling all cells not in G_0-phase of the cell cycle as opposed to PH3 labeling very specific mitotically dividing cells. Additionally, Ki67 staining remains visible in the top 40 μm of the scaffold during imaging and diminishes in the underlying focal planes. This is likely due to limited Ki67 antibody penetration in the scaffold while PH3 easily penetrates the entire construct, allowing for an increased number of focal planes to be imaged.

Experiments utilizing a range of REDVY concentrations in 3D, as well as the 440 mM REDVY/440 mM RGD combination scaffold, failed to show any process extension that would indicate cell attachment to the matrix or ability of cells to push extensions out against the matrix. However, this morphological difference did not appear to affect the proliferation of cells in any of the scaffolds when compared to cells in the salmon fibrin control, in which strong process extension was seen. Because hNSPCs can be cultured in suspension as neurospheres, the rounded appearance of the cells may not influence proliferation. It could, however, have an effect on differentiation. GFAP staining, which is indicative of astrocytes, was seen in all scaffolds that were kept in astrocyte differentiation conditions, though only the 0.4% (w/v) Glycosil and 0.2% (w/v) Extralink scaffold held cells that extended processes. Neuronal differentiation was not attempted in this study due to the low percentage of neurons that differentiate from this particular set of hNSPCs.

Attachment can affect cell functions through signaling proteins at the cell surface. Proliferation of NSPCs, an important consideration in a transplant designed to repopulate

damaged areas of the brain, is partly influenced in this way. Since the hNSPCs used in this study do not bind to HA (Fig. 6.3, no attachment to HyStem), interactions between the cells and the matrix occur mainly through the added peptides. REDVY and RGD, the two most effective peptides at binding these hNSPCs, are both derived from fibronectin. Fibronectin binds to several integrins, including α3β1, α4β1, α5β1, α8β1, αVβ1, αVβ3, and α4β7[27]. Specifically, the REDV binding site of fibronectin is known to bind to the integrin α4β1, and the RGD sequence is known to bind αIIbβ3, α3β1, α5β1, α8β1, αVβ3, αVβ6, αVβ1, and αVβ5[28, 29]. HNSPCs express the α3, α4, α5, αV, and β1 subunits at high or moderate levels (See Chapter 4), but it is unknown whether these integrins are binding the REDVY and RGD binding sites in the scaffolds. Due to the increased cell proliferation in the REDVY 440 mM/RGD 440 mM, as measured via PH3 staining, it is possible that RGD is binding to an integrin that directs proliferation.

6.5 CONCLUSIONS

This study focused on attachment and proliferation of NSPCs in HA-based scaffolds. These two parameters must be optimized for cells in scaffolds in order to consider use of these materials in transplant settings. A combination of 0.71% (w/v) thiolated HA (Glycosil), 0.2% PEGDA (Extralink), 440 mM REDVY, and 440 mM RGD induced proliferation of hNSPCs in the absence of cellular extension. Cellular process extension was only observed in a scaffold composed of less concentrated HA with stiffness below 100 Pa, as opposed to 340 Pa for all other scaffolds in the study. This suggests that a key parameter to obtaining hNSPC process extension within these HA-based scaffolds is the mechanical compliance. Future studies must focus on whether differentiation is impacted by the rounded morphology of the cells in the HA scaffolds, and if using an MMP-degradable cross-linker in a softer HA scaffold encourages outgrowth of cellular processes.

6.6 REFERENCES

1. Skop, N.B., Calderon, F., Cho, C.H., Gandhi, C.D. & Levison, S.W. Improvements in biomaterial matrices for neural precursor cell transplantation. *Mol Cell Ther* **2**, 19 (2014).
2. Silver, J. & Miller, J.H. Regeneration beyond the glial scar. *Nat Rev Neurosci* **5**, 146-156 (2004).
3. Okano, H. & Sawamoto, K. Neural stem cells: involvement in adult neurogenesis and CNS repair. *Philos Trans R Soc Lond B Biol Sci* **363**, 2111-2122 (2008).
4. Arvidsson, A., Collin, T., Kirik, D., Kokaia, Z. & Lindvall, O. Neuronal replacement from endogenous precursors in the adult brain after stroke. *Nature medicine* **8**, 963-970 (2002).
6. Hicks, A.U. et al. Transplantation of human embryonic stem cell-derived neural precursor cells and enriched environment after cortical stroke in rats: cell survival and functional recovery. *Eur J Neurosci* **29**, 562-574 (2009).
6. Guzman, R. et al. Intracarotid injection of fluorescence activated cell-sorted CD49d-positive neural stem cells improves targeted cell delivery and behavior after stroke in a mouse stroke model. *Stroke* **39**, 1300-1306 (2008).
7. Kallur, T., Darsalia, V., Lindvall, O. & Kokaia, Z. Human fetal cortical and striatal neural stem cells generate region-specific neurons in vitro and differentiate extensively to neurons after intrastriatal transplantation in neonatal rats. *J Neurosci Res* **84**, 1630-1644 (2006).
8. Bakshi, A. et al. Caspase-mediated cell death predominates following engraftment of neural progenitor cells into traumatically injured rat brain. *Brain Res* **1065**, 8-19 (2005).
9. Parr, A.M., Kulbatski, I. & Tator, C.H. Transplantation of adult rat spinal cord stem/progenitor cells for spinal cord injury. *J Neurotrauma* **24**, 835-845 (2007).
10. Darsalia, V. et al. Cell number and timing of transplantation determine survival of human neural stem cell grafts in stroke-damaged rat brain. *J Cereb Blood Flow Metab* **31**, 235-242 (2011).
11. Ricks, C.B., Shin, S.S., Becker, C. & Grandhi, R. Extracellular matrices, artificial neural scaffolds and the promise of neural regeneration. *Neural Regen Res* **9**, 1573-1577 (2014).
12. Johnson, P., Tatara, A., McCreedy, D., Shiu, A. & Sakiyama-Elbert, S. Tissue-engineered fibrin scaffolds containing neural progenitors enhance functional recovery in a subacute model of SCI. *Soft matter* **6**, 5127-5137 (2010).
13. Hwang, d.W. et al. In vivo bioluminescence imaging for prolonged survival of transplanted human neural stem cells using 3D biocompatible scaffold in corticectomized rat model. *PLoS One* **9**, e105129 (2014).
14. Jin, K. et al. Transplantation of human neural precursor cells in Matrigel scaffolding improves outcome from focal cerebral ischemia after delayed postischemic treatment in rats. *J Cereb Blood Flow Metab* **30**, 534-544 (2010).
16. Wang, J.Y. et al. Neurorestorative effect of urinary bladder matrix-mediated neural stem cell transplantation following traumatic brain injury in rats. *CNS Neurol Disord Drug Targets* **12**, 413-425 (2013).
16. Moshayedi, P. & Carmichael, S.T. Hyaluronan, neural stem cells and tissue reconstruction after acute ischemic stroke. *Biomatter* **3** (2013).
17. Liang, Y., Walczak, P. & Bulte, J. The survival of engrafted neural stem cells within hyaluronic acid hydrogels. *Biomaterials* **34**, 5521-5529 (2013).
18. Vanderhooft, J., Alcoutlabi, M., Magda, J. & Prestwich, G. Rheological properties of cross-linked hyaluronan-gelatin hydrogels for tissue engineering. *Macromolecular bioscience* **9**, 20-28 (2009).
19. Misra, S., Hascall, V.C., Markwald, R.R. & Ghatak, S. Interactions between Hyaluronan and Its Receptors (CD44, RHAMM) Regulate the Activities of Inflammation and Cancer. *Front Immunol* **6**, 201 (2015).
20. Brizzi, M.F., Tarone, G. & Defilippi, P. Extracellular matrix, integrins, and growth factors as tailors of the stem cell niche. *Curr Opin Cell Biol* **24**, 645-651 (2012).
21. Davidenko, N., Campbell, J.J., Thian, E.S., Watson, C.J. & Cameron, R.E. Collagen-hyaluronic acid scaffolds for adipose tissue engineering. *Acta Biomater* **6**, 3957-3968 (2010).

22. Park, S.H., Cui, J.H., Park, S.R. & Min, B.H. Potential of fortified fibrin/hyaluronic acid composite gel as a cell delivery vehicle for chondrocytes. *Artif Organs* **33**, 439-447 (2009).
23. Lam, J., Carmichael, S.T., Lowry, W.E. & Segura, T. Hydrogel design of experiments methodology to optimize hydrogel for iPSC-NPC culture. *Adv Healthc Mater* **4**, 534-539 (2015).
24. Saha, K. et al. Substrate modulus directs neural stem cell behavior. *Biophysical journal* **95**, 4426-4438 (2008).
26. Seidlits, S. et al. The effects of hyaluronic acid hydrogels with tunable mechanical properties on neural progenitor cell differentiation. *Biomaterials* **31**, 3930-3940 (2010).
26. Li, X. et al. Short laminin peptide for improved neural stem cell growth. *Stem Cells Transl Med* **3**, 662-670 (2014).
27. Johansson, S., Svineng, G., Wennerberg, K., Armulik, A. & Lohikangas, L. Fibronectin-integrin interactions. *Front Biosci* **2**, d126-146 (1997).
28. Massia, S.P. & Hubbell, J.A. Vascular endothelial cell adhesion and spreading promoted by the peptide REDV of the IIICS region of plasma fibronectin is mediated by integrin alpha 4 beta 1. *J Biol Chem* **267**, 14019-14026 (1992).
29. Plow, E.F., Haas, T.A., Zhang, L., Loftus, J. & Smith, J.W. Ligand binding to integrins. *J Biol Chem* **275**, 21785-21788 (2000).

CHAPTER 7

RECOMBINANT COLLAGEN SCAFFOLDS AS SUBSTRATES FOR HUMAN NEURAL STEM CELLS

Authors: Janahan Arulmoli[1,2*], Richard Que[1*], Nancy A. Da Silva[1,3], Szu-Wen Wang[1,3], Lisa A. Flanagan[1,2,4]

Author Affiliations:

[1]Department of Biomedical Engineering

[2]Sue & Bill Gross Stem Cell Research Center

[3]Department of Chemical Engineering and Materials Science

[4]Department of Neurology

*Denotes equal contribution to this work

[1-4]University of California, Irvine, Irvine, CA, 92697, USA

7.1 INTRODUCTION

Great strides have been made in the field of regenerative medicine in identifying the importance of the cellular microenvironment with regards to cell proliferation, differentiation, and overall development. Biomaterials can mimic the extracellular matrix (ECM) by means of tuning the material's chemical and physical properties, polymerization and degradation rates, nanoscale architecture, and cell adhesion sites in order to modulate cell behavior[1-3]. The utilization of naturally-derived biomaterials as ECM components is stymied by large scale manufacturing bottlenecks and batch-to-batch variation of materials sourced from animals in clinical settings[4, 5]. One of the most commonly found naturally-derived ECM materials is triple-helical collagen, comprising more than 90% of the natural ECM in mammals[6, 7]. Collagen has been studied broadly as an ECM substrate for tissue engineering applications but native collagen is typically acquired from animal sources, thereby permitting minimal control over cell-material interactions and amino acid sequence[8].

To combat these issues, we have developed recombinant human collagen III that can have specific functional sites inserted at desired locations and frequencies on the polymer, making it a highly customizable system[9, 10]. Collagen III, which is a fibrillar collagen composed of a homotrimer and found in elastic tissues such as skin and vasculature[11, 12], was chosen as the collagen in our work due to its expression as a single gene. This recombinant human collagen III system (rCol) yields stable triple-helical collagen that can be used as an effective biomaterial to support mammalian cells[13].

Collagen has been developed as a biomaterial for neural stem/progenitor cells (NSPCs), as these cells can remain in a stem-like state or efficiently differentiate into neurons, astrocytes,

and oligodendrocytes when cultured within 3-dimensional collagen scaffolds[14, 15]. Furthermore, collagen used as a scaffold for NSPCs in a rotating wall vessel bioreactor culture system promotes their differentiation and supports formation of a two-layered structure mimicking cerebral cortical architecture of the embryonic brain[16, 17]. Cells in the CNS bind to collagen primarily through the α1β1, α2β1, and α3β1 integrin heterodimers[18]. Collagen has been used as a transplant scaffold for NSPCs in brain injury models, supporting both migration and differentiation of transplanted cells[19]. In this study, we investigated the effect of various recombinant collagen III scaffolds with inserted collagen-based integrin-binding peptide sequences (GFOGER) on human NSPC (hNSPC) adhesion, proliferation, and differentiation. The ability of synthetic recombinant collagen to support hNSPC behavior would bode useful for translating NSPC/scaffold-based therapies into the clinic where the size, similarity, and manipulability of collagen batches for manufacturing purposes would be of utmost importance.

7.2 MATERIALS AND METHODS

Substrate Preparation

Recombinant collagen was synthesized as described previously[10, 20]. To prepare coated surfaces, 20 μg/mL native and recombinant collagens (in MEM) were incubated in 96-well non-tissue culture treated polystyrene plates (Corning, NY, USA) for 24 hours at 4^{o}C. Laminin was coated at 20 μg/mL and fibronectin at 10 μg/mL and used as controls. Table 7.1 details the different recombinant collagen variants used in these studies.

Table 7.1 Summary of recombinant collagen variants and native human collagen controls. The abbreviated names of the variants, number of GFOGER sites, and descriptions are listed. Reformatted by permission from Elsevier: Biomaterials[20], copyright 2015.

Name of collagen	Description of collagen variant
hCol I	Human collagen I from native source; 1 native GFOGER site
hCol III	Human collagen III from native source (no GFOGER sites, but contains GROGER, GAOGER, GLOGEN, GLKGEN, and GMOGER sites)
rCol	Human collagen III from native source (no GFOGER sites, but contains GROGER, GAOGER, GLOGEN, GLKGEN, and GMOGER sites)
rCol-0G	Human collagen III with GROGER, GAOGER, GLOGEN, GLKGEN, and GMOGER integrin-binding hexamers replaced with non-binding GSPGGK
rCol-1G-8	rCol-0G with GFOGER inserted
rCol-2G-8,11	rCol-0G with 2 GFOGER sites inserted
rCol-4G	rCol-0G with 4 GFOGER sites inserted
rCol-0G-1I	rCol-0G with 1 IKVAV site inserted
rCol-1I	rCol with 1 IKVAV site inserted

Cell Culture

Fetal-derived hNSPCs (SC27) were isolated from the cerebral cortices of brain by the National Human Neural Stem Cell Resource and were grown as adherent cultures on 6-well plates coated with 10 μg/mL fibronectin (human; Fisher Scientific, Hampton, NH, USA)[21].

HNSPC basal medium included DMEM/F12 (Fisher Scientific, Hampton, NH, USA), 20% BIT 9500 (bovine serum albumin, insulin, and transferrin; Stem Cell Technologies, Vancouver, CA), and 1% antibiotic/antimycotic (penicillin/streptomycin/amphotericin; Thermo Fisher Scientific, Waltham, MA, USA). Proliferation media was prepared from basal media via addition of 40 ng/mL epidermal growth factor (EGF; PeproTech, Rocky Hill, NJ, USA), 40 ng/mL basic-fibroblast growth factor (bFGF; PeproTech), and 40 ng/mL platelet-derived growth factor (PDGF-AB; PeproTech,). Adhesion of SC27s to the substrate was measured at 1 day post cell-seeding and proliferation was measured at 1 or 3 days post seeding in proliferation media onto coated 96 well plates. Differentiation media consisted of 96% Neurobasal (Thermo Fisher Scientific, Waltham, MA, USA), 2% B-27 (Thermo Fisher Scientific), 1% GlutaMAX (Thermo Fisher Scientific), and 1% pen/strep (penicillin/streptomycin; Thermo Fisher Scientific) with 20 ng/mL brain-derived neurotrophic factor (BDNF; PeproTech), 20 ng/mL glial-derived neurotrophic factor (GDNF; PeproTech), and 0.5 μM dibutyryl cyclic AMP (cAMP; Sigma-Aldrich, St. Louis, MO, USA) (modified from[22]). HNSPCs were differentiated for 14 days in this media formulation for assessment of neuron and astrocyte formation. Cells were routinely passaged 1:2 or 1:3 and seeded at $1x10^4$ hNSPCs in 100 μL of media per well for experiments and equal numbers of viable cells (Trypan Blue staining) were used for each experimental group. Proliferation media was refreshed every day (50%) for passaging and every other day (100%) for proliferation assays to minimize mechanical disruption of the gels with daily media changes. Differentiation media was refreshed (100%) every other day.

Integrin Blocking and Adhesion Analysis

HNSPCs were dissociated and incubated for 30-45 minutes in 20 μg/mL function blocking (β1, α1, α2, α3, α7) or IgG1 isotype control antibodies (Millipore). Cells were then

plated and imaged using phase contrast microscopy (EVOS) at 24 hours post seeding. To determine how many living cells were adhered to each substrate, cells were washed once with MEM and subsequently incubated with 4 μM Calcein-AM in 0.1% bovine serum albumin (BSA)/PBS at 37^{o}C for 1 hour. After 1x5 minute wash in DPBS, solutions were removed and hNSPCs were lysed with CelLytic M (Sigma) and fluorescence was measured on a plate reader at 494/517 nm (excitation/emission) (SpectraMax M2) and normalized to readout values for hCol I.

Immunostaining and Imaging

HNSPCs were fixed with 4% paraformaldehyde for 10 min as described previously[23]. Fixed cells were treated with 0.3% Triton X-100 in PBS for 5 minutes prior to blocking for 1 hour in 5% BSA in PBS. Cells were incubated in primary antibody in 1% BSA/PBS overnight at 4^{o}C. For differentiation experiments, neurons were stained with 1:200 mouse anti-MAP2 (Sigma, M9942) and astrocytes with 1:200 rabbit anti-GFAP (Sigma, G9269). For proliferation experiments, cells not in G_0 of the cell cycle were stained with 1:500 rabbit anti-Ki67 (Leica Biosystems, KI67P-CE) and cells undergoing mitosis were stained with 1:200 mouse anti-phosphohistone H3 (Cell Signaling Technology, 9706S). Following 3x5 minute PBS washes, samples were incubated with secondary antibodies at a 1:200 dilution in 1% BSA/PBS at room temperature in the dark for 2 hours. The secondary antibodies used were donkey anti-mouse 488 (Thermo Fisher Scientific, A21202) and donkey anti-rabbit 555 (Thermo Fisher Scientific, A-31572). Following 3x5 minute PBS washes, cell nuclei were counterstained for 1 minute with Hoechst 33342 at 1:500 in PBS and wells were covered with 20 μL Vectashield (Vector Labs) and imaged using a Nikon Eclipse Ti microscope with a 20X objective and images were acquired

using NIS element AR3.10 software. ImageJ was used to quantitate positively stained cell nuclei for proliferation.

7.3 RESULTS AND DISCUSSION

7.3.1 hNSPCs adhere to recombinant collagen-coated surfaces

Several variants of collagen were generated to investigate as substrates for hNSPCs (Table 1). Human collagen I and III were used as controls for the mimetic collagens. Recombinant collagen (rCol) is the recombinant version of human collagen III and several modifications to this variant were made by manipulating adhesion sites in the triple-helical domain. A variant of rCol that had several non-binding GSPGGK peptide sequences inserted (rCol-0G) was used as a negative control. Three other recombinant collagens with 1, 2, or 4 GFOGER peptide sequences inserted were used as experimental surfaces (rCol-1G-8, rCol-2G-8,11, rCol-4G). The rCol substrates with incorporated GFOGER sites support the adhesion and expression of the focal adhesion protein vinculin in HT-1080 cells, with highest vinculin expression on rCol-4G compared to both native and all other recombinant collagens[20].

Equipped with these various collagen-mimetic substrates, we set out to test whether hNSPCs would bind and spread on the surfaces presented in Table 7.1. HNSPCs adhered to human collagen I, III, rCol, and all surfaces that contained at least 1 GFOGER site (Fig. 7.1). To our knowledge, there are no previous reports of neural stem cell binding to GFOGER peptide sequences. Fibronectin and laminin were used as positive controls in the study. Adhesion was not as robust on rCol surfaces compared to others, likely due to the instability of rCol compared to its native hCol III form. There was no adhesion observed on rCol-0G, the substrate with all integrin-binding hexamers replaced with the inert GSPGGK sequence. This can be seen by the

lack of cellular extension and spreading on the surface and the prevalence of clumped spheres (Fig 7.1h).

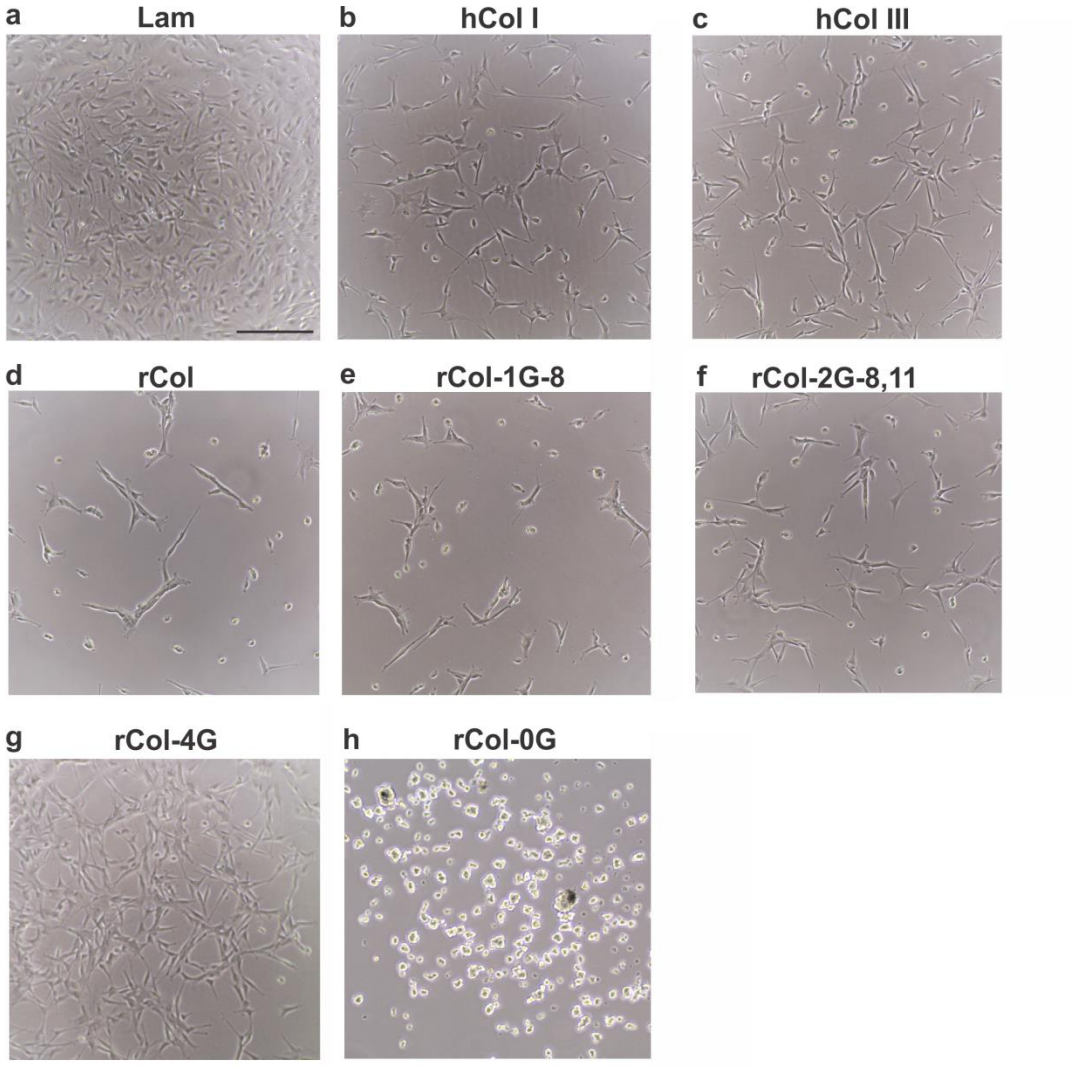

Figure 7.1. Adhesion of hNSPCs to recombinant collagen substrates. HNSPCs adhere and spread on (a) laminin (Lam), (b) hCol I, (c) hCol III, (d) rCol, (e) rCol-1G-8, (f) rCol-2G-8,11, and (g) rCol-4G. There was no binding in the recombinant collagen variant (g) rCol-0G containing inert integrin-binding sites. Scale bar is 200 μm.

Additionally, we tested hNSPC adhesion onto rCol substrates with the laminin-based integrin-binding sequence IKVAV (rCol-0G-1I and rCol-1I). Interestingly, we did not see any adhesion whatsoever on these substrates as the cells behaved similarly to seeding on rCol-0G

(data not shown). We believe this lack of binding to the laminin-binding sequence may be due to the absence of flanking amino acid sequences that have typically been used with IKVAV to achieve binding of NSPCs[24] (See Chapter 6).

7.3.2 α1 and β1 integrins play a role in hNSPC binding to recombinant collagen substrates

Since there could be several mechanisms facilitating the adhesion of hNSPCs to the recombinant collagen substrates such as charge, integrins, or non-integrin collagen receptors, we wanted to delve deeper into which could be playing the largest role. Based on our RNA-Seq data, hNSPCs express several α and β integrin subunits at various expression levels that mediate binding to the ECM (See Chapter 4, Fig. 4.6) (Fig. 7.2). HNSPCs pertinently express collagen-binding integrins α1, α2, and α3 at moderate to high levels (Table 7.2).

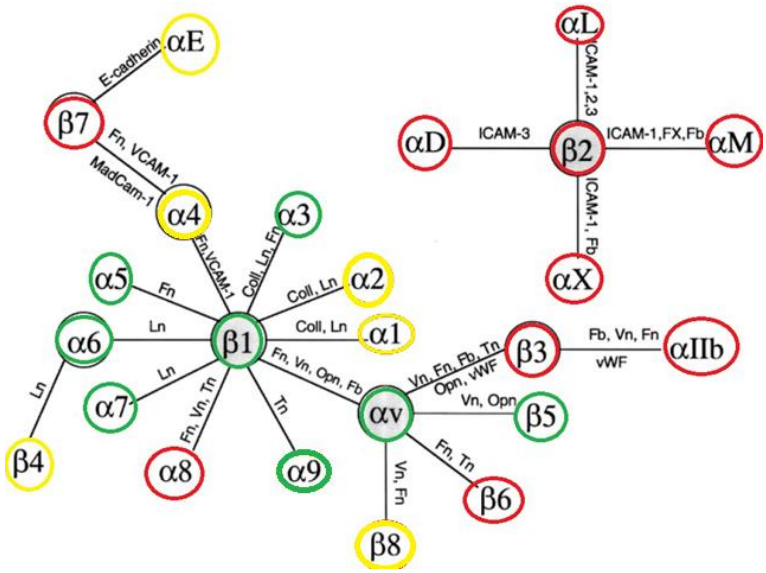

Figure 7.2. Integrin α-β subunits and their expression levels in hNSPCs. Integrins are expressed at the cell surface as α and β heterodimers. α subunits dimerize with β subunits and their expression levels are displayed as high (green), moderate (yellow), or low-none (red) as established in Fig. 3.6, Chapter 3. Ligand abbreviations are: Coll, collagen; Fb, fibrinogen; Fn, fibronectin; FX, factor X; ICAM-1,2,3, intercellular adhesion molecule-1,2,3; Ln, laminin; MadCAM-1, mucosal addressin cell adhesion molecule-1; Opn, osteopontin; Tn, tenascin;

VCAM-1, vascular cell adhesion molecule-1; Vn, vitronectin; vWF, von Willebrand's factor. Reprinted by permission from John Wiley and Sons: Journal of Neuroscience Research[18], copyright 2002.

Table 7.2 Expression levels of collagen-binding integrins in hNSPCs by RNA-Seq analysis. Expression levels are categorized as high (>10 RPKM) or moderate (1-10 RPKM).

Integrin	RPKM (reads per kilobase per million mapped reads)	Relative Expression Level
α1	4.91	Moderate
α2	1.47	Moderate
α3	52.71	High

Based on these data, we first wanted to study whether the most promiscuous and highest-expressed integrin in hNSPCs, β1, is involved in cell binding. We did this by using a function blocking antibody against β1 to observe whether it would have any effect on adhesion to the substrates. We found that blocking the β1 integrin fully disrupts binding to any of the collagen-based substrates, regardless of native or recombinant source. This clarified that collagen-binding integrins α1, α2, or α3 which link to β1 are probably facilitating hNSPC binding to the recombinant collagen substrates. There was not a noticeable effect of blocking β1 integrin on hNSPC binding to laminin or fibronectin (Fig. 7.3). The laminin-binding integrin heterodimer α6β4 is likely compensating for the absence of β1 and enabling adhesion. The αVβ8 likely mediates hNSPC adhesion to fibronectin in the event of blocking the prevalent fibronectin-binding β1-based integrins α3β1, α4β1, α5β1, and αVβ1.

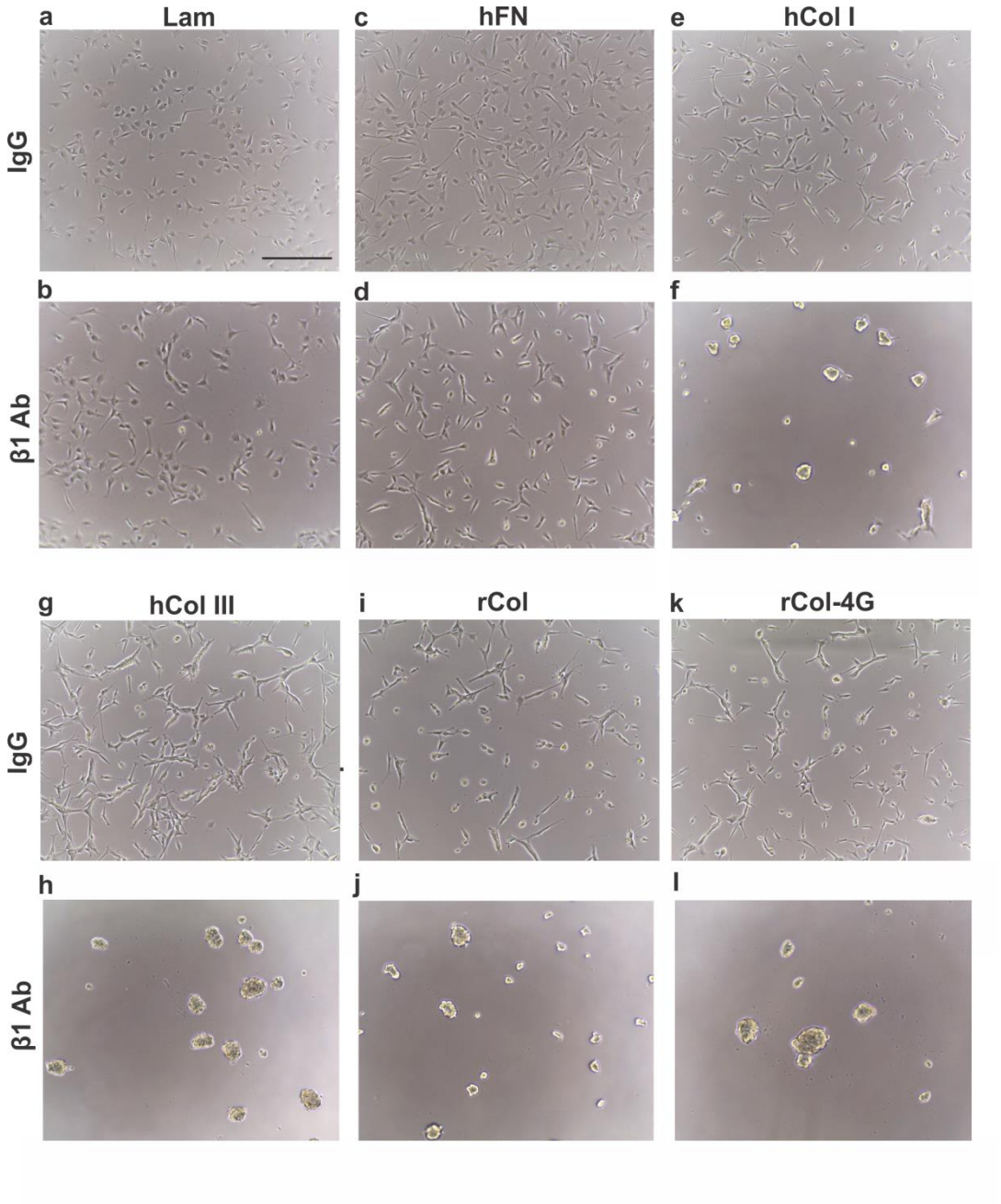

Figure 7.3. Blocking β1-integrin inhibits hNSPC binding to collagen substrates. HNSPCs were incubated with an IgG1 control or function blocking β1 antibody prior to seeding onto (a-b) laminin (Lam), (c-d) fibronectin (hFN), (e-f) hCol I, (g-h) hCol III, (i-j) rCol, and (k-l) rCol-4G substrates. There was an undetectable effect of the β1 antibody treatment on hNSPC adhesion to control hFN and Lam substrates, but binding was fully blocked on all collagen surfaces. Scale bar is 200 μm.

Since β1 is involved in mediating hNSPC adhesion to the substrates, we wanted to test whether its collagen-binding α subunit counterparts are also involved. We chose to test α3 first

since it is highly expressed in hNSPCs based on RNA-Seq data (Table 7.2), and found that blocking α3 did not have a visible effect on adhesion to any of the collagen surfaces (data not shown). We previously found that blocking α2 integrin impeded binding of HT-1080 cells to these collagen substrates[20]. We did not see any effect of perturbing α2 on hNSPC binding to collagen (data not shown). However, blocking the moderately expressed α1 integrin in hNSPCs had a significant effect on binding (Fig. 7.4). A non-specific IgG1 control antibody demonstrated similar effects on adhesion to untreated cells, as shown by Calcein-AM quantification. These findings suggest that hNSPCs bind our novel recombinant collagen substrates at least partially through the α1β1 integrin heterodimer.

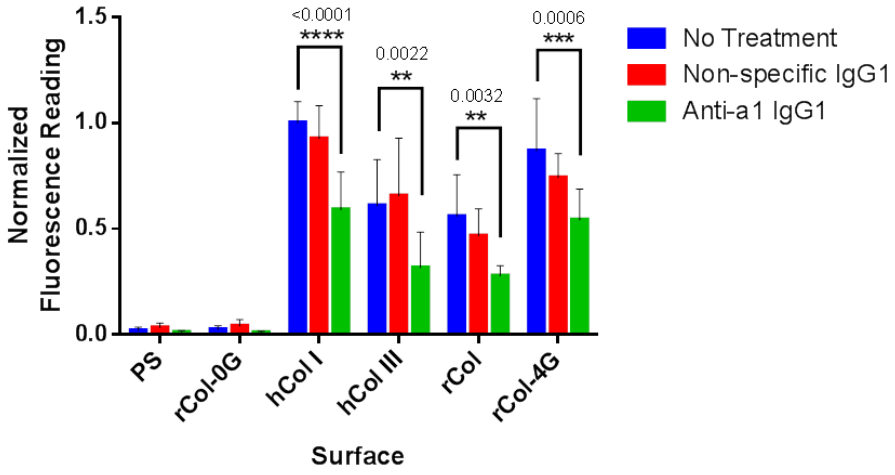

Figure 7.4. HNSPC adhesion after α1-integrin blocking. HNSPCs were incubated with no antibody, non-specific IgG1 antibody, or anti-α1 antibody prior to seeding on various collagen substrates. The fluorescence readout quantifies the relative number of cells adhered to the substrate via Calcein-AM assay. Fluorescence readings were normalized to the No Treatment hCol I group. We note a significant decrease in hNSPC adhesion in α1 blocking antibody-treated groups compared to no treatment on hCol I, hCol III, rCol, and rCol-4G. **P < 0.01. ***P < 0.001. ****P < 0.0001. Error bars represent SEM. N = 3 independent biological repeats.

7.3.3 hNSPCs proliferate and differentiate on recombinant collagen substrates

Since hNSPCs can bind to recombinant collagen substrates through cell surface integrins, we next wanted to assess the proliferation and differentiation capacity of hNSPCs to gauge the ability of the substrates to support hNSPC function. We evaluated the proliferation of hNSPCs via Ki67 and phosphohistone H3 (PH3) immunostaining. Ki67 is expressed in cycling cells that are not in G_0-phase of the cell cycle and PH3 marks cells that are undergoing mitosis in M-phase of the cell cycle. We observe similar proliferation of hNSPCs on laminin compared to hCol I, hCol III, rCol, rCol-1G-8, rCol-2G-8,11, and rCol-4G based on Ki67 immunostaining (Fig. 7.5). However, there is a decrease in total cell number on collagen substrates compared to laminin controls. PH3 staining labels very few cells since a small percentage of the population is undergoing mitosis at any given time, indicating that any difference in percentage between groups may be the result of many imaged fields containing no PH3-positive cells.

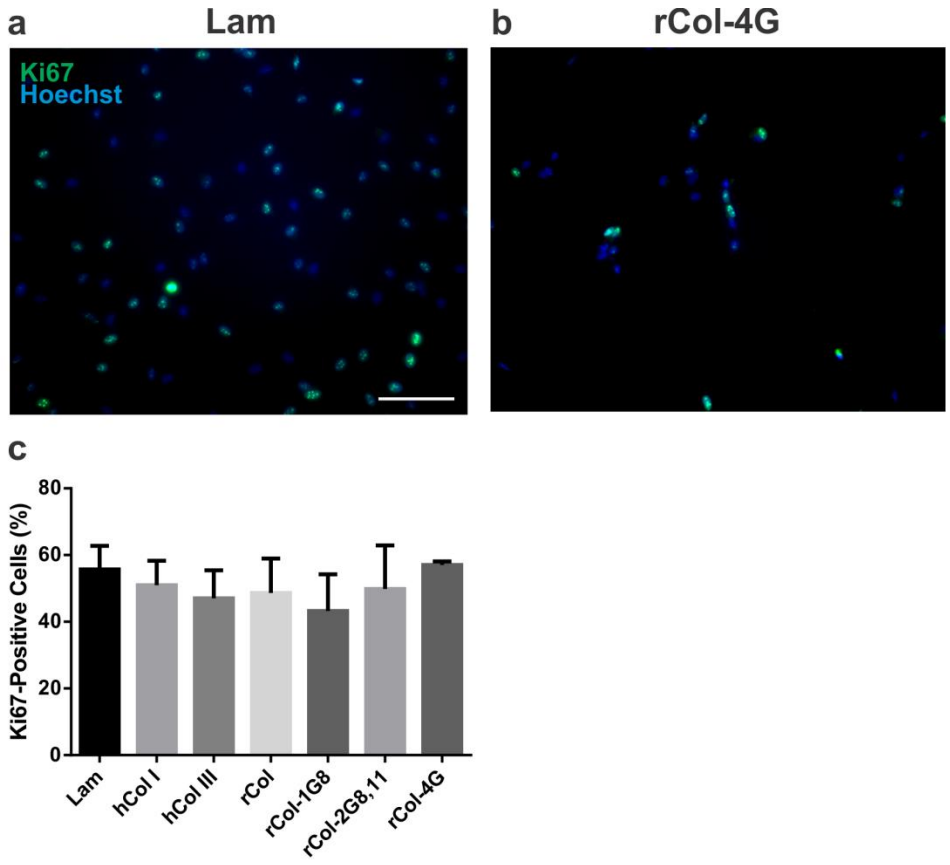

Figure 7.5. HNSPCs proliferate on collagen substrates. Proliferating hNSPCs not in G_0-phase of the cell cycle were detected by immunostaining for Ki67. Representative fields of cells on (a) laminin (Lam) and (b) rCol-4G are shown. (c) Ki67-positive nuclei were quantified after 1 day in proliferating conditions and indicate similar proliferation of the cells across all substrates. Scale bar is 100 μm. N=1 biological repeat.

A critical attribute of substrates for hNSPCs is their ability to promote differentiation, which may stimulate repair in CNS transplant situations. We probed differentiation of hNSPCs into neurons and astrocytes on all the recombinant collagen substrates. These particular cells do not efficiently generate oligodendrocytes *in vitro*, so we did not pursue this lineage. We observed differentiation of hNSPCs into neurons as shown by staining with the neuronal marker MAP2 and astrocytes with the marker glial fibrillary acidic protein (GFAP) on all substrates including controls (Fig. 7.6).

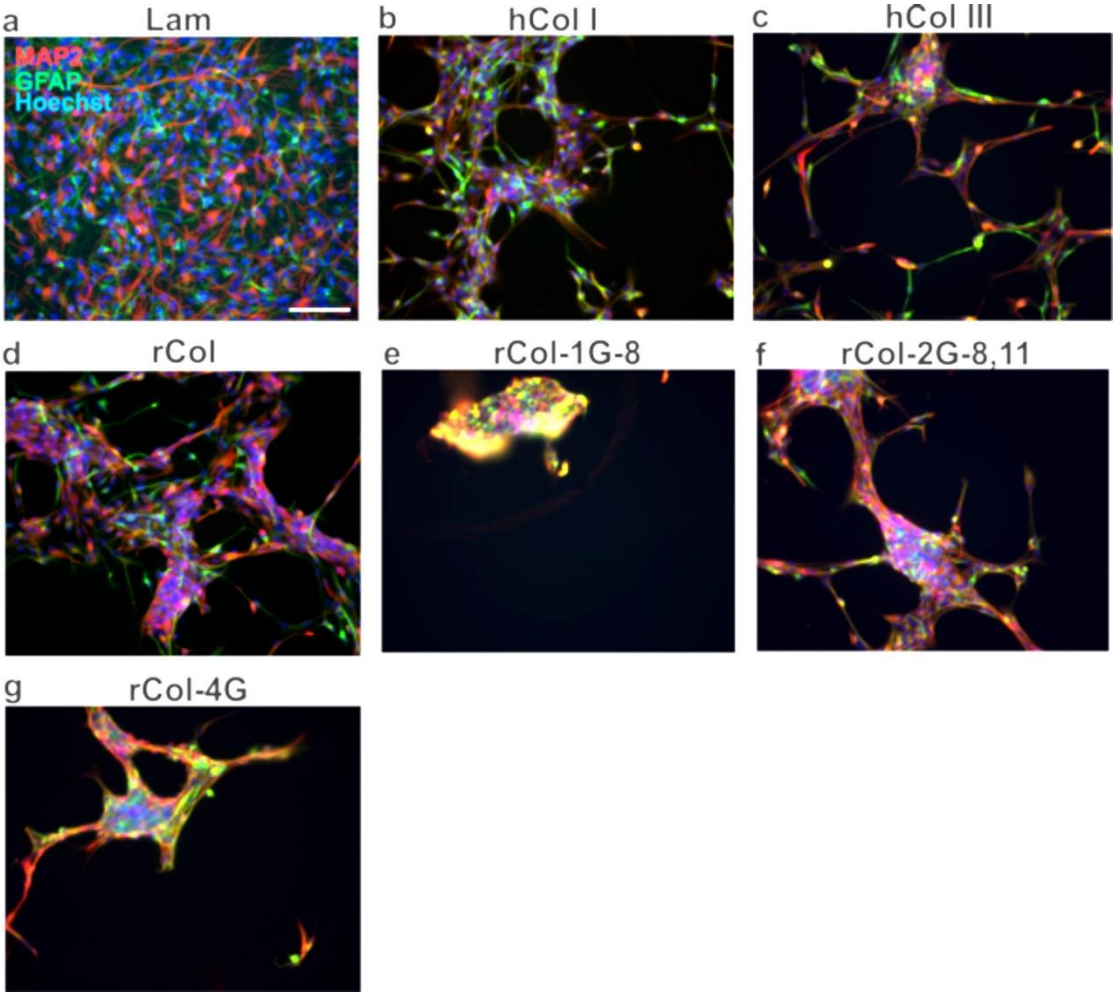

Figure 7.6. Neuronal and astrocyte differentiation of hNSPCs on collagen substrates. HNSPCs were differentiated for 14 days and differentiation was assessed using the markers MAP2 (red) for neurons and GFAP (green) for astrocytes. Cells differentiated down both lineages on (a) laminin (Lam), (b) hCol I, (c) hCol III, (d) rCol, (e) rCol-1G-8, (f) rCol-2G-8,11, and (g) rCol-4G though cells were more clumped together on the collagen surfaces than laminin control. Nuclei were counterstained with Hoechst (blue). Scale bar is 100 μm.

It was impractical to quantitatively analyze differentiated cells across samples because of the clustering of cells on collagen substrates over 14 days of differentiation. The clustering was not as apparent on rCol-4G compared to rCol, hCol I, and hCol III, suggesting that the increased number of GFOGER sites may support cell adhesion to the surface. Since the initial binding of hNSPCs to the collagen substrates is not as strong as on laminin controls (Fig. 7.1), the strength of adhesions likely weakens over the course of 2 weeks of differentiation. However, it is evident

from immunostaining that hNSPCs are at least able to differentiate into neurons and astrocytes on both native and recombinant collagen substrates. This result suggests that recombinant collagen substrates provide a novel platform that supports hNSPC behavior in 2-dimensional culture.

7.4 CONCLUSIONS AND FUTURE DIRECTIONS

This work highlighted the development of novel recombinant collagen substrates that can be used for the culture of hNSPCs. HNSPCs adhered to collagen III-mimetic substrates that contained varying amounts of inserted GFOGER adhesion peptides. Since no group has previously demonstrated interaction of hNSPCs with GFOGER, this finding adds to the body of literature pertaining to short adhesion sequences that facilitate binding of NSPCs. Recombinant collagen surfaces enable proliferation and differentiation of hNSPCs, and blocking of the α1 and β1 integrins perturbs binding to the substrate indicating cells interact with rCol variants through the α1β1 integrin heterodimer. These substrates serve as favorable biomaterials for hNSPC culture in 2D, though further studies are needed to investigate the morphological changes of clumped cells differentiated on collagen substrates. These findings still provide ample motivation to develop rCol-based substrates as 3D scaffolds. Analysis of hNSPC function within 3D rCol matrices would then set the stage for its use as a cell delivery scaffold for the treatment of stroke.

7.5 REFERENCES

1. Discher, D.E., Mooney, D.J. & Zandstra, P.W. Growth factors, matrices, and forces combine and control stem cells. *Science* **324**, 1673-1677 (2009).
2. Lutolf, M.P. & Hubbell, J.A. Synthetic biomaterials as instructive extracellular microenvironments for morphogenesis in tissue engineering. *Nat Biotechnol* **23**, 47-55 (2005).
3. von der Mark, K., Park, J., Bauer, S. & Schmuki, P. Nanoscale engineering of biomimetic surfaces: cues from the extracellular matrix. *Cell Tissue Res* **339**, 131-153 (2010).
4. Uemura, M. et al. Matrigel supports survival and neuronal differentiation of grafted embryonic stem cell-derived neural precursor cells. *J Neurosci Res* **88**, 542-551 (2010).
5. Lynn, A.K., Yannas, I.V. & Bonfield, W. Antigenicity and immunogenicity of collagen. *J Biomed Mater Res B Appl Biomater* **71**, 343-354 (2004).
7. Abraham, L.C., Zuena, E., Perez-Ramirez, B. & Kaplan, D.L. Guide to collagen characterization for biomaterial studies. *J Biomed Mater Res B Appl Biomater* **87**, 264-285 (2008).
7. Birk, D.E., Silver, F.H. & Trelstad, R.L. in Cell biology of extracellular matrix 221-254 (Springer, 1991).
8. Jia, X. & Kiick, K.L. Hybrid multicomponent hydrogels for tissue engineering. *Macromol Biosci* **9**, 140-156 (2009).
9. Chan, S.W. et al. Recombinant human collagen and biomimetic variants using a de novo gene optimized for modular assembly. *Biomacromolecules* **11**, 1460-1469 (2010).
10. Que, R., Mohraz, A., Da Silva, N.A. & Wang, S.W. Expanding functionality of recombinant human collagen through engineered non-native cysteines. *Biomacromolecules* **15**, 3540-3549 (2014).
11. Royce, P.M. & Steinmann, B. Connective tissue and its heritable disorders: molecular, genetic, and medical aspects. (John Wiley & Sons, 2003).
12. Bourhis, J.-M. et al. Structural basis of fibrillar collagen trimerization and related genetic disorders. *Nature structural & molecular biology* **19**, 1031-1036 (2012).
13. Jabaiah, A. et al. Nanoscale architecture and cellular adhesion of biomimetic collagen substrates. *J Biomater Appl* **28**, 1354-1365 (2014).
14. Ge, D. et al. Culture and differentiation of rat neural stem/progenitor cells in a three-dimensional collagen scaffold. *Appl Biochem Biotechnol* **170**, 406-419 (2013).
15. Huang, F., Shen, Q. & Zhao, J. Growth and differentiation of neural stem cells in a three-dimensional collagen gel scaffold. *Neural Regen Res* **8**, 313-319 (2013).
17. Lin, H.J., O'Shaughnessy, T.J., Kelly, J. & Ma, W. Neural stem cell differentiation in a cell–collagen–bioreactor culture system. *Developmental brain research* **153**, 163-173 (2004).
17. Ma, W. et al., Vol. 227, Edn. 1 327-334 (Wiley Online Library.
18. Milner, R. & Campbell, I. The integrin family of cell adhesion molecules has multiple functions within the CNS. *Journal of neuroscience research* **69**, 286-291 (2002).
19. Elias, P.Z. & Spector, M. Implantation of a collagen scaffold seeded with adult rat hippocampal progenitors in a rat model of penetrating brain injury. *J Neurosci Methods* **209**, 199-211 (2012).
20. Que, R.A. et al. Tuning cellular response by modular design of bioactive domains in collagen. *Biomaterials* **53**, 309-317 (2015).
21. Schwartz, P.H. et al. Isolation and characterization of neural progenitor cells from post-mortem human cortex. *J Neurosci Res* **74**, 838-851 (2003).
22. Yuan, S.H. et al. Cell-surface marker signatures for the isolation of neural stem cells, glia and neurons derived from human pluripotent stem cells. *PLoS One* **6**, e17540 (2011).
23. Flanagan, L. et al. Unique dielectric properties distinguish stem cells and their differentiated progeny. *Stem cells (Dayton, Ohio)* **26**, 656-665 (2008).
24. Lam, J., Carmichael, S.T., Lowry, W.E. & Segura, T. Hydrogel design of experiments methodology to optimize hydrogel for iPSC-NPC culture. *Adv Healthc Mater* **4**, 534-539 (2015).

CHAPTER 8

REFLECTIN AS A MATERIAL FOR NEURAL STEM CELL GROWTH

Authors: Long Phan[1,*], Rylan Kautz[1,*], **Janahan Arulmoli**[3,4], Iris Kim[5], Dai Trang T. Le[5], Michael A. Shenk[1], Medha M. Pathak[5], Lisa A. Flanagan[3,4,6], Francesco Tombola[5], Alon A. Gorodetsky[1,2]

Author Affiliations:

[1]Department of Chemical Engineering and Materials Science

[2]Department of Chemistry

[3]Department of Biomedical Engineering

[4]Sue and Bill Gross Stem Cell Research Center

[5]Department of Physiology & Biophysics

[6]Department of Neurology

*Denotes equal contribution to this work

[1-6]University of California, Irvine, Irvine, CA, 92697, USA

Keywords: reflectin, cephalopods, bioelectronics, biointerfaces, stem cells

8.1 ABSTRACT

Cephalopods possess remarkable camouflage capabilities, which are enabled by their complex skin structure and sophisticated nervous system. These animals' unique characteristics have therefore inspired the design of novel functional materials and devices. Within this context, recent studies have focused on investigating the self-assembly, optical, and electrical properties of reflectin, a protein that plays a key role in cephalopod structural coloration. Herein, we report the discovery that reflectin constitutes an effective material for the growth of human neural stem/progenitor cells. Our findings may hold relevance both for understanding cephalopod embryogenesis and for developing improved protein-based bioelectronic devices.

8.2 INTRODUCTION

Cephalopods (squid, octopus, and cuttlefish) are renowned as much for their stunning camouflage displays as for their vertebrate-like behavioral characteristics[1-6]. These abilities stem from the cephalopods' sophisticated nervous system, which has evolved to exhibit a number of anatomical and functional similarities with the nervous systems of vertebrates[4, 6-11]. Consequently, cephalopods have greatly advanced fundamental neurobiology research by furnishing seminal comparative neurophysiological model systems, including giant axons, giant synapses, and chromatophore neuromuscular junctions[12-19]. The study of cephalopods has therefore illuminated basic mechanisms of neuronal communication and greatly advanced scientific understanding of human brain function[4, 6-11].

Outside of neuroscience, the complex skin structure of cephalopods has served as a source of inspiration for the development of novel functional devices from both artificial[20-25] and natural materials[26-29]. For example, several groups have fabricated stimuli-responsive optical coatings from proteins known as reflectins, which play a crucial role in cephalopod structural coloration and possess unique self-assembly properties[26-34]. Moreover, the reflectin A1 isoform from *Doryteuthis (Loligo) pealeii* has been shown to function as an effective proton conduction medium, enabling its use in protonic transistors[35, 36]. These findings have indicated that reflectins possess untapped potential as active materials not only for adaptive optics but also for bioelectronic devices.

Recently, cephalopods, and specifically the cuttlefish *Sepia officinalis*, have been touted as promising comparative models for ecological and evolutionary developmental biology[37-39]. Within this context, the presence of both mRNA and iridescence associated with reflectin were

recently noted during the later stages of embryogenesis in *Sepia officinalis*[40, 41]. Interestingly, reflectin was detected during developmental stages that correlate to some of the major steps of neurogenesis, precisely when brain maturation and growth occurs in *Sepia officinalis* embryos[40, 41]. These observations hinted at undiscovered roles for reflectin in cephalopod neural development and inspired us to consider the possibility that reflectin could promote neural stem cell growth.

Herein, we report the finding that reflectin constitutes an effective substrate for human neural stem/progenitor cells (hNSPCs). We first fabricate reflectin films according to standard protocols[26, 27, 35, 36]. We next show that these substrates support the growth of murine and human cells. We subsequently demonstrate that reflectin films support the adhesion, proliferation, and differentiation of relatively difficult-to-culture hNSPCs. Our findings represent a crucial step towards the direct electrical monitoring and triggering of cellular biochemical events with reflectin-based bioelectronic devices.

8.3 RESULTS AND DISCUSSION

We began our studies by fabricating reflectin films on quartz or silica substrates. We first expressed a histidine-tagged *Doryteuthis (Loligo) pealeii* reflectin A1 isoform in *E. coli*. We then coated the substrates with reflectin via a modified doctor blading procedure (Fig 8.1), yielding films that were similar to those reported in our previous studies.[26,27] The resulting reflectin-coated substrates were used directly for cell culture experiments (Fig. 8.1).

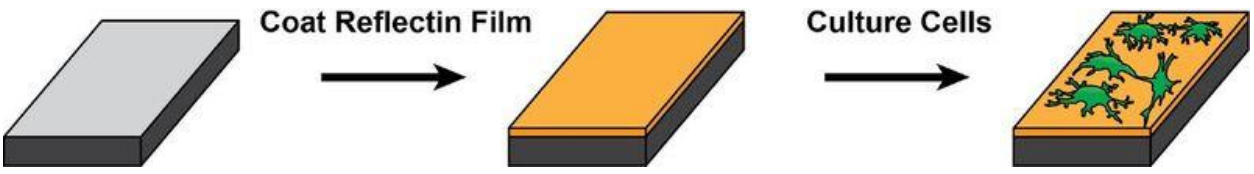

Figure 8.1. General illustration of cell culture experiments on reflectin-coated substrates. Reflectin films were fabricated via a modified doctor blading procedure and then used directly for the growth of mammalian cells.

We initially evaluated the ability of reflectin to support the growth of inherently adherent murine and human cells (before transitioning to a more challenging cell type). For these experiments, we specifically selected three established cell lines that are well-known to grow on varied surfaces: HEK293A (human embryonic kidney cells that are widespread in cell biology)[42, 43], MDA-MB-231 (human mammary cells employed in breast cancer research)[44, 45], and BV2 (murine microglial cell lines used for exploring the immune response of the central nervous system)[46-48]. The use of these established cell lines facilitated our exploratory protocol optimization.

We incubated reflectin-coated substrates with HEK293A, MDA-MB-231, or BV2 cells. After 1 day, we visualized the substrates with bright-field microscopy (Fig. 8.2). The three cell types exhibited morphologies that were consistent with literature precedent and indicative of adhesion and/or division. Indeed, HEK293A cells grew together in islands and possessed relatively flat bodies[42, 43], MDA-MB-231 cells featured granular and spindle-like bodies[44, 45], and BV2 cells varied between flat spinous and small rounded bodies[46-48]. These observations demonstrated that reflectin films were capable of supporting mammalian cell adhesion and portended favorably for subsequent experiments.

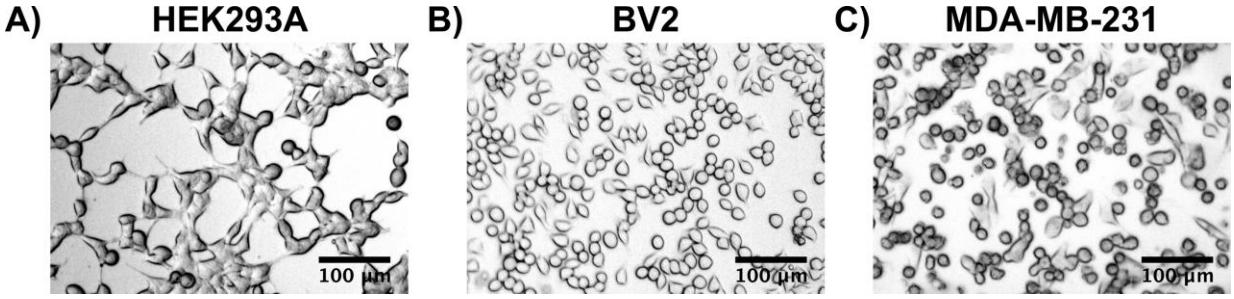

Figure 8.2. Typical bright-field microscopy images of (a) HEK293A, (b) BV2, and (c) MDA-MB-231 cells on reflectin films. The images were collected 1 day after seeding and show that the cells have adhered to the substrates.

We proceeded to challenge our substrates with hNSPCs, which play an essential role in brain and spinal cord development[49-51]. As a general rule, stem cells are exquisitely sensitive to chemical and physical cues from their surrounding environment, making them relatively difficult to culture on arbitrary surfaces[52-58]. Here, we focused our efforts on SC27 hNSPCs derived from the cerebral cortex of a post-mortem fetal brain[59, 60]. These cells express standard neural stem cell markers, including SOX2, nestin, and CD 133, and can potentially differentiate into three major cell types of the brain (i.e. astrocytes, neurons, and oligodendrocytes)[59-63]. They have also been shown to possess therapeutic potential in mouse models of Sandhoff disease[64]. Furthermore, we have previously explored the adhesion, proliferation, an differentiation of SC27 hNSPCs under varied conditions on different substrates[61, 62, 65]. Thus, SC27 hNSPCs represented a particularly advantageous choice for our studies.

We seeded reflectin-coated and uncoated substrates with undifferentiated SC27 hNSPCs and visualized them with phase contrast optical microscopy over a period of 15 days (Fig. 8.3). For the coated substrates, we were gratified to observe that the hNSPCs were bound to the surface after 1 day. Indeed, most of the cells adopted a predominantly elongated morphology, and some of the cells displayed a rounded morphology while maintaining attachment to the substrate, as might be expected during cell division (Fig. 8.3a). After 15 days, we found a marked >10-fold increase in the cell density, confirming division (Fig. 8.3d). In contrast, uncoated substrates showed no hNSPC attachment or growth under identical conditions over the same time period (Figure 3D). In contrast, uncoated substrates showed no hNSPC binding or growth under identical conditions over the same time period (Fig. 8.3d). Together, these

observations indicated that reflectin coatings facilitated hNSPC attachment and subsequent proliferation on their surfaces (and supported cell viability for an extended period of time).

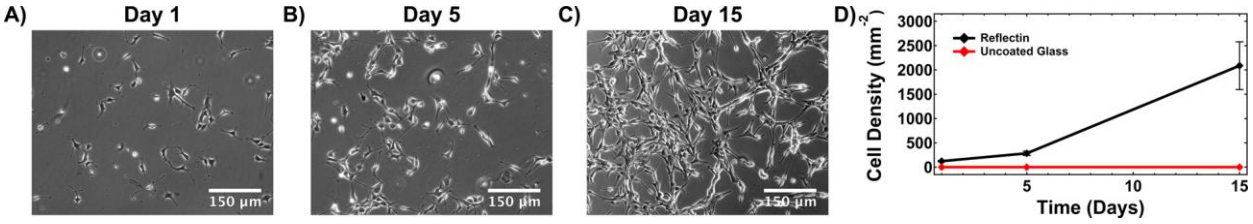

Figure 8.3. Typical phase contrast optical microscopy images of hNSPCs on reflectin films, which demonstrate cell proliferation over time. The images were collected (a) 1 day, (b) 5 days, and (c) 15 days after seeding. (d) The plot of the cell density on both reflectin-coated and uncoated substrates after 1 day, 5 days, and 15 days. The error bars indicate the standard error of the mean per film.

We next directly compared hNSPC growth on reflectin and more established materials (Fig. 8.4). Due to their significance in both the fetal and adult central nervous systems, hNSPCs have been cultured on various substrates, including ceramics, polymers, polysaccharides, synthetic peptides, and naturally occurring proteins[52-54]. For our comparison, we selected fibronectin, laminin, and poly-D-lysine. These coatings were specifically chosen because they are in the same materials class as reflectin (i.e. proteins and peptides)[52-54] and have been previously used for the growth of hNSPCs[61, 62, 65].

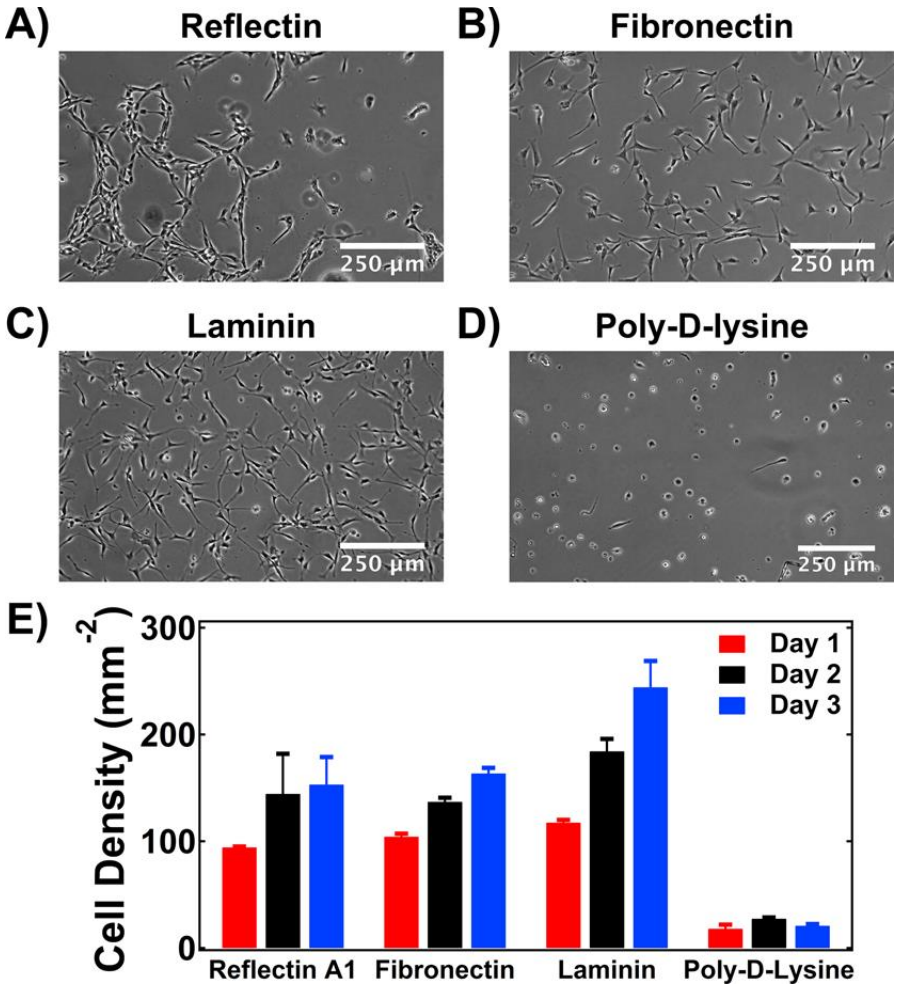

Figure 8.4. Typical phase contrast optical microscopy images of hNSPCs on (a) reflectin, (b) fibronectin, (c) laminin, and (d) poly-D-lysine. The cell cultures were prepared under identical conditions, and the images were collected 3 days after seeding. (e) The corresponding plot of the cell density for each of the 4 substrates over the initial 3 days after seeding. Note that the cell density on reflectin is comparable to the cell density on fibronectin and laminin. The error bars indicate the standard error of the mean per film.

Phase contrast optical microscopy images of cells cultured under identical conditions on reflectin, fibronectin, laminin, and poly-D-lysine are shown in Figure 8.4. Here, because stem cells often produce their own extracellular matrices, which contribute to cell adhesion and proliferation over extended periods of time, we limited our analysis to the first three days of growth. Although hNSPCs were not always uniformly distributed on reflectin-coated substrates (Fig. 8.4a), the cell morphologies were similar to those observed on fibronectin- and laminin-

coated substrates (Fig. 8.4b,c), but quite distinct from those observed on poly-D-lysine-coated substrates (Fig. 8.4d). Moreover, we observed that the cell densities on reflectin, fibronectin, and laminin were comparable and much higher than on poly-D-lysine (Fig. 8.4e). Overall, the performance of reflectin was comparable to that of common validated neural stem cell growth matrices.

We proceeded to assess the behavior of hNSPCs cultured on reflectin-coated substrates. Because stem cell/matrix interactions influence cell fate[52-54], we investigated whether reflectin affected typical physiological processes previously documented for membrane-bound proteins at the cell-substrate interface. Thus, we studied the activity of the Ca^{2+}-selective ion channel Piezo1, which influences stem cell differentiation via the transduction of matrix mechanical information[65]. For this purpose, we utilized total internal reflection fluorescence microscopy (TIRFM), a technique that reduces intracellular background fluorescence and specifically reports on events at the cell-substrate interface (Fig. 8.5)[66, 67]. We postulated that reflectin would be especially well suited for TIRFM experiments due to its favorable optical properties, including a high refractive index of 1.54[26, 27].

We visualized hNSPCs on reflectin-coated substrates with TIRFM, monitoring them in real time (Fig. 8.5). The fluorescent Ca^{2+} indicator Fluo-4AM facilitated imaging of individual cells (Fig. 8.5b), enabling us to measure spontaneous Ca^{2+} transients that have been previously linked to Piezo1 activity.[67] As an example, two arbitrary representative areas are marked with blue and red boxes in Figure 8.5b, and the corresponding spontaneous transients are shown in Figure 8.5c. In general, the appearance of the hNSPCs, as well as the amplitude and frequency of the associated transients, closely resembled those found on fibronectin-coated substrate[65].

Overall, our TIRFM measurements provided additional evidence for hNSPCs exhibiting "typical" behavior and activity on reflectin.

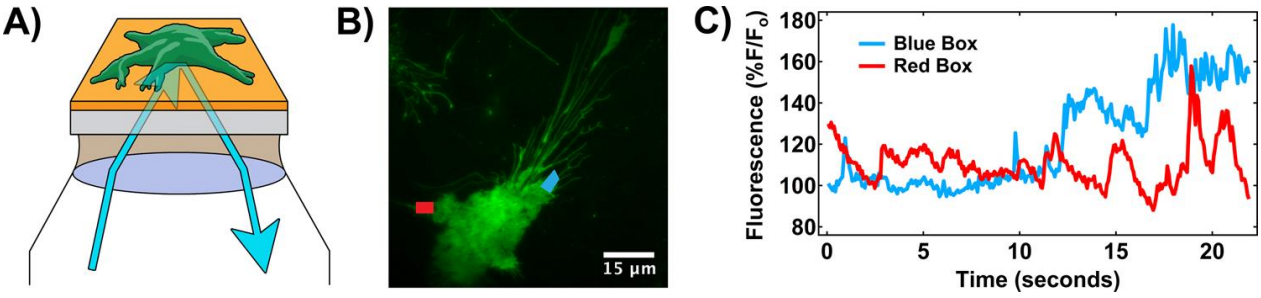

Figure 8.5. Total internal reflection fluorescence microscopy (TIRF) of hNSPCs on reflectin. (a) An illustration of total internal reflection fluorescence microscopy of an hNSPC (green) on a reflectin-coated substrate. The reflectin film is orange, and the reflected light is indicated by a blue arrow. (b) A typical total internal reflection fluorescence microscopy image obtained of an hNSPC loaded with the fluorescent Ca^{2+} indicator Fluo-4 AM. Two arbitrary representative areas are marked with blue and red boxes. (c) A plot of the fluorescence intensity as a function of time for the blue and red boxes in panel b. The plot shows the presence of spontaneous Ca^{2+} transients, which are associated with Piezo1 channel activity.

Having validated that reflectin-coated substrates support hNSPC adhesion and proliferation, we investigated the differentiation potential of reflectin-bound neural stem cells. Thus, after 2 days of growth in proliferation media, we induced differentiation of the hNSPCs by substituting proliferation media with differentiation media. After another 14 days in differentiation media, we fixed, immunostained, and imaged the substrate-bound hNSPCs via standard protocols[61, 62, 65]. We sought to detect the presence of neurons and astrocytes but not oligodendrocytes, as they are not efficiently generated via standard differentiation protocols.

Fluorescence microscopy images of two different immunostained sets of hNSPCs are shown in Figure 8.6. To detect astrocytes, we labeled cells for SOX2, a stem/progenitor cell marker (Fig. 8.6b), and GFAP, a typical astrocytic marker (Fig. 8.6c). This co-staining approach identified the SOX2-negative and GFAP-positive cells as fully differentiated astrocytes (Fig. 8.6d). To detect neurons, we labeled cells for a combination of MAP2 and DCX, which are

common neuronal markers (Fig. 8.6f,g). This co-staining approach identified the MAP2- and DCX-positive cells as differentiated neurons (Fig. 8.6h). Here, we note that immunostained differentiated cells grown on reflectin (Fig. 8.6) were almost indistinguishable from those grown on laminin under identical conditions (Fig. 8.S1). For example, the percentages of hNSPCs on reflectin that transformed into astrocytes and neurons were 64.2 ± 0.6 % and 3.9 ± 0.7 %, respectively, and the percentages of hNSPCs on laminin that transformed into astrocytes and neurons were 68.1 ± 6.1 % and 4.2 ± 0.8 %, respectively. Overall, our experiments confirmed that reflectin-coated substrates were fully capable of supporting neural stem cell differentiation.

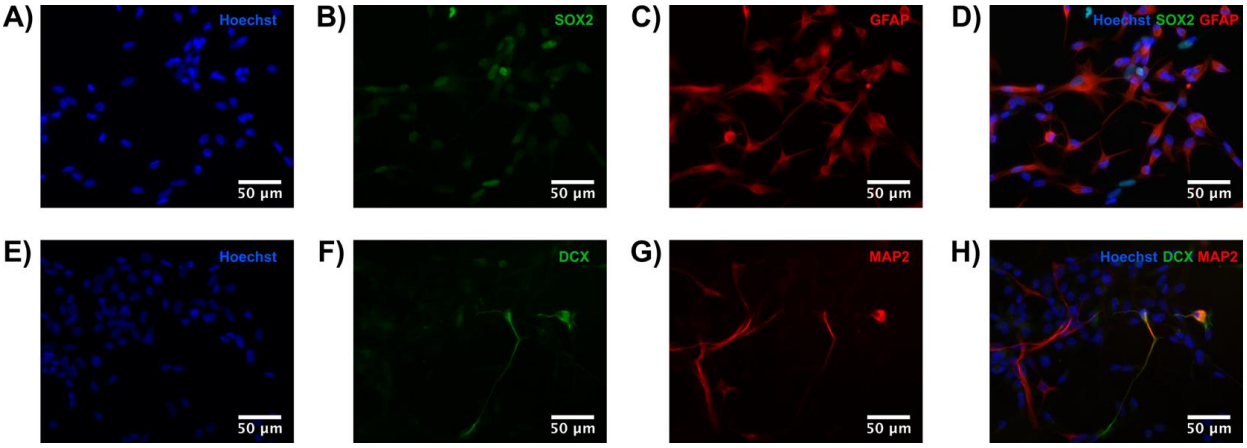

Figure 8.6. Typical fluorescence microscopy images of two separate sets of immunostained hNSPCs on reflectin-coated substrates after differentiation into (a-d) astrocytes and (e-h) neurons. The cells were co-stained with (a) the nuclei marker Hoechst, (b) the stem/progenitor cell marker SOX2, and (c) the astrocyte marker GFAP. The image corresponding to all three markers is shown in (d), where SOX2-negative/GFAP-positive cells are differentiated astrocytes. The neurons were co-stained with (e) the nuclei marker Hoechst, (f) the neuronal marker DCX, and (g) the neuronal marker MAP2. The image corresponding to all three markers is shown in (h), where MAP2-positive and DCX-positive cells are neurons.

8.4 CONCLUSIONS

In summary, we have discovered that reflectin constitutes an effective material for cell growth and differentiation, as demonstrated for traditionally difficult-to-culture hNSPCs. The

viability of the reflectin-bound neural stem cells was assessed with a combination of phase-contrast, bright-field, and fluorescence microscopy techniques. Overall, our studies indicate that reflectin is quite comparable to alternative neural stem cell matrix materials.

Here, we note that our experiments may be quite interesting from the perspective of developmental and cell biology. For example, reflectin's unexpected presence during key stages of brain development in *Sepia officinalis* embryos, together with its functionality as a surface for hNSPC growth, hint that the protein may potentially play some as-of-yet undetermined general role in cephalopod nervous system development. Moreover, given that positively-charged reflectin is similar to fibronectin and laminin, but superior to positively-charged poly-D-lysine, as a cell growth substrate, its unusual amino acid sequence[30-33] may influence stem cell binding and/or proliferation. These possibilities are exciting and certainly warrant further exploration, especially within the context of cephalopods as general comparative model systems for vertebrates.

Finally, our findings hold particular significance from the perspective of bioelectronic applications. Indeed, relatively few materials have been shown to simultaneously exhibit excellent electrical properties and support stem cell attachment, proliferation, and differentiation[52-58]. Reflectin's ability to serve as a substrate for neural stem cell growth therefore establishes the groundwork for interfacing hNSPCs with protein-based protonic devices and raises the intriguing possibility of directly regulating neurogenesis with protonic currents. Moreover, in contrast with some traditional neural stem cell growth materials, reflectin possesses a similar refractive index to glass, making it nearly ideal for TIRFM measurements. The protein's combination of favorable optical and electrical properties thus opens an opportunity for the spectroelectrochemical triggering and monitoring of ion channel activity in single isolated

neural stem cells. Together, these advantages portend favorably for the future of reflectin as an inherently biocompatible active layer in a diverse array of bioelectronic devices.

8.5 MATERIALS AND METHODS

Statement of Ethics

Informed written consent was obtained for all human subjects. All human cell research involved cells with no patient identifiers and was approved by the University of California, Irvine Institutional Review Board and the Human Stem Cell Research Oversight Committee.

Expression, Purification, and Characterization of Reflectin

Reflectin was prepared according to previously reported protocols[26, 27, 35, 36]. An *E. coli* codon optimized gene coding for 6X histidine-tagged reflectin A1 protein from *Doryteuthis pealeii* (Genbank: ACZ57764.1) was synthesized and cloned into the pJExpress414 vector (DNA2.0). The vector was transformed into BL21(DE3) cells (Novagen). Reflectin was expressed at 37°C using Overnight Express Instant Terrific Broth (TB) media (Novagen) supplemented with 100 μg mL^{-1} Carbenicillin. Reflectin was completely insoluble when expressed at 37°C and was sequestered in inclusion bodies prepared using BugBuster (Novagen) according to the manufacturer's suggested protocols. The inclusion bodies were then solubilized in denaturing buffer (pH 8.4, 50 mM sodium phosphate, 300 mM sodium chloride, 6 M guanidine hydrochloride) and purified under denaturing conditions on a HisPur Cobalt Resin gravity column (Thermo Scientific) according to the manufacturer's protocols (elution was performed using denaturing buffer supplemented with 250 mM imidazole). The fractions containing the reflectin protein were pooled and concentrated on an Amicon Concentrator (Millipore) before being purified with high performance liquid chromatography (HPLC) on an

Agilent 1260 Infinity system using a reverse phase C18 column. The gradient was evolved from 95% Buffer A:5% Buffer B to 5% Buffer A:95% Buffer B at a flow rate of 0.5 mL min^{-1} over 20 minutes (Buffer A: 99.9% water, 0.1% trifluoroacetic acid; Buffer B: 95% acetonitrile, 4.9% water, 0.1% trifluoroacetic acid). After purification, the identity of the protein was confirmed with Sodium dodecyl sulfate polyacrylamide gel electrophoresis (SDS-PAGE) and in-gel tryptic digestion, followed by mass spectrometry analysis. The pure reflectin was pooled, flash frozen in liquid nitrogen, and lyophilized. Protein concentrations and yields were quantified via the Bradford protein assay (BioRad) with BSA as the standard.

Fabrication of Reflectin-Coated Substrates

Reflectin-coated substrates were prepared according to previously reported procedures[26, 27, 35, 36]. For bright-field microscopy experiments, reflectin films were fabricated on silica substrates (SQI), and for phase contrast optical microscopy and fluorescence microscopy experiments, reflectin films were fabricated on glass cover slips (ThermoFisher). In a typical experiment, uncoated substrates were first cleaned sequentially with MilliQ water, acetone, and isopropanol, as well as flame-sterilized with a bunsen burner. A fresh 10 mg/mL – 20 mg/mL reflectin solution was then prepared and filtered through sterile 0.45 μm and 0.22 μm filters (ThermoFisher). Subsequently, teflon tape (McMaster-Carr) was applied to edges of the substrates to act spacer for coating. The reflectin protein solution was then cast onto the substrate in front of a plastic blade, which was translated at a constant speed across the surface to produce films. To promote water evaporation, the coating procedure was performed at 80°C. Note that the absence of a graphene oxide adhesion layer reduced film uniformity over large areas.

Growth of HEK, BV2, and MDA-MB-231 Cell Cultures

The HEK cells were a gift from Dr. Naoto Hoshi, the BV2 cells were a gift from Dr. Heike Wulff, and the MDA-MB-231 cells were purchased from ATCC. HEK, BV2, and MDA-MB-231 cells were plated at densities of 20,000 – 105,000 cells/cm^2. The cells were grown as adherent cultures according to known procedures[42-48] at 37°C and under 5% CO_2 in DMEM (Life Technologies), supplemented with 10% fetal bovine serum (Gemini Bio-Products) and 1% Penstrep.

Growth of Adherent Human Neural Stem/Progenitor Cell Cultures

hNSPCs denoted as SC27 were procured from the National Human Neural Stem Cell Resource[59-61]. The hNSPCs were originally derived from brain subventricular zone (SVZ) tissue of a premature neonate that died shortly after birth, as previously described[59, 60]. For donation of the requisite brain tissue, informed consent was obtained prior to tissue acquisition, and this process was approved by the Institutional Review Board[59, 60]. In our studies, the cells were plated at densities of 40,000 – 80,000 cells per 18 mm cover slip. The cells were grown as adherent cultures at 37°C and under 5% CO_2 in base proliferation media, which consisted of DMEM:F12 (Gibco/Invitrogen), 20% (vol/vol) BIT 9500 (bovine serum albumin, insulin, and transferrin) (Stem Cell Technologies), and 1% (vol/vol) antibiotic/antimycotic (penicillin, streptomycin, and amphotericin) (Gibco/Invitrogen). This media was supplemented with 40 ng/ml epidermal growth factor (EGF) (BD Biosciences), 40 ng/ml fibroblast growth factor (FGF) (BD Biosciences), and 20 ng/ml platelet-derived growth factor (PDGF-AB) (Peprotech). To induce differentiation, the base media was exchanged for the differentiation media, which consisted of a 1:1 mixture of the base media and Neurobasal media (Invitrogen) supplemented with 0.5% (vol/vol) B27 (Life Technologies), 20 ng/ml brain-derived neurotrophic factor (BDNF)

(Peprotech), 20 ng/ml neurotrophin-3 (NT3) (Peprotech), 1% (vol/vol) fetal bovine serum (FBS) (Gibco/Invitrogen), 2.5 ng/ml FGF, and 0.1 μM all-trans-retinoic acid (Sigma). The cells were maintained in the differentiation media for a minimum of 14 days.

Optical Microscopy of Adherent Mammalian Cells

Bright-field microscopy images of HEK, BV2, and MDA-MB-231 cells were obtained with a Carl Zeiss Axio Imager A1M Microscope in a 145 mM NaCl, 3 mM KCl, 3 mM $CaCl_2$, 2 mM $MgCl_2$, 5 mM Hepes, pH = 8.3 buffer solution. Phase contrast optical microscopy images of hNSPC cells were obtained with either an EVOS XL (Advanced Microscopy Group) microscope or an Olympus IX71 (Olympus) microscope, which was outfitted with a Hamamatsu C8484 digital camera. The hNSPC images were collected in the base proliferation media. To quantify cell densities, the images were analyzed with FIJI software[68].

Fluorescence Microscopy of Immunostained Human Neural Stem/Progenitor Cells

Fluorescence microscopy images of immunostained hNSPCs were obtained with a Nikon Eclipse Ti microscope and acquired with NIS element AR3.10 software. For imaging, the differentiated hNSPCs were first fixed by treatment with 4% paraformaldehyde for 10 minutes. These fixed cells were then treated with 0.3% Triton X-100 in phosphate-buffered saline (PBS) for 5 minutes, followed by blocking in 5% bovine serum albumin in PBS for 1 hour. All cell nuclei were stained with Hoechst 33342 at 1:500 (2 μg/mL) in PBS for 1 minute. To detect astrocytes, the cells were stained with mouse anti-GFAP (Sigma) and goat anti-SOX-2 (Santa Cruz Biotechnology) primary antibodies for 2 hours at room temperature. To detect neurons, the cells were stained with mouse anti-MAP2 (Sigma) and goat anti-DCX (Santa Cruz Biotechnology) primary antibodies for 2 hours at room temperature. Both neurons and astrocytes were stained with donkey anti-mouse Alexa-Fluor 555 (Life Technologies) and donkey anti-goat

Alexa-Fluor 488 (Life Technologies) secondary antibodies for 1 hour in the dark at room temperature. The primary and secondary antibodies were diluted at 1:200 in 1% bovine serum albumin in PBS solution. To compensate for a lower neuron differentiation percentage, hNSPCs were plated at densities of 80,000 cells per 18 mm cover slip for neurons and at 40,000 cells per 18 mm cover slip for astrocytes. The images were analyzed with FIJI software[68].

Total Internal Reflection Fluorescence Microscopy Imaging of hNSPCs

Fluorescence microscopy images were obtained by using an Olympus IX71 microscope equipped with an Ixon EMCCD camera (Andor), a 488-nm solid-state laser (Melles Griot), and a 1.49 NA Olympus 100x objective lens. The images were collected with an exposure time of 0.04081 s at 13.7 Hz. For Ca^{2+} imaging, the hNSPC cells were loaded with a solution of 1 μM Fluo-4 AM in phenol red-free DMEM/F12 (Invitrogen) for 10 min at 37°C. The cells were then washed three times and further incubated at room temperature for another 10 – 15 minutes to allow for cleavage of the AM ester. The total internal reflection fluorescence microscopy images were obtained in a 148 mM NaCl, 3 mM KCl, 3 mM $CaCl_2$, 2 mM $MgCl_2$, 8 mM glucose, 10 mM Hepes, pH = 8.3 buffer solution. The images were analyzed with FIJI[68] and Origin 9.1 software.

8.6 ACKNOWLEDGMENTS

We thank Dr. Phillip Schwartz, Dr. Naoto Hoshi, and Dr. Heike Wulff for the gift of hNSPCs, HEK293A, and BV2s, respectively. We are grateful to Dr. Albert Yee for the use of an optical microscope. Portions of this work received support from the Air Force Office of Scientific Research grant FA9550-14-1-0144, as well as by the University of California, Irvine (to A.A.G.). The work was also supported by the National Institute of Health grants GM098973

and NS085628 (to F. T.) and the National Science Foundation CAREER award IOS-1254060 (to L.A.F.). R. K. acknowledges the National Science Foundation Graduate Research Fellowship DGE-1321846 Program, and J. A. acknowledges the National Institute of Neurological Disorders and Stroke grant T32 NS082174 for financial support. We are also grateful to the Sue and Bill Gross Stem Cell Research Center at the University of California, Irvine for additional funding.

8.7 SUPPLEMENTAL MATERIAL

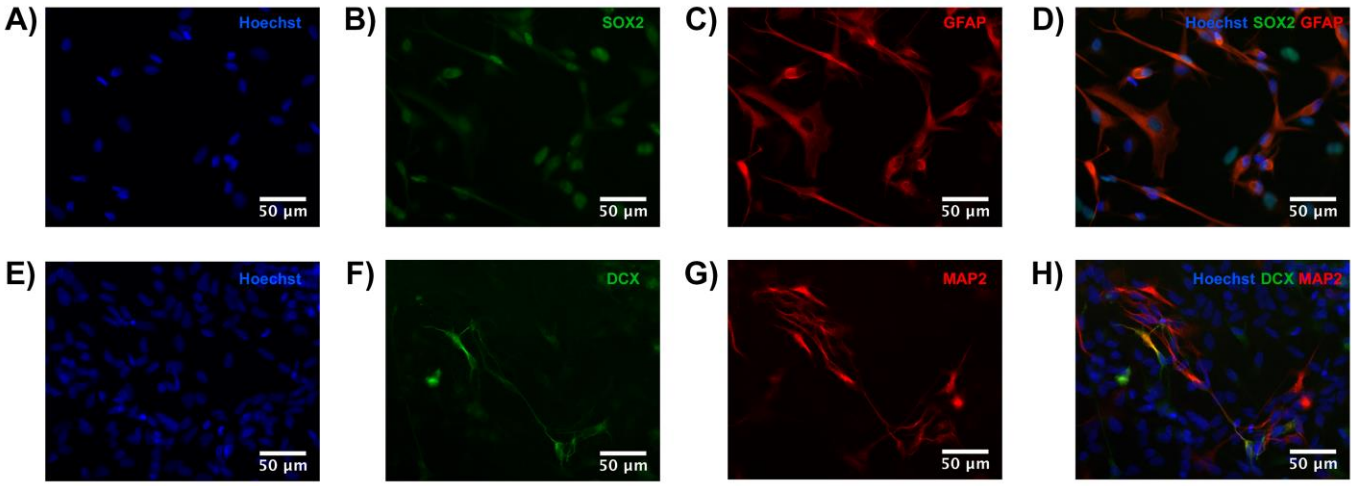

Figure 8.S1. Typical fluorescence microscopy images of two separate sets of immunostained hNSPCs on laminin-coated substrates after differentiation into (a-d) astrocytes and (e-h) neurons. The cells were co-stained with (a) the nuclei marker Hoechst, (b) the stem/progenitor cell marker SOX2, and (c) the astrocyte marker GFAP. The image corresponding to all three markers is shown in (d), where SOX2-negative/GFAP-positive cells are differentiated astrocytes. The neurons were co-stained with (e) the nuclei marker Hoechst, (f) the neuronal marker DCX, and (g) the neuronal marker MAP2. The image corresponding to all three markers is shown in (h), where MAP2-positive and DCX-positive cells are neurons.

8.8 REFERENCES

1. Hanlon, R.T. & Messenger, J.B. Cephalopod behaviour. (Cambridge University Press, 1998).
2. Mäthger, L.M., Denton, E.J., Marshall, N.J. & Hanlon, R.T. Mechanisms and behavioural functions of structural coloration in cephalopods. *J R Soc Interface* **6 Suppl 2**, S149-163 (2009).
3. Stevens, M. & Merilaita, S. Animal camouflage: mechanisms and function. (Cambridge University Press, 2011).
4. Abbott, N.J., Williamson, R. & Maddock, L. Cephalopod neurobiology: neuroscience studies in squid, octopus and cuttlefish. (1995).
5. Nixon, M. & Young, J.Z. The brains and lives of cephalopods. (Oxford University Press, 2003).
6. Borrelli, L. & Fiorito, G. Behavioral analysis of learning and memory in cephalopods. *Learning and memory: a comprehensive reference. Academic Press, Oxford*, 605-627 (2008).
8. Sandeman, D. Homology and convergence in vertebrate and invertebrate nervous systems. *Naturwissenschaften* **86**, 378-387 (1999).
8. Williamson, R. & Chrachri, A. Cephalopod neural networks. *Neurosignals* **13**, 87-98 (2004).
9. Grant, P., Zheng, Y. & Pant, H.C. Squid (Loligo pealei) giant fiber system: a model for studying neurodegeneration and dementia? *Biol Bull* **210**, 318-333 (2006).
10. Hochner, B., Shomrat, T. & Fiorito, G. The octopus: a model for a comparative analysis of the evolution of learning and memory mechanisms. *Biol Bull* **210**, 308-317 (2006).
11. Walters, E.T. & Moroz, L.L. Molluscan memory of injury: evolutionary insights into chronic pain and neurological disorders. *Brain Behav Evol* **74**, 206-218 (2009).
12. Williams, L.W. The anatomy of the common squid Loligo pealii, Lesueur. (1909).
13. Young, J.Z. Structure of nerve fibres in Sepia. *J Physiol* **83**, 27P (1935).
14. BULLOCK, T.H. Properties of a single synapse in the stellate ganglion of squid. *J Neurophysiol* **11**, 343-364 (1948).
15. Sereni, E. & Young, J.Z. Nervous degeneration and regeneration in cephalopods. *Pubbl. Staz. Zool. Napoli* **12**, 173-208 (1932).
16. HODGKIN, A.L. & HUXLEY, A.F. A quantitative description of membrane current and its application to conduction and excitation in nerve. *J Physiol* **117**, 500-544 (1952).
18. Bloedel, J., Gage, P.W., Llinás, R. & Quastel, D.M. Transmitter release at the squid giant synapse in the presence of tetrodotoxin. *Nature* **212**, 49-50 (1966).
18. Katz, B. & Miledi, R. Input-output relation of a single synapse. *Nature* **212**, 1242-1245 (1966).
19. Florey, E., Dubas, F. & Hanlon, R.T. Evidence for L-glutamate as a transmitter substance of motoneurons innervating squid chromatophore muscles. *Comp Biochem Physiol C* **82**, 259-268 (1985).
20. Kreit, E. et al. Biological versus electronic adaptive coloration: how can one inform the other? *Journal of The Royal Society Interface* **10**, 20120601 (2013).
21. Manakasettharn, S., Taylor, J.A. & Krupenkin, T.N. Bio-inspired artificial iridophores based on capillary origami: fabrication and device characterization. *Applied Physics Letters* **99**, 144102 (2011).
22. Morin, S.A. et al. Camouflage and display for soft machines. *Science* **337**, 828-832 (2012).
23. Rossiter, J., Yap, B. & Conn, A. Biomimetic chromatophores for camouflage and soft active surfaces. *Bioinspir Biomim* **7**, 036009 (2012).
24. Yu, C. et al. Adaptive optoelectronic camouflage systems with designs inspired by cephalopod skins. *Proc Natl Acad Sci U S A* **111**, 12998-13003 (2014).
25. Wang, Q., Gossweiler, G.R., Craig, S.L. & Zhao, X. Cephalopod-inspired design of electro-mechano-chemically responsive elastomers for on-demand fluorescent patterning. *Nature communications* **5** (2014).
26. Phan, L. et al. Reconfigurable infrared camouflage coatings from a cephalopod protein. *Adv Mater* **25**, 5621-5625 (2013).
28. Phan, L. et al. Infrared invisibility stickers inspired by cephalopods. *Journal of Materials Chemistry C* **3**, 6493-6498 (2015).
28. Kramer, R.M., Crookes-Goodson, W.J. & Naik, R.R. The self-organizing properties of squid reflectin protein. *Nat Mater* **6**, 533-538 (2007).

29. Qin, G. et al. Recombinant reflectin-based optical materials. *Journal of Polymer Science Part B: Polymer Physics* **51**, 254-264 (2013).
30. Crookes, W.J. et al. Reflectins: the unusual proteins of squid reflective tissues. *Science* **303**, 235-238 (2004).
31. Izumi, M. et al. Changes in reflectin protein phosphorylation are associated with dynamic iridescence in squid. *J R Soc Interface* **7**, 549-560 (2010).
32. Tao, A.R. et al. The role of protein assembly in dynamically tunable bio-optical tissues. *Biomaterials* **31**, 793-801 (2010).
33. DeMartini, D.G., Izumi, M., Weaver, A.T., Pandolfi, E. & Morse, D.E. Structures, Organization, and Function of Reflectin Proteins in Dynamically Tunable Reflective Cells. *J Biol Chem* **290**, 15238-15249 (2015).
34. DeMartini, D.G., Krogstad, D.V. & Morse, D.E. Membrane invaginations facilitate reversible water flux driving tunable iridescence in a dynamic biophotonic system. *Proc Natl Acad Sci U S A* **110**, 2552-2556 (2013).
35. Ordinario, D.D. et al. Bulk protonic conductivity in a cephalopod structural protein. *Nat Chem* **6**, 596-602 (2014).
36. Ordinario, D.D., Phan, L., Jocson, J.-M., Nguyen, T. & Gorodetsky, A.A. Protonic transistors from thin reflectin films. *APL materials* **3**, 014907 (2015).
38. Bonnaud-Ponticelli, L. & Bassaglia, Y. Cephalopod development: what we can learn from differences. *OA Biol* **18** (2014).
38. Bassaglia, Y. et al. Sepia officinalis: A new biological model for eco-evo-devo studies. *Journal of Experimental Marine Biology and Ecology* **447**, 4-13 (2013).
39. Navet, S. et al. Neurogenesis in Cephalopods:" Eco-Evo-Devo" Approach in The Cuttlefish Sepia officinalis (Mollusca-Cephalopoda). *Journal of Marine Science and Technology* **22**, 15-24 (2014).
40. Bassaglia, Y. et al. ESTs library from embryonic stages reveals tubulin and reflectin diversity in Sepia officinalis (Mollusca—Cephalopoda). *Gene* **498**, 203-211 (2012).
41. Andouche, A., Bassaglia, Y., Baratte, S. & Bonnaud, L. Reflectin genes and development of iridophore patterns in Sepia officinalis embryos (Mollusca, Cephalopoda). *Dev Dyn* **242**, 560-571 (2013).
42. Graham, F.L., Smiley, J., Russell, W.C. & Nairn, R. Characteristics of a human cell line transformed by DNA from human adenovirus type 5. *J Gen Virol* **36**, 59-74 (1977).
43. Thomas, P. & Smart, T.G. HEK293 cell line: a vehicle for the expression of recombinant proteins. *J Pharmacol Toxicol Methods* **51**, 187-200 (2005).
44. Cailleau, R., Young, R., Olivé, M. & Reeves, W.J. Breast tumor cell lines from pleural effusions. *J Natl Cancer Inst* **53**, 661-674 (1974).
45. Holliday, D.L. & Speirs, V. Choosing the right cell line for breast cancer research. *Breast Cancer Res* **13**, 215 (2011).
46. Blasi, E., Barluzzi, R., Bocchini, V., Mazzolla, R. & Bistoni, F. Immortalization of murine microglial cells by a v-raf/v-myc carrying retrovirus. *J Neuroimmunol* **27**, 229-237 (1990).
48. Bocchini, V. et al. An immortalized cell line expresses properties of activated microglial cells. *J Neurosci Res* **31**, 616-621 (1992).
48. Stansley, B., Post, J. & Hensley, K. A comparative review of cell culture systems for the study of microglial biology in Alzheimer's disease. *J Neuroinflammation* **9**, 115 (2012).
49. Gage, F.H. Mammalian neural stem cells. *Science* **287**, 1433-1438 (2000).
50. Kornblum, H.I. Introduction to neural stem cells. *Stroke* **38**, 810-816 (2007).
51. Gage, F.H. & Temple, S. Neural stem cells: generating and regenerating the brain. *Neuron* **80**, 588-601 (2013).
52. Willerth, S.M. & Sakiyama-Elbert, S.E. Combining stem cells and biomaterial scaffolds for constructing tissues and cell delivery. (2008).
53. Little, L., Healy, K.E. & Schaffer, D. Engineering biomaterials for synthetic neural stem cell microenvironments. *Chem Rev* **108**, 1787-1796 (2008).
54. Yao, S. et al. Directing neural stem cell fate with biomaterial parameters for injured brain regeneration. *Progress in Natural Science: Materials International* **23**, 103-112 (2013).

55. Discher, D.E., Mooney, D.J. & Zandstra, P.W. Growth factors, matrices, and forces combine and control stem cells. *Science* **324**, 1673-1677 (2009).
56. Lutolf, M.P., Gilbert, P.M. & Blau, H.M. Designing materials to direct stem-cell fate. *Nature* **462**, 433-441 (2009).
58. Celiz, A.D. et al. Materials for stem cell factories of the future. *Nat Mater* **13**, 570-579 (2014).
58. Murphy, W.L., McDevitt, T.C. & Engler, A.J. Materials as stem cell regulators. *Nat Mater* **13**, 547-557 (2014).
59. Palmer, T.D. et al. Cell culture. Progenitor cells from human brain after death. *Nature* **411**, 42-43 (2001).
60. Schwartz, P.H. et al. Isolation and characterization of neural progenitor cells from post-mortem human cortex. *J Neurosci Res* **74**, 838-851 (2003).
61. Flanagan, L., Rebaza, L., Derzic, S., Schwartz, P. & Monuki, E. Regulation of human neural precursor cells by laminin and integrins. *Journal of neuroscience research* **83**, 845-856 (2006).
62. Labeed, F.H. et al. Biophysical characteristics reveal neural stem cell differentiation potential. *PLoS One* **6**, e25458 (2011).
63. Pistollato, F., Chen, H.-L., Schwartz, P., Basso, G. & Panchision, D. Oxygen tension controls the expansion of human CNS precursors and the generation of astrocytes and oligodendrocytes. *Molecular and cellular neurosciences* **35**, 424-435 (2007).
64. Lee, J.P. et al. Stem cells act through multiple mechanisms to benefit mice with neurodegenerative metabolic disease. *Nat Med* **13**, 439-447 (2007).
65. Pathak, M.M. et al. Stretch-activated ion channel Piezo1 directs lineage choice in human neural stem cells. *Proc Natl Acad Sci U S A* **111**, 16148-16153 (2014).
66. Axelrod, D. Total internal reflection fluorescence microscopy in cell biology. *Traffic* **2**, 764-774 (2001).
68. Axelrod, D. Chapter 7: Total internal reflection fluorescence microscopy. *Methods Cell Biol* **89**, 169-221 (2008).
68. Schindelin, J. et al. Fiji: an open-source platform for biological-image analysis. *Nature methods* **9**, 676-682 (2012).

CHAPTER 9

CONCLUSION

9.1 SUMMARY

Neural stem cells open a hopeful avenue of potential cures for stroke sufferers living with deficits that inhibit normal daily function. However, transplantation of exogenous NSPCs into the stroke-injured brain results in low cell survival. Injectable biomaterial scaffolds provide NSPCs with protection from shear forces during transplantation, physical shielding from the toxic microenvironment of the infarct site, and may support cell function post-transplant. In this work, we investigated the interactions of ECM materials and NSPCs in the context of physical cues such as substrate stiffness and static stretch, and based on these findings designed and tested the effects of novel scaffolds on NSPC behavior *in vitro* and *in vivo.*

Prior to this study, it was recognized that NSPCs have an exquisite sensitivity to their mechanical environment, particularly substrate stiffness. However, little was known of NSPC sensitivity to alternate mechanical stimuli such as stretch. This type of stimulus occurs in the brain within the context of development as well as traumatic injury. There is no effect of static stretch on neuron and astrocyte generation from NSPCs, but it elicits a significant reduction in oligodendrocyte formation which is dependent on the engagement of laminin-binding integrins. Thus, NSPCs *in vivo* that are in laminin-rich niches encountering a stretch stimulus may alter their oligodendrocyte generation. Furthermore, the stretch-activated ion channel (SAC) Piezo1 mediates lineage choice of NSPCs based on the mechanical properties of the substrate, thus providing insight into how these cells interpret mechanical stimuli. Further studies will be

necessary to determine the functional significance of these findings *in vivo*, but it directly impacts the design of biomaterials for NSPC tissue engineering and transplantation. Inclusion of laminin in 3D scaffolds would be beneficial since it is found in the native *in vivo* NSPC niche and supports NSPC function *in vitro*.

A critical problem with the use of naturally-derived materials as *in vivo* scaffolds for neurological injury is rapid degradation upon transplant into a CNS lesion site. This renders these types of scaffolds incapable of long-term support for transplanted cells. We developed unique combination scaffolds of salmon fibrin, HA, and laminin that support hNSPC proliferation and differentiation, which are vital for the success of a stem-cell based CNS transplant construct to treat injury. Additionally, the combination scaffold attenuates rapid cell-mediated degradation seen with fibrin alone, directly addressing the aforementioned degradation issue in the biomaterials field. These scaffolds are also advantageous because they possess ideal material properties for transplantation into the CNS. This study marks the first of its kind in including human-derived endothelial and neural cells within this unique combination scaffold to encourage vascularization *in vitro*. This sets a benchmark in the field for developing human-based therapies utilizing multiple cell types and provides motivation for the use of this particular construct in creating a transplanted neurovascular niche to treat the injured CNS.

Biomaterials that utilize short peptide sequences for cell adhesion portend favorably for approval from the FDA for use with a cellular therapeutic due to reduced immunogenicity and increased manufacturability. Since HA has already been FDA-approved as a hydrogel for various applications, we developed HA-based scaffolds conjugated with several adhesion peptide sequences for hNSPCs. The peptide sequence serves as a replacement for salmon fibrin since the latter is a non-recombinantly expressed full length protein and therefore would be challenging to

pass through FDA regulations. Recombinant collagen may also be easier to translate as a scaffold material into the clinic since it has higher manipulability in terms of engineering cell adhesion sequences to various sites on the protein. The ability to manufacture recombinant collagen allows for more exhaustive *in vivo* immunoreactivity testing for CNS applications. Through the creation of novel and more simplistic systems that can mimic or improve currently used biomaterials that facilitate NSPC adhesion, it will become easier to design and manufacture scaffolds that can be used as cell devices for clinical trials and eventually as approved treatments for neurological injury.

9.2 DIRECTIONS FOR FURTHER RESEARCH

This thesis is comprised of a comprehensive study that employs a combination of engineering and biology to develop biomaterials that can be used as scaffolds for NSPCs to treat stroke. It also adds to the growing body of literature highlighting the sensitivity of NSPCs to their biophysical microenvironment and the materials they interact with. Due to the clinical relevance of using biomaterials as NSPC scaffolds for CNS injury, there are several avenues that can be explored in order to further appreciate the impact of the findings in this work on the neural tissue engineering and regenerative medicine field.

9.2.1 What are the downstream mechanisms regulating the effect of static stretch on NSPC differentiation?

As described in Chapter 2, applying a 10% equibiaxial static stretch to NSPCs cultured on laminin elicits a significant reduction in production of oligodendrocytes. Although we

identified the α6 integrin as being a key mediator of this effect, it is still unclear what intracellular downstream mechanisms are at play. We showed in Chapter 3 that substrate stiffness sensing in NSPCs and its relationship with cell fate is mediated by the SAC Piezo1. Piezo1 is likely also playing a role in stretch-sensing and additional studies investigating nuclear transcription factors, nuclear structural proteins, and cytoskeletal rearrangements associated with mechanical perturbations would shed light on phenotypic regulators downstream of integrins. Knowledge of intracellular processes involved in mechanotransduction would provide a more complete overall depiction of the effect of these types of mechanical stimuli on NSPC differentiation.

9.2.2 What are the effects on hNSPCs when co-cultured with hECFC-ECs within combination scaffolds?

In Chapter 4, a novel combination scaffold was introduced that can enhance vascularization from endothelial cells in co-cultures with hNSPCs. Although we were able to identify changes in hECFC-EC behavior as a function of biomaterial and hNSPC co-culture, we have yet to investigate the complementary effects on hNSPC behavior. By studying proliferation and differentiation of hNSPCs in co-cultures with hECFC-ECs, we would gain a deeper understanding of the behavior of both cell types within this system and of the neurovascular niche. This would be beneficial in the preparation of this type of transplant construct for *in vivo* applications.

9.2.3 How do hNSPCs behave long-term when transplanted into a rodent stroke model?

Chapter 5 outlines the use of biomaterials as scaffolds for hNSPC transplants to treat stroke. The study focuses on the short-term (2 weeks) effects of transplanting hNSPCs with scaffolds into stroke-injured rat brain. Since hNSPC differentiation *in vivo* requires at least 1 month, a long-term study on the order of months would be necessary to identify effects of the transplant on exogenous cell differentiation. This would also provide the ability to study long-term behavioral recovery in animals as a function of hNSPC differentiation. The increased time frame of the preclinical study would make it more comparable to a human stem cell stroke clinical trial study, which requires months to years to obtain reliable data.